NASA TECHNICAL NOTE

NASA TN D-4881

NASA TN D-4881

NIMBUS II FLIGHT EVALUATION AND ENGINEERING REPORT, LAUNCH THROUGH ORBIT 5275

by

Joseph J. McNaney and Bennie A. Palmer
General Electric Company

and

Ralph Shapiro
Goddard Space Flight Center

NATIONAL AERONAUTICS AND SPACE ADMINISTRATION • WASHINGTON, D. C. • FEBRUARY 1969

NASA TN D-4881

NIMBUS II FLIGHT EVALUATION AND ENGINEERING REPORT, LAUNCH THROUGH ORBIT 5275

By Joseph J. McNaney and Bennie A. Palmer
General Electric Company

Ralph Shapiro
Goddard Space Flight Center
Greenbelt, Md.

NATIONAL AERONAUTICS AND SPACE ADMINISTRATION

For sale by the Clearinghouse for Federal Scientific and Technical Information
Springfield, Virginia 22151 – CFSTI price $3.00

ABSTRACT

Nimbus II, an earth-stabilized, long-life observatory satellite, is part of the NASA research and development program for meteorological applications. Experiments include advanced vidicon camera subsystem (AVCS), high-resolution infrared radiometer (HRIR) subsystem, medium-resolution infrared radiometer (MRIR) subsystem, automatic picture transmission (APT) subsystem with data code grid, and direct readout infrared radiometer (DRIR). This report covers the flight history of Nimbus II from its launch on May 15, 1966, through orbit 5275 on June 15, 1967, providing an engineering evaluation of the performance during this period. The mission successfully met all technological and scientific objectives, the only failures being the tape recorders, PCM, MRIR, AVCS, and HRIR; these failures occurred during orbits 949, 985, 1443, and 2455, respectively. As of March 15, 1968 (22 months, orbit 9020), the spacecraft was performing satisfactorily with little change in performance since June 15, 1967, except for the solar array drive. After October 1967, the drive system evidenced occasional erratic behavior and since then has been operated in the high-torque mode. The real-time data systems are still being used.

CONTENTS

CONTENTS (Continued)

CONTENTS (Continued)

CONTENTS (Continued)

CONTENTS (Continued)

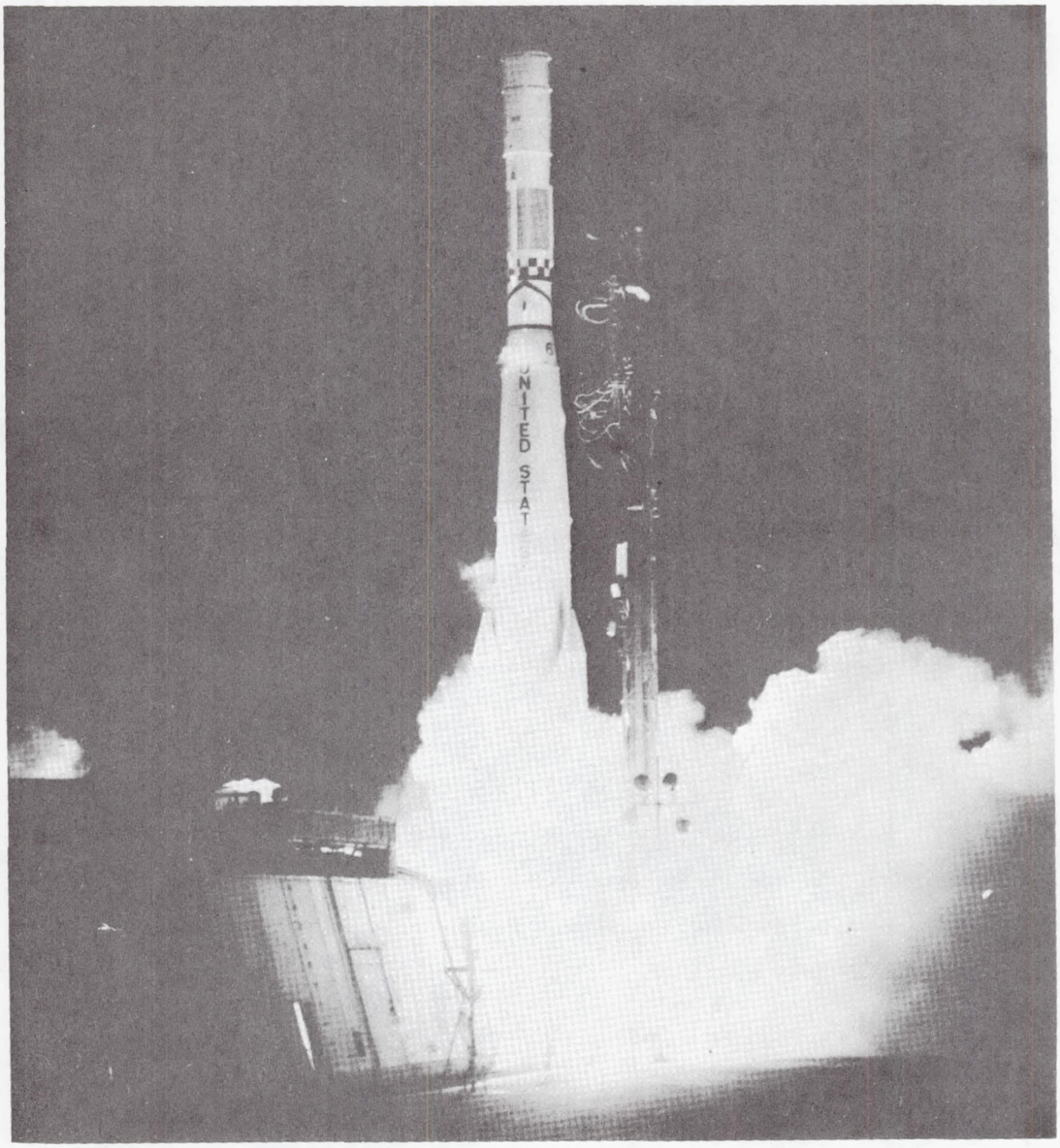

Frontispiece—Nimbus II launched May 15, 1966 (00:55:34 PDT).

NIMBUS II FLIGHT EVALUATION AND ENGINEERING REPORT, LAUNCH THROUGH ORBIT 5275

by

Joseph J. McNaney and Bennie A. Palmer

General Electric Company

Ralph Shapiro

Goddard Space Flight Center

SECTION 1
INTRODUCTION

During the 13 months of the Nimbus II flight reported in this document (May 15, 1966 to June 15, 1967), a continuous on-line and off-line evaluation of spacecraft performance was maintained by the Nimbus Technical Control Center (NTCC) at Goddard Space Flight Center. This report summarizes the results of the engineering flight evaluation for the period between launch on May 15, 1966, and orbit 5275 on June 15, 1967. Addendums to this report will be published to cover subsequent flight operations.

Sensory data obtained from Nimbus II have been cataloged by the Nimbus Data Utilization Center. Copies of these catalogs or sensor data can be obtained from the National Space Science Data Center, Goddard Space Flight Center, Code 601, Greenbelt, Maryland 20771.

SECTION 2

FLIGHT OBJECTIVES

The Nimbus program resulted from the need for a meteorological satellite system capable of meeting the research and development needs of the nation's meteorological scientists and weather services. The general objective of the program is to establish an earth-oriented platform for developing and flight-testing a variety of advanced meteorological experiments. This platform must be capable of viewing the entire earth daily for a prolonged period of time. The end objective of the program is to collect and distribute the meteorological data gathered so that the data may be used immediately, both operationally and in the study of atmospheric processes. With these general views in mind, the immediate objective of Nimbus II becomes one of demonstrating the capability of the basic spacecraft as a long-life observatory with technological and scientific operational characteristics.

Technological success requires that the spacecraft attain earth-stabilization in three axes to ±1-degree precision, that the power supply support the payload in full-time operation for a prolonged period, and that global sensory data be collectable and retrievable on an operational and near-real-time basis. The power supply requirements, in turn, dictate that the improved solar array drive (SAD) has long-life capability.

Scientific success depends on the effective operation of each of the spacecraft experiments. The advanced vidicon camera subsystem (AVCS) and high-resolution infrared radiometer (HRIR) must collect a body of high-resolution television (TV) and infrared (IR) data over a prolonged period. The medium-resolution infrared radiometer (MRIR) must measure the earth's terrestrial and atmospheric radiation and reflected solar radiation in five spectral bands between 0.2 and 30 microns. The automatic picture transmission (APT) subsystem and direct readout infrared radiometer (DRIR) must provide real-time data to local users on a continuous basis. The AVCS, HRIR, and MRIR experiments not only must perform their functions, but also must perform them on a global basis if their potential is to be realized fully.

All of the foregoing objectives were met. However, the premature failure of the MRIR, AVC, and HRIR subsystem tape recorders eliminated global coverage capability. Table 2-1 is a breakdown by subsystem of Nimbus II flight objectives and results.

Table 2-1

Nimbus II Flight Objectives and Results.

Subsystem	Flight Objectives	Remarks	
		6 Months	13 Months
Power	Demonstrate the capability of the Power Subsystem to provide normal spacecraft power demand with the required voltage regulations, for a period of at least 6 months following orbit injection.	The Power Subsystem maintained all of its functional requirements within limits during the first 6 months despite a solar paddleboard failure that resulted in a 0.6-amp reduction in total solar array output. At the end of 6 months, the array current output was 12.3 amps.	The Power Subsystem continued to supply enough power for spacecraft operation despite an additional loss of 0.6 amp from the solar array caused by a paddleboard failure and 13 months degradation because of particle damage. The array output was 9.85 amps on 15 June 1967.
PCM	(1) Demonstrate the ability of the PCM Subsystem to continuously record, and playback on command, high-quality telemetry data for reception at the Nimbus DAF stations. (2) Demonstrate the capability of the PCM Subsystem to provide high-quality telemetry data in real time to designated receiving stations.	(1) The PCM Subsystem provided data with a quality of 98% good data prior to failure of the PCM tape recorder during orbit 949. This failure precluded further reception of A stored data. (2) Good quality A real time continued to be received from the spacecraft.	(1) The PCM tape recorder remained inoperative. It was periodically commanded into playback to eliminate 10-kHz interference on the AVCS pictures caused by the time code on the real time telemetry. (2) Good quality A real time continued to be received from the spacecraft.
Control	(1) Demonstrate that the Control Subsystem is capable of: (a) Initial attitude acquisition following orbit injection. (b) Maintain three-axis stabilization. (c) Provide paddle deployment and solar array pointing for a period of at least 6 months following orbit injection.	(1a) The spacecraft acquired the earth reference and stabilized the spacecraft within 3.6, 3.4, and 6.1 minutes in pitch, roll, and yaw, respectively, after each of these loops was enabled. (b) In the absence of cold clouds, fine limit cycle control of the pitch, roll, and yaw axes had been to within 1 degree of the required reference. (c) The SAD pointed the array surface properly toward the sun within 5.5 minutes after the drive loop was enabled and continued to track properly.	(1a) (See 6-month comment) (b) In the absence of cold clouds, fine limit cycle control of pitch, roll, and yaw axes continued to be maintained within 1 degree of the required reference. (c) Solar array pointing continued to be maintained well within specifications.

Table 2-1

Nimbus II Flight Objectives and Results (Continued).

Subsystem	Flight Objectives	Remarks	
		6 Months	13 Months
Control (Continued)	(2) Demonstrate the adequacy of the Control Subsystem thermal control system.	(2) Since launch, the controls temperatures maintained within the specified range of 25 ± 10°C. The controls housing average at the end of 6 months was 26.3°C.	(2) The controls temperatures continued within limits with the average control housing temperature at 26.9°C.
	(3) Demonstrate that the improvements to the SAD will preclude the failure experienced in Nimbus I.	(3) The array continuously tracked the sun with no observed signs of degradation in the electronic or mechanical system.	(3) The array continuously tracked the sun with no observed signs of degradation in the electronic or mechanical system.
	(4) Demonstrate that the reduced pitch nozzle size plus reduced gating time will eliminate the pitch oscillation experienced on Nimbus I.	(4) There was no observed pitch oscillation.	(4) There was no observed pitch oscillation.
Command Receiver	Demonstrate the capability of the Command Subsystem to properly and consistently receive, store, and execute encoded commands and to receive and execute unencoded commands.	The Command Subsystem operated successfully for the first 6 months. The only problems were: (1) noise entry into the clock causing erroneous data on the data code and grid (DCG), and (2) unintentional unencoded command executions. Neither of these affected spacecraft operation. The clock stability was excellent (gaining an average of 1.15 milliseconds per orbit).	The Command Subsystem continued to operate successfully with only those problems listed under the 6 months remarks. Clock stability continued to be excellent (gaining an average of 1.15 milliseconds per orbit).
Thermal	Demonstrate the ability of the Thermal Subsystem to maintain the sensory ring components within the prescribed temperature limits.	The Thermal Subsystem performed in an excellent manner, maintaining temperatures within prescribed limits. The average sensory ring and H-frame temperatures were 21.5° and 23.5°C, respectively.	The Thermal Subsystem continued to perform in an excellent manner. The average sensory ring and H-frame temperatures were 19.1°C and 20.6°C, respectively.
AVCS	Demonstrate the capability of the AVCS to record high-quality cloud photographs of the entire earth surface and play back upon command.	The performance of the AVCS was satisfactory until orbit 1444 during which the subsystem tape recorder failed, eliminating the data storage capability of the subsystem. Since then, pseudo-direct photographs were received. The quality of the photographs was degraded by 10-kHz RF interference.	Pseudo-direct photographs of good quality continued to be received from the spacecraft. With the PCM tape recorder in playback, photographs are interference-free.

Table 2-1

Nimbus II Flight Objectives and Results (Continued).

Subsystem	Flight Objectives	Remarks	
		6 Months	13 Months
S-Band	Provide a high quality transmission medium for the AVCS and HRIR tape recorder playbacks and direct AVCS frames.	The performance of the S-band transmitter was excellent with signal reception levels ranging (DAF) from -70 to -90 dbm.	The S-band transmitter performance continued to be excellent with no evidence of long-term degradation.
APT	(1) Demonstrate the capability of the APT Subsystem to provide high-quality photographs of the earth surface and cover and transmit in real time.	(1) The performance of the APT Subsystem was entirely satisfactory.	(1) The APT Subsystem continued to perform satisfactorily. A gradual shift in the dc level of the video occurred but this can be compensated for in the ground processors.
	(2) Provide feasibility of providing ephemeris data (DCG) to APT users via the satellite.	(2) The DCG portion of the APT pictures proved to be a complete success.	(2) The DCG continued to be satisfactory.
DRIR	Demonstrate the feasibility of direct readout of high resolution infrared using the APT transmitter.	The HAX Module provided good quality, interference-free transmission of IR video from the HRIR Subsystem until orbit 2455 at which time the HRIR tape recorder failure precluded further reception of data.	The status is the same as listed for the 6-month results.
HRIR	Demonstrate the capability of the HRIR Subsystem to record high-quality IR measurements of the earth surface and cover and provide real-time IR to the HAX Module.	The HRIR Subsystem performance was excellent until orbit 2455, at which time the subsystem tape recorder failed. This failure precluded further reception of data from this subsystem. Prior to the failure, the HRIR Subsystem provided good quality data to the HAX Module.	Subsystem status remained unchanged since orbit 2455.
MRIR	Demonstrate the ability to measure the earth terrestrial and atmospheric radiation and reflected solar radiation in five spectral bands between 0.2 and 30 microns.	The MRIR Subsystem performed excellently until a malfunction within the subsystem tape recorder during orbit 985 eliminated the data recording/transmission capability. A subsequent failure of the radiometer chopper motor occurred during orbit 1170.	Subsystem status remained unchanged since orbit 1170.

SECTION 3

VEHICLE DESCRIPTION AND FLIGHT SUMMARY

SPACECRAFT DESCRIPTION

Structure

The Nimbus II spacecraft consists primarily of a lower sensory ring structure and an upper housing, separated by truss supports. The upper housing contains the attitude controls required for spacecraft orientation and provides solar paddle attachment. The sensory ring is composed of 18 compartments. Each compartment consists of an upper and lower section, in which the solid-state modularized subsystems and assemblies are located. Modules are positioned around the ring to maintain an isothermal temperature balance of 25 ± 10°C. Units dissipating large amounts of heat are located in the lower sections which never face the sun directly.

The attitude controls, sensory ring systems, and the solar paddles are thermally independent. Venetian blind-type shutters, located in the control housing and on the outer area of the sensory ring, provide radiant cooling, when open. Magnesium is the basic structural material because of its high strength-to-weight ratio and its favorable stiffness and damping characteristics.

Thermal Control

Independent thermal control has been established for the three major elements of the spacecraft—the solar paddles, the sensory ring, and the control housing.

Solar Paddles

The front and rear surfaces of the solar paddles are designed with absorptivity and emissivity carefully chosen to yield an average solar-paddle equilibrium temperature of approximately +25°C. The excellent thermal conductivity of the side of the paddle honeycomb structure opposite the sun tends to cool the heated side and minimize temperature gradients.

Sensory Ring

The sensory ring is designed for an isothermal temperature balance of +25 ± 10°C. Temperature control is maintained both by the shutters on each compartment and by the lining on the top and bottom of the sensory ring. This lining consists of multiple layers of aluminized Mylar. The sensory ring also serves as a heat sink for the electronics modules, which are mounted for maximum heat transfer to the ring structure through conduction and radiation.

Control Housing

An equilibrium temperature of +25 ± 10°C is maintained in the control housing by both passive and active thermal controls. The pneumatic tank must be kept within specified limits of pressure; therefore, heat conduction to the pneumatic tank is prevented by insulating the bottom surface of the control housing. The control housing active thermal control system consists of two four-shutter panels located on the two sides of the housing; the system operates similarly to the sensory ring thermal controls.

Stabilization and Control

The primary requirements of the Control Subsystem are to orient and stabilize the spacecraft with respect to the earth and orbital plane. The stabilization and control system employs horizon scanners and a rate gyro, with three flywheels and eight Freon-14 gas nozzles as torque generators to provide spacecraft attitude control. A pneumatic tank, located under the control housing, contains the Freon gas supply. The nozzles are used to reduce large stabilization errors, and the flywheels compensate for small errors. A tachometer monitors the speed of the flywheels and operates the gas nozzles to reduce the speed of the flywheels, thus preventing flywheel saturation.

The spacecraft coordinate system is defined by the yaw, roll, and pitch alignment of the optical scanners and inertial devices used for axis orientation. The yaw axis points toward the earth center, and the roll axis is perpendicular to the yaw axis and parallel to the orbital plane. The pitch axis is perpendicular to both the yaw and roll axes and coincides with the solar paddle axis.

Power Supply

The power supply includes an array of N-P silicon solar cells mounted on solar-oriented paddles, nickel-cadmium storage batteries, voltage regulators, and protective devices. The solar cells are mounted on one side of each of the two aluminum honeycomb paddles that are rotated continuously to face the sun. Sun sensors circle the driveshaft of each paddle and detect solar radiation so that the sun can be "acquired" by the solar paddles regardless of the spacecraft attitude or the position of the paddles in respect to the sun-satellite line. A servomotor located in the control housing rotates the driveshaft.

During the 600-nm orbit, 73 minutes are spent in sunlight and 35 minutes in the earth's shadow. When the satellite is on the dark side of the earth, a preset potentiometer continues to turn the paddles until they reach the position for sunrise acquisition. Power for nighttime operation is supplied by the storage batteries. The power supply delivers -24.5 vdc regulated at ±2 percent and a nominal average power of 250 watts during the entire orbit. Eight battery modules provide redundancy.

Command Clock

Stable, accurate, and coherent timing signals are required to relate the satellite operation to orbital position; therefore, time control of the spacecraft systems is mandatory at all times. The

command clock provides a time reference in days, hours, minutes, and seconds; precise, stable, and coherent signals from 400 kHz to 1 Hz; relay closure pulses for commanding subsystems; and a capability for storing 16 commands. The time reference consists of Minitrack time code outputs to the spacecraft subsystems. The relay closure pulses are derived from encoded commands received by the command receiver, error-checked, interpreted, remembered, and ultimately released to trigger spacecraft actions at the desired time. These commands, of which there are 128 possibilities, are executable at the rate of 1 per second. Although there are 128 possibilities, only 16 distinct commands may be stored within the spacecraft at any given time.

Command Receiver

A pair of redundant, highly selective, sensitive command receivers (operating at 149.52 MHz) and selectable FM demodulators are provided; four unencoded commands are available. Three FSK subcarriers at 1.3, 1.7 and 2.3 kHz are demodulated in the receiver to provide bit rate, character sync, and data intelligence to the command clock. The receiving antenna is located on top of the controls structure.

Telemetry

Nimbus II uses a pulse code modulated (PCM) telemetry subsystem to gather information from all subsystems for status and engineering evaluation. A total of 542 analog functions are sampled and digitized at rates varying from once each second to 1 each 16 seconds. A major frame of telemetry containing 1024 8-bit words (7 data bits) is sampled every 16 seconds. Data are mixed with time code and transmitted via a 136.5-MHz, 1/4-watt transmitter through four antennas located on the outer area of the sensory ring. Data are also stored on a tape recorder and played back in 3.75 minutes for a full orbit of data.

Communications

The spacecraft is commanded by ground stations located at the Alaska DAF at Fairbanks and the Nimbus Data Handling Center (NDHS) at Greenbelt, Maryland through transmitters located at the Fairbanks and Rosman, N. Carolina data acquisition facilities (DAF) and at the Orroral, Australia STADAN site. The transmitters operate at 149.52 MHz. Data are transmitted from the spacecraft over the communication links listed in Table 3-1.

Table 3-1

Communication Links.

Subsystem	Frequency (MHz)	Power (watts)	Modulation
Telemetry	136.5	1/4	PCM/AM
APT/DRIR	136.9	5	AM/FM
MRIR	137.2	1-3/4	PCM/FM
Wideband (AVCS/HRIR)	1707.5	5	FM/FM

The telemetry and APT transmitters operate full time. APT data are received directly by worldwide users for making weather pictures of local areas using facsimile equipment. Telemetry, MRIR, and wideband data are received at the two DAF facilities, generally 10 passes at Alaska and two at Rosman with two "blinds" per day. Reception of telemetry data is available at the Orroral STADAN site during blind orbits. Interrogations average 10 minutes.

Advanced Vidicon Camera System (AVCS)

The Advanced Vidicon Camera Subsystem consists of three vidicon cameras, a 4-track magnetic tape recorder, a frequency multiplexer, and associated timing and power control electronics. The three AVCS cameras are arranged in a trimetrogon array to obtain almost complete coverage of the earth's sunlit side. The three cameras are mounted so that the one in the center points straight down, with the two adjacent cameras tilted 35 degrees. The field-of-view for each camera is 37 degrees with a 2-degree overlap, as shown in Figure 9-3. Operating in a polar orbit at an altitude of 600 nm, the camera area covered is approximately 400-by-1900 nautical miles. Successive frames, taken at 91-second intervals, provide approximately 20-percent overlap of earth coverage. Camera readout requires one scan and is approximately 6.25 seconds; the video bandwidth is 60 kHz. A ground resolution of approximately one-half mile per TV line is obtained. Each camera is equipped with a variable iris to compensate automatically for latitudinal changes in earth illumination. Self-contained calibration for both sweep and gray scale linearity is incorporated in the camera sensors. A precision reticle pattern, deposited in the image area of the vidicon, provides the dimensional reference for measuring system linearity. A calibrated gray scale appears on each picture for white-to-black reference.

High-Resolution Infrared Radiometer (HRIR)

The HRIR Subsystem consists of a scanning radiometer, associated electronics, a 4-channel tape recorder, and a multiplexer. The system is designed to detect radiation in the 3.5- to 4.1-micron range for determining cloud and terrestrial temperatures for making nighttime cloud cover pictures and IR mapping of the earth surface.

The radiometer has an approximate 1/2-degree field-of-view, equivalent to 5-nm resolution at 600-nm altitude. A mirror rotating at 44.7 rpm scans 360 degrees in a plane perpendicular to the orbital motion of the spacecraft. The radiation reflected from the scan mirror is chopped at the focus of a 4-inch f/1 Cassegrainian telescope. It is then refocused at a lead selenide (PbSe) detector by a reflective relay optical system containing a 3.5 to 4.1-micron filter. The detector is radiatively cooled to -75°C. The data are stored on an analog recorder along with reference Minitrack time code, which is played back through the S-band transmitter at eight times the recorded speed.

Automatic Picture Transmission (APT) Subsystem and Direct Readout (DRIR)

The Automatic Picture Transmission Subsystem (Figure 10-1) is a supplementary meteorological system that provides real-time transmission of daylight cloud-cover photography to local

ground stations for weather observation and forecasting applications. The HRIR video signal is also transmitted over the APT transmitter for real-time reception of nighttime cloud-cover pictures (DRIR).

The APT Subsystem consists of a camera assembly, electronics module, automatic sync generator (ASG), and a VHF transmitter. The subsystem is programmed for continuous operational cycles of picture-taking and transmission. The 1-inch vidicon tube is designed for long-duration storage and slow readout of the cloud cover images viewed by a wide-angle lens (108 degrees). Ground coverage at a 600-nm altitude is in the order of 1250-by-1250 nm, imaged by a 108-degree Tegea Kinoptic, wide-angle lens. The picture cycle is 208 seconds, including 3 seconds of start tone, 5 seconds of phasing signals, and 200 seconds of picture readout. The picture includes a data code readout along one edge that provides information on the picture exposure time and satellite ephemeris data used for geographic referencing of the picture.

Medium-Resolution Infrared Radiometer (MRIR)

The MRIR Subsystem, consisting of a 5-channel scanning radiometer and associated electronics and tape recorder, is designed to measure the earth's terrestrial and reflected solar radiation in five different spectral bands between 0.2 and 30 microns. The channels and their application are as follows:

Spectral range (microns)	Application
0.2 to 4.0	Visible and near-infrared
6.4 to 6.9	Water vapor absorption band (upper troposphere)
10 to 11	Atmospheric window (earth's surface and clouds)
14 to 16	Carbon dioxide absorption (stratosphere)
5 to 30	Total infrared (earth heat budget)

The radiometer consists of a scan mirror rotating at 8 rpm, five 4.2-inch focal length f/2.4 Cassegrainian telescopes, a rotating chopper dish, five filters, five thermistor bolometer detectors, and five preamplifiers. The system has approximately a 3-degree field-of-view, equivalent to 30-nm ground resolution at 600-nm altitude. The analog signal is converted into 7-bit digital data, stored on an 8-track tape recorder, and played back at 26 times recorded speed through the 137.2 MHz transmitter.

NIMBUS II SPACECRAFT CHANGES

The Nimbus II is essentially identical to Nimbus I; major differences include:

a. Addition of the MRIR Subsystem,

b. Addition of Battery Module No. 8,

c. Addition of HAX affording HRIR real-time readout from the APT Subsystem transmitter,

d. Increase in the command clock memory capability and addition of data code gridding and timeout capability,

e. A larger SAD motor (size 8 to 11) with a high (26 vac) and low (10.5 vac) drive voltage selection and thermally strapped to Panel No. 2; the motor rotor design was changed to increase the radiative cooling to lower the temperature.

f. Decrease in the pitch and roll solenoid gating durations from 0.52 to 0.105 second.

g. Cutback of the Control Subsystem sun shades on Panels 2 and 5 to minimize sun shading of the SAD shaft sun sensors.

CONFIGURATION

The Nimbus II configuration and coordinate system definition is shown in Figure 3-1. Figures 3-2 and 3-3 show inboard profile views of the Control Subsystem housing and sensory ring. Spacecraft mass properties are summarized in Table 3-2.

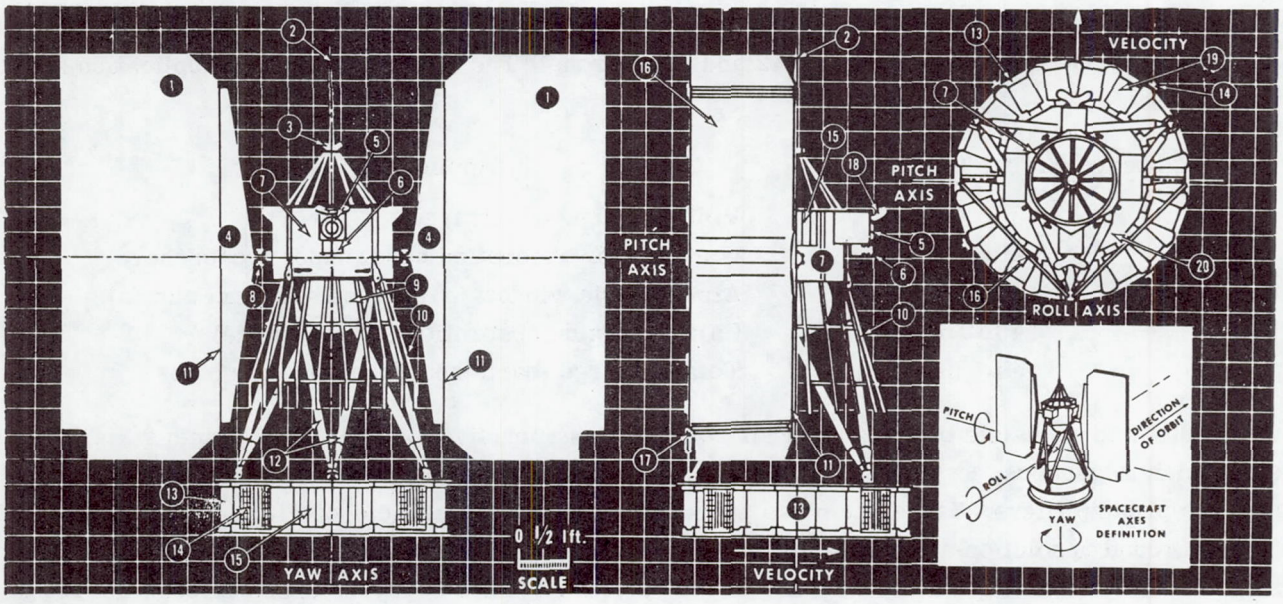

1. SOLAR PADDLE (extended) (2)
2. COMMAND ANTENNA
3. PITCH AND ROLL NOZZLES
4. TRANSITION SECTION (2)
5. HORIZON SCANNER (2)
6. YAW SUN SENSOR (2)
7. CONTROL SUBSYSTEM
8. PADDLE-POSITION SUN SENSOR (2)
9. PNEUMATIC TANK (freon)
10. COMMAND ANTENNA GROUND PLANE
11. SOLAR-PADDLE HINGE LINE
12. TRUSS STRUCTURE
13. PAYLOAD RING
14. BEACON/TELEMETRY ANTENNA (4)
15. THERMAL-CONTROL SHUTTERS
16. SOLAR PADDLE (folded) (2)
17. PADDLE-RELEASE MECHANISM
18. HORIZON-SCANNER SUN SHADE (2)
19. PAYLOAD RING COMPARTMENT (18)
20. YAW NOZZLES

WEIGHT BREAKDOWN (lb)

STRUCTURE	118.5	
THERMAL CONTROL	51.2	WITH FLIGHT ADAPTER
HARNESS	78.0	TOTAL WT. 984 LB
AVCS HRIR	130.2	
MRIR	35.9	
PCM	45.7	
CLOCK & COMMAND	33.0	
APT	30.5	
POWER SUPPLY	142.9	
ATTITUDE CONTROL	181.8	
SOLAR PADDLES	75.5	
TOTAL WT.	923.2	

Figure 3-1—Nimbus II spacecraft configuration.

FLIGHT HISTORY

Launch and Orbit Insertion

Following an uninterrupted terminal countdown, Nimbus II was launched from the Western Test Range (WTR) at Vandenberg AFB into a near-circular polar orbit at 00:55:34 PDT on May 15, 1966. The launch vehicle was a thrust-augmented Thor with an Agena B second stage. Figure 3-4 shows a launch sequence diagram, and Table 3-3 lists the launch sequence of events. Table 3-4 lists the initial orbital parameters.

Telemetry contact was maintained with the spacecraft throughout the launch and orbit insertion phase from Vandenberg AFB; Johannesburg, South Africa; Winkfield, England; and the Fairbanks, Alaska (Ulaska) tracking station. The spacecraft/booster separation and paddle-unfold was confirmed, and achievement of spacecraft stabilization to the earth reference

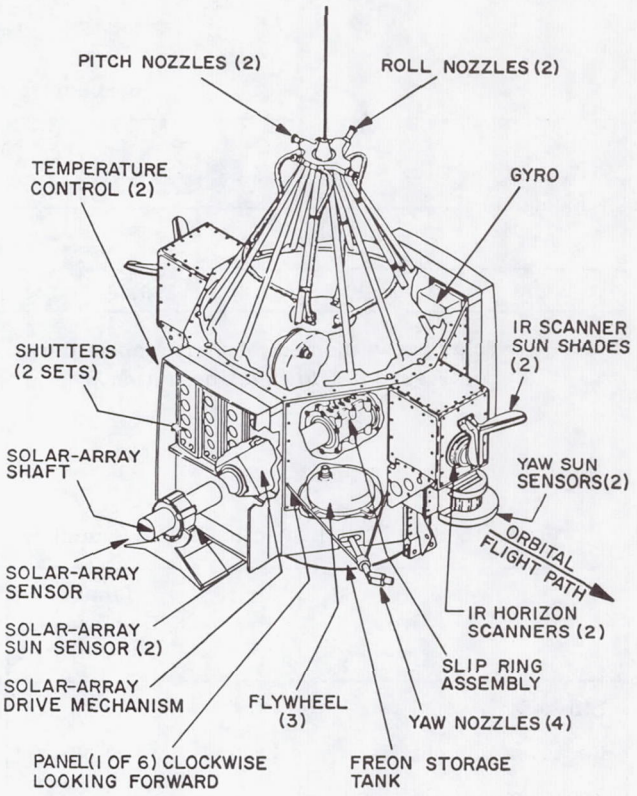

Figure 3-2—Nimbus II control subsystem housing (inboard profile).

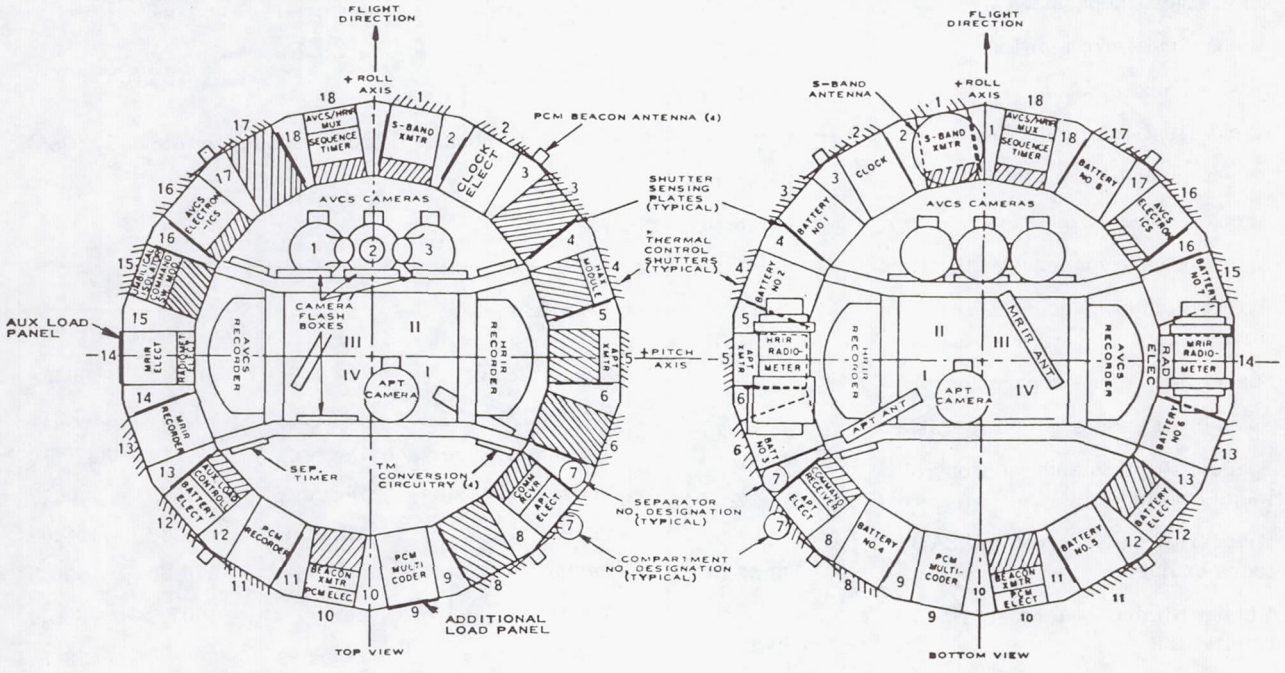

Figure 3-3—Nimbus II sensory ring (inboard profile).

Table 3-2

Spacecraft Mass Properties.

Weight (pounds)	CG (inches)			Moment of Inertia (slug-ft^2)			Product of Inertia (slug-ft^2)		
	X	Y	Z	I_{xx}	I_{yy}	I_{zz}	I_{xy}	I_{xy}	I_{zy}
915.9	+0.240	-0.425	196.26	241.0	209.0	105.0	+0.86	+0.45	+1.59

Note: (1) Solar array moment of inertia about drive shaft = 13.8 slug-ft^2.
(2) See Figure 3-1 for axes definition.

Table 3-3

Powered Flight and Orbit Injection Event Summary.

Event	Time of Occurrence (GMT)
Lift-off	07:55:34
Rocket motor cutoff	07:56:17
Rocket motor ejection	07:56:39
Meco	07:58:03
Veco	07:58:12
Thor/Agena separation	07:58:19
Agena first-burn ignition	07:58:47
Nose shroud ejection	07:58:57
Agena first-burn cutoff	08:02:43
Agena second-burn ignition	08:48:14
Agena second-burn cutoff	08:48:20
Agena pitchup maneuver initiation	08:51:11
Agena pitchup maneuver termination	08:52:31
Spacecraft/Agena separation	08:52:44
Spacecraft paddle unfold initiation	08:52:46
Spacecraft pitch and roll control loops enabled	08:52:57
Spacecraft yaw control and SAD loops enabled	08:53:37
Ulaska Nimbus beacon signal acquisition	09:23:34
Ulaska Nimbus beacon signal loss	09:42:34

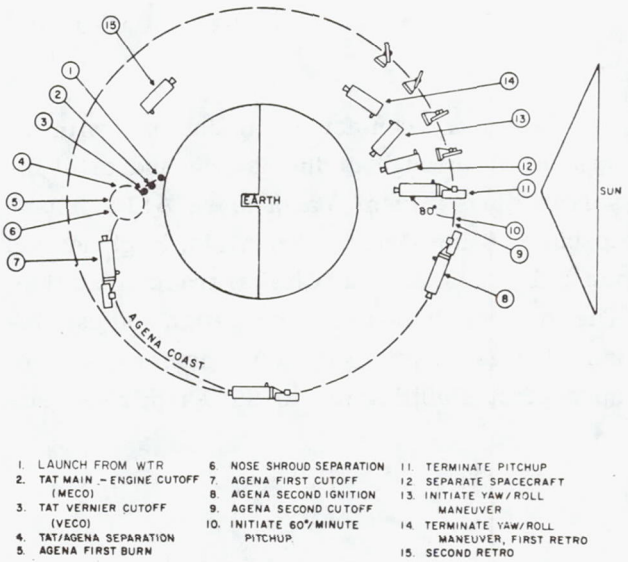

Figure 3-4—Nimbus II launch sequence (May 15, 1966).

Table 3-4

Initial Orbital Parameters.

Parameter	Units	Values*	
		Prelaunch	Actual
Eccentricity	-	0.00341	0.00558
Inclination	Degrees	99.957	100.311
Argument of perigee	Degrees	227.114	337.710
Nodal regression	Deg/day	0.9865	1.0017
Period	Minutes	107.28	108.06
Perigee	nm	579.80	590.5
Apogee	nm	607.3	636.0
Solar incidence	Degrees	-	9.74

*Source: NASA Tracking and Data Systems.

within 4 minutes was verified by real-time telemetry data received at Johannesburg. A clock-reset was performed during the first Ulaska station pass to correct the clock time upset which occurred during separation.

Initial Spacecraft Activation

The prelaunch plan adhered to in initially activating the Nimbus II spacecraft is shown in Table 3-5.

Table 3-5

Initial Activation of Nimbus II Spacecraft.

Orbit	Comment
1U	Confirmed initial Johannesburg report that spacecraft stabilization was proper. Performed power management based on the 14 amp array observed in telemetry. Reset the Clock to accurate time.
2U	Turned off the backup telemetry power supply. Performed power management based on actual array output of 13.6 amp (error in telemetry conversion circuit). Checked hot and cold memory locations in clock.
3U	Initiated S-band tracking. Played back prelaunch data stored on AVCS and HRIR tape recorders. Initiated the recording of HRIR data.
4U	Recorded short interval of MRIR and played it back. Playback of first HRIR recorded data achieved.
5R-5U	Obtained initial daytime DRIR pictures. Turned on APT. Disabled the yaw pneumatics.
6R-6U	Turned on AVCS Camera No. 3 and obtained pseudo-direct pictures at DAF at Rosman, N. Carolina.
7U	Turned on all AVCS cameras. Played back Camera No. 3 data.
8U	Played back AVCS data. Turned off all sensors. Established coast-through power management for blind period.
9U	Verified that power management was correct for blind orbits.

Significant Orbital Events

Significant Orbital Parameters

The 13-month (5275 orbits) histories of the significant orbital parameters are illustrated in Figure 3-5.

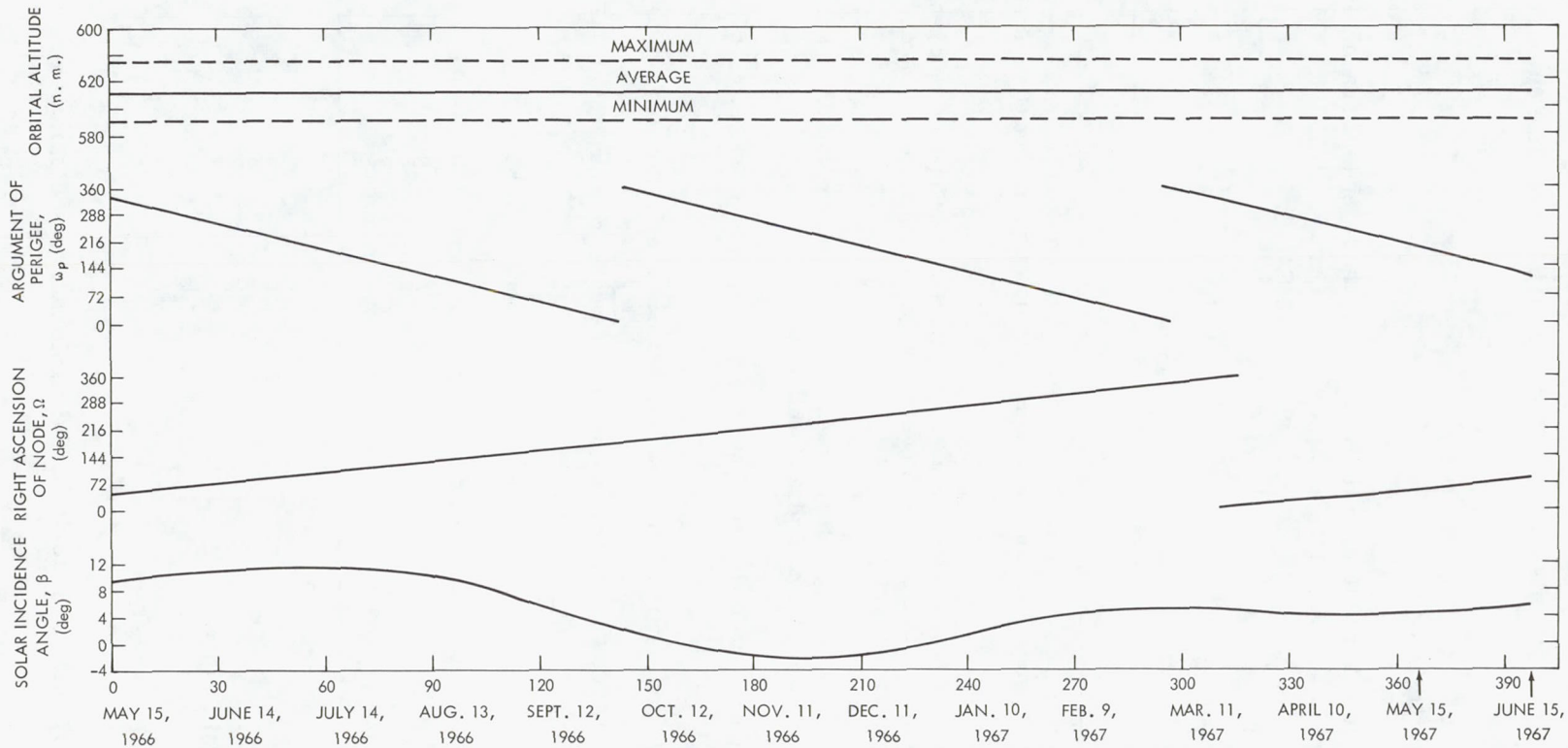

Figure 3-5—Significant Nimbus II orbital parameters in a 13-month flight (launch to June 15, 1967).

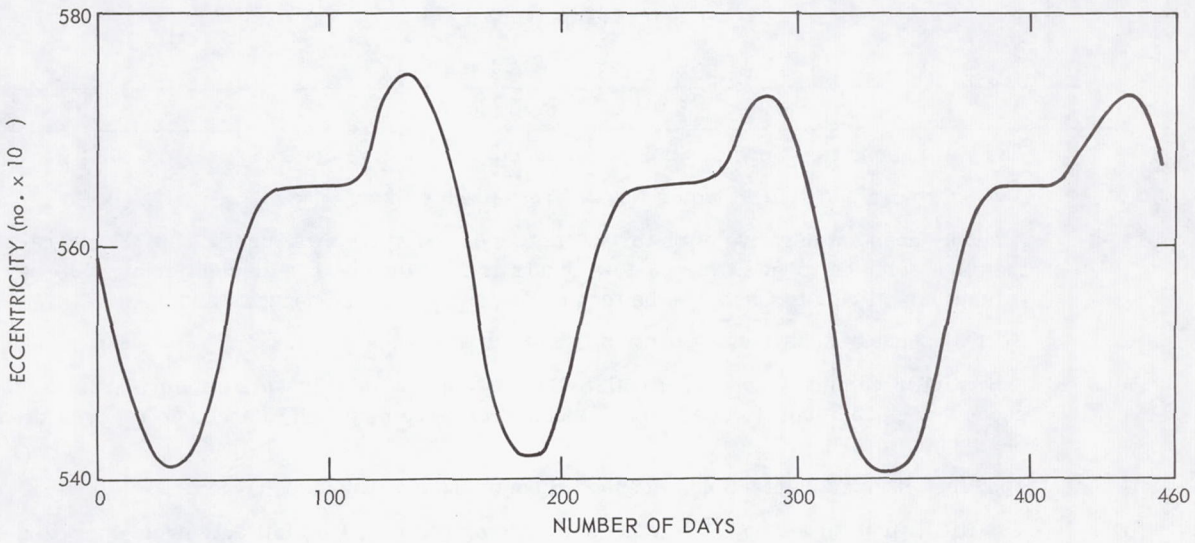

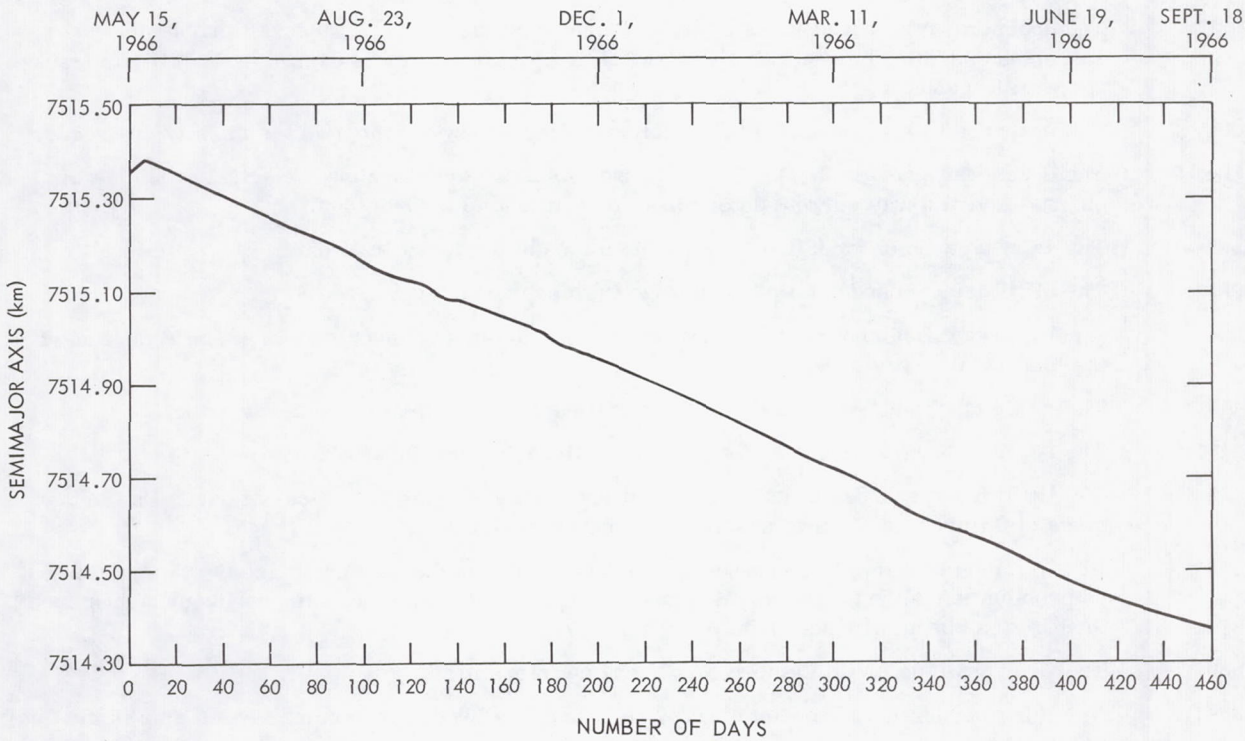

Figure 3-5 (continued)—Significant Nimbus II orbital parameters in a 13-month flight (launch to June 15, 1967).

Significant Flight Events

Flight events of significance are shown in Table 3-6.

Table 3-6

Significant Flight Events.

Orbit	Comment
5	The yaw pneumatics were disabled, as planned, to conserve control gas.
8U	AVCS Camera No. 1, IRIS Motor No. 2, first failed to drive.
13	A nearly constant negative pitch torque, acting on the spacecraft since Orbit 13, has caused the pitch solenoid to gate every 3-to-4 orbits at the satellite day-to-night or night-to-day transitions. Prior to Orbit 13, the torque alternated between negative and positive.
20U	Normal sensory subsystem operation first realized.
28U	A HAX OFF command occurring with S-Band ON during the Ulaska station pass caused the second clock time upset. Operational procedures were modified to preclude recurrence of the problem.
45U	The first of many unintentional unencoded command executions occurred.
48U	The HRIR first turned on for full day and night operation. This full duty cycle operation continued until Orbit 170. This mode of operation caused the subsystem temperatures to exceed the upper specified operating temperature limits without deliterious effect on the equipment or data.
53U	The spacecraft was not contacted during a planned station pass. Spacecraft problems were suspected and PCM Beacon No. 1 was switched ON. Problem was caused by inability to track spacecraft manually.
68U	The spacecraft experienced a partial eclipse of the sun by the moon in the vicinity of Greece.
788–804	The spacecraft put into the APT "coast-through" mode to determine the actual array power output. Actual array current determined to be 12.6 amp in Orbit 800.
949	The PCM tape recorder failed resulting in a loss of A-stored PCM data.
985	The MRIR tape recorder failed resulting in a loss of MRIR data.
1066	A solar array paddleboard (Board M) failed resulting in an approximate 0.6 amp reduction of the total solar array output.
1443	The AVCS tape recorder failed resulting in the loss of the total solar array output.
2413	The spacecraft experienced a partial solar eclipse over South America.
2455	The HRIR tape recorder failed in the playback mode resulting in the loss of data. Due to the mode of failure, the HAX Subsystem was no longer operable.
3293	PCM Transmitter No. 2 was turned on due to an error in the command tape but this presented no problem since the quality of the signal from this transmitter was as good as at launch even though it had been off since Orbit 53 (8 months).
3520	The Grey Scale on AVCS Camera No. 3 became intermittent.
4384	A failure occurred to the solar array resulting in a loss of approximately 0.6 amp in the total array output.
4784	The spacecraft experienced a partial solar eclipse near Alaska.
4862	Nimbus II completed one year in space thus demonstrating the capability of the Controls, Power, PCM, Command/Clock, APT, and AVCS* Subsystems.

*Pseudo–direct pictures only.

Orbit-Sun Relationships

Lift-off of Nimbus II occurred at 0755:34.857 GMT. The first northbound equator crossing approximately 63 minutes later occurred at 0858:39.72 GMT at longitude 37.44°E. The corresponding local mean time was 1128:25.32. Thus, the first ascending node occurred 0031:34.68 prior to local noon, and the orbit plane lay 7.89 degrees west of the mean apparent sun. (Because of the inclination of the earth axis and the eccentricity of its orbit, the apparent sun never coincides with the mean apparent sun). The seasonal variations shown in Figure 3-6 cover a range of +23.44 degrees in latitude, and as much as +4.12 to -3.58 degrees in longitude. On May 15, 1966, the position of the apparent sun (heavy dot) and time of launch were such as to make the orbit plane 9.74 degrees west of the apparent sun-earth line. The mean precessional rate of the orbit plane (1.00171 degrees per day) exceeded the mean rotational rate of the earth about the sun (0.9856 degree per day); thus, the orbit plane approached the mean apparent sun at 0.0161 degree per day, or 0.483 degree per month. The relationship of the orbit plane to the apparent sun shown in Figure 3-6 is for mid-May and November 1966, and for mid-May 1967.

The sun angle did not exceed 11.6 degrees during the Nimbus II flight until August 1966. The orbit plane contained the apparent sun-earth line (sun angle 0) on two occasions—in October 1966 and again in late December 1966. Thus, the objective of an essentially high-noon sun synchronous orbit was achieved, and the desired spacecraft-sun relationship will be maintained for at least 2 years.

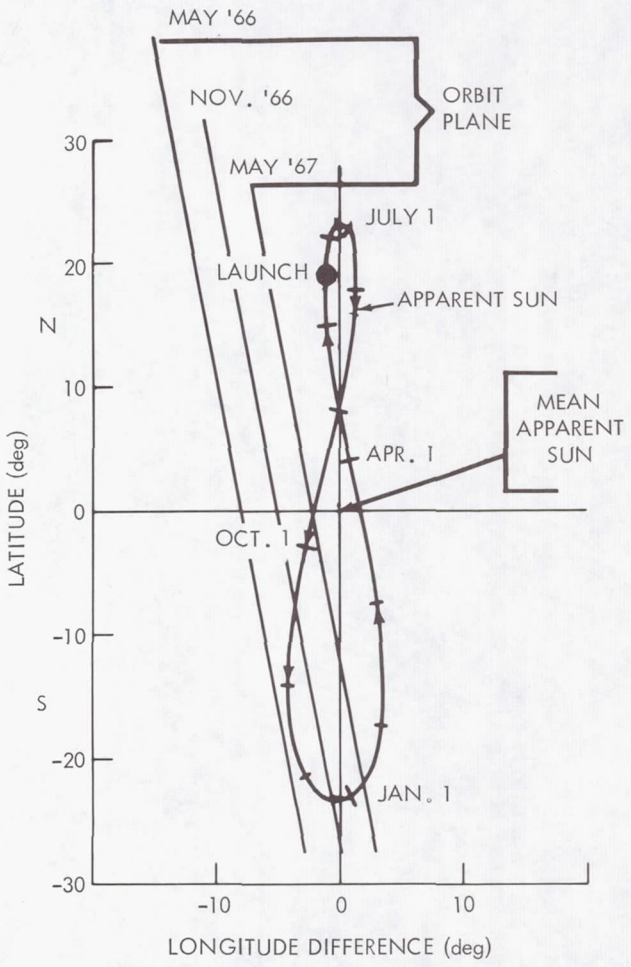

Figure 3-6—Projection of Nimbus II orbit plan in relation to sun.

Current Status

During the 31-day period of flight from May 15, 1967, to June 15, 1967, (orbit 4862 through orbit 5275), the Nimbus II spacecraft continued to perform well. There were no failures during this period.

SECTION 4

POWER SUBSYSTEM

FUNCTIONAL DESCRIPTION

The Nimbus II Solar Conversion Power Supply Subsystem (Figure 4-1) is a solid-state, electromechanical assembly that provides all of the electrical energy required to operate the satellite subsystems. Basically, this subsystem acquires incident solar radiation and changes it into electrical energy by photovoltaic conversion. The energy is stored electrochemically during the satellite day for use in supplying satellite night and peak daytime loads. Regulation of the electrical output provides a voltage level suitable for distribution to the spacecraft subsystems.

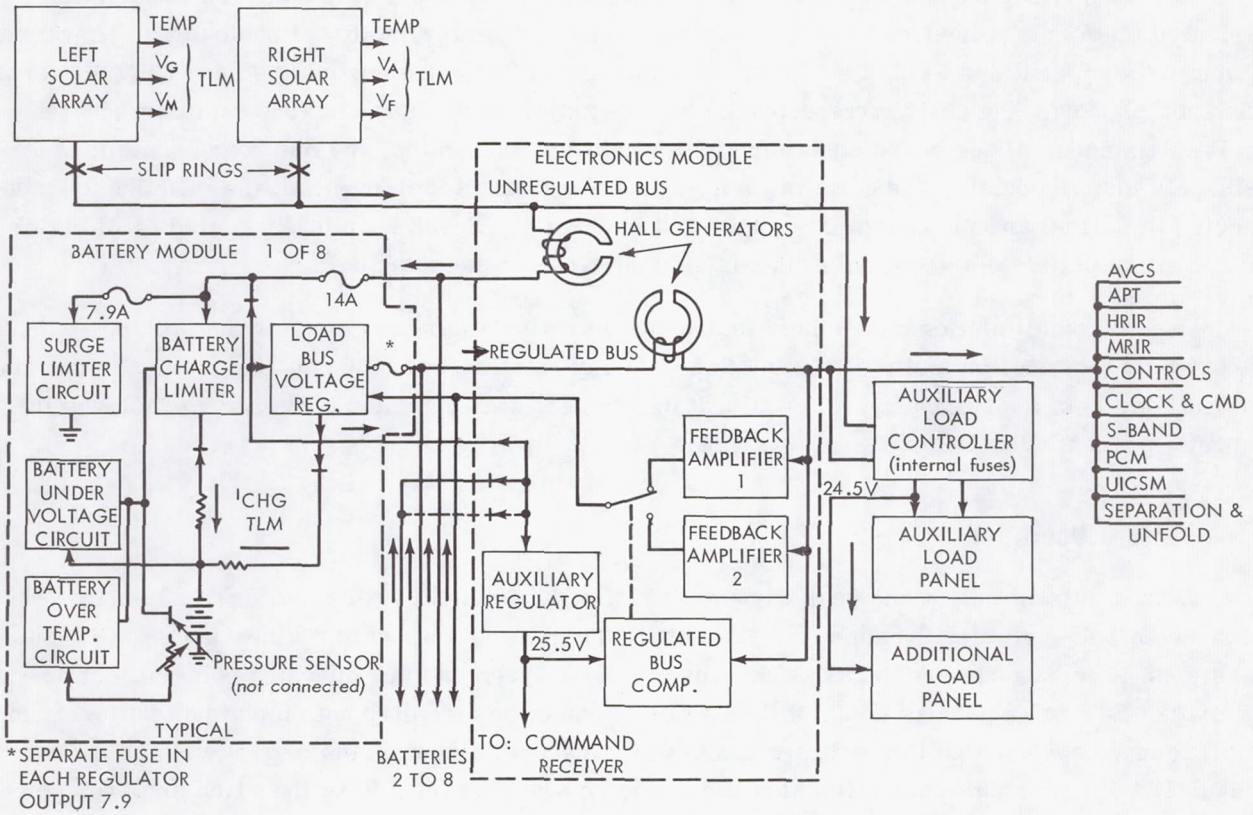

Figure 4-1—Power-supply subsystem block diagram.

Solar Acquisition

The spacecraft was launched in an 80-degree retrograde polar orbit that contains the earth-sun line. Acquisition of the sun was therefore simplified, requiring only one axis of rotation for the solar platform. The solar cells, mounted on one side of the two aluminum honeycomb platforms,

are continuously incident to the earth-sun line and, therefore, are able to intercept a maximum amount of solar energy during the satellite day period. Sun sensors circling the driveshaft of each platform detect solar radiation and are used to control the position of the platforms with respect to the sun-satellite line. A servomotor, located in the control housing, rotates the driveshaft to keep the sun sensor output nulled when the paddles are normal to the sun. With a 600-nm orbit, 73 minutes are spent in satellite day, and 35 minutes in satellite night. When the satellite enters the umbra, there is no output from the sun sensors; the paddles are then slewed at six times normal speed to a "night rest" position ready for acquisition of the sun (exit the umbra). During this slew period, the paddle drive motor is driven at voltage levels established by a potentiometer coupled to the paddle shaft.

Energy Conversion

During satellite day, an array of N-P junction silicon solar cells, mounted on two solar-oriented platforms, converts solar radiation to electrical energy, in direct photovoltaic conversion. Each platform contains 5472 solar cells, which cover the outside sun-facing skins of the platforms. On each platform, the cells are grouped on six boards with four of the boards containing 98 ten-cell solar modules, one board containing 97 ten-cell solar modules, and one board containing 97 six-cell solar modules. The cells in each module are connected in parallel, the modules are connected in series, and the boards are connected in parallel. Special, optically coated 6-mil-thick fused silica platelets are bonded to the outside surfaces of the solar cells.

The solar cell platform assembly intercepts an active solar energy equivalent to approximately 5800 watts (nominal intensity of 140 mw/cm^2) during satellite day. By considering the actual array output (day 1) of approximately 460 watts, it can be seen that the solar conversion efficiency is about 8 percent overall.

Battery Operation

During satellite night and peak daytime loads, eight identical battery packs of 23 series-connected 1.45-volt nickel-cadmium cells supply the power required to operate the satellite subsystems. The batteries are rated at 4.5 ampere-hours each and are operated nominally at approximately 8 to 12 percent depth of discharge. Protection circuitry puts individual batteries in trickle charge when high temperature limits are exceeded, and when the battery voltage is less than -19 volts. Circuit protection also limits the charge current to less than 1.65 amperes per battery. The battery electronics are adjusted so that the load-sharing of each battery should be 12.5 ± 2.5 percent.

Voltage Regulation and Distribution

The power supply subsystem provides a single power source of -24.5 vdc at ±2 percent regulation. An auxiliary voltage regulator provides -25.5 ± 1 vdc to the comparator circuit of the main voltage regulator. This provides a base level independent of regulated bus load. It also provides

power to portions of the clock receiver, thereby providing unencoded command capability independent of regulated bus voltage for switching feedback amplifiers in the voltage regulator.

FLIGHT OBJECTIVES AND SUMMARY OF OPERATION

The flight objectives of the Power Subsystem were to demonstrate the system capability to meet normal spacecraft regulated power demands for at least 6 months following orbit injection. The Power Subsystem has met requirements from launch through the period covered by this report.

The array output has been adequate to meet spacecraft operating requirements, which have decreased progressively as some of the sensory subsystems failed. There were two momentary losses of voltage regulation under similar circumstances observed during testing before launch. The battery performance has indicated no sign of degradation since launch, and charge-sharing has been maintained uniformly. Based on the battery voltage pattern and the limited data available, there is no sign of any decrease in the charge capacity. The batteries are being operated in an 8 to 13 percent depth-of-discharge duty cycle. There have been two solar array board failures observed, one of which was intermittent. The array degradation caused by charged particles followed a pattern predicted for the flux rate estimated for the Nimbus II orbit with an 18 percent loss at orbit 5200.

The initial solar array output was estimated to be 13.6 amperes at -34 vdc or 462 watts operating at an 8.3 percent efficiency, compared to a prediction of 7.9 percent. In the first 100 orbits, the output dropped to 13 amperes, and at orbit 200 to 12.7 amperes. Thereafter, the array output fluctuated with the seasonal sun intensity and beta angle variations, in addition to the loss caused by particle degradation and the sharp losses when the paddleboard cells failed. During orbit 1066, the array output decreased by 600 milliamperes because of a board failure, with another loss of 600 milliamperes occurring about orbit 4384. The latter failure was intermittent in that for most of the orbits following the failure, the 600-milliampere decrease did not occur until 10 to 25 minutes after the satellite reentered the sunlight portion of the umbra (implying a thermal effect). The array output at orbit 5275 was 9.85 amperes (8.3 amperes required for minimum spacecraft operation), permitting the APT and AVC subsystems to be operated full time.

POWER SYSTEM PERFORMANCE

Solar Array Performance

Because of subsystem failures, the solar array power output has been consistently higher than required to operate the spacecraft at maximum capacity during the various phases of operation. The initial array output was estimated to be 13.6 amperes at -34 vdc, or 462 watts, requiring a dissipation of 65 ampere-minutes per orbit with a fully operated spacecraft. The actual array output current has been difficult to determine. The unregulated bus current telemetry sensor has been unreliable, reading high during the early flight phase and then reading progressively lower.

The alternative method of computing the array output from the summation of spacecraft load currents and battery charge currents also is unreliable because of the uncertainty imposed on the regulated bus current value and battery charge currents by the controls gyro heater, as well as a possible changing error in the regulated bus current telemetry value. The 13.6-ampere output was determined by the charge management prediction technique which has been used throughout the life of the spacecraft. This technique is used to keep the batteries at their full charge state without overcharge by calculating the loads required to provide the correct battery recharge current based on prelaunch values of spacecraft subsystem load currents (some load currents checked in flight) and battery charge ratios. The accuracy of the array output used in this calculation is judged on the basis of the battery end-of-day and end-of-night terminal voltages as well as the temperature profile of the batteries. A plot of the solar array output, as determined by power management calculations, versus orbit number is shown in Figure 4-2 along with the response of the two solar cell experiments and the percentage of loss in array output caused by sun intensity, beta angle variations, and board failures.

For the estimated array output of 13.6 amperes at -34 vdc, the efficiency of the array was 8.3 percent, based on a net illumination at the paddles of 5590 watts because of seasonal intensity and beta angle at launch. This compares with 7.9 percent predicted before launch (Reference 1). At orbit 5275, the average array output was 9.85 amperes at -34 vdc, or 336 watts. With AVCS and APT operating full time during this phase of spacecraft operation, 25 ampere-minutes were dissipated in auxiliary loads.

During the early months of flight, the 9.75-degree solar incidence angle resulting from the spacecraft being launched early in the window (see Figure 4-2) caused the Controls Subsystem to shade a corner of one paddle before entering and after leaving the umbra. This caused a 1.4-ampere decrease in array output for 3 to 8 minutes.

The spacecraft passed through three solar eclipses that affected the solar array output. The array output dropped approximately 2 amperes during orbits 68 and 4784, and during orbit 2413 (Figures 4-3 and 4-4), the array output dropped to zero for approximately 80 seconds. Paddle temperature dropped 10°C, and the unregulated bus voltage dropped from 30.4 to 26.5 volts, although there was sufficient sunlight on the paddle shaft sun sensors to prevent the paddles from being driven to the nighttime rest position (see Figure 5-19).

Orbital profiles of typical array power output are shown in Figure 4-5 for an early orbit (51) and in Figure 4-6 for an orbit around 5300 (developed from real-time telemetry over a number of orbits). The humps at the beginning and end of the data represent the earth albedo inputs over the polar regions.

The unregulated bus voltage telemetry reading has consistently followed the paddle voltage. The difference has been 0.3 to 0.7 volt (0.3 volt/PCM count). This voltage drop, which includes the losses across blocking diodes, slip rings, harness, and connectors, was estimated to be 1.8 volts. An error in the unregulated bus voltage telemetry is suspected. The telemetry circuit does not have a separate return to the telemetry encoder, resulting in an encoder input that includes a

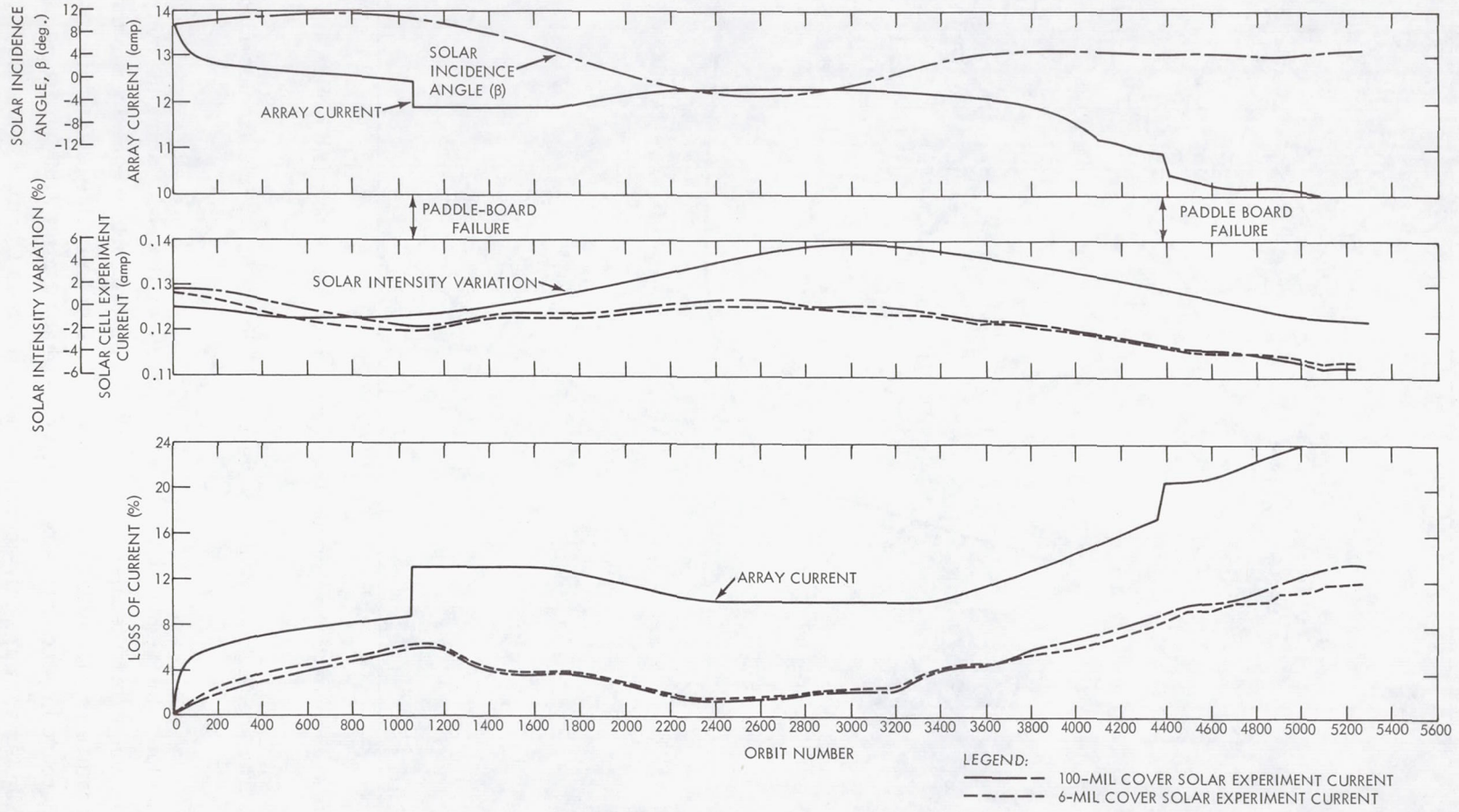

Figure 4-2—Array and solar-cell experiment current history.

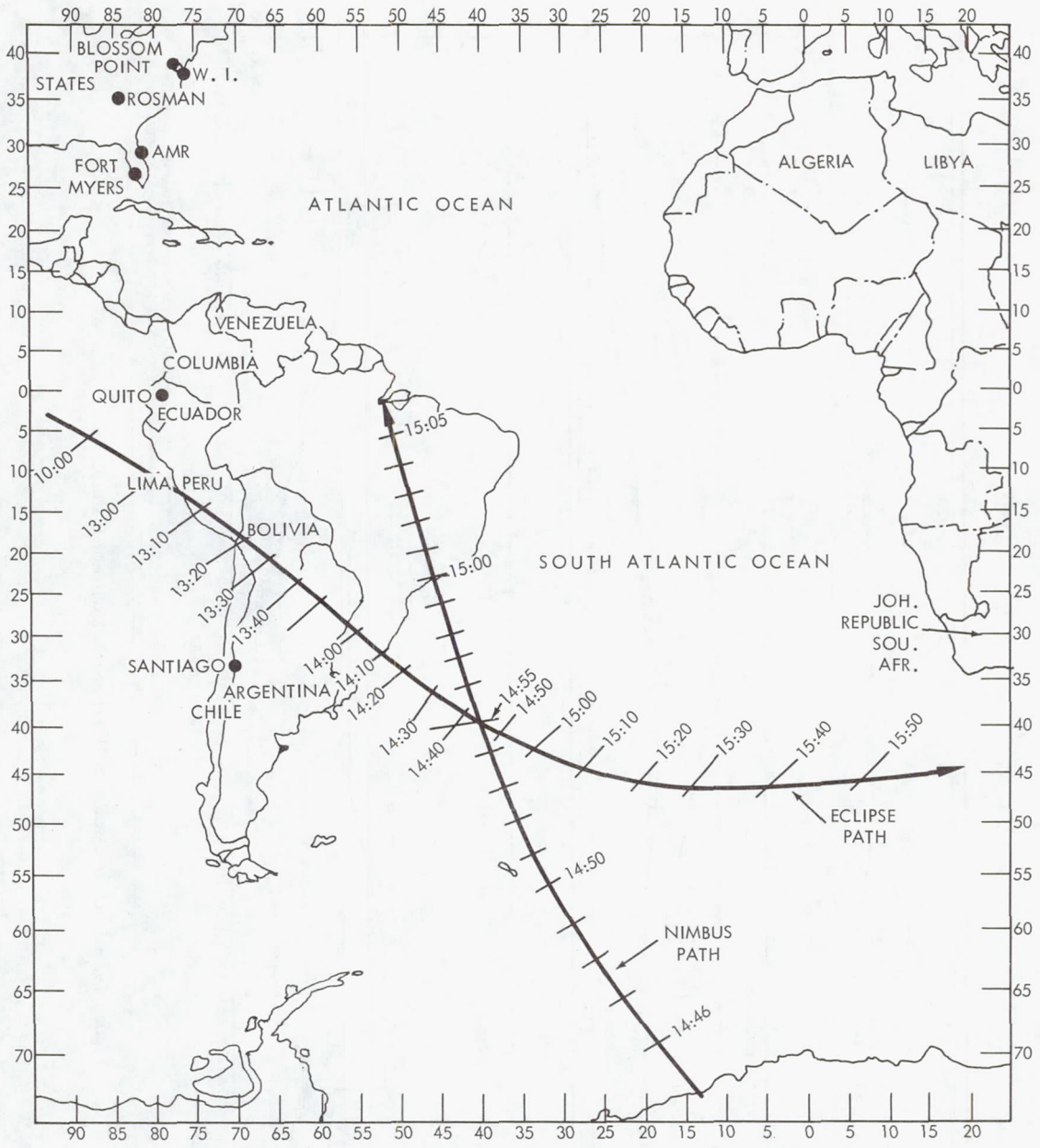

Figure 4-3—Intersection of Nimbus II orbit and path of solar eclipse (orbit 2413).

voltage drop caused by the high currents in the ground leads in the electronics module (Reference 2).

Figure 4-7 is a plot of the right-hand paddle (the paddle on the right facing the sun and in the velocity vector direction) orbital temperature profile for several orbits compared to the predicted values. The temperature remained relatively constant during the initial 1000 orbits and then increased with the increase in solar intensity, which peaked about orbit 3100 (6 percent higher). By orbit 4720, the paddle temperature only decreased a few degrees from the peak value at orbit 3100,

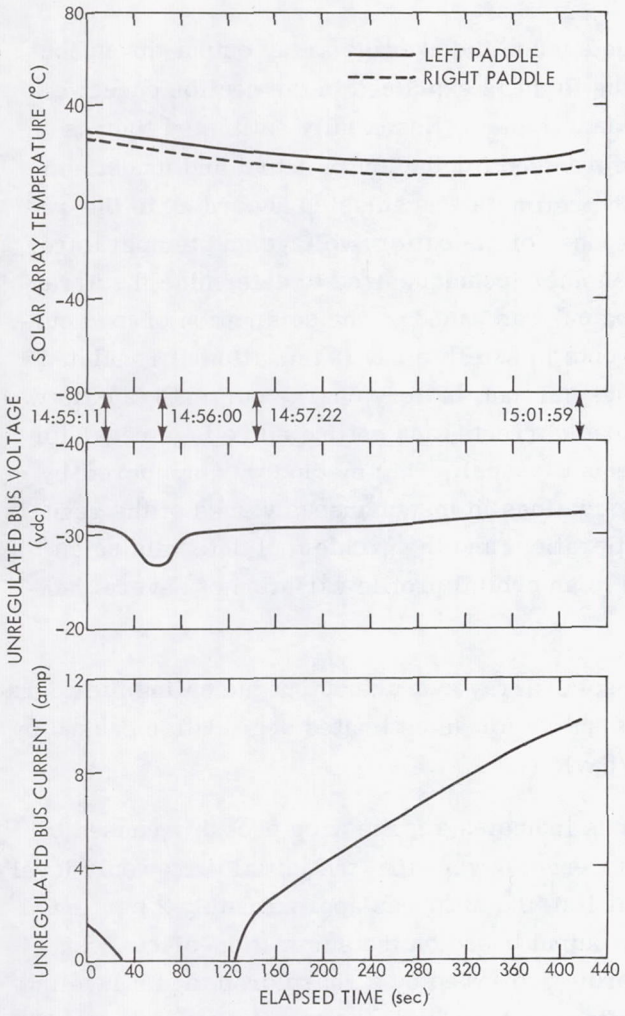

Figure 4-4—Solar-array power generation characteristics illustrating effects of solar eclipse.

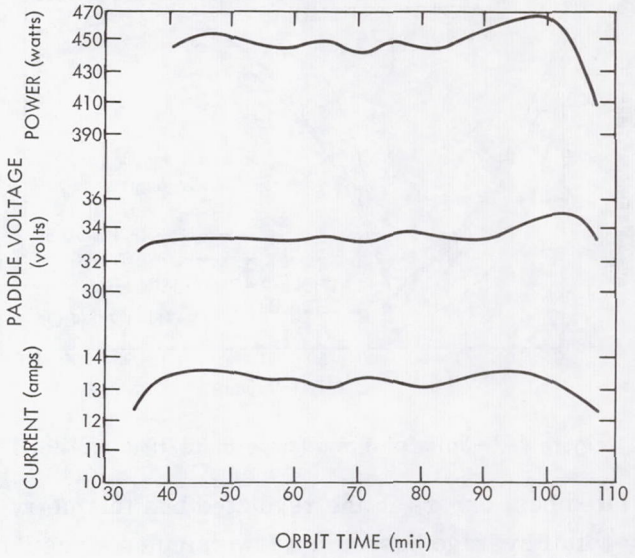

Figure 4-5—Typical profile of early orbit (orbit 51).

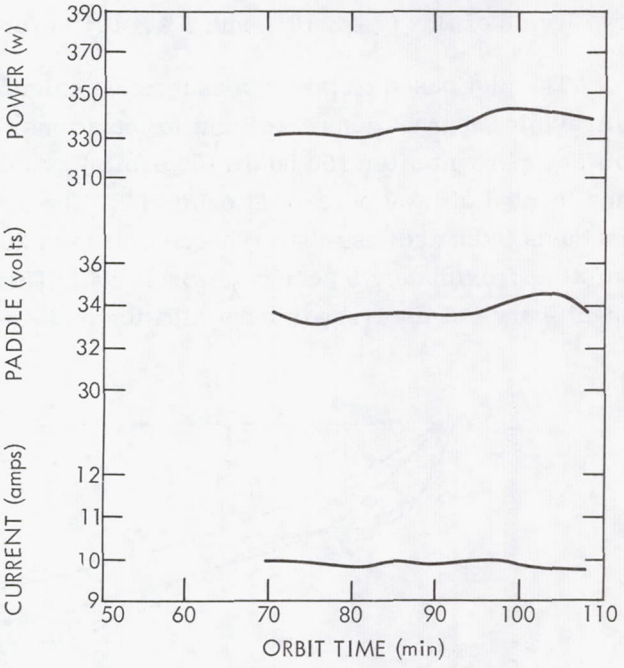

Figure 4-6—Data extracted from several orbits in the vicinity of orbit 5300 (APT and AVCS ON only).

with the same sun intensity at launch. The decrease in solar conversion efficiency (down approximately 18 percent since launch) and a coating degradation contributed to the higher temperatures. The left-hand paddle exhibited the same profile except that the maximum temperature indicated is 10°C lower. A telemetry error is suspected and will be discussed later.

Solar Array Degradation

The exact solar array output has been difficult to determine, primarily because the unregulated bus current telemetry point provided for this purpose has been unreliable. The technique used to

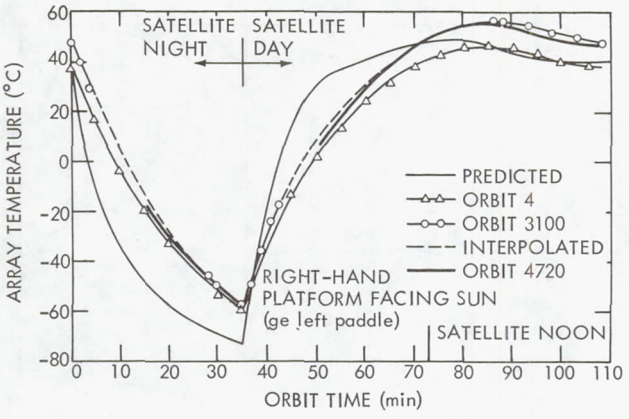

Figure 4-7—Solar platform temperature/time profile.

determine the average array output throughout the flight is explained in the section on Power Management. Essentially estimated figures were used for the array output and loads, and the estimate was adjusted according to the response of the battery voltage and temperature. Another technique used to determine the array output was based on the summation of load currents in satellite day (summation of regulated bus current, battery charge currents, auxiliary load currents, and estimated voltage regulator shunt losses). This method was hampered by variations in instantaneous values of the regulated bus, errors in the regulated bus telemetry calibration, and the problem of determining an orbital average based on a few samples since there is an orbital profile variation of several hundred milliamperes in the array output.

Figure 4-8 is a time history of the normalized solar array average output indicating the degradation of the array. The normalized array output is shown for an estimated degradation caused by two levels of flux (7.2×10^{11} and 9.4×10^{11} e/cm^2/day).

The plot based on power management calculations indicates a large drop probably caused by ultraviolet degradation. Preflight expectations (Reference 3) were that the initial drop would level off at 4 percent after 100 hours (60 orbits). At orbit 100, the drop was approximately 2 percent and leveled off at 6 percent at orbit 500. The array output based on the summation-of-current methods indicated less than 1-percent drop in 200 orbits, followed by a sharp drop, again leveling off at approximately 6 percent at orbit 500. Thereafter, both techniques show the same trend. The significance of the irregular degradation pattern is uncertain; it may be caused by errors in

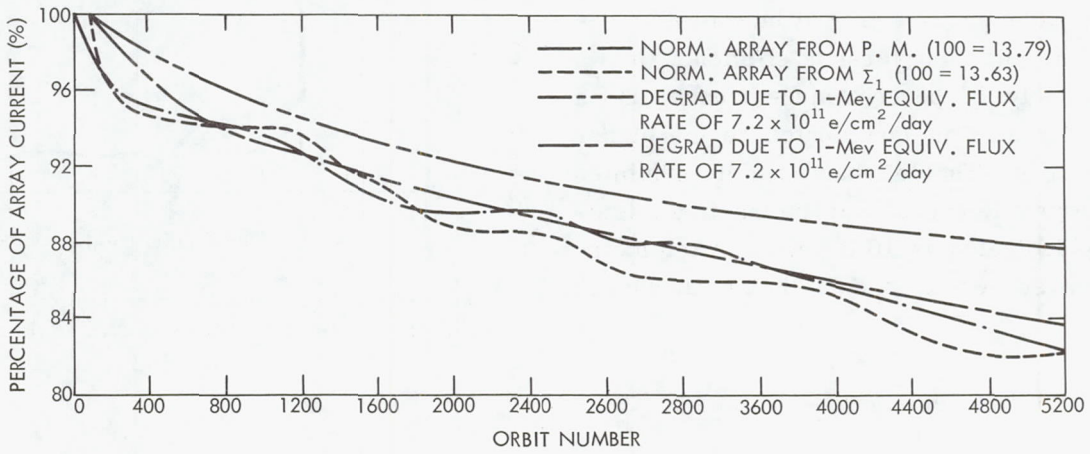

Figure 4-8—Degradation of normalized solar array.

determining average array output, or it may be caused by short-term, cyclic variations in the flux rate or errors in normalizing for the board failures after orbit 1000. Two fixed corrections were used during the orbit when the failures occurred, although telemetry data indicated that, after the second array board failure, some output was still obtained from the board for some portion of the orbit. The loss of the PCM tape recorder in orbit 949 made a quantitative understanding of this phenomenon very difficult. Any intermittent output would therefore make the normalized array output plot be irregular and show high points. Refer to the paragraphs under Solar Cell Experiment for a description of the degradation of the two solar cell experiments.

Solar Paddleboard Failure No. 1

Between orbits 1065 and 1070, the solar array output dropped from a level of 12.5 to 11.9 amperes. Spacecraft attitudes were verified to be normal, and the solar array drive was operating properly. Paddleboards M and L, located on the left-hand paddle (the paddle on the left side of the spacecraft when one is looking along the velocity vector) are normally shaded by the sensory ring (with a positive β angle) before entering and after leaving the umbra. This condition was verified by a distinct pattern of decreased solar array output at these points in the orbit.

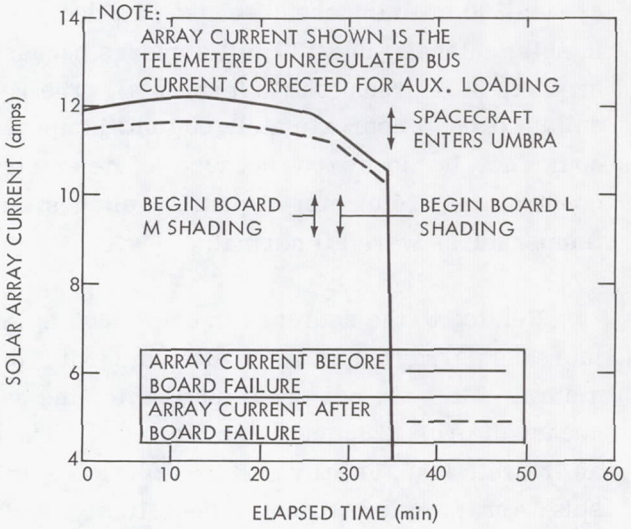

Figure 4-9—Shading effects on solar array output before and after paddleboard failure.

A comparison of the solar array current output trailoff (before entering the umbra) before and after the drop in total output is shown in Figure 4-9. From the figure it can be seen that the telemetered value of array current (after the board failure) averaged approximately 700-milliamperes lower before shading and approximately 0.2 amperes lower during maximum shading than it did before the failure. Assuming that all cells delivered the same amount of current, board L (with 980 cells) and board M (with 582 cells) would provide 1.04 amperes and 0.645 amperes, respectively, based on the telemetered array current value of 12.2 amperes (sensor reading plus auxiliary load losses). The decrease (approximately 600 milliamperes) compares favorably with the 645 milliamperes that would be provided by board M. From Figure 4-9 it is noted that, since the failure, shading does not affect the total output until approximately 5.5 minutes before entering the umbra, whereas before the failure it affected the output up to 3 minutes earlier. The reason for this is that board M, because of shading, is affected normally before board L (because of the manner in which the shading occurs; see Figure 4-10). Therefore, if board M has failed, the dropoff would be delayed (Figure 4-9).

The 200-milliampere difference during the period of maximum shading may be attributed to telemetry resolution of the unregulated bus sensor, which is approximately ±150 milliamperes in the 10- to 12-ampere range. No voltage telemetry is available on either board M or board L; voltage telemetry on boards A, F, G, and J was normal.

Solar Paddleboard Failure No. 2

The solar array output decreased by approximately 600 milliamperes between orbits 4384 and 4386. Figure 4-11 is a plot of the unregulated bus current before and after the decrease. The array output dropped approximately 1.00 ampere between orbits 4000 and 4700. During this interval, the output was expected to decrease 300 milliamperes because of a decrease in solar intensity and 100 milliamperes because of particle degradation (Reference 4). The resultant drop of approximately 600 milliamperes could not be localized because of telemetry constraints. Telemetered paddle voltages and temperatures were all normal.

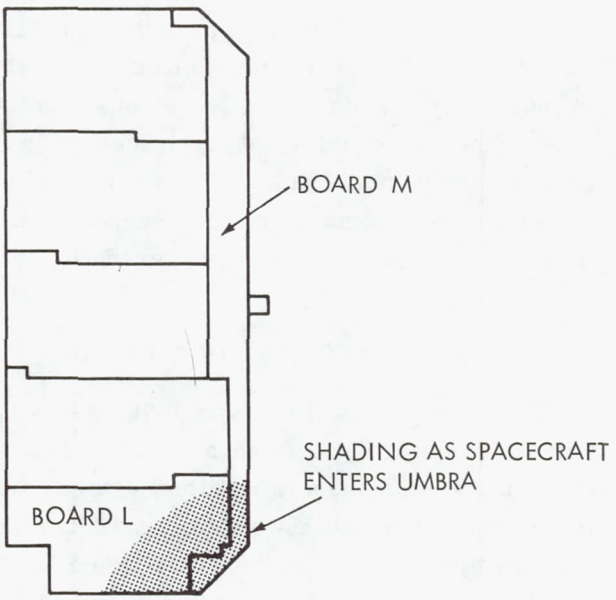

Figure 4-10—Shading of spacecraft left array (orbit 212U) during transition from satellite day to night.

Related to the decrease in orbit 4386 is the increased array output noted after the exit from umbra. This did not occur until after the decrease of orbit 4385 and is still present. The drop (Figure 4-12) to the normal value, established after orbit 4385, usually occurred: (1) with paddle temperature between 7°C and 23°C; (2) with solar array shaft position between 10 and 30 degrees; and (3) with the spacecraft within ±10 minutes of the earth night-to-day transition. The initial magnitude of the increase was approximately 600 milliamperes (orbit 4443) and is presently approximately 490 milliamperes (orbit 5275). Examination of available telemetry has revealed no additional information. The most probable cause is thermal cycling of the associated panel board failure in orbit 4385.

Power Storage

The battery system has performed extremely well, with no failures of any kind observed and no sign of degradation indicated. The batteries were operated at depth-of-discharge levels ranging from 12.5 percent during the early phases to 8 percent when only APT and AVCS were in operation. Figure 4-13 represents the approximate depth-of-discharge history. There were occasional fluctuations from the various plateaus shown of ±0.5 percent caused by programming sensor operation rather than operating them continuously (which was normal). Adjustments in the power management of the batteries were generally accomplished with auxiliary loads that operated directly from the unregulated bus, thus not affecting the depth of discharge of the batteries. There were no occasions during this reporting period when the spacecraft had to be placed in a minimum load configuration; therefore, there was never any severe overcharging of the batteries. The nominal charge ratio recommended by the battery supplier for +25°C was used throughout: a charge/discharge ratio of 1.1 for the first 430 ampere-minutes below full charge and a 1.0 ratio beyond that.

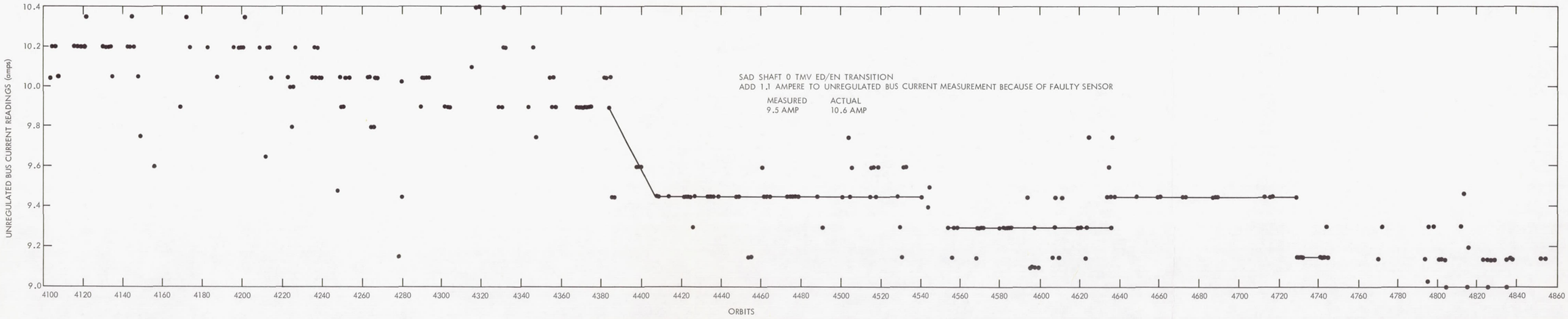

Figure 4-11—Unregulated bus history during second paddleboard failure.

Page Intentionally Left Blank

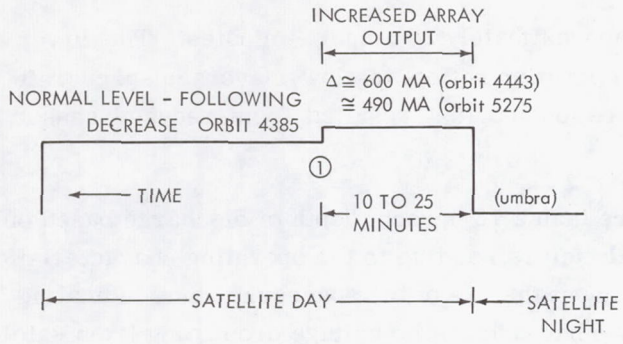

Figure 4-12—Increased array output following transition from satellite night to satellite day.

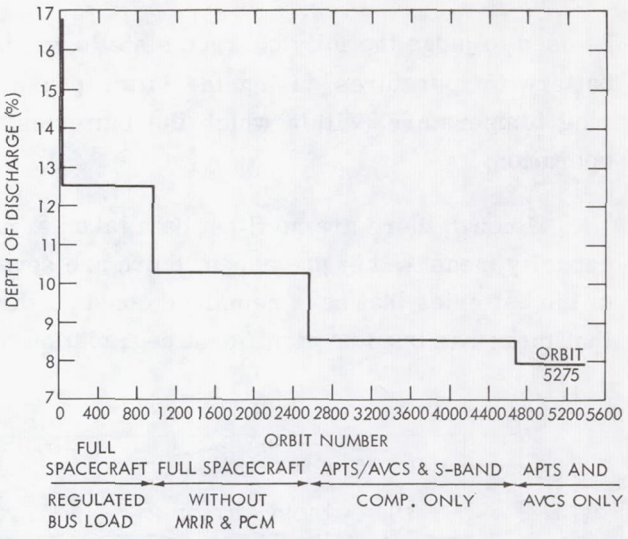

Figure 4-13—Approximate depth-of-discharge history.

Figure 4-14 is a history plot of the system operating characteristics (average of eight batteries). The lower end-of-charge terminal voltages during the first 1000 orbits reflect the operational plan to maintain the charge state 50 to 100 ampere-minutes below full charge. After the loss of the PCM tape recorder, the power management plan was changed to recharge the batteries to their full charge state at the end of satellite day. The battery end-of-charge voltages and temperatures were sensitive enough parameters to

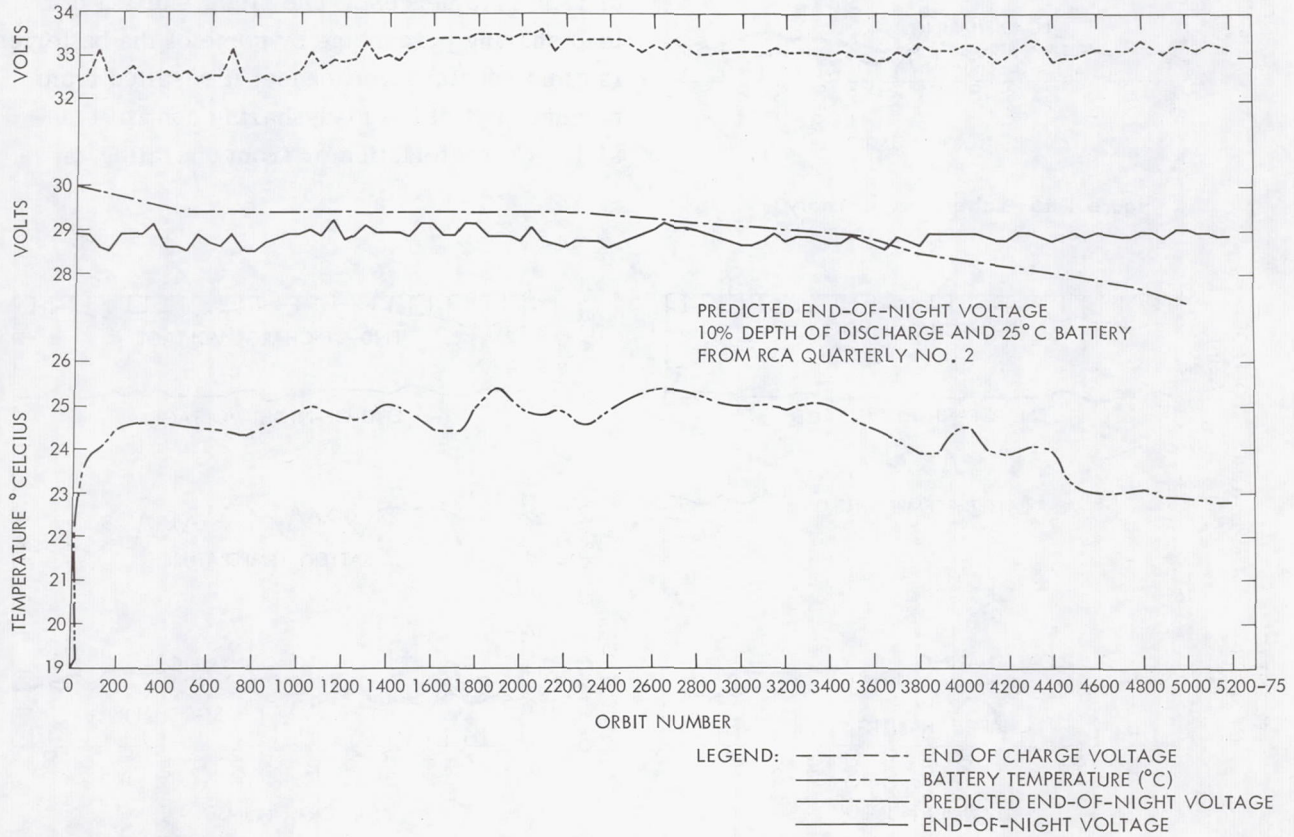

Figure 4-14—Battery system history.

be used to judge the fully charged state to within approximately 20 ampere-minutes. The lower battery temperatures during the latter phase of operation reflect the lower average spacecraft ring temperature (within which the batteries were located that resulted from reduced sensor operation.

Although there are no flight data taken at more than a 13 percent depth of discharge based on capacity measured at prelaunch, there are several factors relating to the operating characteristics of the batteries that have remained constant throughout the life of the spacecraft, thus indicating that there has been no significant degradation of the batteries. The voltage drop going from satellite day to night has remained constant at 1.2 to 1.8 volts. The battery voltage-versus-discharge profile has remained essentially constant as has the temperature orbital profile. The system charge ratio has not changed nor have the individual battery charge ratios.

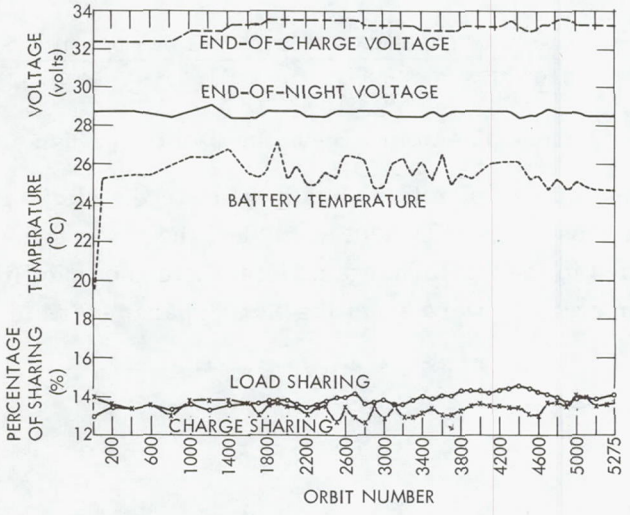

Figure 4-15—Battery no. 1 history.

The operating parameters of the individual batteries are listed in Table 4-1 and plotted in Figures 4-15 through 4-22. Load sharing throughout the flight was within the design specification of 12.5 ± 2.5 percent. The slight shifting of the load sharing percentage by some of the batteries is of no special significance; it resulted from normal drift of the load-sharing control transistor characteristics or from operating on

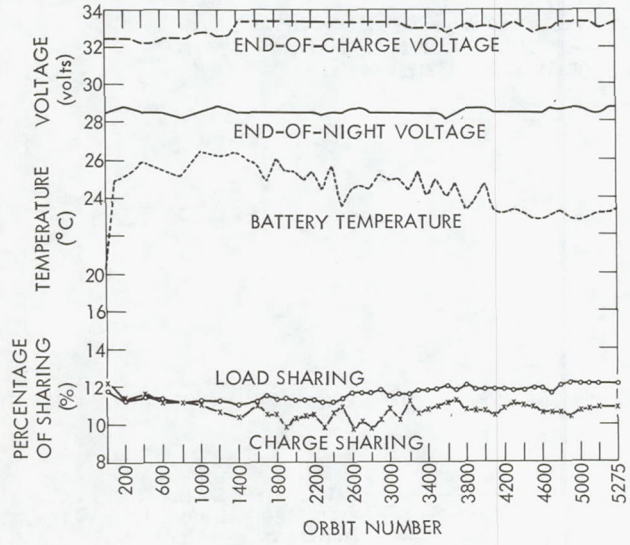

Figure 4-16—Battery no. 2 history.

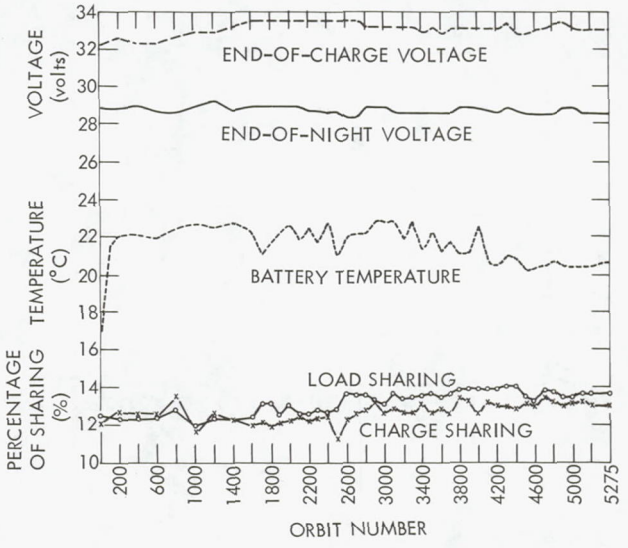

Figure 4-17—Battery no. 3 history.

Table 4-1

Battery Performance Summary.

Battery No.	Parameter	Orbit Number														
		2	200	400	600	800	1000	1200	1400	1600	1700	1800	1900	2000	2100	2200
1	% load sharing	13.0	13.5	13.4	13.6	13.3	13.7	13.4	13.6	13.6	13.8	13.9	13.8	13.9	13.6	13.5
	% charge sharing	14.0	13.5	13.4	13.6	13.2	13.7	13.8	13.9	13.7	13.1	13.8	13.9	13.6	13.5	13.1
	Temperature (°C)	19.7	25.4	25.5	25.5	23.3	26.4	26.4	26.9	25.6	25.3	25.8	27.2	25.2	25.9	25.0
2	% load sharing	13.9	13.4	13.6	13.4	13.3	13.4	13.4	13.2	13.3	13.7	13.4	13.5	13.4	13.4	13.4
	% charge sharing	14.3	13.4	13.6	13.3	13.4	13.2	12.8	12.5	13.3	12.7	12.7	12.0	12.5	12.6	12.7
	Temperature (°C)	20.7	25.2	25.9	25.5	24.4	26.5	26.3	26.5	25.9	24.9	26.2	25.5	25.5	25.0	25.5
3	% load sharing	12.6	12.5	12.5	12.5	13.0	12.1	12.5	12.4	12.5	13.2	13.3	12.6	13.1	12.7	12.7
	% charge sharing	12.2	12.6	12.5	12.6	13.5	11.7	12.5	12.4	12.1	12.3	12.0	12.2	12.3	12.6	12.3
	Temperature (°C)	17.3	22.2	22.2	22.0	24.5	22.8	22.6	22.9	22.4	21.2	21.8	22.4	22.8	21.9	22.6
4	% load sharing	11.2	11.2	11.5	11.5	12.0	11.9	11.9	11.7	11.8	11.5	11.5	11.9	11.7	12.0	12.0
	% charge sharing	9.9	11.1	11.5	11.5	11.9	11.8	11.6	11.6	11.7	12.0	11.0	12.0	11.9	12.0	12.0
	Temperature (°C)	21.5	26.5	26.4	26.1	26.8	26.5	25.9	26.5	26.6	25.6	27.7	27.0	27.8	27.2	28.1
5	% load sharing	10.6	11.2	11.3	11.3	11.5	11.4	11.0	11.2	11.0	10.8	10.5	10.9	10.6	11.0	10.9
	% charge sharing	10.7	11.3	11.3	11.2	11.4	11.0	11.0	10.7	11.3	11.3	11.0	11.0	10.9	11.2	11.8
	Temperature (°C)	18.1	24.0	23.4	23.0	21.6	23.3	21.8	22.4	23.4	21.8	24.3	22.8	24.3	22.6	24.3
6	% load sharing	12.5	12.4	12.2	12.2	12.0	12.1	12.0	11.9	12.3	12.3	12.4	12.1	12.2	12.2	12.2
	% charge sharing	13.3	12.9	12.5	12.5	12.1	12.1	12.5	12.8	12.9	12.9	12.8	12.9	12.9	12.8	12.7
	Temperature (°C)	18.6	25.3	24.4	24.2	21.2	24.6	23.7	24.3	23.8	23.3	24.5	25.4	24.9	24.4	24.6
7	% load sharing	12.1	12.2	12.2	12.3	12.0	12.8	12.5	12.7	12.6	12.3	12.4	12.6	12.5	12.7	12.7
	% charge sharing	11.9	12.2	12.2	12.4	11.9	13.0	13.1	13.4	12.5	13.0	12.8	13.7	13.4	13.0	13.2
	Temperature (°C)	17.2	24.2	24.0	24.2	20.0	25.3	25.4	26.0	23.8	23.8	24.1	27.5	25.5	25.5	25.5
8	% load sharing	13.8	13.4	13.2	13.0	12.8	12.9	13.2	13.1	12.8	12.5	12.6	12.6	12.5	12.5	12.7
	% charge sharing	13.8	12.9	13.0	13.0	12.5	13.2	12.8	12.8	12.5	12.8	12.6	12.2	12.5	12.2	12.0
	Temperature (°C)	19.5	24.4	24.8	24.6	22.5	25.2	25.1	25.4	24.5	24.7	24.6	25.4	23.5	24.9	23.7

Table 4-1

Battery Performance Summary (Continued).

Battery No.	Parameter	Orbit Number														
		2300	2400	2500	2600	2700	2800	2900	3000	3100	3200	3300	3400	3500	3600	3700
1	% load sharing	13.7	13.8	14.0	14.0	14.3	13.7	13.8	13.9	13.7	13.7	13.9	14.1	14.0	14.1	14.1
	% charge sharing	13.5	13.6	12.8	13.5	13.0	12.8	13.6	12.9	13.7	13.0	13.0	13.3	13.5	13.2	13.1
	Temperature (°C)	25.0	25.6	25.3	26.5	26.5	26.2	24.8	24.8	25.1	26.4	25.4	26.3	25.2	26.6	24.9
2	% load sharing	13.3	13.3	13.5	13.8	13.7	13.7	14.0	13.6	13.7	13.7	13.9	13.9	14.0	14.1	14.0
	% charge sharing	12.0	12.8	13.1	11.9	12.3	11.9	12.4	13.1	12.4	13.6	12.7	12.9	13.0	13.2	13.3
	Temperature (°C)	24.5	25.9	23.5	24.6	24.7	24.5	25.4	25.0	25.1	24.4	25.6	24.1	25.1	24.1	24.9
3	% load sharing	12.9	12.7	12.9	13.8	13.7	13.7	13.4	13.2	13.7	13.5	13.5	13.6	13.7	13.6	13.8
	% charge sharing	12.4	12.6	11.6	12.4	12.7	12.9	13.3	12.8	13.0	12.8	12.8	13.2	12.8	13.0	12.8
	Temperature (°C)	21.8	23.2	21.0	22.2	22.3	22.3	23.0	22.9	23.0	22.0	23.1	21.4	22.5	21.2	22.0
4	% load sharing	12.2	12.0	12.0	11.7	11.4	12.0	11.7	12.0	11.8	11.5	11.6	11.5	11.5	11.3	11.1
	% charge sharing	12.3	12.4	12.6	12.2	12.4	11.5	11.9	13.4	12.1	12.5	11.9	11.8	12.2	12.2	12.2
	Temperature (°C)	27.2	28.8	26.9	27.9	27.9	28.0	29.0	28.5	28.3	27.2	28.0	26.4	26.8	25.6	26.2
5	% load sharing	10.8	10.9	10.5	10.0	10.0	10.2	10.0	10.3	10.2	10.2	10.1	10.0	10.0	10.0	9.9
	% charge sharing	11.4	11.0	10.8	11.3	11.2	11.2	11.5	11.2	10.9	11.1	11.5	11.0	10.6	10.7	10.4
	Temperature (°C)	23.2	24.8	23.6	24.1	24.0	23.5	25.0	24.3	24.2	23.1	24.3	22.4	23.6	21.6	23.2
6	% load sharing	12.4	12.1	12.4	12.2	12.3	12.9	11.7	12.0	11.8	12.1	12.1	12.1	12.1	12.2	12.4
	% charge sharing	12.8	12.6	12.6	13.4	12.6	12.6	12.0	12.5	12.2	12.5	11.9	12.9	13.0	12.0	12.8
	Temperature (°C)	24.7	25.5	25.6	26.3	26.1	25.6	25.0	24.7	24.8	25.0	24.5	24.4	24.3	24.2	24.3
7	% load sharing	12.4	12.7	12.6	12.8	13.1	12.9	13.2	13.0	12.9	12.9	13.0	13.1	13.1	13.2	13.2
	% charge sharing	13.5	12.6	12.2	13.5	13.6	12.0	13.2	12.6	13.5	12.8	13.5	13.1	13.0	13.2	13.3
	Temperature (°C)	24.8	26.4	26.8	27.6	27.4	27.4	25.6	25.6	25.8	26.7	25.9	26.1	25.5	26.5	25.2
8	% load sharing	12.4	12.5	12.0	11.7	11.6	11.8	11.7	11.6	11.8	11.9	11.9	11.8	11.7	11.8	11.8
	% charge sharing	12.3	12.4	12.3	11.9	12.1	12.1	11.8	11.8	12.2	11.7	12.8	11.9	11.9	12.5	12.2
	Temperature (°C)	24.3	24.2	23.2	24.3	24.3	24.2	23.1	23.3	23.5	24.3	23.8	24.3	23.7	24.7	23.4

Table 4-1

Battery Performance Summary (Continued).

Battery No.	Parameter	Orbit Number														
		3800	3900	4000	4100	4200	4300	4400	4500	4600	4700	4800	4900	5000	5100	5275
1	% load sharing	14.4	14.4	14.4	14.3	14.4	14.5	14.6	14.0	13.8	14.1	14.0	13.8	13.9	14.0	13.9
	% charge sharing	13.4	13.6	13.8	13.6	13.6	13.5	13.5	13.2	13.1	13.8	13.9	13.6	14.2	14.1	13.6
	Temperature (°C)	25.6	25.3	25.6	26.1	26.2	26.2	26.2	25.3	25.0	24.8	25.3	24.8	25.2	24.9	24.8
2	% load sharing	14.2	14.0	14.0	14.0	14.0	13.9	14.0	14.0	14.0	13.8	14.2	14.3	14.3	14.3	14.3
	% charge sharing	12.9	12.8	12.9	12.6	12.9	13.2	13.1	13.0	12.8	12.7	12.8	12.5	12.9	12.9	13.0
	Temperature (°C)	23.4	23.8	25.0	23.4	23.3	23.5	23.4	23.0	22.9	23.2	23.4	23.1	23.3	23.3	23.5
3	% load sharing	14.0	14.0	14.0	14.0	14.0	14.2	14.2	13.6	13.3	14.0	14.0	13.6	13.6	13.8	13.8
	% charge sharing	13.5	13.4	12.7	13.3	13.2	13.1	13.0	13.3	13.1	13.6	13.4	13.1	13.3	13.4	13.2
	Temperature (°C)	21.2	21.3	22.8	20.8	20.6	21.2	21.0	20.3	20.5	20.6	20.9	20.6	20.6	20.6	20.8
4	% load sharing	10.9	11.0	11.1	11.0	11.0	10.9	11.2	11.4	11.4	11.3	11.4	11.5	11.5	11.5	11.5
	% charge sharing	11.5	11.2	12.0	11.8	11.8	11.9	11.9	12.0	12.2	11.8	11.7	12.4	11.7	11.8	12.1
	Temperature (°C)	25.6	25.6	26.8	25.5	25.1	25.6	25.6	24.8	24.9	25.1	25.3	25.1	25.0	24.9	24.8
5	% load sharing	9.4	9.4	9.5	9.4	9.4	9.3	9.3	10.5	10.3	9.9	10.1	10.3	10.1	10.3	10.3
	% charge sharing	10.7	10.7	10.2	10.6	10.5	10.4	10.5	10.9	10.8	10.4	10.4	10.7	10.2	10.4	10.4
	Temperature (°C)	22.1	21.7	23.6	21.6	21.2	21.6	21.2	20.0	19.9	19.9	19.9	19.8	19.3	19.2	19.4
6	% load sharing	12.2	12.2	12.2	12.2	12.3	12.3	12.1	12.0	12.1	11.9	11.9	11.9	11.9	11.7	11.7
	% charge sharing	12.3	12.4	12.7	12.4	12.6	12.6	12.7	12.6	12.8	12.4	12.5	12.8	12.6	12.2	12.4
	Temperature (°C)	24.4	23.8	24.4	23.9	23.8	24.3	24.0	23.0	22.9	22.8	22.8	22.7	22.4	22.1	22.1
7	% load sharing	13.2	13.2	13.2	13.2	13.1	13.2	13.4	13.1	13.0	13.0	13.1	13.0	12.9	13.1	13.0
	% charge sharing	13.5	13.3	13.7	13.5	13.5	13.5	13.5	13.0	13.1	13.2	13.4	13.1	13.1	13.2	13.1
	Temperature (°C)	24.4	25.0	26.0	25.6	25.7	26.1	26.1	24.4	24.4	23.7	24.0	23.7	23.9	23.6	23.5
8	% load sharing	11.7	11.7	11.7	11.7	11.7	11.8	11.7	11.9	11.9	11.5	11.6	11.5	11.7	11.5	11.5
	% charge sharing	12.3	12.0	12.1	12.1	12.1	12.1	11.8	12.1	12.1	12.0	12.0	11.9	12.0	12.0	12.1
	Temperature (°C)	23.8	23.7	23.8	23.8	23.8	24.1	24.1	23.5	23.4	23.5	23.9	23.5	23.8	23.6	23.5

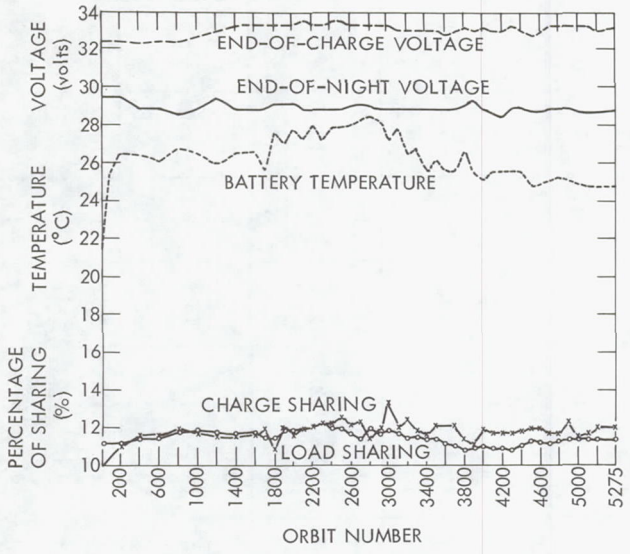

Figure 4-18—Battery no. 4 history.

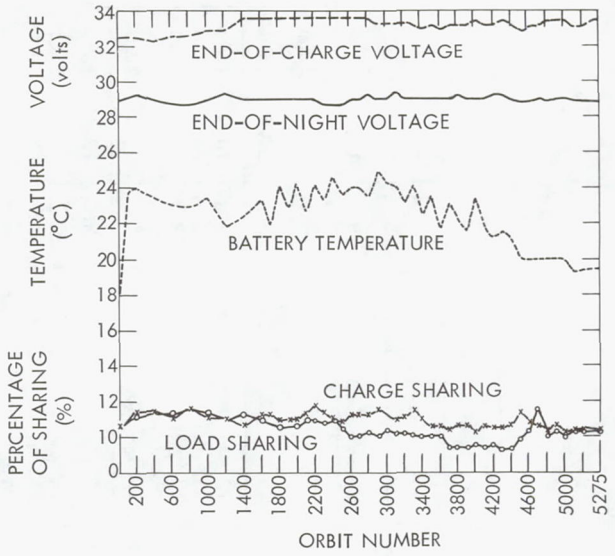

Figure 4-19—Battery no. 5 history.

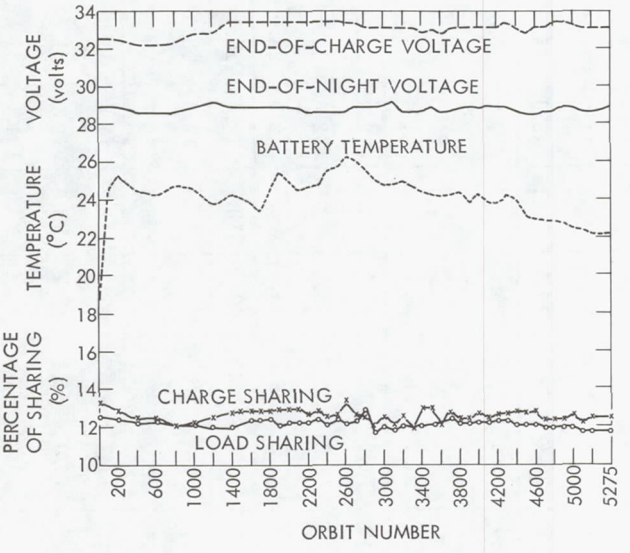

Figure 4-20—Battery no. 6 history.

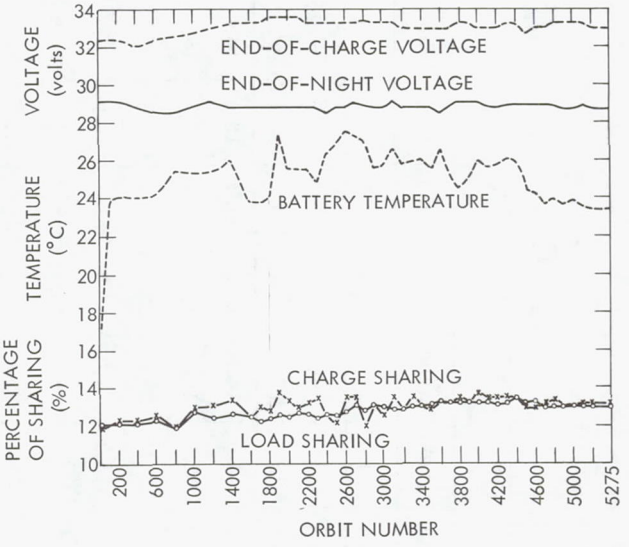

Figure 4-21—Battery no. 7 history.

different points of their characteristic curve because of changes in individual battery temperatures. Charge sharing generally was proportional to the load sharing, indicating that there were no cell failures. Because sharing is not controlled by active components but is generally established by the actual battery characteristics, a uniformity of characteristics is indicated.

Voltage Regulation

Except for two momentary losses in voltage regulation, there have been no malfunctions in this system. The first one, which was the most severe, resulted from a transient during the paddle-unfold sequence. This transient caused a clock upset, loss of a PCM word in the PCM bit stream, and the firing of the APT shutter (this may have been caused by a mechanical vibration). By manually decoding the PCM bit stream and beacon time code, it was determined that there were really two voltage transients spaced seconds apart. This loss of voltage regulation at paddle-unfold was also experienced during the test of the spacecraft before launch.

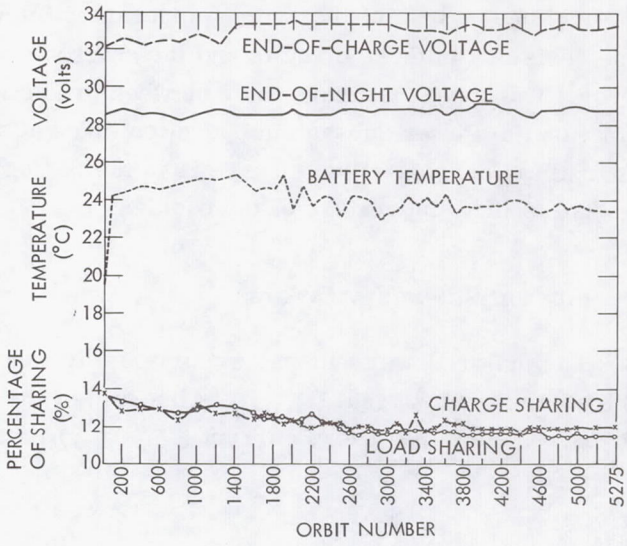

Figure 4-22—Battery no. 8 history.

The other out-of-regulation condition occurred during orbit 28 and resulted from a transient developed by turning the HAX (DRIR) off while the S-band transmitter was on. This transient caused a clock upset and a ringing current transient that appeared on the HRIR video for 0.4 second (see Figure 7-4). A clock upset occurred once in preflight testing when the HAX was commanded off with the S-band transmitter on. Operating procedures were established to avoid turning HAX off with the S-band transmitter on. However, the feedback amplifiers did not switch in either of the foregoing cases, indicating that the voltage transient may not have exceeded specification limits.

There were many instances in which the voltage regulation feedback amplifier switched because of spurious, unencoded command execution (refer to the Command Subsystem section). The switching between prime and redundant feedback is done either automatically or by unencoded command, but there is no way to identify directly which took place. Because there was an obvious unencoded command problem and many indications of spurious command-receiver input activity at the time of an amplifier switch as well as no clock upsets at the time of the switches (the clock has been a reliable transient indication on the spacecraft), it is assumed that no automatic switching of the feedback amplifier occurred. All of the switches occurred in a few zones around the world. There were no switches observed over South America whenever the STADAN stations squelched the spacecraft receiver with the command carrier signal, although this was ordinarily a high occurrence area. During the period when continuous telemetry was available, approximately nine switchings per 100 orbits were observed with no noticeable adverse effect on the regulation system.

Telemetry Sensor Errors

Solar Array Temperature Error

The high temperature of the right-hand paddle has consistently been approximately 10°C colder than the left-hand paddle. This difference in platform temperatures is probably caused by constant

error in one or both of the array temperature telemetry circuits. The use of carbon composition-type resistors in these circuits and the environmental effects on them may be the cause of the error. The apparent discrepancy between predicted and measured array temperature has little effect on the Power Subsystem operation since at all times the voltage operating region on the solar array current-voltage curve is in the region of relatively constant current output and independent of the temperature of the paddles.

Current Telemetry Errors

The major Power Subsystem currents are shown in the simplified block diagram in Figure 4-23. The solar array current (I_{array}) is the sum of the output currents of the left and right solar platforms. The auxiliary load current ($I_{aux.\ load}$) is the sum of the currents in each of the three resistive ground commandable loads, which are between the solar array bus and ground. The battery current (I_{batt}) is the sum of the eight individual battery currents (either charge or discharge). The shunt loss current ($I_{shunt\ loss}$) is the total current existing in the various resistive paths to ground in the Power Subsystem. The -24.5 volt regulated bus current (I_{reg}) is the total load current supplied external to the power subsystems. From Figure 4-23, the following system current relationship may be written:

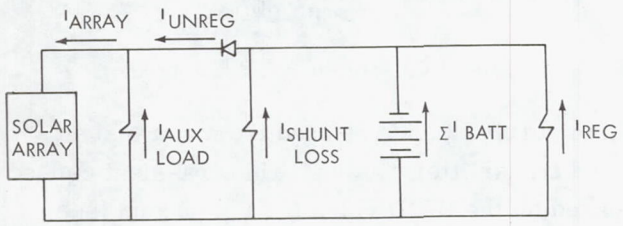

Figure 4-23—Simplified block diagram of power subsystem currents.

$$I_{reg} = I_{batt\ dischg} - I_{shunt\ loss} \text{ (satellite night)}$$

$$I_{unreg} = I_{shunt} + I_{batt\ chg} + I_{reg} \text{ (satellite day)}$$

$$I_{array} = I_{unreg} + I_{aux\ load} \text{ (satellite day).}$$

From the first equation, the regulated bus current error was determined to be zero below 5.5 amperes, gradually increasing to 150 to 200 milliamperes at 7.0 amperes. At 9.4 amperes on the regulated bus, the regulated bus current indicated high by 300 milliamperes. The unregulated bus current telemetry error was determined by the same summation of system currents with satellite daytime telemetry data. The resulting unregulated bus current error is a function of time in orbit. In the initial 200 orbits, the unregulated bus current error decayed almost exponentially from a positive 0.900 milliampere to a 0-ampere error. The decay continued in the same manner up to orbit 800. At this point, the slope remained constant out to about orbit 3200 where the error was 1.1 amperes lower than actual. The error from orbit 3200 to the present has remained in the vicinity of 1.1 amperes. Values of Power Subsystem shunt loss currents are approximately 1.25 amperes during satellite day and 0.45 ampere during satellite night.

The actual determination of regulated and unregulated bus current is difficult since the sensor is a Hall-effect generator operating at 400 Hz, which is coherent with the operation of other systems

within the spacecraft such as the controls gyro heater. The output of the Hall-effect generator is filtered (30-millisecond time constant), thereby inhibiting the observation of transients and variable duty-cycle surges such as the 400-Hz gyro heater causes. Also, because of the coherent 400-Hz frequency used by the Hall-effect generator and other spacecraft subsystems, it is possible that the sensor could read anywhere from peak current to minimum current, depending on the relative phasing and duty cycle.

There is also a slight error (approximately 5 percent) in the summation of the charge and discharge currents because of the pulsing 400-Hz nature of the gyro heater power requirements. The charge and discharge telemetry points are shunt resistors showing instantaneous values. The relationship of the actual duty cycle of the gyro heater to the position of these telemetry points in the PCM matrix causes an error with changes in the duty cycle. It is estimated that the duty cycle varied in flight from approximately 40 to 20 percent or less, although the actual duty cycle cannot be determined from available telemetry.

SOLAR CELL EXPERIMENT

Description

The solar cell radiation experiment consisted of two planar panels, each having 30 series-connected solar cells bonded to an aluminum honeycomb substrate. The cells on one panel are provided with 6-mil thick fused silica coverglass, bonded to the cells with Furane 15E adhesive. This panel is located on the transition section of the right-hand solar array platform, viewing the array from the sun. The 100-mil thick fused silica coverglass has the same optical filter properties as the 6-mil experiment and is bonded to the cells of the panel located on the transition section of the left-hand platform. The radiation experiments receive solar illumination at the same incidence angle and for the same period of time as the solar array. Each solar cell in the experiment is loaded with a 1.46-ohm resistance for monitoring current near the short-circuit point.

Discussion

Figure 4-24 is a plot of the normalized percentage of current loss versus orbit for both experiments. The data points for these plots were taken at the same paddle position at all times. This permitted normalizing for sun angle and sun intensity seasonal variations, but introduced a possible error caused by temperature variations at that paddle position, ranging from 16° to 20°C.

Both experiments, in the early orbits, showed a smaller loss caused by ultraviolet damage than the solar array indicated. The degradation at orbit 5200 was near the predicted

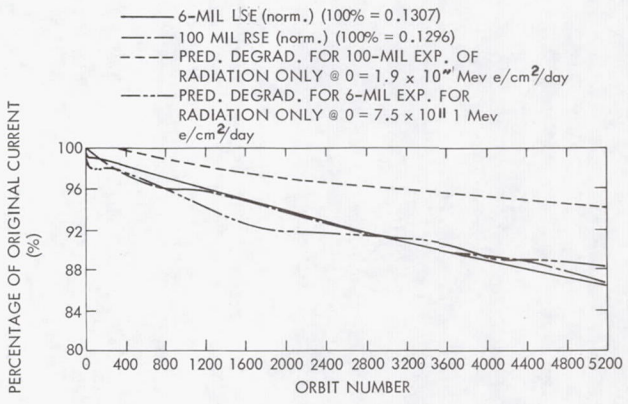

Figure 4-24—Current loss versus orbit for solar-cell experiments.

value at a flux level of 7.5×10^{11} e/cm^2/day (3 to 4 percent for first 100 hours predicted) predicted for the 6-mil experiment, which has the same characteristics as the actual array cells. The 100-mil experiment had a much higher degradation than anticipated. The extra thick coverglass on this experiment yielded a calculated flux rate of 1.9×10^{11} e/cm^2/day on the actual cell. A 4-percent degradation was predicted at orbit 3100, yet 10 percent was actually observed.

Telemetry data on experiment current and temperature have been insufficient to allow an exact analysis of the unusual 100-mil experiment degradation. At this point it is possible, however, to make tentative inferences as to likely causes of the loss of the 100-mil experiment current referred to in Reference 4.

The specially made 100-mil thick coverglass platelets may be inadequately shielding the solar cells. Inadequate shielding could be caused by insufficient dimensions or mispositioning of the cells, and would allow unattenuated particles to reach the cells. Or, ultraviolet exposure may be causing anomalistic degradation of the 100-mil coverglass transmission characteristic. Although laboratory experiment has yet to prove the effect, it is conceivable that ultraviolet radiation could so affect the thicker coverglass without affecting the thinner, 6-mil coverglass.

Mechanical stresses could be exerting enough pressure to loosen the cell contacts or even crack the silicon. The different expansion coefficients of glass and silicon is a possible source of pressure that might become worse with cycle life. Another is the soldering process during the nonproduction line assembly of the experiment.

Changes in the values of the load resistances that comprise the printed circuit load resistor network could be caused by environmental effects, although the 6-mil experiment data indicated no change in load resistance values.

SECTION 5

CONTROLS SUBSYSTEM

DESCRIPTION

Functional Description

The Nimbus II Controls Subsystem is required to initially stabilize the satellite's earth orientation, maintain the body axis system in alignment with the orbit axis system, initiate deployment of the solar array paddles, and continually align the paddles with respect to the sun. After the satellite separates from the launch vehicle, its direction and rates are stabilized and refined until the yaw axis points toward Earth's center, and the roll axis parallels the orbital plane. Pointing accuracy about all axes—roll, pitch, and yaw—must be maintained to within 1 degree with the instantaneous angular rate of the satellite body axis relative to the orbit axis always less than 0.05 degree per second. The solar array paddles are oriented perpendicular to the earth-sun line during satellite day to enable the solar array to collect radiant energy for conversion to electrical energy.

Physical Description

Stabilization System

The 3-axis stabilization of the spacecraft is achieved by a combination of flywheels and gas jets for each axis (Figures 5-1 and 3-2). Error signals for controlling the pitch and roll axes are derived from a pair of infrared scanners operating in the 12- to 18-micron range, mounted fore and aft on the control housing. The yaw-axis error signal is derived from an integrating gyro operating in the rate mode and mounted with the input axis in the roll-yaw plane, inclined 12 degrees to the roll axis. The gyro generates an error signal proportional to the yaw rate sensed directly, and to the yaw position error developed indirectly from the roll rate because of the gyro inclination to the roll axis. This method of determining yaw error applies accurately for low roll rates (which the spacecraft is expected to have). The yaw-rate input acts as a damping function in the yaw flywheel servo loop. A backup yaw control mode using two sun sensors mounted fore and aft in place of the gyro is also available.

A simplified block diagram of the pitch and roll attitude control loops (which operate identically) is shown in Figure 5-2. The horizon scanners generate a conical scanning aperture of 3×10 degrees rotating at 16.2 Hz about a 90-degree apex angle (Figure 5-3). At the nominal 600-nm orbit, the scan cone intersects the earth over an 84-degree segment of the scan, generating a voltage pulse as the earth is intercepted. The pitch error is developed in the horizon attitude digital computer as a function of the difference in the widths of the front and rear earth pulses. Roll is computed on the basis of the offset of the front scanner pulse with respect to a reference voltage coincident with the yaw axis of the spacecraft, switching to the rear scanner when the pitch

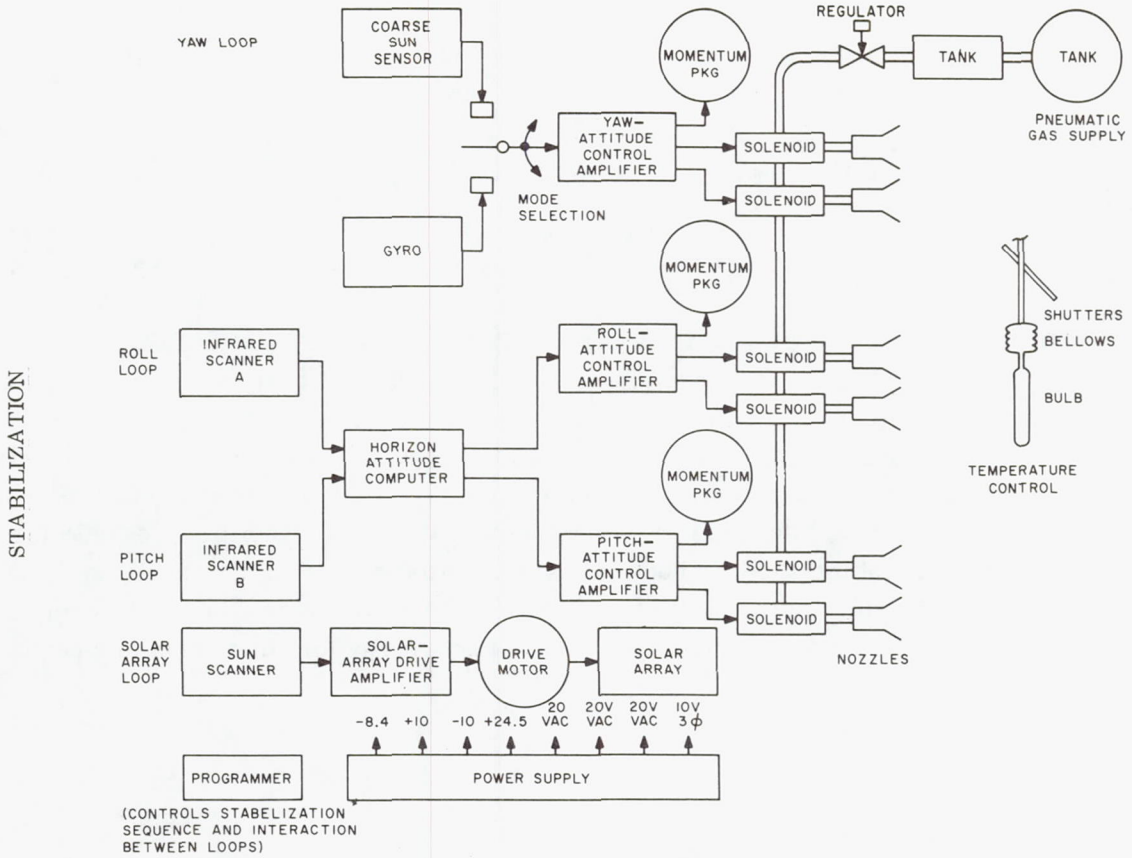

Figure 5-1—Control subsystem block diagram.

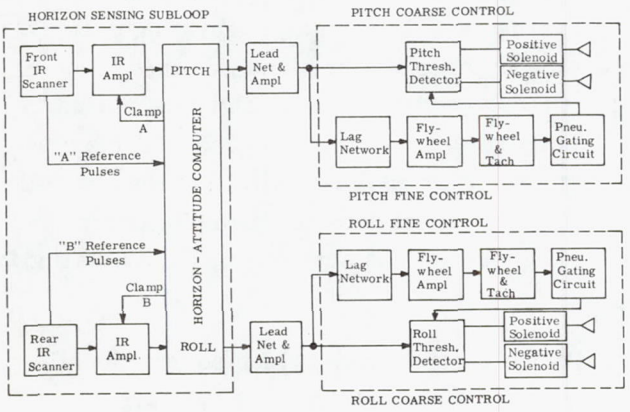

Figure 5-2—Pitch and roll control loops.

error is greater than 8 degrees. Pitch and roll error computations are illustrated in Figure 5-4.

Freon-14 gas provides the pneumatic impulses; 16.4 pounds pressurized at 1250 psig are available at launch. The jets are arranged to deliver momentum changes of 0.115, 0.083 and 0.183 ft-lb sec per gate in pitch, roll and yaw, respectively. Gating speed is set at 80 percent of rated flywheel speed in pitch, 84 percent in roll, and 65 percent in yaw (equivalent to steady-state errors of approximately 0.17, 0.33, and 0.14 degree, respectively). Each gate changes the associated flywheel speed by approximately 362, 263, and 576 rpm, respectively. A summary of pneumatic subloop parameters is given in Table 5-1.

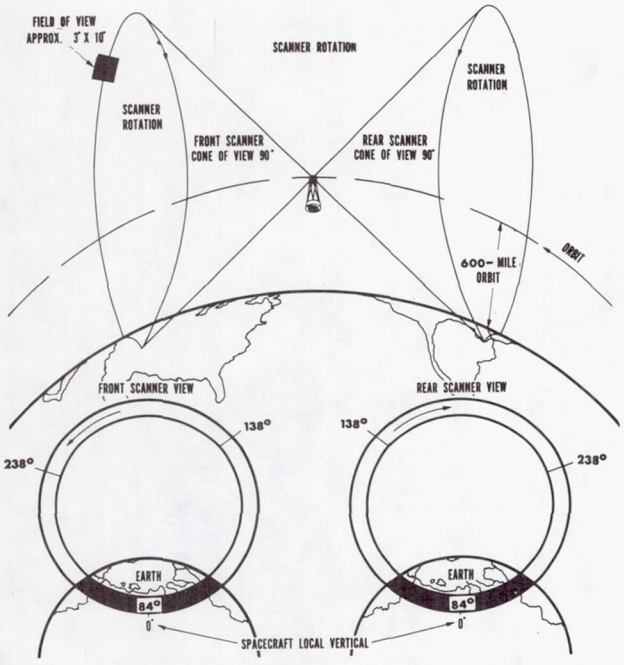

Figure 5-3—Intersection of scan cone and earth.

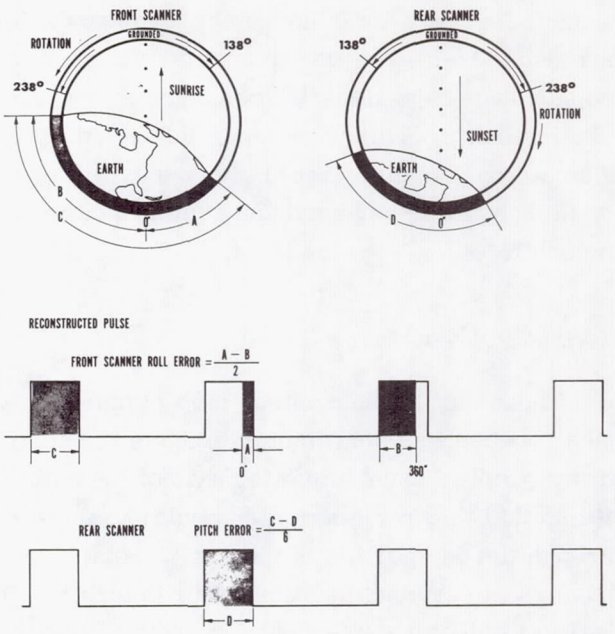

Figure 5-4—Pitch and roll error computation.

If the combined error and error rates in any axis exceed a prescribed threshold as shown in Figure 5-5, continuous firing of the appropriate jet occurs. This does not apply to yaw control in the gyro mode where gate firings can be no closer than 30 seconds apart. Commands are available to turn off yaw pneumatics and all pneumatics. There are also commands to introduce steps

Table 5-1

Pneumatic Subloop Parameters (Measured Data).

Axis	Vehicle Inertia (slug ft^2)	Pneumatic Moment Arm (ft)	Nozzle Thrust (lb)	Mass Flow Rate Per Nozzle (lb per sec)	Vehicle Accel. (deg/sec)	Momentum Removed Per Gate (ft-lb sec)	Momentum Removed (Per % of Wheel Capacity†)	Gating Speed (% of Rated Speed)	Equivalent Body Rate at Gating Speed Momentum (deg/sec)	Gating Interval (sec)
Pitch	243.5	5.98	0.099	0.00214	0.139	0.115	29	84	0.077	0.100
Roll	268	3.50	0.155	0.00335	0.116	0.084	21	84	0.076	0.100
Yaw	125	2.52	0.134	0.00290*	0.155	0.188	47	64	0.115	0.52

Pneumatic System	
Gas: Freon 14 (CF_4-tetrafluoromethane) Tank volume: 930 cu in = 0.522 cu ft Charge pressure: 1250 psig Gas weight: 15.2 lb	Usable weight (including leakage and 50 psi min): 14.6 lb Specific impulse: 46.2 seconds Stored usable impulse: 675 lb sec

*Total flow rate in yaw is twice single-nozzle rate.
†Wheel capacity = 0.4 ft lb sec at 1250 rpm; max rpm at 26 vac ≈ 1350 − 1400 rpm.

of fine yaw correction of up to 7 degrees to compensate for gyro drift and other commands to introduce 24-degree yaw bias into the control loop in 6-degree steps to compensate for sun misalignment. This yaw bias is varied by a solar array potentiometer to give opposite polarity biases in the northern and southern parts of the orbit.

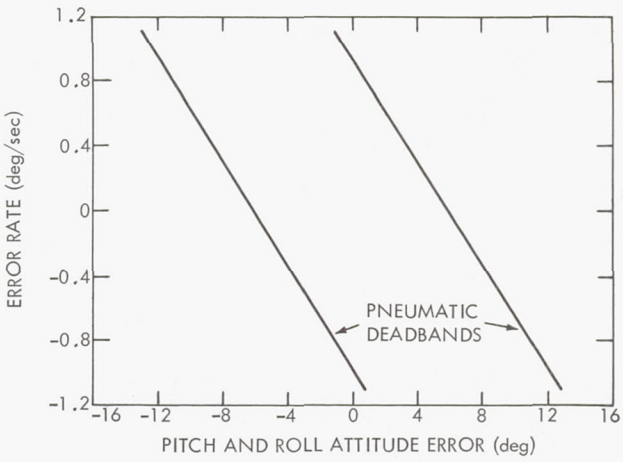

Figure 5-5—Attitude error versus error rate.

Solar Array Drive

The solar array control loop (Figure 5-6) uses a two-phase servomotor to drive the solar array paddles about the pitch axis of the satellite so that they remain perpendicular to the sun through the day portion of the orbit. Solar array sensors mounted on each end of the solar array drive shaft serve as position error detectors. The sun sensors are cylindrical and provide a 360-degree field-of-view (except for earth albedo shields mounted beneath each sensor). The sensor has a zero output with the shaft oriented such that the solar array paddles are perpendicular to the sun. The output signal, which is proportional to the pointing error, drives the variable voltage phase of the servomotor (Figure 5-7). The motor is coupled to the array driveshaft through a 84, 847:1 gear reduction mechanism and a ball detent clutch which is used primarily to protect the gear mechanism during ground handling.

Several steps were taken to prevent the degradation of the motor lubricant (G300 grease), which was the cause of the Nimbus I failure. A larger motor (Size 11) was used; it had a larger rotor with a high emissivity surface. A heat strap also was connected between the motor housing and the base structure (Panel 2). The motor can be operated in either of two modes, selectable by

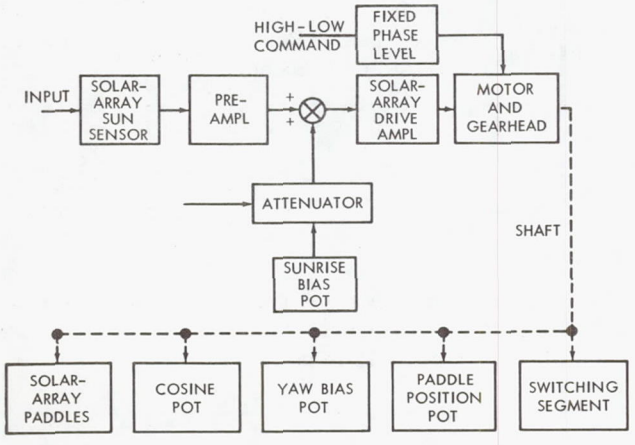

Figure 5-6—Solar-array control loop.

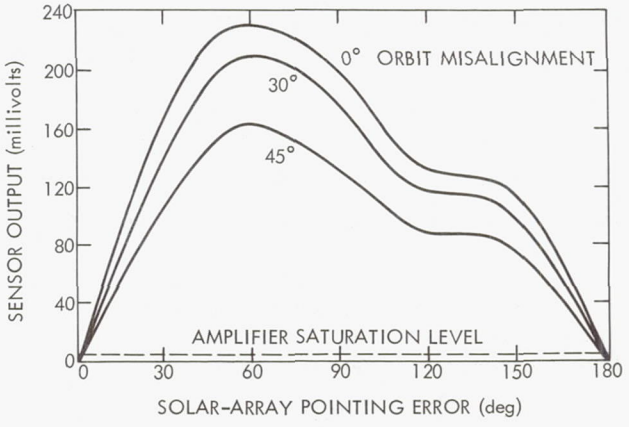

Figure 5-7—Solar-array sun sensor characteristics.

ground command, thus providing either high-torque output or a derated output. The low-torque mode, which generates less heat, is the normal operating mode.

The paddles track the sun during the sun day with less than a degree of error. When the spacecraft enters the umbra, control of the drive is taken over by a sunrise bias potentiometer coupled to the driveshaft, which causes the array to be driven at six times orbital speed to the nominal sunrise position. The paddles resume tracking at sunrise when the sun sensors are again illuminated by the sun. The effect of this sunrise bias potentiometer during satellite day is to offset the paddle null position only slightly from perpendicular to the sun, since the gain of the sun sensor preamplifier is large. Slip rings in the Controls Subsystem housing carry the solar array current and telemetry signals from the array shaft to the spacecraft and allow continuous rotation of the array.

Initial Stabilization

After injection into orbit, the Agena is allowed 2 minutes to stabilize. Then a 1-degree per second pitchup maneuver is initiated and maintained for 80 seconds. The Agena is stabilized at a pitch attitude of 10 degrees from the vertical. Separation is then initiated by severing a Marmon clamp holding the spacecraft to the adapter section affixed to the Agena; the clamp is severed by firing two sets of squibs that activate two bolt cutters. Compressed springs in the adapter impart a separation velocity of 4 feet per second to ensure diverging orbits between the spacecraft and the rocket.

Two microswitches sense separation from the rocket, initiate a paddle-unfold sequence, and enable the Command Subsystem. A 2.5-second timer then fires a squib to cut the cable latching the two paddles closed. A backup 5-second timer is provided to fire a redundant cable cutter should the first firing not succeed. The severing of the cable, sensed by a microswitch, initiates the paddle-unfold motors and stars a Controls Subsystem programmer. The paddles are opened by a combination of springs and drive motors. The drive motors are turned off individually when each paddle latches in the open position; this is accomplished by a motor housing reaction windup system triggering a switch.

The controls programmer in the reset condition inhibits the operation of all pneumatics, the yaw flywheel amplifier, and the solar array drive. In 10 seconds after programmer activation, the pitch and roll pneumatics are enabled, allowing time for the paddles to clear the scan field of the rear IR horizon scanner. Then 50 seconds after paddle-unfold starts, the yaw control loop is enabled, allowing time for the spacecraft to start stabilizing in roll because of the interaction between roll and yaw. The yaw flywheel is maintained at zero speed until the loop is enabled to minimize pitch and roll cross-coupling during the initial period after separation and to allow for maximum absorption of yaw body momentum by the wheel. The solar array drive is also enabled at that time. This delay allows time for the paddles to open fully.

The Controls Subsystem operating in the gyro mode is capable of initial stabilization for a variety of combinations of pitch, roll, and yaw rates up to approximately 2 degrees per second.

However, to ensure initial stabilization, the rates in any axis due to a combination of Agena and separation springs are limited to less than 1 degree per second. The individual axis rates imparted by the springs are limited to 0.5 degree per second. Initial stabilization is expected to take place in 3 to 5 minutes.

FLIGHT OBJECTIVES

Table 5-2 lists the flight objectives and results of the Controls Subsystem over periods of 6 and 13 months.

Table 5-2

Controls Subsystem Flight Objectives and Results.

Objective	6 Months	13 Months
Demonstrate that the Controls Subsystem is capable of:		
Initial attitude acquisition following orbit injection.	The spacecraft acquired the earth reference and stabilized the spacecraft within 3.6, 3.4, and 6.1 minutes in pitch, roll, and yaw, respectively, after each of these loops was enabled.	(See 6-month comments)
Maintaining three-axis stabilization.	In the absence of cold clouds, fine limit cycle control of the pitch, roll, and yaw axes was to within 1 degree of the required reference.	In the absence of cold clouds, fine limit cycle control of pitch, roll, and yaw axes continued to be maintained within 1 degree of the required reference.
Providing paddle deployment and solar array pointing for a period of at least 6 months following orbit injection.	The SAD pointed the array surface properly toward the sun within 5.5 minutes after the drive loop was enabled and continued to track properly.	Solar array pointing continued to be maintained well within specifications.
Demonstrate the adequacy of the Control Subsystem thermal control system.	Since launch, the controls temperatures were maintained within the specified range of 25 ± 10°C. The controls housing average at the end of 6 months was 26.3°C.	The controls temperatures continued within limits with the average control housing temperature currently at 26.9°C.
Demonstrate the improvements to the SAD.	The array continuously tracked the sun with no observed signs of degradation in the electronic or mechanical system.	The array continuously tracked the sun with no observed signs of degradation in the electronic or mechanical system.
Demonstrate that the reduced pitch nozzle size plus reduced gating time will eliminate the pitch oscillation experienced on Nimbus I.	There were no observed pitch oscillations.	There were no observed pitch oscillations.

DISCUSSION

Launch and Initial Stabilization

The Controls Subsystem performed successfully following spacecraft/booster separation. The subsystem acquired the earth reference and stabilized the spacecraft within 3.6, 3.4, and 6.1 minutes in pitch, roll, and yaw, respectively, after each of these loops was enabled. The SAD pointed the array surface properly toward the sun within 5.5 minutes after the drive loop was enabled. The usable pneumatic impulse available at lift-off was 690 pound-seconds, which corresponds to 16.43 pounds of Freon-14 gas. At separation, rates of 0.05, 0.10, and 0.12 degree per second were imparted to the spacecraft pitch, roll, and yaw axes, respectively (Reference 5).

When the pitch and roll control loops were enabled, the positive pitch solenoid fired continuously for 6 to 7 seconds and turned off as the pitch error and error rate came within the pneumatic deadbands. As the pitch error became positive, the negative pitch solenoid fired continuously for 3 to 4 seconds. This firing was followed by two additional, short negative firings as the combined pitch error and error rate "walked" down the pneumatic switching line. These firings were subsequently followed by a negative pitch solenoid gate. No roll solenoid firings were required to stabilize the spacecraft on this axis (Figure 5-8). After enabling of the yaw loop, yaw flywheel pneumatic gating occurred seven times before yaw fine limit control was achieved.

Satellite Day-to-Night Transition

Since orbit 13, a nearly constant negative pitch disturbance torque caused the pitch flywheel to absorb momentum continuously. Each third or fourth orbit, as the pitch flywheel speed approached -900 rpm, the torque caused by accelerating the solar array to the maximum slew rate (upon entering the earth's umbra) induced a negative pitch error that, in turn, caused the flywheel to attain gating speed. Following the solenoid gate, the flywheel speed was reduced to approximately -400 rpm, thus beginning the momentum buildup cycle again (Figure 5-9). Occasionally, the flywheel did

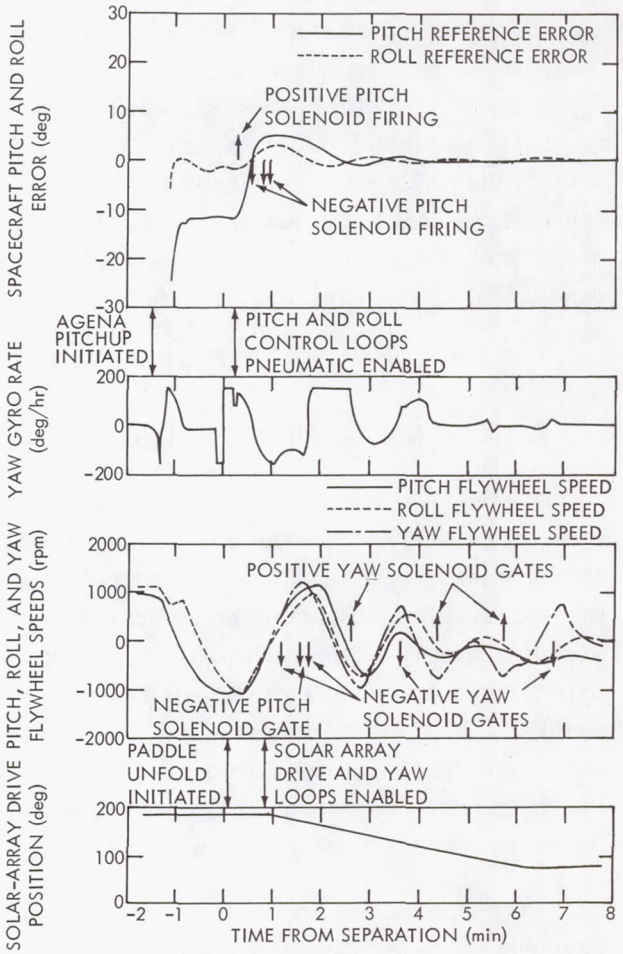

Figure 5-8—Control subsystem parameter history of spacecraft initial attitude-reference acquisition.

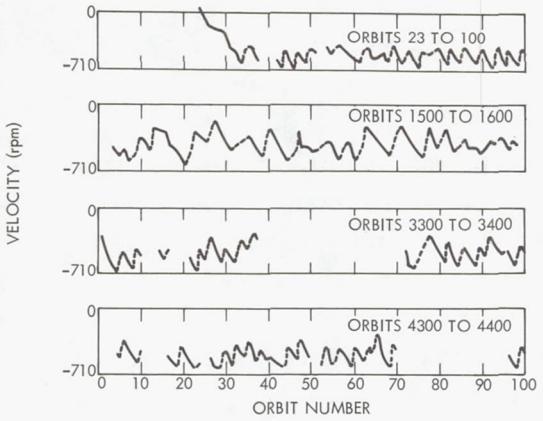

Figure 5-9—Pitch velocity profile.

not quite attain the gating speed during this period of time. When a gate did not occur at this time, it occurred during the night-to-day transition when the array was accelerated to the sunrise position. The pitch control characteristics were similar in both cases. During these transition periods, little or no effect was seen in the yaw and roll control loops.

The pitch disturbance that occurred during the satellite day-to-night transition period is illustrated in Figure 5-10. This figure shows that the pitch flywheel was capable of overcoming the negative pitch error. However, since the flywheel speed was -800 rpm at the initiation of the disturbance, the -200 rpm additionally required to control the disturbance was sufficient to cause the positive solenoid to gate. This gate reinforced the rate induced by the flywheel and caused an overshoot of the fine limit cycle deadbands in the positive direction. Approximately 1 minute was required to regain pitch fine limit cycle control. Before orbit 21, when the pitch flywheel was maintaining a positive momentum vector, the pitch error (induced by the acceleration of the SAD to the maximum satellite night slew rate) did not exceed the fine limit cycle deadbands at any time during these transition periods.

Satellite Night-to-Day Transition

Figure 5-11 illustrates the typical spacecraft pitch response to the solar array slew to the sunrise position, which occurs each time the spacecraft exits from the umbra. The response shown is attributable to flywheel torquing in response to array motion, without solenoid firings. A similar response is experienced each time the spacecraft enters the umbra, during the satellite day-to-night transition, without the occurrence of a pitch solenoid gate.

Torque resulting from accelerating the array induced a negative-going pitch error of 0.2 degree, which resulted in a proportional change in flywheel speed. This flywheel deceleration

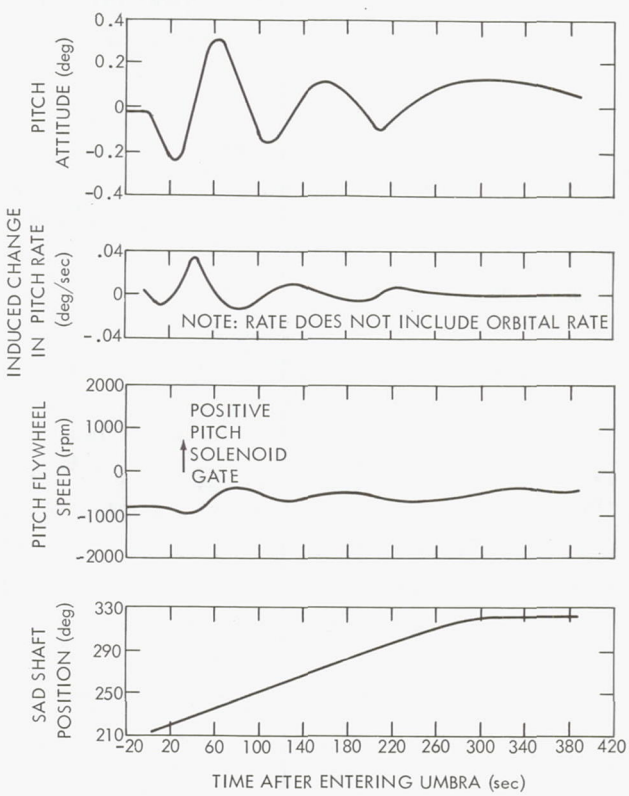

Figure 5-10—Pitch stabilization control characteristics during transition from satellite day to satellite night (orbit 1220).

torqued the spacecraft in a positive sense that, combined with array deceleration, caused an overshoot of approximately 0.24 degree beyond the initial attitude of 0.2 degree. The perturbation was subsequently damped, and the pitch attitude returned to its initial condition of 0.2 degree within 2 minutes. The pitch attitude error was approximately 0.2 degree initially (Figure 5-11) because during the early orbits, a positive pitch disturbance torque was acting on the spacecraft thus effecting a positive pitch offset error. In later orbits, the pitch disturbance torque became negative and resulted in a small negative average pitch error. However, the direction and relative magnitudes of the error induced during the satellite night-to-day transition remained the same.

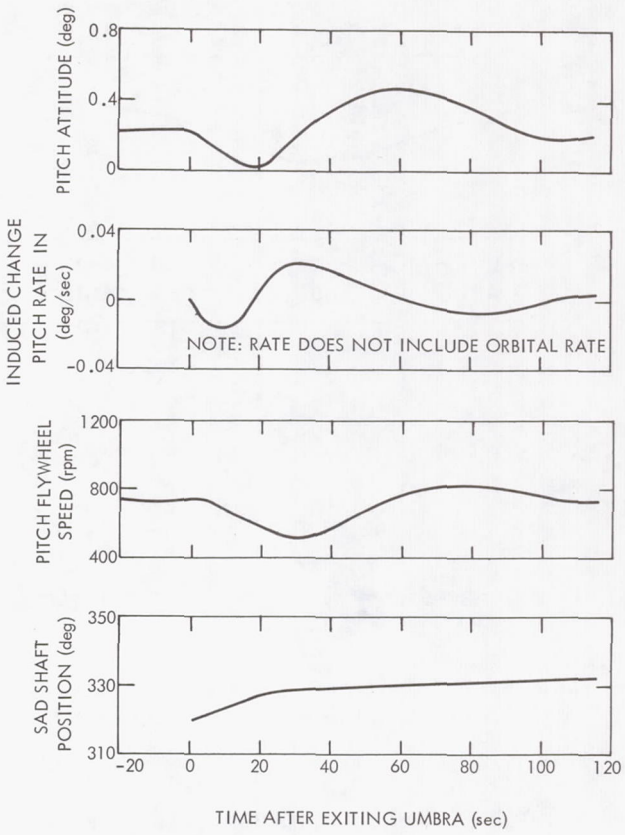

Figure 5-11—Pitch stabilization control characteristics during transition from satellite night to satellite day (orbit 60).

IR Disturbances

Throughout each orbit, perturbations in the roll reference error output channel of the horizon attitude computer were noticeable. These perturbations were caused by cold clouds within the scanner field-of-view, particularly on the horizon portions of the earth scan. In the equatorial regions they lasted 1 to 4 minutes. These apparent attitude error signals caused the roll flywheel to accelerate or decelerate proportionately in a direction that reduced the apparent attitude error. Changing the roll flywheel speed caused the spacecraft to move about the roll axes. This motion was sensed by the yaw gyro, which in turn generated a signal proportional to the sensed rate to drive the yaw flywheel, with polarity that reduced the apparent heading error. For cold-cloud IR disturbances, roll attitude errors of 2 to 3 degrees were observed that caused yaw attitude errors of approximately 8 to 10 degrees. The pitch reference error channel output from the horizon attitude computer seemed to be much less affected by cold clouds.

Roll Yaw Momentum Exchange

During the Nimbus II flight there has been a continuing interchange of momentum between the roll and yaw flywheels. The spacecraft has rotated at a constant rate about the pitch axis and has completed one revolution each orbit. With no appreciable torques acting on the spacecraft, the total system momentum vector is fixed in inertial space. Therefore, the component of system momentum lying in the orbit plane must be continually interchanged between the yaw and roll flywheels. This phenomenon is shown in Figure 5-12. The interchange is brought about as the pitch

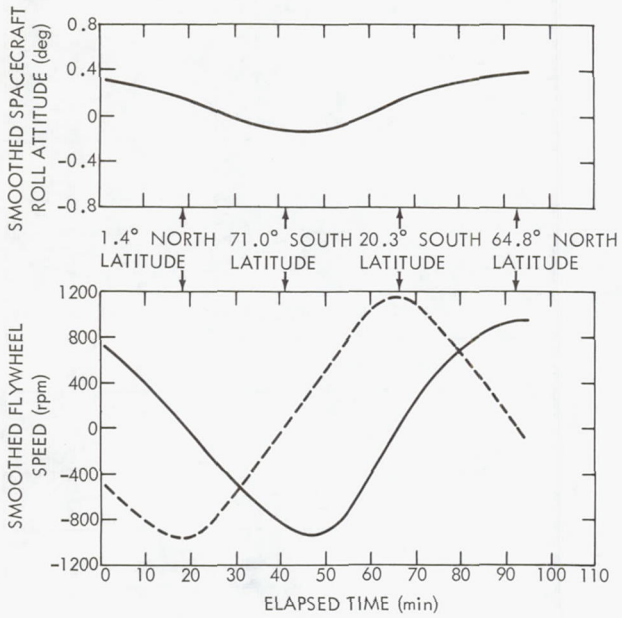

Figure 5-12—Roll-yaw momentum exchange showing induced mean roll attitude error (orbit 450).

rate induces a gyroscopic moment in the yaw and/or roll flywheels proportional to their respective rotational speeds. This moment is applied to the opposite axis. For example, the yaw flywheel gyroscopic moment induces motion about the roll axis, which increases the roll attitude reference error and the roll flywheel speed. The imparted roll rate is sensed by the yaw gyro, which in turn decreases the yaw flywheel speed. This continuing effect is such that during a single orbit, the yaw and roll flywheel speeds respond in a sinusoidal manner, 90 degrees out of phase with each other (Figure 5-12). The maximum roll flywheel momentum periodically stored each orbit was greater than predicted. This increased momentum has been attributed to a disturbance torque caused by the interaction of the magnetic force field of the spacecraft.

Pitch Disturbance Torque

From the time of initial orbit injection, a pitch disturbance torque was observed. Within the first 13 orbits, the torque was alternating positive and negative. Since orbit 13, it has been mostly negative with a fairly constant magnitude of approximately -0.045×10^{-4} foot-pounds (this is a gravity gradient effect). The condition before orbit 13, also observed during the early orbits of Nimbus I, is not understood.

Solar Array Drive Pointing

When the SAD loop was enabled following spacecraft booster separation, it drove backwards from the 180-degree position for approximately 5.5 minutes before the SAD sun sensors became nulled. However, the loop has been functioning satisfactorily ever since. The improved SAD can operate in either a "low" voltage mode (which is normal), or a "high" voltage mode (which increases the voltage to the drive motor). The spacecraft has operated in the low mode since launch.

The average satellite day array drive rate has been approximately 3.3 degrees per minute at an average SAD amplifier output voltage of 0.72 to 0.78 vrms. The maximum drive rate while slewing to the array night rest position has been approximately 22.5 to 24.5 degrees per minute with a maximum SAD amplifier output of 11.6 to 11.9 vrms. The earth day and night signals have been occurring at approximately 6 degrees and 171 degrees of shaft position, respectively; and the shaft night rest position has been between 319.5 and 320.5 degrees.

Figure 5-13 presents the history of the SAD functions. During the first month of flight, the solar array was observed to advance 0.5 to 1.0 degree after settling in its night rest position. This was attributed to noise on the 400-Hz power supply used by the SAD and flywheel motors. This phenomenon is no longer observed.

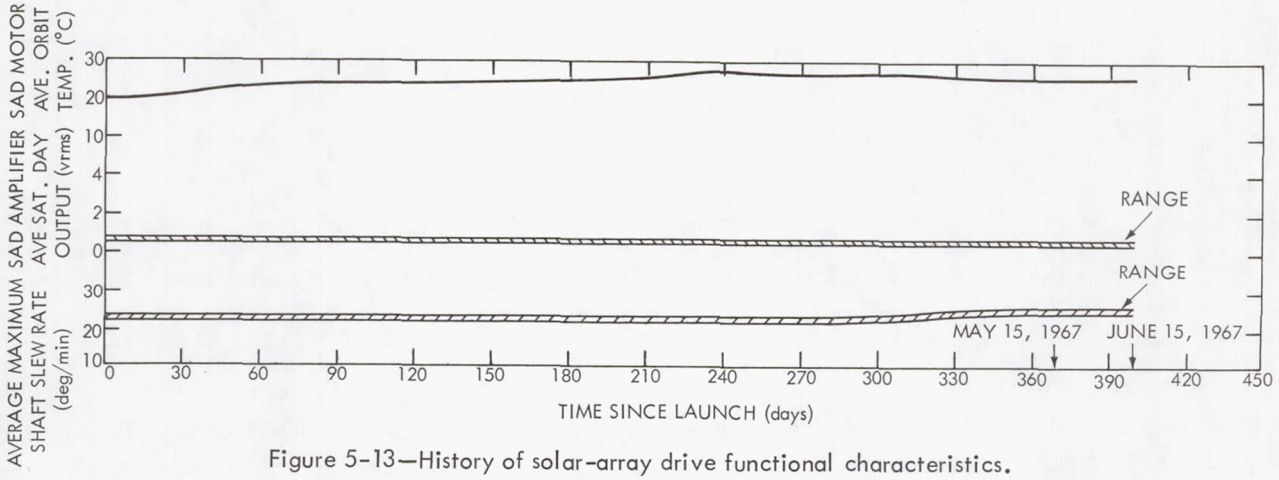

Figure 5-13—History of solar-array drive functional characteristics.

Also, in the early parts of flight, the high solar incidence angle β, when combined with negative yaw error caused deviations in the SAD shaft tracking (Figure 5-14). A review of the SAD performance showed that the drive occationally slowed down and/or reversed for 1 to 2 minutes, at which time deviations from nominal approached 5 degrees of tracking error. These deviations occurred between the earth day (0 degrees) and high noon (90 degrees) orbit position and were accompanied by large excursions of the roll and yaw flywheels because of cold cloud patterns. These deviations in shaft tracking, as noted from flight data, occurred only when the vehicle roll and yaw positions were perturbed by a cloud pattern. Therefore, it was concluded that the cause of the deviations was a negative yaw error, adding to the existing 10-degree orbit plane misalignment, resulting in uneven shading of the solar array sun sensor. This problem ceased when the β angle became lower. If the orbit plane solar β angle had become much larger, it is assumed that this anomaly would have occurred more often.

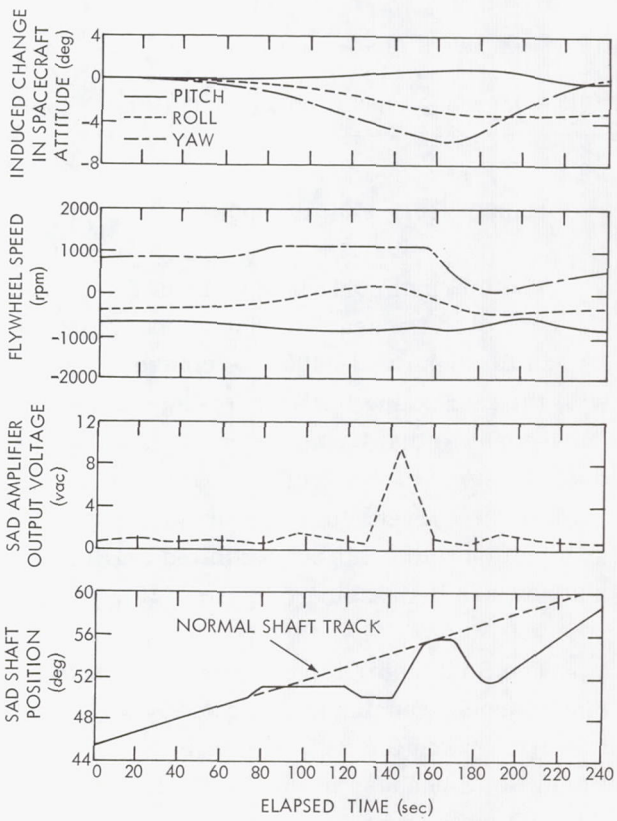

Figure 5-14—Solar-array drive reversal characteristics correlated with change in spacecraft attitude (orbit 1590).

Power Conversion

Power Conversion from -24.5 vdc to the required ac and dc voltages was satisfactory throughout the flight (Table 5-3).

Table 5-3

Control Voltages.

Power Supply Output	Orbit Number												
	1 to 400	400 to 800	800 to 1200	1200 to 1600	1600 to 2000	2000 to 2400	2400 to 2800	2800 to 3200	3200 to 3600	3600 to 4000	4000 to 4400	4400 to 4860	4860 to 5275
400 Hz, phase 1 (26 ± 1.8 vac)	25.96	25.95	25.95	25.95	25.93	25.92	25.93	25.94	25.92	25.92	25.92	25.91	25.91
400 Hz, phase 2 (20.0 ± 1.0 vac)	20.38	20.34	20.34	20.32	20.33	20.33	20.27	20.25	20.25	20.25	20.25	20.25	20.25
+24.5 ± 0.5 vdc	24.51	24.51	24.55	24.51	24.50	24.53	24.51	24.52	24.53	24.52	24.51	24.51	24.50
-10.0 ± 0.2 vdc	-9.9	-9.9	-9.9	-9.9	-9.91	-9.91	-9.88	-9.86	-9.88	-9.89	-9.89	-9.88	-9.89
+10.0 ± 0.2 vdc	10.06	10.07	10.09	10.07	10.08	10.08	10.06	10.06	10.06	10.06	10.06	10.06	10.06

Temperature Maintenance

The thermal control of Nimbus II is essentially the same as that for Nimbus I. Since launch, the controls temperatures have been maintained within the specified range of 25 ± 10°C. From launch through orbit 3400, the controls exhibited a general warming trend, which was consistent with the increasing intensity of the sun as the earth approached its perihelion (near winter solstice). Subsequent to that time, the controls exhibited a general decrease in temperature (Table 5-4) but did not return to the original level. This was probably caused by degradation of the thermal coatings. (The current control housing temperature is 26.9°C.) The IR scanner temperatures were low at injection into orbit but exhibited a gradual increase similar to the rest of the controls functions and now are decreasing (Figure 5-15).

The SAD motor temperature has varied with the temperature of Control Housing Panel No. 2 since launch, running approximately 3°C lower than Panel No. 2 (Figure 5-16). Since Panel No. 2 is warmer than the SAD motor, it is assumed that the SAD motor is possibly absorbing heat from Panel No. 2 because of the thermally conductive heat path that exists between the two. In this case, the SAD motor would probably run at a lower temperature if it were not "heat-sinked" to Panel No. 2. This situation has caused no detrimental effects since the temperature of the SAD motor is well within the specified limits, averaging 24 ± 3°C for the 13-month period. Since the thermistor for Panel No. 2 is located at the opposite end from the heat sink, the temperature indicated may not be

Table 5-4

Component Temperature Summary.

Component	Average Temperature (°C)													
	Orbit 1	Orbit 25	Orbit 400	Orbit 600*	Orbit 800	Orbit 1000	Orbit 1200	Orbit 1400	Orbit 1600	Orbit 1800	Orbit 2000†	Orbit 2200	Orbit 2400	Orbit 2600
Freon tank	7.6	7.1	8.2	9.5	9.6	9.7	10.0	10.9	11.4	11.7	12.3	13.0	13.4	14.0
Gyro fluid	73.7	73.8	73.7	73.7	73.8	73.8	73.8	73.8	73.8	73.8	73.7	73.7	73.7	73.7
Yaw flywheel	29.1	27.8	29.1	30.0	30.5	30.6	31.2	31.6	31.7	31.9	32.1	32.4	32.8	33.7
Roll flywheel	30.8	27.2	28.6	29.2	29.5	30.0	30.5	30.4	30.7	30.9	31.6	32.1	32.0	32.8
Control housing	22.3	19.2	20.8	21.3	21.5	23.3	23.8	24.2	24.5	24.7	25.2	25.8	26.3	26.6
SAD motor	21.2	20.5	21.0	22.8	22.8	23.4	23.7	23.3	23.3	23.6	24.0	24.4	24.7	25.3
Panel no. 2	26.0	24.0	25.3	25.9	26.2	27.3	28.0	27.9	27.7	27.0	26.9	27.4	27.7	27.7

Component	Average Temperature (°C)												
	Orbit 2800	Orbit 3000†	Orbit 3200‡	Orbit 3400	Orbit 3600	Orbit 3800	Orbit 4000	Orbit 4200	Orbit 4400	Orbit 4600	Orbit 4860	Orbit 5060	Orbit 5275
Freon tank	14.2	14.7	15.0	15.0	14.9	14.7	14.5	14.1	14.0	13.8	13.7	13.59	13.53
Gyro fluid	73.7	73.7	73.7	73.8	73.8	73.8	73.8	73.8	73.7	73.7	73.7	73.69	73.71
Yaw flywheel	34.2	34.2	35.1	34.7	34.8	34.3	34.5	34.1	34.3	33.4	33.9	34.34	33.85
Roll flywheel	32.9	33.5	33.6	33.5	33.5	33.6	33.3	33.0	32.6	31.4	31.9	32.16	31.69
Control housing	26.6	27.9	28.7	27.1	28.0	26.9	27.3	27.0	27.6	26.6	26.6	27.11	26.93
SAD motor	25.4	25.7	26.7	27.0	27.1	27.1	26.8	26.0	25.5	25.6	25.3	25.28	25.36
Panel no. 2	27.5	28.9	29.7	29.8	30.0	29.6	29.5	29.2	29.1	28.3	28.5	28.83	28.76

*β angle = 11.37°
†β angle = 0°
‡β angle = 1.6°

One year in orbit

the same as the heat sink, and the desired effect may be occurring (i.e., Panel No. 2 dissipating heat from the SAD motor).

Pneumatics

Following initial stabilization, the usable pneumatic impulse showed a nearly constant decrease of approximately 1 pound of Freon-14 gas (42 pound-sec of impulse) per 1950 orbits. This can be attributed to the yaw pneumatics being disabled in orbit 5U, and pitch and roll loops averaging only one and two solenoid gates, respectively, every 3 to 4 orbits (Figure 5-17). Based on this rate and on the fact that on June 15, 1967 there were 13.40 lb of usable gas remaining, there

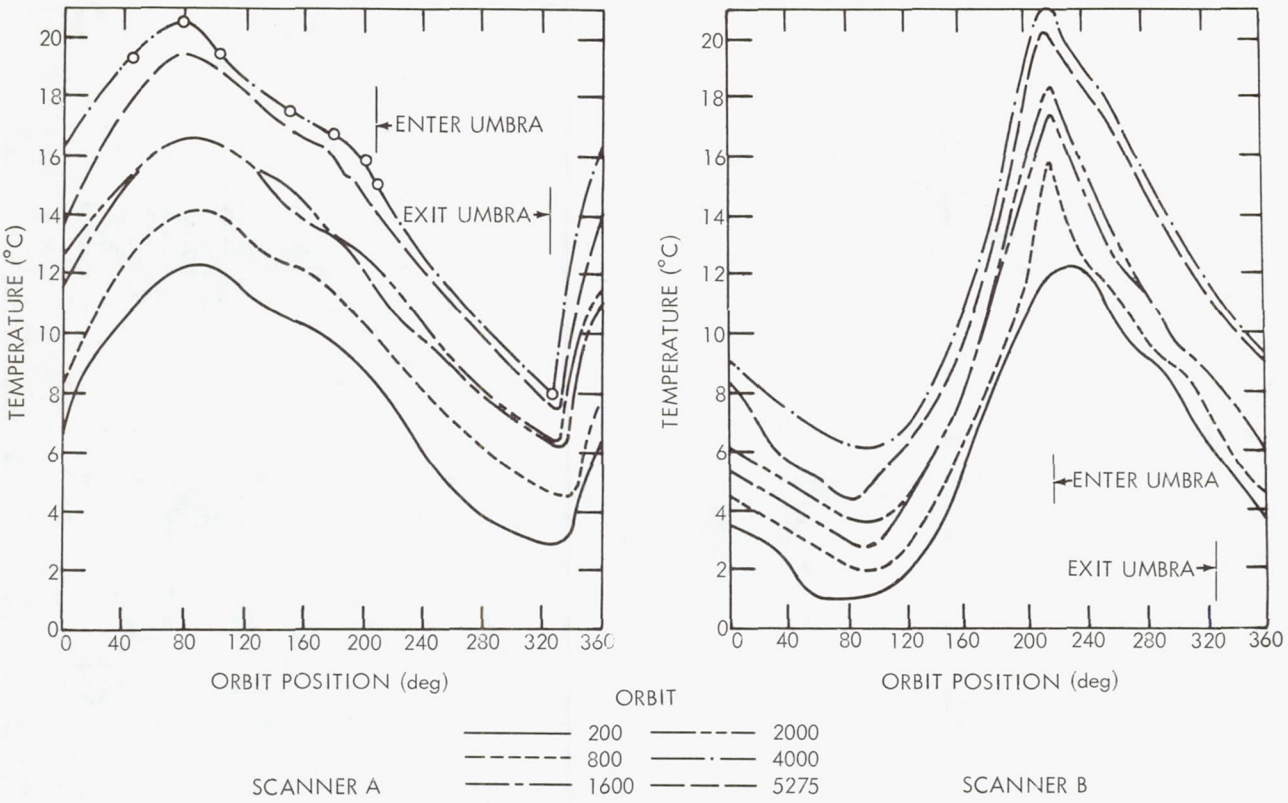

Figure 5-15—Scanner A and scanner B temperature history.

are approximately 26,000 orbits worth of gas remaining; this is equivalent to approximately 5.4 years. Throughout the flight, the average regulated manifold pressure was maintained within 35 ± 1 psig, which is within the 35 ± 2 psig requirement.

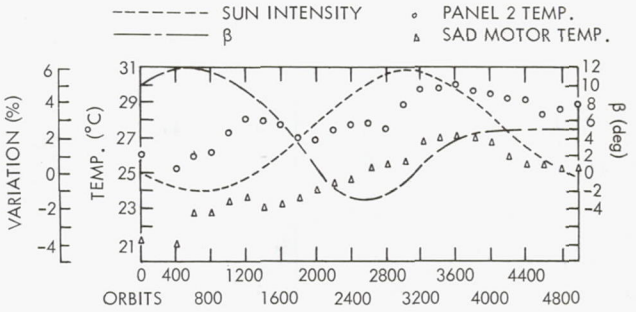

Figure 5-16—SAD motor temperature versus panel no. 2 temperature.

Solar Eclipses

Nimbus II has passed through three eclipses: during orbits 68, 2413, and 4784. The

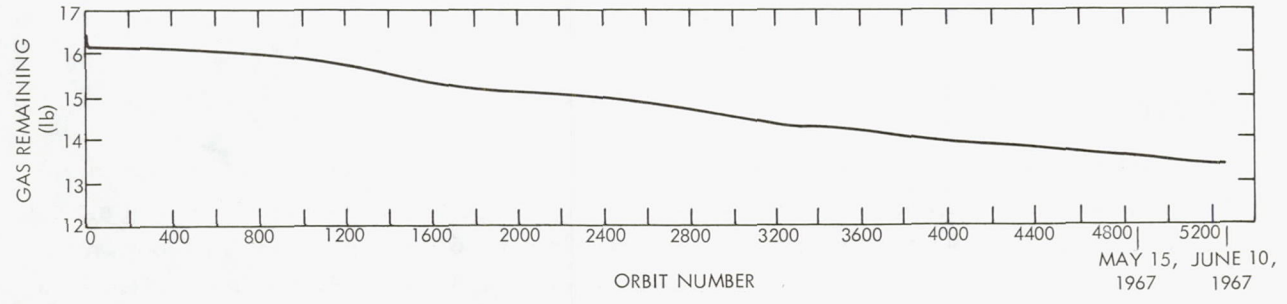

Figure 5-17—Freon-14 gas consumption.

first, a partial eclipse of the sun by the moon, had no effect on the Controls Subsystem. Neither did the third, which was a partial solar eclipse encountered by the spacecraft before transition from Rosman to Ulaska at 15422 on May 9, 1967.

However, during orbit 2413, the spacecraft passed through the region of a partial eclipse. Figure 5-18 shows the performance of various control functions during the eclipse. The spacecraft entered the eclipse at approximately 1445Z and exited at approximately 1502Z. The PCM data were received at Santiago, Chile, from 1454Z to 1501Z. Therefore, the spacecraft was in the eclipse area approximately 9 minutes before the receipt of PCM data.

At the beginning of the data the roll and yaw flywheels and the gyro were fairly quiet, the SAD motor was stalled at an orbital position of 65 degrees, and the unregulated bus current was zero (0.9 TMV ⇒ Telemetry Volt). Two minutes after the start of data (1456Z), the SAD motor resumed normal sun tracking, and unregulated bus current started to increase back to its normal value for daytime operation. The stalled condition of the SAD was caused by the reduced sun sensor amplifier output, which was still sufficient to override the feedback pot voltage, thus preventing the SAD from driving to the array sunrise position; however, it was not sufficient to perform normal sun tracking. The SAD did drive backwards approximately 4 degrees toward the sunrise position as the spacecraft passed through the area of least sun illumination and then drove rapidly forward for approximately 45 seconds just before the resumption of normal sun tracking.

At 1458Z, the spacecraft underwent a severe perturbation lasting almost 2 minutes. This disturbance is shown by the fine gyro off-scale readings and the increased activity of the roll and yaw

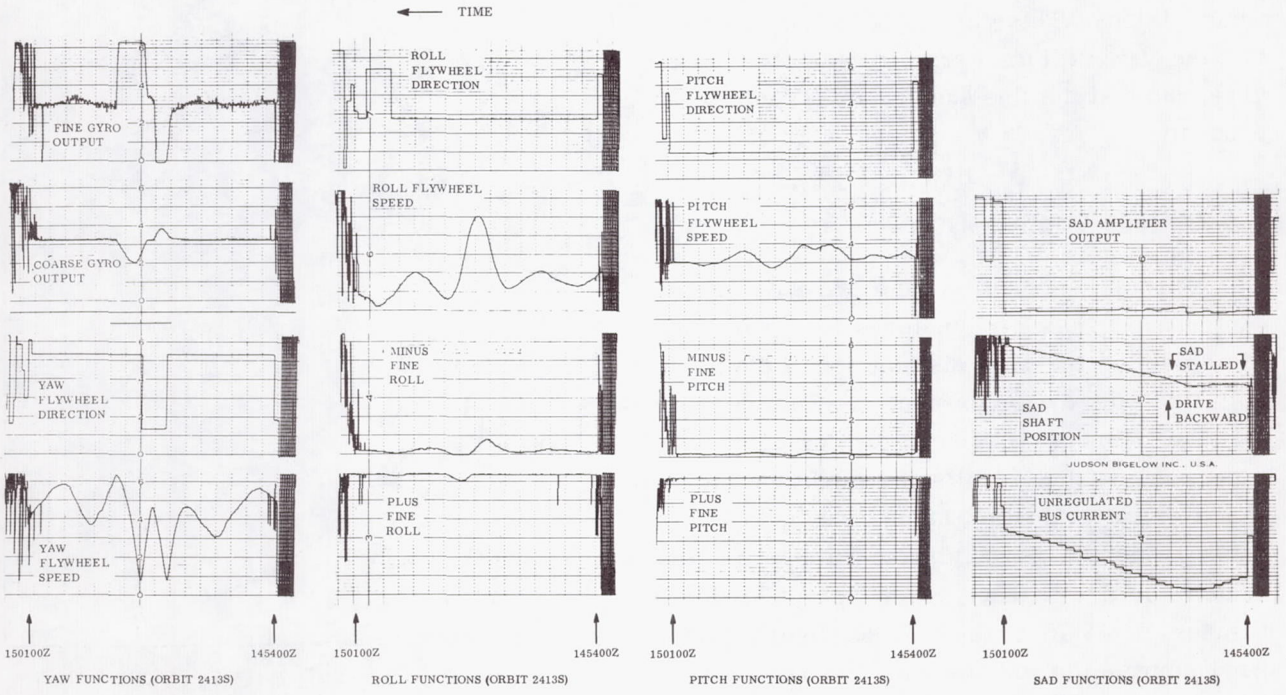

Figure 5-18—Control function performance during eclipse (orbit 2413S).

flywheels. Two factors indicate that this was a normal cold cloud-induced disturbance and was not caused by the eclipse:

a. Cold cloud disturbances are common at this orbital position (approaching high noon).

b. HRIR pictures taken at the time of the perturbation show a concentration of clouds on the horizon immediately preceded by a realtively cloud-free area.

Fine Sun Sensors (Yaw Sun Sensors)

Figure 5-19 shows fine sun sensor readings around the North Pole at various β angles. Typical curves are shown for β angles of 10, 5.58, 5, 0, and -1.5 degrees. The data were plotted as the sun angle (angle of the sun with the pitch-roll plane of the spacecraft) varied around zero degrees to verify the accuracy of the fine sun sensor readings. In general, data were selected for minimum evidence of IR disturbances. At the zero sun angle (the position of the maximum accuracy of the sun sensor) and in the absence of yaw errors, the sun sensor reading should approximate the β angle—which it does. This close correlation indicates that the yaw attitude error is less than 1 degree, and that the fine sun sensor is functioning properly.

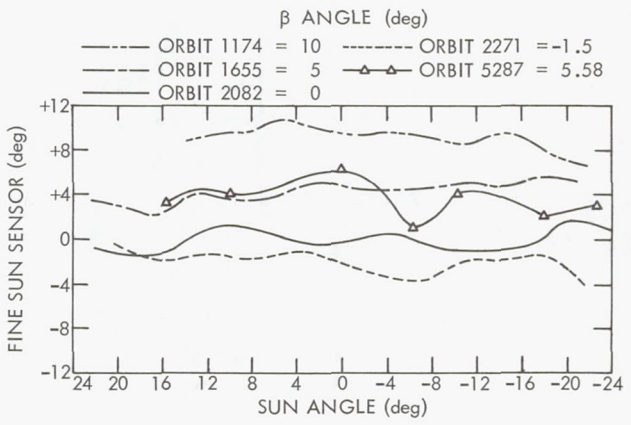

Figure 5-19—Fine sun-sensor readings in North Pole region (at various β angles).

Attitude Error Analysis

A dynamic control system error evaluation (Reference 6), using telemetered data, was made to determine the time distribution of the pitch, roll, and yaw dynamics control system errors for the Nimbus II spacecraft. Figure 5-20 superimposes the results of an independent attitude error evaluation using a method (Reference 7) which employed a photogrammetric film reader-digitizer that could accept reduced Nimbus II AVCS frames. The figure yields good correlation for the yaw axis and reasonably good agreement for roll. The close agreement for yaw is caused by the absence of

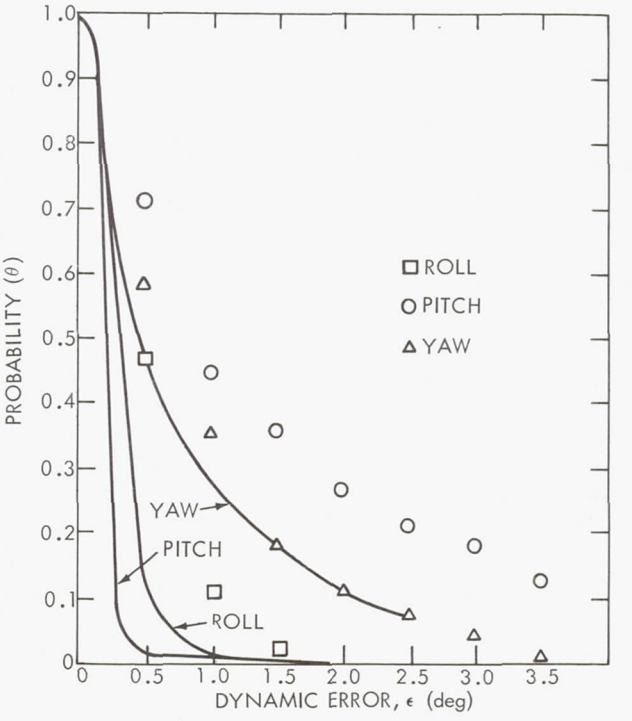

Figure 5-20—Comparison of data with independent evaluation (Reference 7).

time-base errors in the picture evaluation and the relative insensitivity to camera alignment compared to roll. Since determining the pitch attitude error from pictures requires knowledge of an exact orbit position when the picture was taken, a 1-second time error induces a 0.5-degree pitch error. This factor and potential camera misalignment are believed to be the cause of the appreciably higher pitch error variance and means shown by the picture analysis method.

SECTION 6

THERMAL SUBSYSTEM

DESCRIPTION

Functional Description

The Thermal Subsystem controls the heat absorption and rejection rates, maintaining average sensory subsystem structure temperature within 25 ± 10°C. Passive control (coatings and/or insulation) is used on the large areas of the top and bottom surfaces of the sensory subsystem. Active control (movable insulated shutters) is used in the peripheral areas of the sensory subsystem. Figure 6-1 illustrates how thermal balance is achieved.

Physical Description

Passive thermal control uses the absorptivity and emissivity of the external surface to limit the temperature excursion. Between the external surface and the inner volume of the sensory subsystem is insulation in the form of 32 layers of 1/4-mil Mylar, aluminized on both sides to provide high resistance to heat flow. This insulation is described as multibarrier radiation insulation since, in the vacuum of space, the predominant mode of heat transfer is by radiation; conduction contributes a negligible effect. A large temperature difference is required to transfer a small amount of heat because (a) there must be a potential difference for heat to flow, (b) radiant heat transfer occurs as the fourth power difference in the temperatures, and (c) the heat transfer rate is a constant between any two layers. Surfaces that are coated only, and have no insulation, control temperature by limiting the quantity of heat absorbed and rejected. These coatings work in conjunction with the thermal capacity of the components or structure being coated.

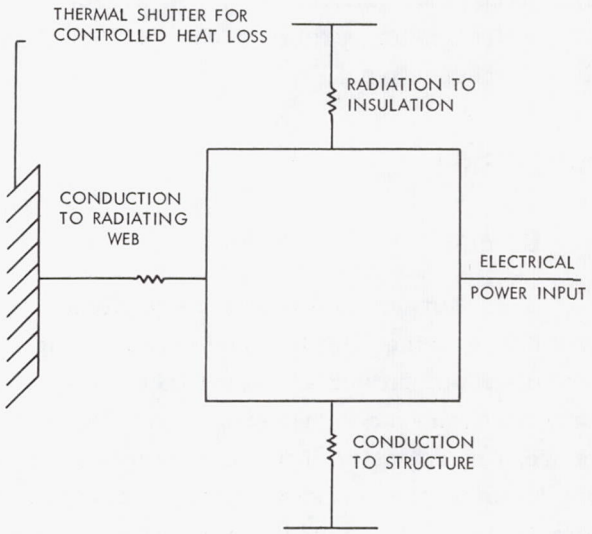

Figure 6-1—Thermal balance schematic.

Active control (Figure 6-2) is provided by sensing component temperature and positioning movable insulation in the form of shutters to increase or decrease the heat rejection capacity.

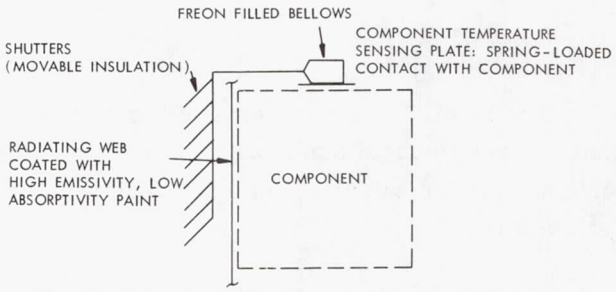

Figure 6-2—Temperature controller schematic.

Behind the shutters are surfaces having high emissivities and low solar (and albedo) absorptivities. The coating and the shutter maximize the heat rejection at full open, but minimize the heat absorption.

FLIGHT OBJECTIVES

The flight objective of the Thermal Subsystem is to demonstrate the ability of the subsystem to maintain the sensory ring and its components within the temperature limits prescribed in Table 6-1. After 6 months, the subsystem performance was excellent, maintaining the average sensory ring and H-frame temperatures at 21.5°C and 23.5°C, respectively. After 12 months, the subsystem continued its excellent performance, with the sensory ring and H-frame temperatures now at 19.1°C and 20.6°C, respectively.

Table 6-1

Sensory Ring Thermal Limits.

Parameter	Temperature Limit (°C)
Structure	25 ± 10
Components	25 (+15, -10)
Day-to-night differential (structure)	10 maximum
Component-to-structure differential	5 maximum
Instantaneous differential in structure	10 maximum

DISCUSSION

General

The Thermal Subsystem has performed in an excellent manner, maintaining temperatures within prescribed limits. The sensory ring and H-frame temperature, following postlaunch stabilization, showed a general increasing trend through approximately orbit 3200; since that time they have shown a decreasing trend (Figure 6-3). This trend is consistent with the increasing and decreasing intensity of the sun because of the orbit of the earth about the sun. Another contributing factor in the decrease in temperature is the inoperative state of the HRIR, HAX, and MRIR Subsystems. This trend is also reflected in the compartment and bay plots presented in individual monthly flight evaluation reports.

Orbital Trends

General

The profile or characteristic temperature of the various bays has remained essentially the same since thermal stabilization. However, the reference level has shifted because of the varying intensity of the sun along with the variations in programming the sensory subsystems within the spacecraft.

Table 6-2 lists the predicted thermal performance of the spacecraft. The thermal performance for a typical orbit in the latest mode of operation is shown in Figure 6-4. The information

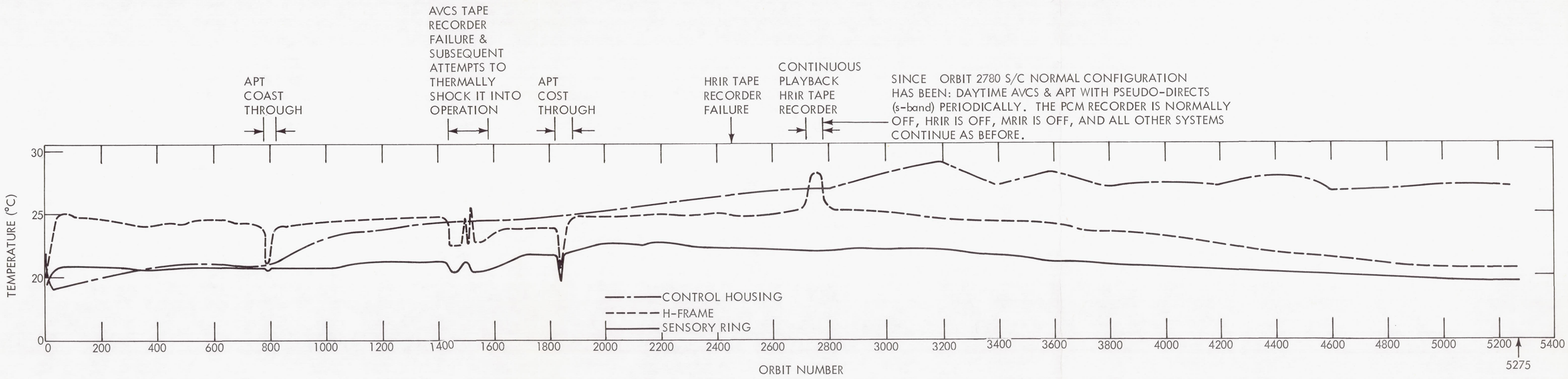

Figure 6-3—Spacecraft thermal performance.

Page Intentionally Left Blank

was derived by selecting data from various orbits between orbits 5275 and 5287, and, by correlation of the SAD shaft position, piecing the data together and extrapolating when necessary to obtain the equivalent of one complete orbit of continuous data. Also shown in Figure 6-4 are the data from the first monthly report. These data are from orbit 46, and the curves agree more closely with the predicted temperatures listed in Table 6-2.

Sensory Ring Structure Temperatures

Average orbital sensory ring temperature varied generally less than 1°C. The average sensory ring temperature for 13 months in flight was 21 ± 2°C.

Center Section Structure Temperature (H-Frame)

Structural temperature variations in the center section are less than 3°C (Figure 6-4). The average temperature difference between the center section and the sensory ring structure was approximately 1.5°C (Figure 6-3). Average center section temperature for 13 months in flight was 23 ± 3°C.

Control Housing Temperature

The control housing temperature has reflected the trend discussed earlier (i.e., a warming trend through orbit 3200 and a trend towards lower temperature since that time). The temperature currently is running at 26.9°C (Figure 6-3) with an orbital variation of ± 1.5°C. The average control housing temperature for 13 months was 24 ± 5°C.

Table 6-2

Expected Thermal Performance of the Nimbus II Sensory Subsystem.

Compartment No.	Expected Temperature (°C)	
	Components	Structure
1	26.0	23.0
2	27.0	24.0
3	25.0	22.0
4	25.7	22.0
5	26.0	22.0
6	25.5	21.0
7	25.0	22.0
8	23.0	21.0
9	23.5	22.0
10	24.0	22.0
11	24.0	22.0
12	25.0	23.0
13	25.0	22.0
14	29.0	25.0
15	25.0	22.0
16	23.5	21.0
17	23.0	21.0
18	24.0	22.0
Center section:	—	27.0 (avg)
HRIR recorder	24.5	—
AVCS recorder	26.0	—
AVCS camera	25.0	—
APT camera	44.0 (max)	—
External:		
HRIR radiometer	11.0	—
MRIR radiometer	23.0	—

Temperature Controller Performance

The performance of the temperature controllers was about as expected (Figure 6-4). The inherent characteristic of lagging behind the temperature increase within the compartments is clearly illustrated in Compartments 3, 5, 8, and 11. Temperature control has been maintained

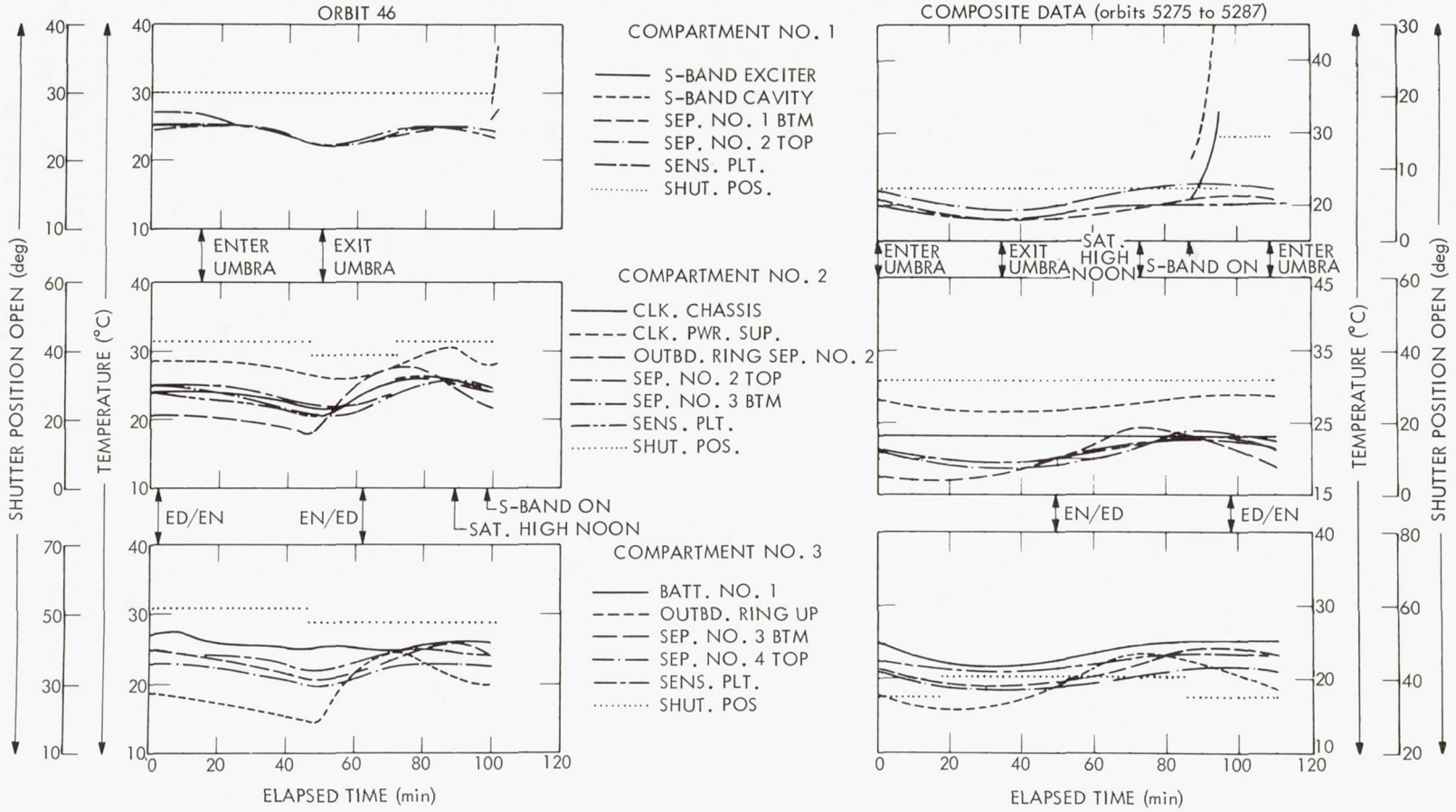

Figure 6-4—Comparison of orbital temperature histories of sensory-ring structure and components (orbit 46 and composite data from orbits 5275 to 5287).

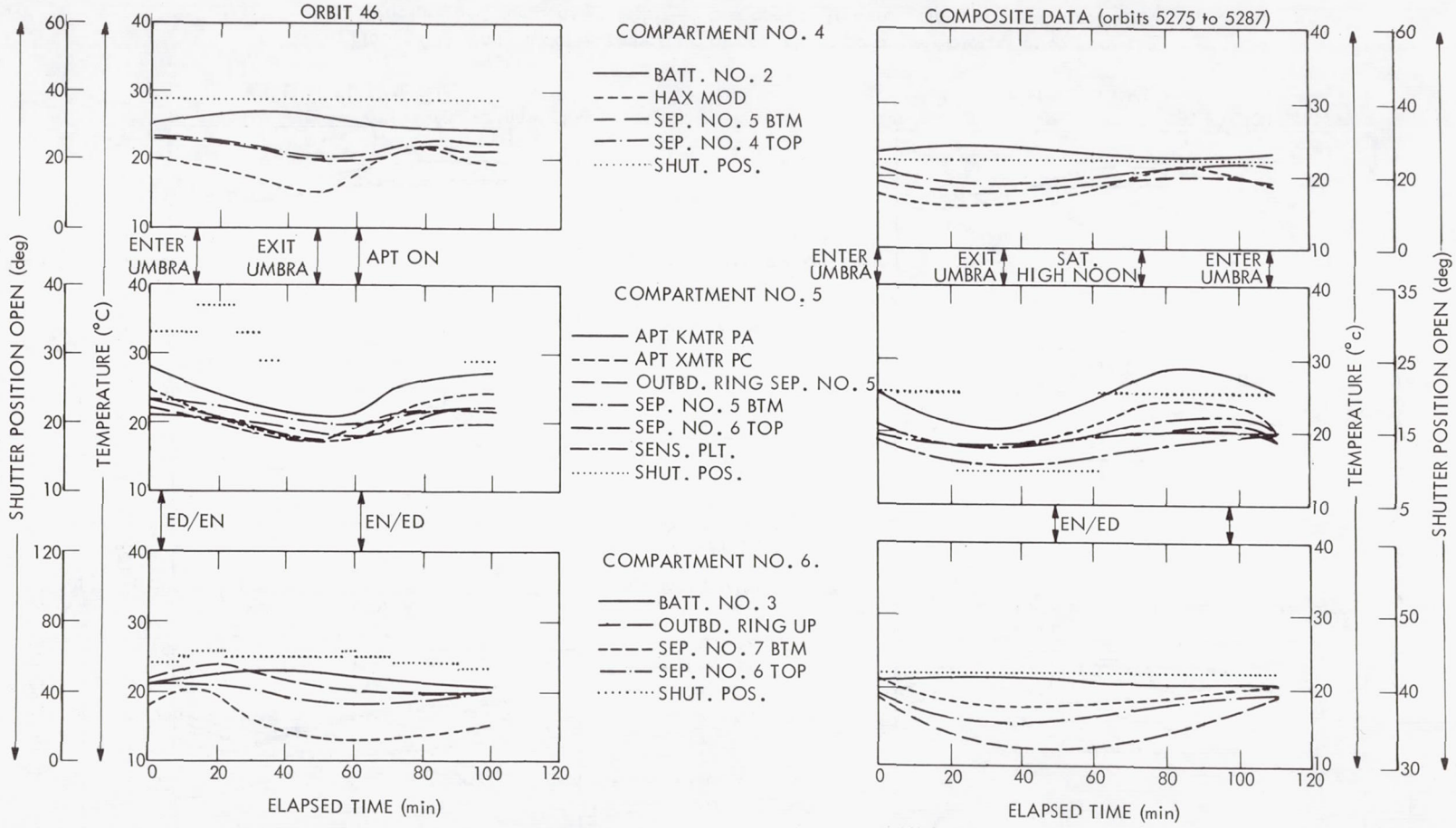

Figure 6-4 (continued)—Comparison of orbital temperature histories of sensory-ring structure and components (orbit 46 and composite data from orbits 5275 to 5287).

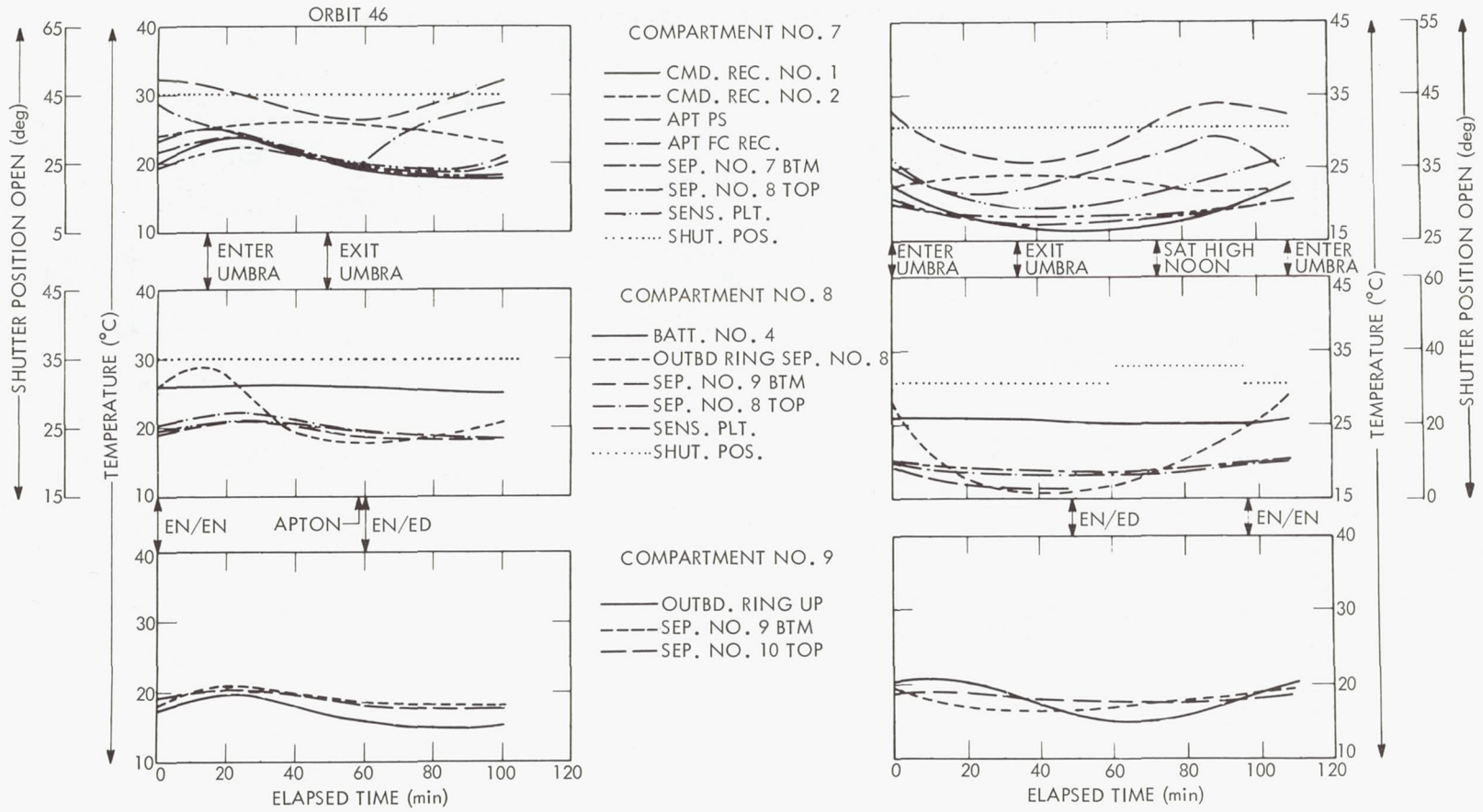

Figure 6-4 (continued)—Comparison of orbital temperature histories of sensory-ring structure and components (orbit 46 and composite data from orbits 5275 to 5287).

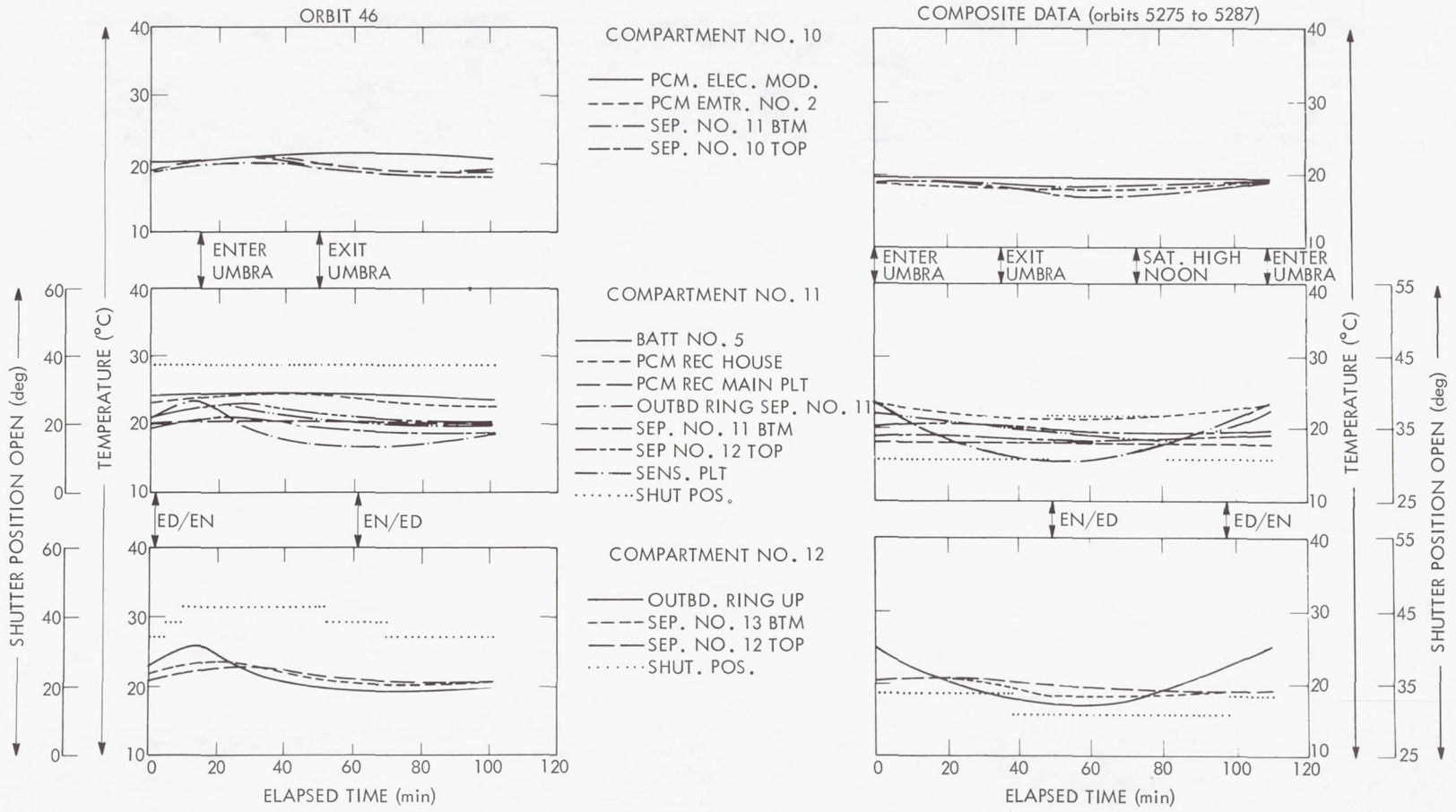

Figure 6-4 (continued)—Comparison of orbital temperature histories of sensory-ring structure and components (orbit 46 and composite data from orbits 5275 to 5287).

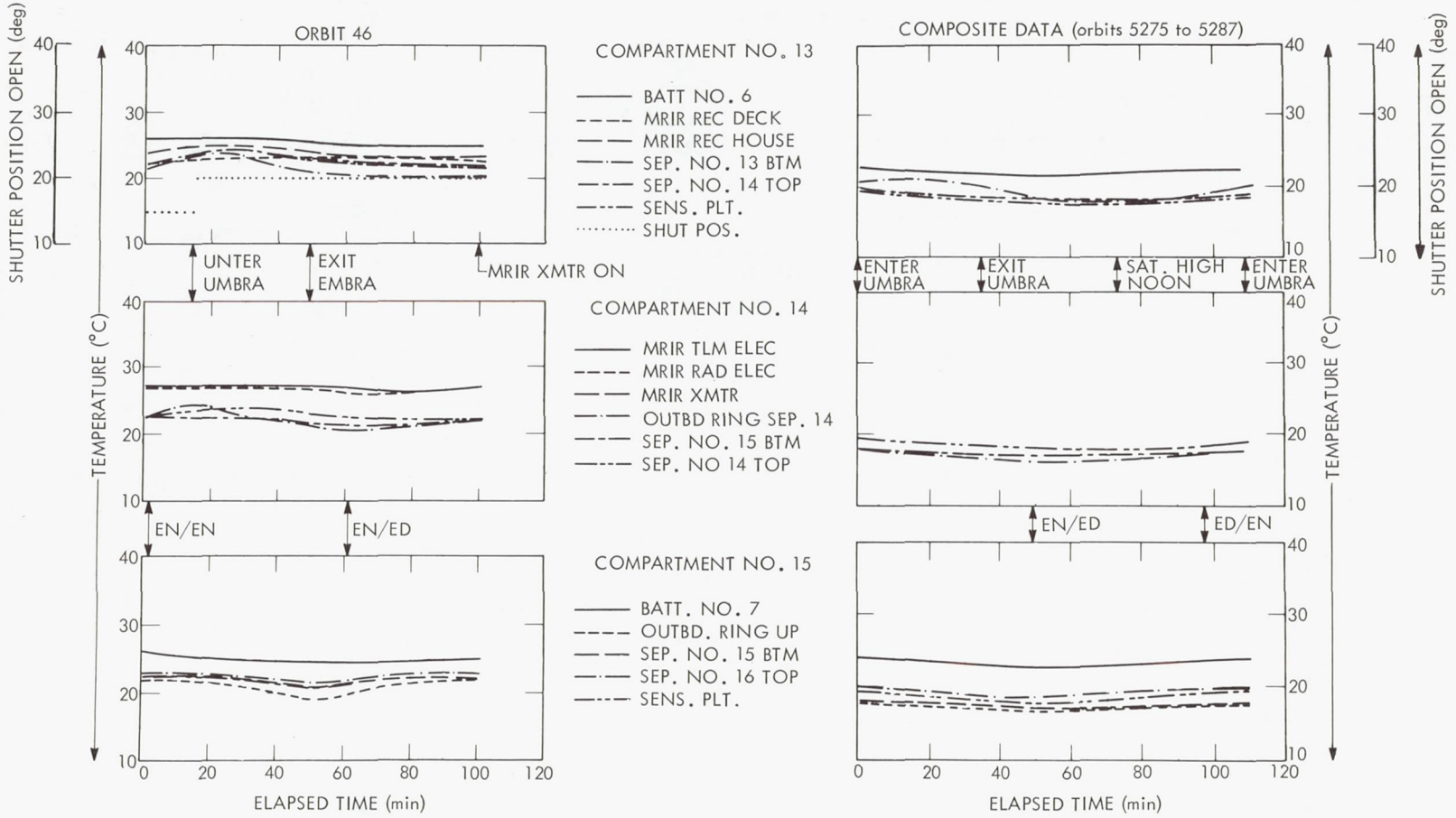

Figure 6-4 (continued)—Comparison of orbital temperature histories of sensory-ring structure and components (orbit 46 and composite data from orbits 5275 to 5287).

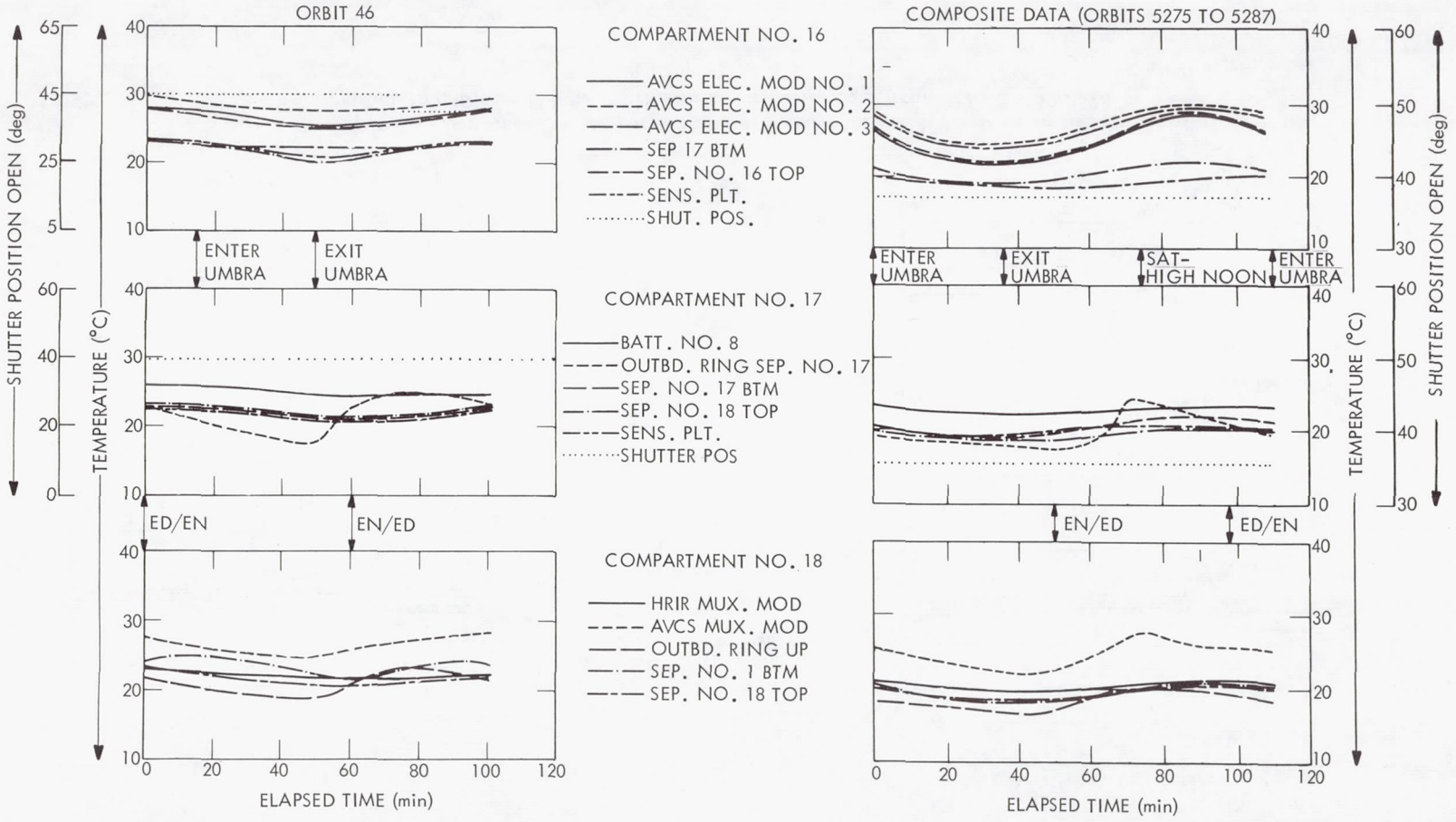

Figure 6-4 (continued)—Comparison of orbital temperature histories of sensory-ring structure and components (orbit 46 and composite data from orbits 5275 to 5287).

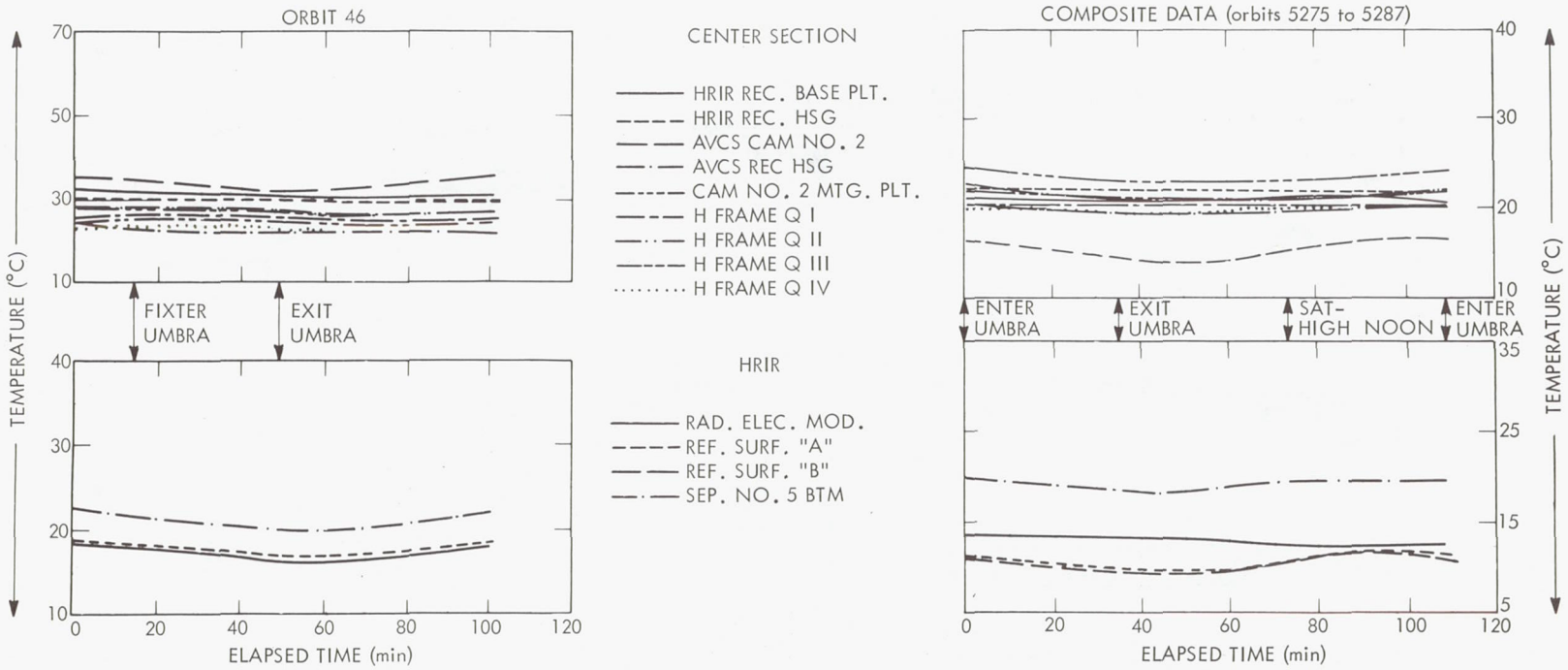

Figure 6-4 (continued)—Comparison of orbital temperature histories of sensory-ring structure and components (orbit 46 and composite data from orbits 5275 to 5287).

within the specified limits of 25 (+15, -10) °C. However, the telemetry resolution of the shutters (temperature controllers) does not allow thorough analysis of performance.

Investigation of the early orbits of the Nimbus II flight revealed battery no. 7 temperatures and sensing plate no. 15 temperatures to be normal; that is, they gradually warmed up from 17.0 to 23.5 degrees and 15.75 to 20.16 degrees, respectively. However shutter no. 15 indicated possible erratic movement with positions ranging from 10.08 to 25.6 degrees and back to zero degrees, allowing no apparent correlation with the sensing plate temperature. In orbits 12 through 34, the same trend appeared, with battery and sensing plate temperatures slightly warmer and more consistent, indicating normal shutter operation. Battery no. 7 has been one of the coolest batteries; if the shutter was closed, it would certainly be much warmer. Digitized listings of shutter no. 15 position on orbit 34 in both engineering units and PCM counts verified the computer output. It was therefore concluded that shutter no. 15 position monitor failed in the open position, followed by occasional intermittent shorting. This condition continued throughout the flight.

Telemetry indicated that shutter no. 13 was malfunctioning, beginning with orbit 792. Random position indications were telemetered by the shutter's position monitor. However, correlatable temperatures (battery no. 6 and sensing plate no. 13) were checked and found to be normal. It was concluded therefore that this monitor failed similarly to shutter position monitor no. 15.

Improper Cooling of HRIR Detector Cell

The HRIR detector cell, after stabilizing postlaunch at approximately -76°C, exhibited a warming trend. The temperature after orbit 380 was -68°C. Following the tape recorder failure, the nominal temperature has been -66 ± 1°C. This anomaly is discussed further in Section 11.

AVCS Camera No. 2 Temperature Telemetry Malfunction

The camera no. 2 temperature telemetry point exhibited erratic performance. Initially this sensor read higher than expected. However, during the 10th month in orbit, it showed a marked decrease (Reference 8). This was attributed to an electrical malfunction in the telemetry conditioning circuitry or a mechanical degradation of the thermal bond between the temperature sensor and the camera housing.

Thermal Performance of MRIR Subsystem

Before failure, the MRIR Subsystem thermal performance was essentially as expected. Since that time the subsystem followed the general trend exhibited by the spacecraft (Table 6-3).

Table 6-3

MRIR Subsystem Thermal Performance.

Function	Orbit 984 (normal operation)	Suspended Operation					
		Orbit 1629	Orbit 1922	Orbit 3679	Orbit 3459	Orbit 4810	Orbit 5252
Recorder housing temp.	21.2	16.4	17.0	17.0	17.0	15.9	14.8
Radiometer housing temp. 1	19.4	16.2	16.9	16.9	16.9	15.0	14.1
Radiometer housing temp. 2	22.7	20.7	21.3	21.3	21.3	19.3	18.7
Recorder deck temp.	24.6	22.7	22.7	24.0	23.1	20.9	20.1
Chopper temp. 1	18.1	14.0	15.0	15.0	14.5	13.5	11.5
Chopper temp. 2	18.1	14.1	15.0	15.0	14.5	13.6	11.8
Radiometer electronics temp.	23.7	21.2	21.2	23.1	22.5	19.4	18.3
Recorder housing temp.	24.0	21.3	21.3	24.0	23.3	20.7	19.3
Transmitter temp.	*19.4	*17.5	N/A	*18.7	*18.1	*18.1	16.9
Recorder pressure (psi)	14.9	14.9	14.9	14.9	14.9	14.9	14.9

*Temperature of transmitter at turn-on.

SECTION 7

COMMAND SUBSYSTEM

SUBSYSTEM OPERATION

The Nimbus II Command Subsystem has operated successfully for the entire 13-month flight. Two types of problems were encountered, however, neither of which actually affected spacecraft operation. One problem was noise entry into the clock memory, resulting mainly in erroneous data in the APT Subsystem data code grid. The second problem was the large number of unencoded command executions, resulting in the switching of the primary and redundant receiver FM demodulation selector relay and the switching of the power supply feedback amplifier selector relay (see Table 7-8).

FUNCTIONAL DESCRIPTION

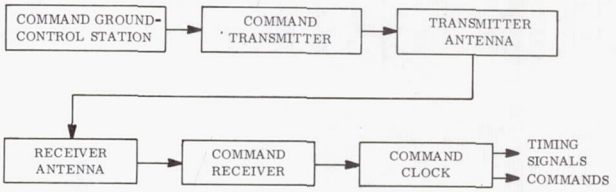

Figure 7-1—Command subsystem block diagram.

The Nimbus II Command Subsystem (Figure 7-1) consists of a command clock, a command receiver, and a receiving antenna located in the satellite and a command control station, a transmitter, and a transmitting antenna located on the ground. The Command Subsystem provides signals for synchronizing all Nimbus subsystems relative to each other and generates and executes commands for controlling the operation of each subsystem in absolute, universal time. The latter capability allows the spacecraft to be controlled according to its orbital position.

Command Receiver

The Command Receiver is a VHF superheterodyne receiver operating at 149.5 MHz and requiring no control other than application of -24.5 volts electrical power. It receives and demodulates command information transmitted from the ground station. In addition to encoded digital command information (W, X, and Y channels), the receiver is capable of demodulating three unencoded commands that are transferred directly (not via the Command Clock) to certain Nimbus subsystems. These unencoded commands are transmitted as audio tones that amplitude-modulate the VHF carrier. The threshold of the receiver is 1 microvolt with an 80-db dynamic range.

The Command Receiver consists of two major subassemblies; an RF receiver subassembly and a demodulation subassembly (Figure 7-2). The receiver assembly consists of two receivers operating in parallel from a common antenna. The demodulation assembly consists of two identical audio amplifiers, each fed by an RF receiver, two switchable FM demodulators, and one AM demodulator. The FM demodulators process the encoded commands and provide this information

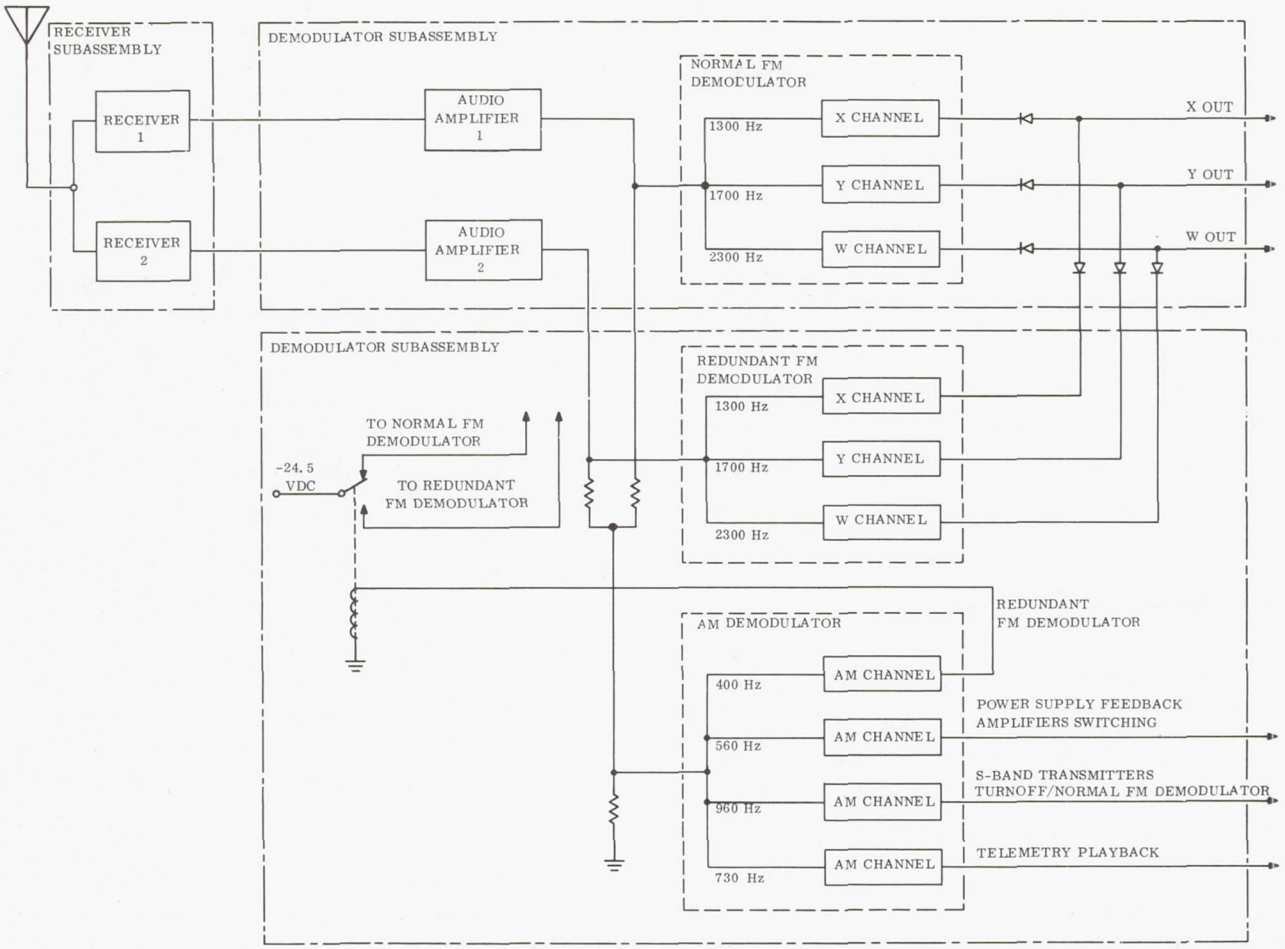

Figure 7-2—Command receiver functional block diagram.

to the Command Clock. The particular FM demodulator to be used is selected by an unencoded command. The AM demodulator processes the unencoded commands.

Command Clock Functional Description

The Nimbus II Command Clock serves a dual purpose: (1) generation of timing signals and (2) processing, storage, and execution of commands. The Command Clock (Figure 7-3) is a space-borne, solid-state electronic package designed to provide Minitrack time code and stable, coherent frequencies for use by other subsystems. A 3.2-MHz oven-controlled crystal oscillator, with a long-term stability of better than 1 part in 10^6, provides the signal source from which the clock time is generated. Time generation and accurate frequency standards are provided through flip-flop division and delay line storage. The clock also provides command signals that activate relay devices associated with other subsystems of the satellite.

The clock accepts command inputs through three synchronous radio command channels (W, X, and Y) from the ground station via the satellite clock receiver. This information, transmitted

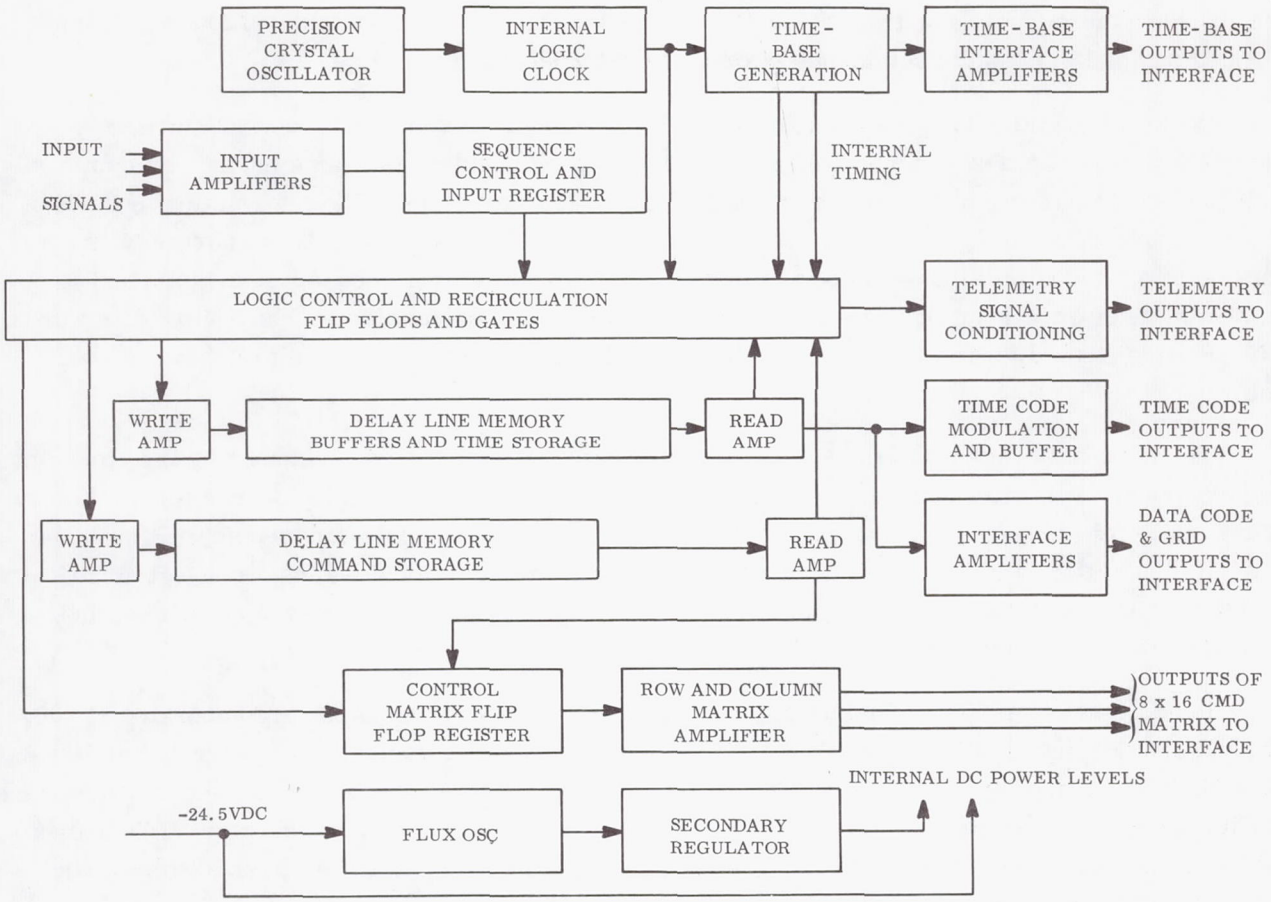

Figure 7-3—Command clock functional block diagram.

in digital form, contains the command intelligence (channel W), bit sync (channel X), and character sync (channel Y). The clock sequence control section enables a ground control station operator to load into the clock commands necessary to drive the various satellite relay devices.

Entry to the command sequencing section of the Nimbus II clock is protected by a key included as part of the command structure. The key that applies to a particular clock must be selected at the time the vehicle harness is wired. By proper selection of key codes, command interference between spacecraft can be eliminated.

Each command sent to the vehicle also includes information that determines the time when that command is to be executed. After receiving the command data, the sequence control buffers these data into the timer loop where they remain until they can be transferred to the memory loop. After the command and command time information have been stored in one of the 16 memory locations, the stored command time information (i.e., seconds, minutes, hours) is compared with the real time word in the timer loop. The timer loop real time contains all readable portions of time (i.e., units of seconds through hundreds of days) and is continually advanced in 1-second increments. When the command time agrees with real time in the timer loop, the command portion of

the word in the memory location will be transferred to the command matrix section, which then issues one of 128 possible commands to drive an associated relay device.

Of the 16 memory locations, 12 are normally reserved for commands, and four are reserved for data words. Data words are loaded into the Command Clock in the same manner as commands, with location instructions to place them in the proper four locations. The information in these four specific data word locations is for presentation on the data code output and normally is not accessible for command time search. However, it is possible by ground-encoded command to make the data word locations accessible, creating a total command storage capability of 16 words. The four data word locations (locations 12 through 15) in the memory are referred to as "cold storage."

The time-base section is the source of the precise frequency standards used by the clock and other subsystems throughout the satellite. It serves as the basic frequency source for the binary time code, coherent frequency standards, and synchronous motor drive frequencies. Binary time code is generated in standard Minitrack (pulse-width modulated) form and as a non-return to zero (NRZ) digital signal in Minitrack code. Two of the frequency standards generated by the clock (10 and 50 kHz) are modulated by the Minitrack time code.

In addition to the 10 and 50-kHz signals, coherent frequency standards are generated at 200, 5, and 2.4 kHz and at 500, 10, and 1 Hz. Two-phase motor drive voltages are generated at 100 and 400 Hz. There are five drive lines at each frequency and phase. The time-base section, by means of its flip-flop registers, defines the clock word and bit rate of the clock subsystem. The Nimbus II clock also provides two signals called data code and grid (DCG) to the APT Subsystem for adding time gridding information to the transmitted APT data.

FLIGHT OBJECTIVES

The flight objective of the Command Subsystem is to demonstrate the ability of the subsystem to receive, store, and execute encoded commands properly and consistently and to receive and execute unencoded commands. At 6 months, only two problems had been encountered and these did not affect spacecraft operation: noise entering the clock caused errors in the DCG data, and some unencoded commands were executed unintentionally. Clock stability was excellent, with an average gain of 1.15 milliseconds per orbit. After 12 months, the subsystem continued to operate exactly as it did at 6 months.

RESULTS OF FLIGHT OPERATION (LAUNCH THROUGH ORBIT 5275)

Overall operation of the Command Clock Subsystem has been successful. The clock provided proper reference frequencies and phasing for other spacecraft subsystems, as well as excellent time stability. The clock has shown an average gain of approximately 1.15 milliseconds per orbit, or approximately 1.75 parts in 10^7—well within the specification for time stability, 1 part in 10^6. The command section was properly enabled at separation and continued to receive, load, and

execute all commands properly throughout the flight. Problems which have been encountered are described in detail in the following subsections.

COMMAND RECEIVER OPERATION

Unencoded Command Executions

The Command Receiver has proved to be much more sensitive than expected, particularly in relation to the unencoded command channels. Unencoded command executions have occurred without apparent receiver input as indicated by telemetry, while others have been associated with very strong receiver input activity. These spurious commands have not affected spacecraft performance, although on two occasions, a U960 command resulted in a premature termination of S-band playback during orbits 346 and 909. In both cases, the S-band transmitter was turned off, and the AVCS and HRIR tape recorders continued to playback to the end of tape. During orbit 346, both the Rosman, North Carolina, and Fairbanks, Alaska (Ulaska), DAF stations had their transmitters up, and it is probable that a beat frequency of approximately 960 Hz was generated and interpreted by the Command Receiver as a U960 command.

While A-stored data were available during the first 2 months of operation, a plot was maintained of the geographical locations of the unencoded command executions (Figure 7-4). Since many of these unencoded commands were executed in the general vicinity of northern South America, a standard operational procedure was developed whereby the STADAN stations at Quito, Ecuador; Santiago, Chile; and Rosman, North Carolina radiated an unmodulated carrier whenever the spacecraft was in range of these stations. There was no instance of unencoded command execution with any single station transmitting an unmodulated carrier. However, to avoid unwanted command executions caused by beat frequencies between two carriers, a 30-second interval was provided between the transmission end time for one station and the transmission start time for the next station. There were several instances of unencoded command executions during these 30-second intervals. This procedure was begun May 20 and terminated November 15, 1966. A summary of observed unencoded command execution is presented in Table 7-1.

Table 7-1

Summary of Observed Unencoded Command Execution.

Unencoded Command	Number of Observed Executions
U400	48
U560	140
U960	58
Total	246

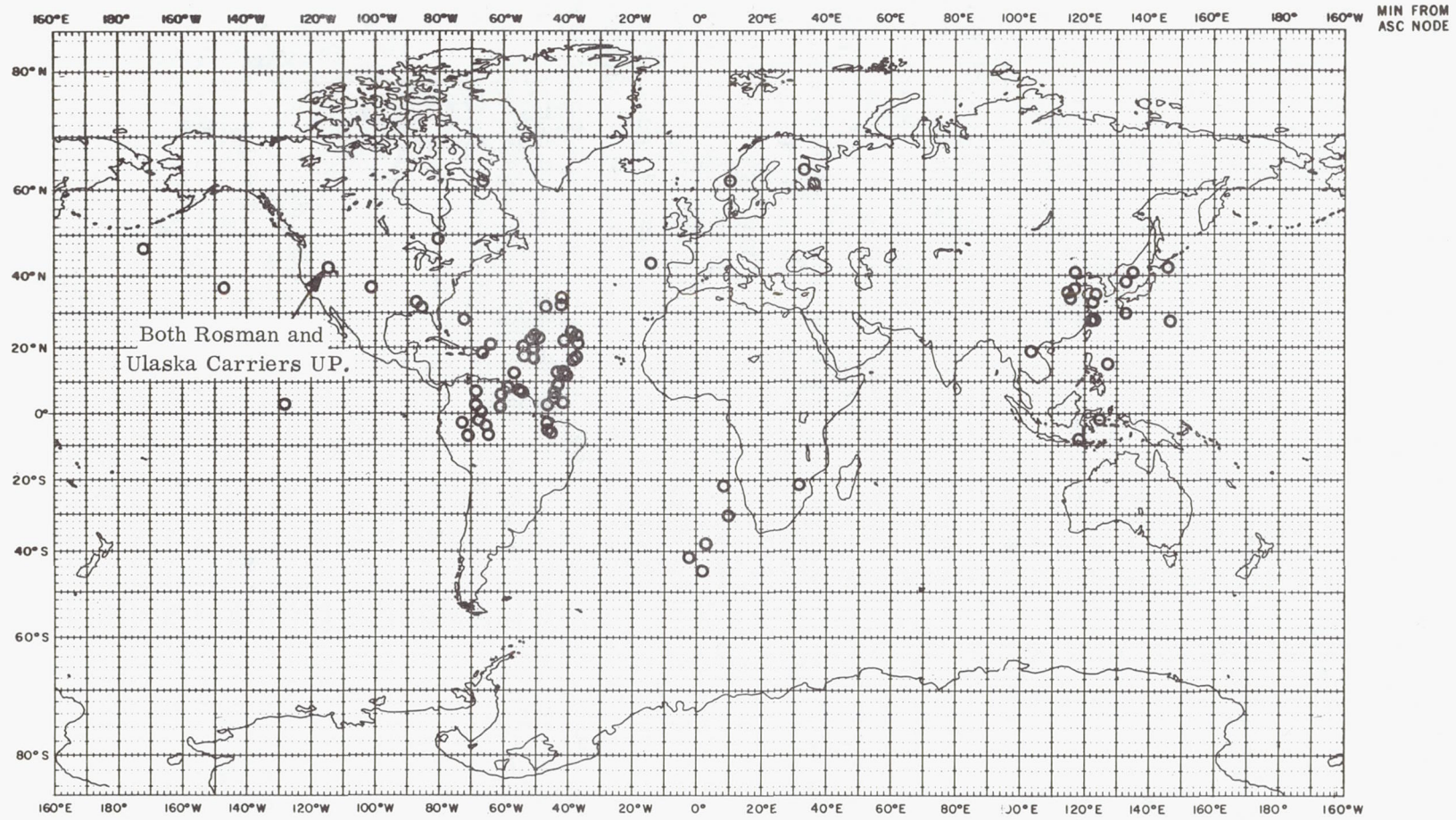

Figure 7-4—Geographic locations of unencoded command executions.

This record may be considered incomplete because only real-time data have been available since the PCM recorder failure in orbit 949. In the last several months of operation, it has been standard procedure to command the spacecraft using the redundant FM demodulator; consequently, only U960 commands have been observed.

Command Receiver EMI

The Command Receiver experienced considerable interference when either the APT or HAX Subsystems was operating. This interference was observed on the Command Receiver output telemetry channels and on the clock input amplifier telemetry channels. It was most noticeable on channel W. This was to be expected because the receiver input channels are 1.3 kHz ± 7.5%, 1.7 kHz ± 7.5%, and 2.3 kHz ± 7.5%, while the APT subcarrier spectrum is 2.4 ± 1.6 kHz; and the HAX subcarrier spectrum is 2.4 ± 1.2 kHz. The video-modulated subcarrier from the APT and HAX subsystems contains sidebands that can be similar to the modulation used for commanding. This type of interference was not experienced during the spacecraft ground test phase because it was rarely, if ever, tested with the Command Carrier off. This interference will be experienced as long as the APT Subsystem is operable.

Suspected Redundant FM Demodulator Problem

During several periods of the Nimbus II flight, a problem was thought to exist with the redundant FM demodulator. In most instances, where verification tones were not received after command transmissions, they appeared to be associated with use of the redundant FM demodulator. Several tests were performed at different times during the flight to try to determine whether such a problem actually existed.

Command Receiver outputs were checked by sending a series of logical 1's to the X, Y, and W channels of each FM demodulator. Results indicated that the command receiver outputs were normal. The operation of the entire Command Subsystem was checked by sending a series of 60 "TAC" (376 and 100) commands through the FM demodulators at 1-second intervals. Commands were then verified on the TMMDC (clock matrix drive current) telemetry, indicating that the subsystem was operating properly.

The point at which commands ceased to be executed was plotted for each FM demodulator and for both command stations. A series of "TAC" commands was sent, and the corresponding slant range of the spacecraft determined by noting the time of the last command executed. Table 7-2 summarizes the results, which indicate that although the spacecraft could be commanded as far away as 3900 km, commands failed to enter the clock as close as 1500 km. The tests showed no conclusive evidence of a redundant receiver problem; when command problems occur, they apparently independent of the receiver in use.

Table 7-2

Command Dropout Points.

Station	FM Demod.	Approx. Maximum Range, No Cmd. Problem (km)	Approx. Minimum Range, Cmd. Problems (km)
Ulaska	N	3900	1700
	R	3900	1500
Rosman	N	3900	2300
	R	3900	2300

COMMAND CLOCK OPERATION

Clock Time Reference

Except for two clock upsets, the Nimbus II Clock provided excellent time reference and stability.

Clock Upsets

The first clock upset occurred at the time of spacecraft/Agena separation as anticipated. A high-speed Visicorder chart was used to extract telemetry data in raw form from the Johannesburg real-time data tape for this time period. No significant transients in regulated bus current or voltage was observed. However, the low sampling rate of the spacecraft telemetry in all probability precluded observation of transients. The short duration of the voltage transient is further substantiated by the fact that feedback amplifier switching did not appear to have occurred. The transient at unfold squib-firing was probably a damped oscillation of insufficient duration to cause switching, as was the situation for orbit 28U (Figure 7-5).

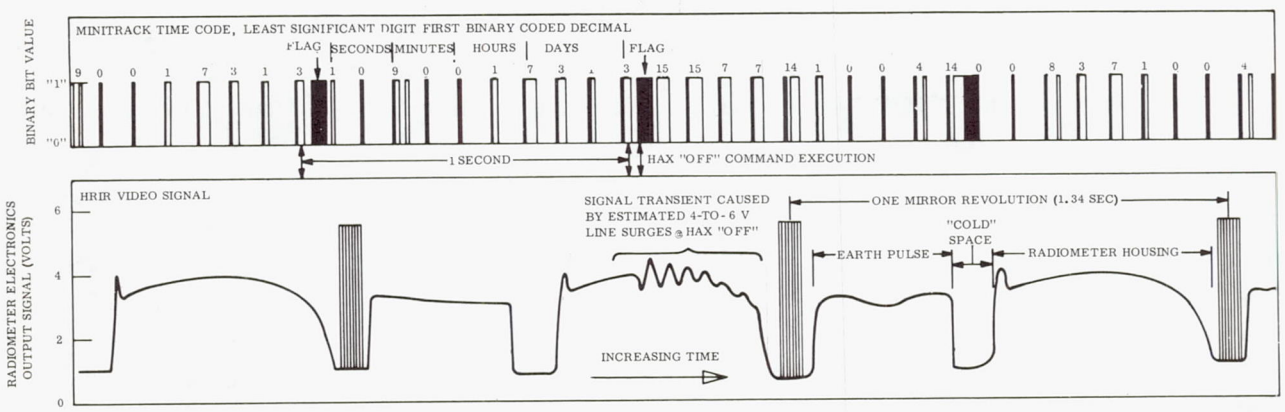

Figure 7-5—Visicorder record of HRIR video signal and minitrack time code at HAX turn-off (Ulaska-station pass orbit 28).

Examination of the visicorder chart revealed two separate clock upsets. There is some ambuguity in the possible time of the first upset, but it could have happened up to 2.23 seconds before the second upset. At the time of the second upset, word 608 or 609 disappeared from the PCM main frame; the station data character changed from its proper "3" to "10" for one readout, then shifted to "0" for the remainder of the chart. Clock and multicoder upsets were expected because of power transients at squib firing (Reference 9). The separation monitor indicated two samples at 2.5 TMV between the clock upsets. These facts indicate that the 2.5-second timer operated at approximately 2.2 seconds and successfully initiated the paddle-unfold sequence.

Another clock upset occurred during the Ulaska station pass on orbit 28. Subsequent investigation showed that the upset coincided with the time of execution of a HAX OFF command. At this time, the AVC Subsystem was ON and the S-band was warming up. A Visicorder readout of the HRIR video signal showed a 1-volt peak-to-peak transient in the 4-volt signal-level with a damped oscillation having a 60-msec period and visible for a 0.4-sec duration. The time code was disrupted, showing several "14" digits in the binary-coded-decimal (BCD) signal (Figure 7-5). An operational procedure was developed to preclude a HAX OFF switching event during S-band operation. A clock time upset also occurred during the thermal-vacuum test phase on February 19, 1966. This "upset" was also caused by execution of HAX OFF command (Reference 9).

Clock Stability

The Nimbus II clock stability has proved excellent throughout the flight, the clock has showed an average gain of approximately 1.15 milliseconds per orbit over the entire flight, or approximately 1.75 parts in 10^7. This is well within the specification for the time stability of 1 part in 10^6. Table 7-3 and Figure 7-6 summarize the operations performed on the spacecraft clock time. With the exception of the two upsets, the time set has always been 1 second.

Table 7-3

Summary of Clock Time Operations.

Orbit	Clock Time Command
1	312 - time set (after clock jump)
28	312 - time set (after clock jump)
41	316 - minus 10 milliseconds (7 commands transmitted)
286	316 - minus 10 milliseconds (10 commands transmitted)
298	316 - minus 10 milliseconds (20 commands transmitted)
535	312 - time set
1415	312 - time set
2285	312 - time set
3106	312 - time set
4024	312 - time set
4876	312 - time set

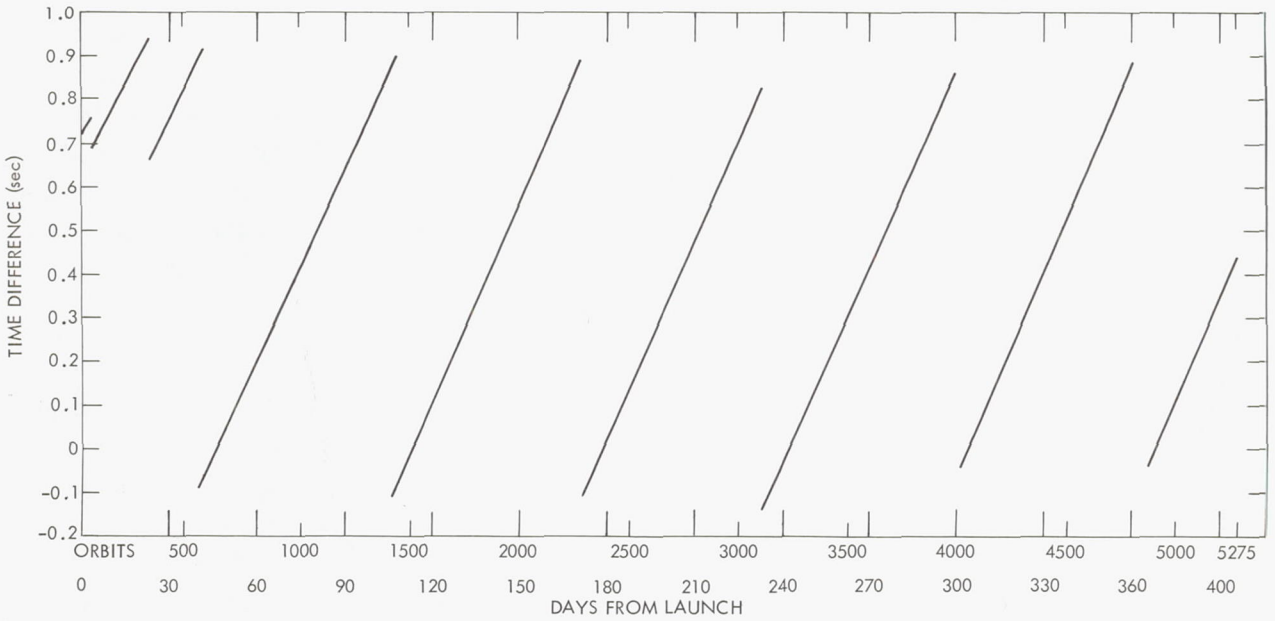

Figure 7-6—History of spacecraft clock/ground-time difference.

Clock Frequency Reference

The Nimbus II clock has continually provided proper reference frequencies and phasing, both for internal clock use and for other subsystem operations. Two types of anomalies were noted; however, neither of them seriously affected spacecraft operation.

A discrepancy observed on several occasions has been a shift in the "beat pattern" between the PCM sampling rate and the clock 1-Hz and 10-Hz telemetry monitors. Although this pattern should remain unchanged, shifts from a pattern containing four "0" values to a pattern containing four "1" values and vice versa sometimes occurred. This discrepancy has been observed to happen only in the period between the start and end of PCM playback and generally when the S-band transmitter is on and regulated bus power demands are high. Analysis of the A-real time data from several orbits has revealed a 2-millisecond "jump" in the PCM multicoder during A-stored playback. This jump does not occur consistently, and no correlation has been found with any other spacecraft events. This is not a clock problem because any change in the 1-Hz or 10-Hz signals would appear as discrepancies in the clock time. A possible explanation for this anomaly is that an extraneous shift occurs in the PCM logic, which counts down from the clock 500 Hz to provide multicoder sequence timing. A shift of 2 milliseconds or an odd multiple of 2 milliseconds would cause the change observed in the 10-Hz and 1-Hz telemetry patterns.

The Data Code and Grid has exhibited on several orbits a "dog leg" pattern (Figure 7-7). This pattern results from the phasing between the clock 1-Hz signal and the APT sequence timer when the APTS is turned on by the day/night switch. Whenever the APT Subsystem is turned on, the sequence timer starts to cycle. This sequence timer uses the 2400-Hz signal from the clock and a countdown chain to generate the internal timing for the APT Subsystem. The Z-7 sync pulse is also generated by the APT for use in the clock to start DCG readout. The Z-7 sync pulse duration

is exactly 8 seconds; after it has ended, the clock will start to read out the Data Code and Grid, starting at the next time that the clock coarse time word is updated by the 1-Hz signal. Consequently, there is a phase difference between the APT sequence timer and the clock 1-Hz signal, between 0 and 2399/2400 second. Thus, when the 1-Hz signal triggers the DCG output flip-flops in the clock and loads new bits into the output flip-flops, the APT Subsystem may be any place in its horizontal sweep. The dogleg pattern on the DCG, therefore, is nothing more than the DCG output flip-flop being triggered to load a new bit. This action will be seen only when the phasing is such that the output flip-flop is loaded in the 12.5-millisecond period of each horizontal scan during which the APT Subsystem reads out the DCG.

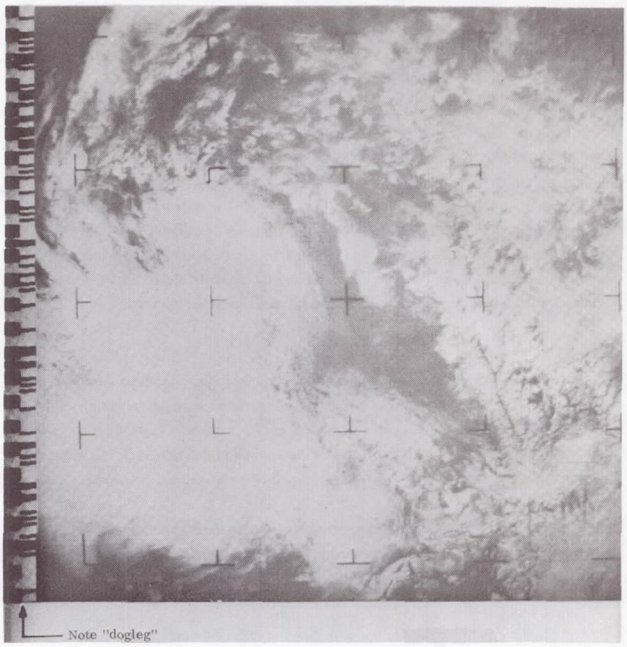

Figure 7-7—APT subsystem photograph showing "dogleg" in the data code and grid.

Noise Entry into Clock Memory

The encoded command logic is apparently susceptible to false triggering. The entry of noise into the clock memory has proven to be the only potentially serious problem with the Nimbus II clock. The specific mechanism of the noise entry into the clock memory is as follows. The EMI experienced by the Command Receiver causes the receiver to provide input signals to the clock. The clock interprets these input signals as command information. The clock will sample the W and Y input channels whenever the X channel input makes a transition from the "1" level to the "0" level, or vice versa. However, there are two points which should be noted. First, the W channel input may change between the "0" and "1" levels many times (or not at all) between each X channel transition and thus may be at either level at the time of an X transition. The second point is that the X transitions need not occur at any fixed frequency, but may vary in frequency between 0 and 2.4 kilobits. The clock will accept information at any rate from 0 to 2.4 kilobits per second.

As long as there is no input to the clock on the Y channel, the W channel information will be shifted into the input buffer as the X transitions occur. Without an input on the Y channel, the clock will make neither parity nor character checks. Thus, if the Y input channel remains at the "0" level, only 48 bits are required to fill the input buffer. If the key and "instruction" characters of this bit sequence are both correct, the contents of the input buffer will be shifted into the clock memory without any further checks being performed. The key character may be a BCD "7", "9", or "15" because only the three least significant bits of the key character are checked, and, in the absence of a Y channel input, neither parity nor character checks are performed. The "instruction" character of the bit sequence must contain the correct 4-bit pattern. There are three legitimate instruction codes.

Even with an occasional Y channel input to the clock, it is possible for spurious data to enter the clock, because the parity and character checks are performed only for the 4-bit "character" contained in input buffer no. 1. This character can be any four bits in the sequence of bits being shifted into the input buffer. In other words, any number of bits between 0 and 44 may have been already shifted into the input buffer, but only those bits contained in input buffer no. 1 and the W bit received at the time the Y bit is detected will be checked for parity. If the parity is incorrect, the input buffers will be cleared. If the parity is correct, the clock will then check the character in input buffer no. 1 for a proper "0" to "9" value. If this check detects an illegal character value, the input buffers will be cleared. However, if the character check is good, the clock will continue to shift bits into the input buffer without clearing the buffers. When 48 bits have been shifted into the input buffers, the clock will then check the "instruction" and "key" characters; and, if these are good, the input buffer contents will be shifted into the clock memory.

To investigate this anomaly more fully, an operational procedure was devised to reveal which memory locations were being entered. The procedure was to fill memory locations 1, 2, 3, and 0 with commands at the end of each pass for execution at the beginning of the next pass. (The last memory location filled was to be location 0.) At the beginning of the next pass, these stored command executions were to be verified on the matrix drive current telemetry channel, and then a command tape containing 11 "TAC" commands was to cycle through the memory locations to reach memory location 11. A command entered in memory location 11 results in a double command verification tone because the command is entered into both memory locations 11 and 0.

As noted above, this procedure was designed to indicate specifically which memory location was being entered. If location 0 were entered, then the stored command in location 0 would not be executed. If locations 1 and 2 had been entered, the stored commands in these locations would not be executed, and the number of unaddressed TAC commands required to be sent to obtain the double command verification tone would be less than 11. For example, if location 1 and 2 had been entered, only nine unaddressed TAC commands would be required to cycle through to location 11. If memory location 12 had been entered, the stored commands would be executed, but the number of unaddressed TAC commands required to cycle through location 11 would be greater than 11. For example, if memory locations 12 and 13 had been entered, then 14 unaddressed TAC commands would be required to obtain the double command verification tone.

This procedure was followed, and the results from orbit 525 to orbit 775 were recorded. A list of the three legal instruction characters and the number of times each was observed to have occurred is shown in Table 7-4. Experience has shown that memory location 12 has been most susceptible to noise, although memory locations 0, 1, 2, and 13 have also been affected.

Operationally, the only action that could be taken to minimize improper command storage was to keep the command sequences as "safe" as possible by not storing commands in memory locations 0, 1, and 2, and by keeping the cold storage memory locations "frozen." A similar procedure was followed between orbits 3200 and 4000. TAC commands were stored in locations 1 and 2 to determine how often these locations were entered by noise. On 54 separate occasions, one or both of these TAC commands were not executed because of noise entering the memory and erasing the

stored commands. Specific noise entry problems in the clock memory are described in subsequent sections.

Table 7-4

Legal Instruction Characters.

Enter Code	Instruction Code	Binary Equivalent	No. of Times Observed
Enter	10	1010	18
Fill 12	12	1100	37
Fill 0	14	1110	20

The basic noise-entry problem exists because the Nimbus II clock checks parity only when receiving a signal from a command ground station. This noise-entry problem has been eliminated in the Nimbus B clock by requiring a parity check; i.e., the Nimbus III clock will require parity even when not receiving a signal from a command ground station.

Data Code Grid Upsets

One of the major clock problems encountered was the repeated upsets of the cold storage memory locations. The only clock memory locations affected by these upsets are locations 12 and 13. This confirms the fact that an internal clock problem does not exist, but rather that the clock is affected by random noise entering the memory loop. This random noise altered the DCG inputs entered in the "cold storage" portion of the memory and resulted in erroneous data appearing in the DCG on pictures transmitted to the APT ground stations. In the first 8 months of operation, there were 110 recorded DCG upsets. However, the APT pictures were not checked routinely, and there may have been more which were not observed.

Command Verification Tones

Noise caused two types of problems associated with the command verification tones—improper duration and phantom beeps. A memory-fill verification signal occurs each time a memory location is filled with a word from the ground station. This signal is a 500-Hz "beep tone" and normally consists of a short, 250-millisecond tone followed by a long, 2-second tone whenever a command is addressed to memory locations F0 and 11 and a short tone only for memory locations 1 through 10. A single, long tone should therefore never occur. But on many occasions such a long tone was observed, indicating that only a second copy of a command entered memory.

This anomaly results from the same process through which noise enters the clock memory. Whenever the clock shifts noise into the input buffer, the buffer is left partially full. Then information bits from the first copy of the first command sent during the pass are shifted into the input buffer until it is full. The clock then clears the buffer because the instruction is sensed as incorrect. The remaining bits of the first command now enter the buffer. Again the buffer is cleared because, though the instruction is correct, the key is now missing.

Clearing the input buffer readies it for the second copy of the command. This copy is accepted if it has not been mutilated in the transmission process. Because only this second copy of the command has been accepted, the command verification tone consists of only a single, long tone.

With the second problem phantom beeps, verification tones frequently were received without commands having been transmitted. Again noise, or "pseudocommands," were being received and accepted by the clock. Apparently, with only one exception, none of these pseudocommands were executed as valid subsystem commands.

Execution of Encoded Command Because of Noise

In orbit 3413, the PCM Power Supply 1 was found to be on, as well as Power Supply 2. Subsequent investigation disclosed that the Power Supply 1 had apparently been turned on sometime in between orbit 2805 and orbit 2807. This was a "blind" period during which no spacecraft telemetry data were received. Both the OGO and AE-B spacecraft were being commanded over the Orroral, Australia, station during this period; but since the bandwidth of the Nimbus command receiver is only 43 kHz at -6 db, the possibility of extraneous command interference should be precluded. There are insufficient data to make a positive conclusion, although it is probable that noise entry into the memory appeared as a valid command with a valid execution time. This is the only instance in the entire flight where this type of anomaly has occurred, and the probability of its occurring again is quite low.

Nonexecution of Encoded Commands Because of Noise

Besides the effect of noise entry on TAC commands noted previously, there have been several occasions when noise prevented execution of operational commands. During orbit 208U, Command 352 (ADDITIONAL LOAD ON) was stored in memory location 1 for execution during a blind orbit (orbit 211, May 31, 1966). The command was not executed; commands were loaded in location F0 in orbit 209U, which left location 1 accessible for any spurious noise entry. A similar problem occurred in orbit 1596 when Command 350 (AUX LOAD OFF), stored in memory location 2 was not executed. This again can be attributed to noise erasing the stored command.

During orbit 3598 at Ulaska, after establishing command capability with TAC commands and transmitting DCG, the normal tape sequence was sent. The 376 and 100 commands in locations F0 and 1 were executed properly. The following 376 in location 2 was not executed, and it is questionable whether the 100 command in location 3 was executed properly. The receiver AGC verified squelch at that time. All the following commands were executed properly, and verification tones were received for all commands transmitted. It is possible that either the time associated with the 376 command (and possibly the 100 command) was altered by noise, or the entire command was altered but still appeared valid to the clock. It is also possible that because of the PCM sampling rate, TMMDC telemetry simply did not show the change in levels.

Command Problems

Although no serious problem was encountered with the Command-Clock-Spacecraft Subsystems link, many command difficulties experienced can be attributed to the causes described below. Other than in the instances cited, there was no evidence of actual nonexecution of an encoded command.

There were many instances where a transmitted command was not executed, but in every such case, no verification tones were received either, indicating that the command was never accepted in the clock memory.

Many commands did not enter the clock because the wrong time was entered at the ground station or because of operator errors. These errors included transmitting two commands with the same execution time and inadvertently erasing stored commands.

Command difficulties occurred most frequently when the spacecraft was either at extreme range or at a low angle in relation to the command antenna. Low transmitter power is included also in this category.

Command Tape Out of Sync

On two occasions, it appeared that encoded commands were not being executed properly, although proper verification tones were being received. Subsequent investigation showed that the verification tones were not normal. Both cases were caused by a sync problem in the command ground station between the time computer and the transmitter modulator. In orbit 4506, this caused a stored command to be erased.

When a command is transmitted, two identical copies are sent to the spacecraft. In orbit 4506, Command 032 (AVCS RECORDER RECORD/S-BAND OFF) was stored in memory location 3. In a later portion of the tape, an S-BAND TRANSMIT sequence was sent, beginning with location F0. At this time, the sync problem developed. Instead of two identical copies of each command being transmitted, each copy of a command was sent with a 1-second time difference. Although the memory was to be cycled only through location 2, actually the sync problem caused a cycling through location 4 and consequently erased the stored 032 command in location 3. The command sequence is shown in Table 7-5 for the pertinent portions of the tape. A similar problem developed in an earlier orbit. However the command tape in that case was a loop tape containing only TAC commands.

Table 7-5

Partial Command Sequence, Orbit 4506.

Printer 1 (copy 1)			Printer 2 (copy 2)		
Command	Execution Time	Memory Location	Command	Execution Time	Memory Location
376	18:23:43	0	376	18:23:43	0
032	18:23:44	1	032	18:23:44	1
100	18:23:45	2	100	18:23:45	2
032	18:31:10	3	032	18:31:10	3
224	18:23:50	4	224	18:23:50	4
306	18:24:15	0	306	18:24:16	0
226	18:24:41	0	226	18:24:42	0
376	18:24:44	1	376	18:24:45	2
226	18:24:48	3	226	18:24:49	4

Odd-Numbered Commands

The proper bit sequence must be present in the clock to ensure execution of a particular command. However, it was discovered that an odd-numbered command with a valid associated time will be executed. This problem occurred on two occasions. During orbit 3293 at Rosman, a 375 command was erroneously transmitted in place of a 376 TAC command. The spacecraft clock interpreted the 375 as a 374 (BEACON TRANSMITTER 2 ON). Because Beacon 1 was in operation at the time, this resulted in a switch to Beacon 2. Although the error was not discovered until several orbits later, it did not affect the operation of the spacecraft. The 375 command was again erroneously transmitted in orbit 3305 at Ulaska. At this time Beacon 2 was already on, and no switching occurred. Table 7-6 gives the bit configuration as interpreted by the clock for any command digit transmitted.

Table 7-6

Clock Interpretation of Bit Configuration.

Actual Digit Transmitted	Digit as Interpreted by Clock					
	Hundreds CMD 8421P		Tens CMD 8421P		Units CMD 8421P	
0	0000	0	0000	0	0000	0
1	0001	1	0001	1	0001	0
2	0010	2	0010	2	0010	2
3	0011	3	0011	3	0011	2
4	0100	0	0100	4	0100	4
5	0101	1	0101	5	0101	4
6	0110	2	0110	6	0110	6
7	0111	3	0111	7	0111	6
8	1000	0	1000	0	1000	0
9	1001	1	1001	1	1001	0
Example: 225 becomes 224 375 becomes 374						

Apparent Partial Encoded Command Execution

During orbit 1452, the HRIR Playback Command (272) appeared to have been only partially executed. The pertinent portion of the command sequence related to this problem is shown in Table 7-7.

The first HRIR playback command (272) did not result in any apparent HRIR playback. However, it did result in power being applied to the AVCS multiplexer. A correct command verification

Table 7-7

Partial Command Sequence, Orbit 1452.

GMT (hr: min: sec)	CMD No.	Command Purpose/Result
09: 33: 00	032	AVCS recorder record and S-band off (stored command)
09: 22: 47	306	HRIR recorder power on
09: 22: 48	272	HRIR playback (playback did not occur)
09: 22: 49	302	HRIR day/night override on
10: 58: 00	274	HRIR recorder power off (stored command)
09: 23: 31	306	HRIR recorder power on (panic command)
09: 23: 38	272	HRIR playback (panic command - playback occurred)

tone was received, and the clock matrix drive current monitor was at the correct level. All command verification tapes indicated that the correct command was sent. Subsequent investigation showed that the HRIR playback command must be executed in order for power to be applied to the AVCS multiplexer. Analysis of the HRIR recorder relay logic and the HRIR video data received indicates that the HRIR playback command was executed just before the time the recorder end-of-tape switch was reached. Therefore, the time between the command execution and the triggering of the end-of-tape switch had to be in the millisecond range. This would have been just enough time for the command to be executed and the relays to apply power to the AVCS multiplexer and the HRIR playback circuits, but not enough time to stop the tape before the end-of-tape switch closed and the recorder was to be automatically switched back to the record mode. However, the AVCS multiplexer and S-band power remained on because of a resistor-capacitor combination in the switching circuit which did not have time to discharge in the short time between the execution of the playback command and the end-of-tape switch actuation.

Clock Exercises

Clock Flag

In orbit 3559 at Ulaska, an experiment was performed in which TAC commands were transmitted using each of the "key" characters (1, 3, 5, 7, and 9) by which the clock may be commanded. Command execution and verification tones were observed only on the 7 and 9 characters, as expected. The Nimbus II clock is keyed with a 7 character, and all Nimbus clocks respond to the 9 master key. The same experiment was attempted in orbit 5078 with identical results.

Command Transmission in 60-Bit (Single Copy) Mode

The command W channel bit rate is normally 120 bits per second. At this bit rate, each command is transmitted twice to ensure successful receipt of at least one copy. An optional W channel

bit rate of 60 bits per second is also available, but at this bit rate only one copy is transmitted. On selected interrogations between 3866 and 3996, the spacecraft was commanded, using this 60-bit mode. Overall results were satisfactory; however, on 12 of 24 interrogations where this mode was used, there were instances where commands did not enter the clock.

Disabling of Y-Channel

During Interrogation 4067 at Ulaska, commanding was attempted with the Y-input channel disabled at the command ground station. The Y channel is one of the three input lines by which command information is transmitted to the clock. The Y channel carries a character sync pulse, a 1 bit approximately in phase with the W channel parity bit. It is a marker pulse by which the clock is told to check each character for parity. With the Y channel disabled, the clock would not check for parity. Without this parity check step, the command word bits enter memory in an abnormal sequence, causing the command number and time of execution to have different values. The enter code could also be erroneous. Although the commands issued in the test were not executed, there is the possibility that commands would be executed under the right conditions. The Nimbus B version of the clock will include a change incorporating an internal parity bit marker pulse, which will enable the clock to check for parity when noise bits enter the clock on the W channel. When the Y channel is transmitted with the X and W channels, the internal parity marker will be phased in with Y-channel marker by the clock, resulting in normal clock operation.

Execution Sequence of Clock Memory Locations

During orbits 3786, 3787, and 3788, a series of TAC commands was stored in the clock in an attempt to check the sequence in which the clock memory locations are executed. Commands with the same execution times were stored in 1, 2, and 3 different selected memory locations. Each time the lowest numbered location was executed first, as expected.

Matrix Current Monitor Telemetry Levels

One method of verifying command execution is to observe the level changes on the TMMDC channel. Although each command does not have a distinct level, this still serves as a very good indicator. The matrix current monitor telemetry indicated incorrect levels for some commands. This is because of the telemetry circuit and is not considered an anomaly. (This same condition was also seen in the testing at General Electric (VFSTC).

Command Capability at STADAN Stations

During orbit 1655 at Rosman, an experiment was conducted to test the feasibility of commanding the spacecraft using "canned" command tapes. This experiment used a sequence of commands pre-recorded on magnetic tape. This tape was then used to modulate the command transmitter. The experiment was successful; the spacecraft accepted and executed all the commands. The plan at that time was to supply selected STADAN stations with sets of pre-recorded tapes, with all

tapes in the set containing the same commands. However, each tape would cover a different time range. Thus, in an emergency, particularly during the blind orbits, the STADAN station could be instructed to send a particular tape. This plan has now been dropped. Instead, the command ground stations at GSFC and Ulaska have been allowed to command the spacecraft through the Orroral, Australia, STADAN station using the data line from Orroral as the command link. This arrangement has been used successfully several times and is expected to be used in the operation of the Nimbus B spacecraft. In this way, much more useful data will be provided by eliminating several blind orbits that occur daily.

Table 7-8

Nimbus II Clock Flight Anomalies.

Anomaly	Cause	Remarks
Clock upset (1st)	Occurred during separation	Orbit 1U; reset clock to accurate time
Clock upset (2nd)	HAX OFF command executed during S-band transmission	Operational procedures modified to preclude recurrence of problem.
Spurious execution of unencoded commands Command Receiver EMI	Modulated RF signals in vicinity of spacecraft APT-HAX transmitter operation	Spurious unencoded commands caused switch of the primary and redundant receiver FM demodulated selector relay and the switching of the power supply feedback amplifier selector relay, but has not affected spacecraft performance; corrected by having STADAN stations at Quito, Ecuador and Santiago, Chile transmit an unmodulated carrier whenever spacecraft in range; procedure discontinued November 15, 1966.
Unencoded command execution while Command Receiver is being jammed	Two stations radiating at same time cause a "beat frequency" unencoded command	A 30-sec interval between end of transmission by a station and start of transmission of next station has been started
Nonexecution of stored commands and DCG upsets	Noise entry into clock memory	--------
Long "beep" tone indicating only one copy of command entering memory	Noise entry into clock memory	--------
APTS DCG "dogleg"	Clock 1 Hz and APTS sequence timer phasing	--------
Shift in "beat pattern" between PCM sampling rate and clock 1 Hz and 10-Hz T/M monitors	PCM/clock phasing	Possibly an extraneous shift in PCM logic of 2 msec or an odd multiple of 2 msec during A-stored P/B
Clock master oven temp. reading 1 PCM count low during S-band transmission	Ground problem spacecraft	EMI effect on T/M levels
Execution of encoded command (not commanded)	Probable noise entry into clock memory	PCM Power Supply No. 1 turned on in blind orbit period 2805-2807
Command tape out of sync	Sync problem in command ground station between time computer and transmitter modulator	On two occasions, this resulted in clock memory being advanced through more locations than intended; this wiped out one stored command.

SECTION 8
PCM SUBSYSTEM

FUNCTIONAL DESCRIPTION

The PCM Subsystem provides a means of monitoring the operational performance of the various subsystems aboard Nimbus II and transmits spacecraft time. The subsystem samples the analog signals of 542 different sensors, converts these signals to a coded digital form, and transmits this information as pulse code modulation (PCM) to a digital data processing station on the ground. The subsystem could transmit data in real time while simultaneously storing the data for later playback. In addition to the primary unit (A Telemetry), the subsystem included a second (B Telemetry) multiplexing and coding unit for emergency purposes. A block diagram of the PCM subsystem is shown in Figure 8-1.

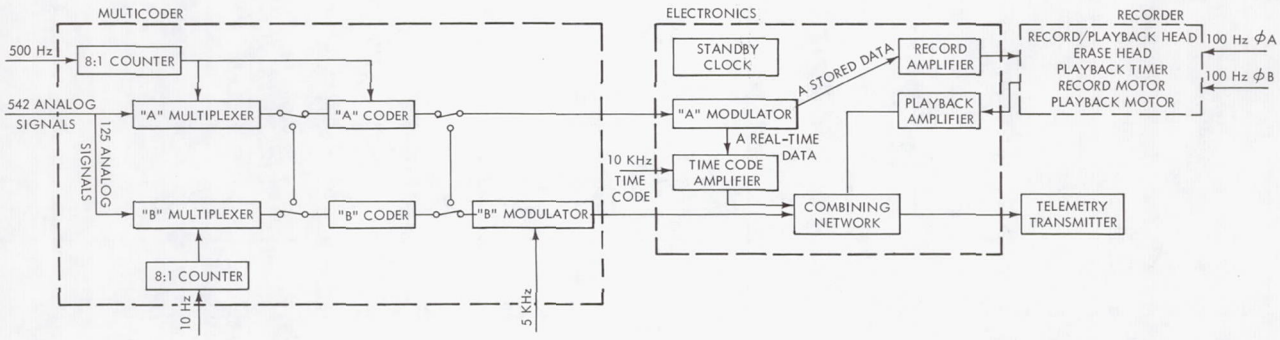

Figure 8-1—PCM subsystem telemetry block diagram.

FLIGHT OBJECTIVES

The flight objectives of the PCM Subsystem are given in Table 8-1.

DISCUSSION

The PCM Telemetry Subsystem performance was excellent for the first 949 orbits at which time a failure of the tape recorder precluded further receipt of stored A data. After that time, only real-time A data have been received, the quality of which has been good. The B telemetry was never commanded during the first 13 months of flight. Table 8-2 is a historical record of the PCM telemetry.

Table 8-1

PCM Subsystem Flight Objectives.

Objective	Results	
	6-month	13-month
Demonstrate the ability of the PCM Subsystem to record continuously and play back, on command, high quality telemetry data for reception at the Nimbus DAF stations.	The PCM Subsystem provided data with a quality of 98% good data before failure of the PCM tape recorder during orbit 949. This failure precluded further reception of stored A data.	The PCM Tape Recorder remained inoperative; it was periodically commanded into playback to eliminate 10-kHz interference on the AVCS pictures caused by the time code on the real-time telemetry.
Demonstrate the capability of the PCM Subsystem to provide high-quality telemetry data in real time to designated receiving stations.	Good quality real-time A data continued to be received from the spacecraft.	Good quality real-time A data continued to be received from the spacecraft.

Table 8-2

History of PCM Recorder Telemetry.

Function	Orbit No.	Telemetry Value (tmv)							
		588	948	949*	1154	1154†	3400	4398	5466
Erase oscillator	174	1.05	1.05	1.05	1.05	1.05	1.05	1.05	1.05
Recorder housing temp.	176	2.15	2.15	2.15	2.2	2.2	1.07	2.25	2.05
Recorder housing pressure	178	4.75	4.75	4.75	4.75	4.75	4.75	4.65	4.7
Recorder motor phase A	179	2.60	2.60	2.60	2.6	2.4	2.40	2.35	2.35
Recorder motor phase B	180	3.00	3.00	3.00	3.0	2.6	2.80	2.80	2.80
Clk pwr 100 Hz phase A/phase B	410	4.55	4.55	4.55	4.55	4.55	4.55	4.55	4.55

*Unmodulated signal received.
†Record motor failure.

Beacon Power

The indicated beacon transmitter power output varied from 390 to 500 milliwatts during the first 80 orbits. Since this variation occurred with two different transmitters (with independent power telemetry points) working into the same antenna system, it may suggest a changing or varying VSWR in the antenna system. Since orbit 80, transmitter power has been nearly constant at approximately 500 milliwatts. In orbit 53U, the transmitters were switched (from Beacon Transmitter No. 2 to Beacon Transmitter No. 1) because of ground station problems which, at the time, resembled a spacecraft problem. During orbit 3293, PCM Transmitter No. 2 was turned on because of an error in the command tape. This presented no problem, and the transmitter was

left on. The signal quality of this transmitter was as good as at launch even though it had been off since orbit 53.

Signal Acquisition

The PCM beacon signal normally rises above the Data Acquisition Facility (DAF) receiver squelch level at approximately -145 dbm. Normally, 1 to 2 minutes later, the Nimbus Data Handling Section (NDHS) PCM ground station at GSFC has been capable of obtaining synchronization, thus processing real-time telemetry data at a signal level of approximately -115 to -120 dbm. Barring ground antenna masking from natural sources, this slant range at signal acquisition and loss has been 3500 to 4000 kilometers. Figure 8-2, a plot of the maximum AGC level obtained over the first 13 months, indicates that the vast majority of passes had a maximum signal varying from -90 to -100 dbm.

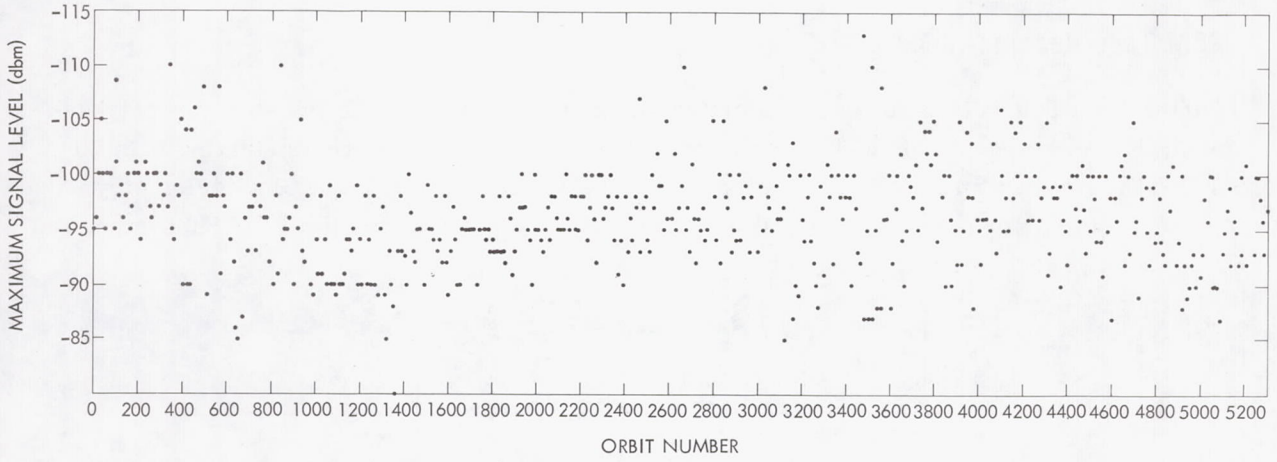

Figure 8-2—Beacon maximum AGC per orbit.

Signal Quality

The quality of the PCM signal has been good. Before orbit 953, the PCM playback was generally timed to occur during the "high angle" portion of the interrogation. The percentage of bad data (no. of bad sub. frames ÷ total no. of sub. frames) was generally less than 5 percent (Figure 8-3). The values in Figure 8-3 reflect such factors as ignition noise, ground equipment malfunctions, spacecraft tracking errors, atmospheric effects, line noise in transmission from the tracking stations, auroral effects, and

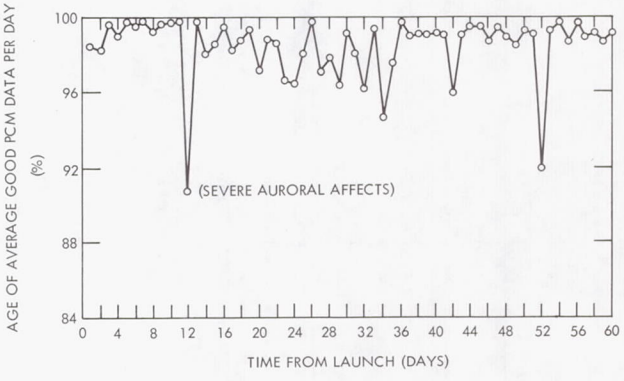

Figure 8-3—Percentage of average good PCM data per day.

low antenna angle interrogations. Another factor contributing to the percentage of bad data was the recorder tape splice, which is discussed later.

Recorder Tape Degradation

From stored telemetry A data it was determined that portions of the tape did not provide recorded data. During the initial orbits, the loss of five words was apparent at the tape splice; however, some loss of data was expected at this point in the continuous tape loop. Another blank spot, two words long, was also discernible 101 words after the splice. By orbit 940, there were three blank spots on the tape. The loss of data because of the splice had increased to eight or nine words. The second blank spot, still 101 words after the splice, grew to six or seven words. The third blank spot was two words long and occurred 11 words after the second. The orbit in which this third blank spot began is not known. (One word is equivalent to approximately 0.0064 inch of tape.)

PCM Tape Recorder Failure

During orbit 949 at Ulaska, an unmodulated signal was received after the stored A playback command was executed. Table 8-3 lists the chronological sequence of events starting with the initial PCM playback command (120) in orbit 949. The PCM Subsystem and Clock telemetry values were normal both before and after the failure. The telemetry values for the PCM Subsystem and Clock before and after the failure are listed in Table 8-4.

Table 8-3

Sequence of Events Following PCM Playback Command 120.

Orbit No.	Time (Z)			Command Executed	Remarks
	Hours	Minutes	Seconds		
949	14	33	00	120	Resulted in unmodulated 136.5-MHz carrier
	14	33	54	132	PCM recorder record command
	14	34	25	120	Resulted in unmodulated carrier
	14	35	16	132	PCM recorder record
	14	35	58	130	T/M A power 1 on
	14	36	05	120	Resulted in unmodulated carrier
	14	36	02	132	PCM recorder record
950	15	59	00	120	Unmodulated carrier. Short playback (1.5 min) because of the short playbacks in the previous pass.
	16	01	25	104	Master clock on
	16	02	04	124	Unmodulated carrier received. Playback terminated after normal playback time of 3 minutes, 43 seconds

Table 8-4

PCM and Clock Telemetry Values.

T/M function	Orbit No.	Telemetry Value (tmv)						
		588	945	946	947	948	949*	950*
Erase oscillator	174	1.05	1.05	1.05	1.05	1.05	1.05	1.05
Rcdr. hsg. temp.	176	2.15	2.15	2.15	2.15	2.15	2.15	2.15
Rcdr. hsg. press.	178	4.75	4.75	4.75	4.75	4.75	4.75	4.75
Rcd. mtr phase A	179	2.60	2.60	2.60	2.60	2.60	2.60	2.60
Rcd. mtr phase B	180	3.00	3.00	3.00	3.00	3.00	3.00	3.00
Clk pwr 100 Hz phase A/phase B	410	4.55	4.55	4.55	4.55	4.55	4.55	4.55

*Unmodulated signal received.

Normal playback duration (3 minutes, 43 seconds) occurred during the command playback in orbit 950, indicating that the timing mechanism was functioning normally. Regulated bus current, recorded on HRIR during the orbit 950 playback, indicated no abnormal current drain during playback. The initial current during the record-to-playback transition appeared normal when compared with the same type data from a previous orbit. The clock matrix current monitor value for the PCM playback commands (120) indicated the correct level, implying that the relays were being driven normally.

Investigation of this failure has revealed the following possible failure modes.

a. The playback amplifier was inoperative because of internal problems.

b. The playback head was inoperative.

c. The recorder tape was broken.

d. Relay K8 (which switches the record/playback head to the record amplifier in the record mode and to the playback amplifier in the playback mode) was stuck in the record position.

e. A wire was broken.

f. The playback motor stalled.

Table 8-5

Stored A Bit Rate as Measured at PCM Ground Station.

Orbit Number	Bit rate (kilobits)
845	14.94
850	14.935
944	14.970
945	14.940
946	14.940
947	14.940
948	14.945

The A-stored bit rate was normal up to orbit 949 as shown in Table 8-5.

It is of interest to note that shortly before the launch of Nimbus II, a NASA technical officer expressed concern over the serviceability of the PCM tape recorder based on a problem that had

developed with a similar tape recorder where the lubricant in the motor bearings broke down and caused the recorder to fail. Accordingly, it was recommended that the tape recorder bearings be replaced; however, none were available, and it was believed that the spacecraft operation could be handled successfully with only real-time telemetry in the event of failure of the PCM recorder. In view of this, the Nimbus Project Office decided to risk flying with an uncertain tape recorder rather than to postpone the launch several months to change the recorder.

Between orbits 1154 and 1155, the PCM Tape Recorder motor appeared to stall, based on a decrease in recorder phase A and phase B telemetry voltage. Table 8-6 shows the telemetry values of the recorder 100-Hz phase A and phase B signals and the clock 100-Hz signals. During orbit 1163, telemetry A power 1 was turned off, and power 2 was turned on. These commands turned off the power to the PCM Tape Recorder.

Table 8-6

Telemetry Values of PCM Tape Recorder and Clock Signals.

Orbit No.	Telemetry Value (tmv)			
	Clock 100 Hz (A & B) TM 100 (410)	Clock 100 Hz (phase A) TM 100F (412)	Recorder phase A (179)	Recorder phase B (180)
1153	4.60	6.00	2.60	2.95
1154U	4.60	6.00	2.60	2.95
1154O	4.60	6.00	2.60	3.00
1155	4.60	6.00	2.40	2.60

Effects of EMI on Telemetry Levels

Some of the telemetry channels showed definite level shifts under certain conditions; these are listed below:

a. The clock master oscillator oven temperature consistently read one PCM count lower than normal when the S-band transmitter was on.

b. The AVCS camera high-voltage cycle consistently showed up on the telemetry channels for the yaw solenoid valve and IRIS control potentiometer.

c. Operating the APT Subsystem caused a level shift in the AVCS camera high-voltage telemetry channels.

d. The HAX module operation caused jitter on the AVCS camera high-voltage telemetry channels. See Section 10 for details.

e. Several of the APT transmitter telemetry channels were affected by the HAX operation.

f. During satellite night, the unregulated bus current telemetry increased from a nominal offset of 0.35 tmv to 0.55 tmv when the S-band transmitter was in warmup and to 1.20 tmv in transmit.

All of these problems were diagnosed as grounding problems within the spacecraft rather than subsystem problems.

Current Subsystem Status

The PCM Subsystem has continued to provide good real-time A data. By replaying the real-time A data post-pass at 30 times its normal bit rate, stored A data are simulated and used to run the computer programs. Although it is impossible to obtain data for a complete orbit, the available data are sufficient to check spacecraft status, to verify most spacecraft events, and to adjust power management for optimum power subsystem performance.

The PCM tape recorder has been commanded periodically into playback to provide AVCS pictures free of 10-kHz interference caused by the clock time code on the PCM carrier during real-time A data transmission. However, no stored A data have been received since orbit 948. The playback time interval has not changed since launch, thus indicating that the compensation motor, which drives the timer, is still functioning properly.

SECTION 9

AVC SUBSYSTEM AND S-BAND TRANSMITTER

INTRODUCTION

The performance of the Advanced Vidicon Camera Subsystem (AVCS) was satisfactory until orbit 1444 when the tape recorder failed, thereby eliminating the data storage capability of the subsystem. Thereafter, pseudo-direct pictures were the only medium by which AVCS sensory data were received. Radio frequency interference (RFI) has been the most serious impediment to the overall quality of the subsystem video. Figure 9-1 is typical of the good output quality of the AVCS. The performance of the S-band transmitter was excellent with no evidence of long-term degradation.

A summary of AVCS anomalies is presented in Table 9-6.

DESCRIPTION

The Advanced Vidicon Camera Subsystem, shown functionally in Figure 9-2, consists of three vidicon cameras, a 4-track magnetic tape recorder, a frequency multiplexer, and associated timing and power control electronics. The three AVCS cameras are arranged in a trimetrogon array that provides almost complete coverage of the earth's sunlit side. The three cameras are mounted so that the one in the center points "straight down," and the adjacent ones are tilted 35 degrees. The field-of-view for each camera is 37 degrees with a 2-degree overlap as shown in Figure 9-3. Operating in a polar orbit at an altitude of 600 nautical miles, the camera area covered is approximately 400-by-1900 nautical miles. Successive frames are taken at 91-second intervals and provide approximately 20 percent overlap of earth coverage.

The camera sensor is a ruggedized, 1-inch, high-resolution vidicon tube, with a usable image area of 0.625 inch diagonal (0.44 by 0.44 inch). External coils provide magnetic

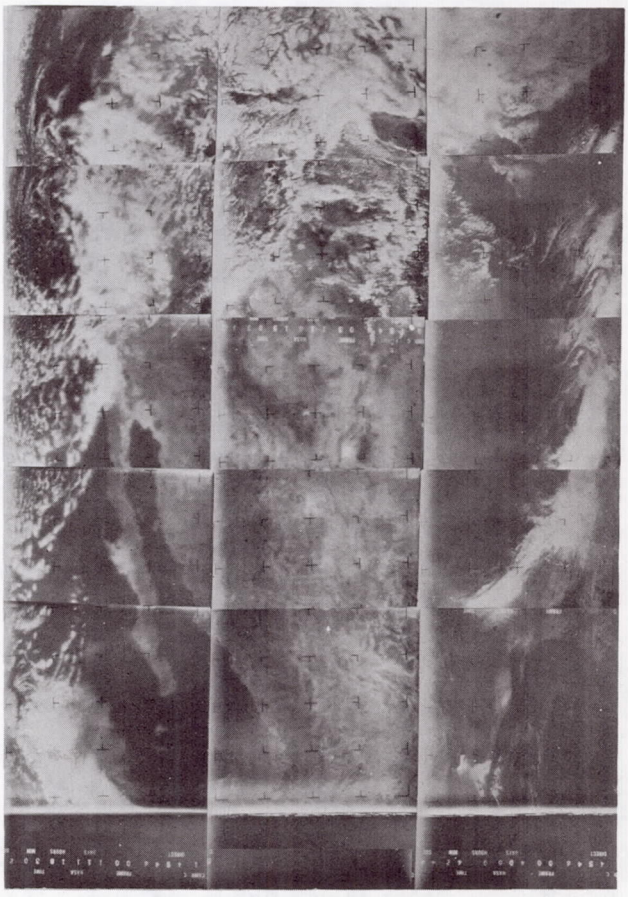

Figure 9-1—Typical AVCS video data quality (orbit 4546).

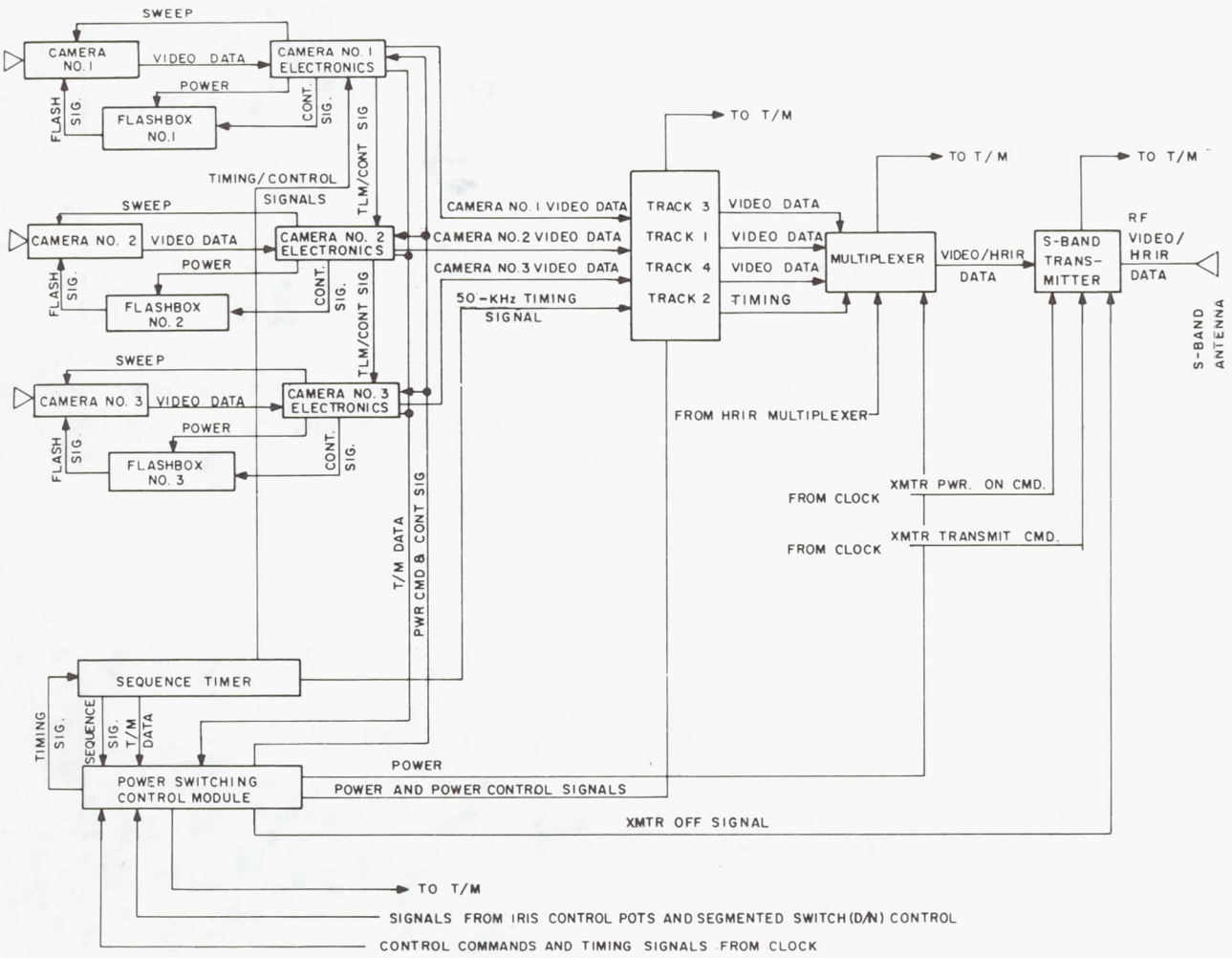

Figure 9-2—AVCS block diagram.

deflection, focusing, and beam alignment. Each camera lens has a speed of f/4, focal length of 17 mm, and an exposure time of 40 milliseconds. The area on the vidicon faceplate used for exposure is 0.625 inch in diameter, but the image is limited to a square by a black level mask and a square scan pattern used in the vidicon. Thus, although the angle of field is 50 degrees (on the diagonal), the angle is limited to a 37- by 37-degree square. Each lens is equipped with a standard Y-10 yellow filter to limit the spectral response, thus eliminating the blue haze effect and enhancing the cloud-cover features.

Camera readout is approximately 6.25 seconds, and the video bandwidth is 60 kHz. A ground resolution of approximately one-half mile per TV line is obtained. Each camera is equipped with a variable iris to compensate automatically for latitudinal changes in earth illumination. Self-contained calibration for both sweep and grey-scale linearity is incorporated in the camera sensors. A precision reticle pattern, deposited in the image area of the vidicon, provides the dimensional reference for measuring system linearity. A calibrated grey scale appears on each picture for white-to-black reference.

The AVCS tape recorder is a 4-channel magnetic tape recording and playback device. The unit is used primarily to store video signals from the three TV cameras and a NASA 50-kHz time-code signal and to play back these signals later on command from the ground station. The video signals are received simultaneously and stored on four parallel tape tracks when the satellite is out of range of the ground receiver. The satellite is commanded to play back these stored signals when the satellite is within communication range of the ground station receiver. These two functions, record and playback, constitute the major modes of operation. A third mode of operation, the direct picture mode, may be commanded. In this mode of operation the tape transport is bypassed; the three video signals and the NASA timing signal then are sent directly into the playback circuits.

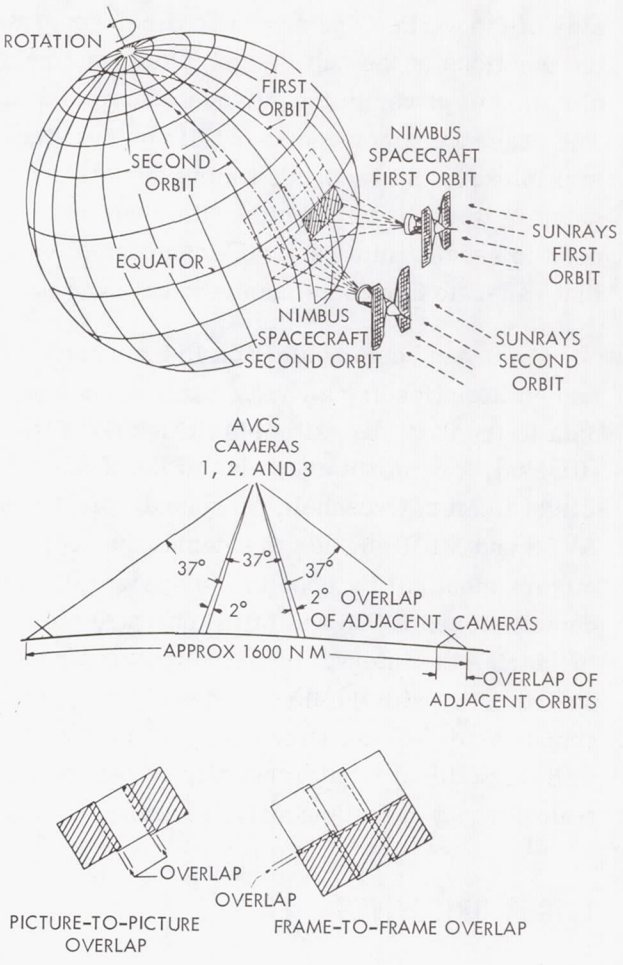

Figure 9-3—AVCS camera coverage.

The multiplexer combines the three video channels and 50-kHz timing signal from the AVCS recorder, along with four other signals from a separate but similar multiplexer associated with the HRIR Subsystem, into a 700-kHz composite baseband for subsequent FM modulation of the main 1707-MHz transmitter in the satellite. The composite signal is applied to the S-band Transmitter for FM transmission to the ground equipment. To provide the required 40-db signal-to-noise ratio, the FM deviation ratio for each of the three AVCS video channels, restricted initially by the response of the tape recorder, is doubled by doubling the instantaneous frequency of each channel. Frequency translation to the proper subcarrier slot in the composite baseband is performed by balanced mixers followed by bandpass filters. The bandpass filters provide both high stop-band attenuation and linear phase response in the pass band, the former to prevent crosstalk and the latter to prevent distortion of the video image. The multiplexer is controlled by applying power to the multiplexer circuits at the appropriate time required for playback or for a direct picture.

Power for operating the AVCS satellite equipment in all three modes is controlled by the power switching control module. Power switching relays in this unit respond to commands transmitted from the ground to select the desired power pattern. A day-night switch removes power from the camera circuits when signals from the solar paddles indicate that the satellite is over the dark (night) side of earth; this switch restores power when the satellite is again over the illuminated

side of the earth. The sequence timer generates the timing signals that control and synchronize the functions of the subsystem. Command relays located in this module control the sequential application of power to the various camera and tape recorder circuits during each camera cycle. The sequence timer counts a 1-Hz output signal from the Nimbus clock and generates camera, multiplexer, and recorder timing signals coherent with the NASA time signal. The time signal is gated in this unit to coincide with, and thus identify, each picture frame. The time signal is also used to reconstitute vertical synchronization on the ground. This module also contains circuits that generate horizontal and vertical sync pulses and the iris-enable signal.

An S-band communication link consisting of a 1707.5-MHz vacuum tube and a 5.75-watt FM transmitter (feeding a cavity-backed, conical, spiral, slot antenna) transmits the AVCS and HRIR data to the data acquisition facilities (DAF's) at Rosman, North Carolina, and Fairbanks, Alaska (Ulaska), for microwave relay to the Nimbus Data Handling Facility (NDHF) at the Goddard Space Flight Center, Greenbelt, Maryland, for processing. At the NDHF, the frequency division-multiplex AVCS and MRIR signals are demultiplexed, using subcarrier filters and frequency-translating mixers identical to those in the spacecraft to return each channel to its original baseband. The demultiplexed AVCS and MRIR data are stored in tape recorders for playback and further processing during the interval between spacecraft interrogations. During this interval, the recorders are played back, with the three video channels each feeding a gridding complex at slow time or the kinescopes at real time. Processing of the AVCS video is performed via kinescopes in a video processor utilizing a Bimat film processing system, which produces a completely processed negative and positive transparency simultaneously. Processed sensory data are presented in the format shown in Figure 9-1.

FLIGHT OBJECTIVES

AVC Subsystem

The flight objectives of the AVCS were to demonstrate its capability to gather high-quality cloud photographs of the entire earth surface and play back upon command. At 6 months, the performance of the AVCS had been satisfactory until orbit 1444, when the subsystem tape recorder failed, eliminating the data storage capability. Since then, pseudo-direct pictures have been received, but with photograph quality degraded by 10-kHz RF interference. At 13 months, pseudo-direct pictures of good quality were being received with the PCM recorder in the playback mode. The pictures are free from interference in this mode.

S-band Transmitter Flight Objectives

The flight objectives of the S-band Transmitter were to provide a high-quality transmission medium for the AVCS and HRIR tape recorder playbacks and direct AVCS frames. At 6 months, the transmitter had been performing well, with signal reception levels ranging (DAF) from -70 to -90 dbm. At 13 months it continued to perform well, with no evidence of long-term degradation.

ELECTROMECHANICAL PERFORMANCE

The electromechanical performance of the AVCS was satisfactory. The only major problem was the failure of the tape recorder during orbit 1444. Minor malfunctions also have occurred although none of them degraded the quality of the subsystem video until a change in the optical system of Camera 1 during the 11th month in orbit resulted in a loss of focus. Subsystem performance is summarized in Table 9-1.

Table 9-1

Summary of AVCS Performance.

Function	Requirement	Outcome
Performance		
Horizontal resolution	700 lines (satellite subpoint)	Satisfactory
Distortion	0.5% maximum V&H dimension	Satisfactory
Focusing	Consistent with 700 lines	Satisfactory (1)
Grey scale	Minimum 6 steps at +25°C	Satisfactory (2)
Shading	Negligible deterioration compared to bench test data	Satisfactory
Quality	Uniform for all cameras	Partially satisfactory (3)
Aspect ratio	1:1 ± 2%	Satisfactory
S-band frequency	1707.54 MHz ± 0.005%	Satisfactory (4)
Telemetry	Adherence to calibration and stability	Satisfactory (5)
Operability	Dependable execution of commands	Excellent (6)
Compatibility	Minimum RFI during operation	Failure (7)
Reliability	Capable of continuous 6-month operation	Failure (8)

Notes: (1) A change in the optical system of Camera 1 during the 11th month in orbit resulted in a loss of focus in this camera's video.

(2) The operation of the flash tubes which illuminate the grey scale of Camera 3 became intermittent during interrogation 3520R and subsequently ceased operation.

(3) The different transfer characteristics of the three cameras required unique processor compensation for each camera to obtain uniform quality photographs.

(4) Frequency measurements showed no long-term degradation in subsystem frequency stability.

(5) Refer to paragraphs entitled Camera 2 Housing Temperature Telemetry Malfunction and Camera 2 Electronics Thermistor Failure.

(6) During interrogation 221U, the encoded command "AVCS 6V Power Supply A Off" (062) was transmitted during the period between To +32.5 and To +39.5. This would have resulted in the AVCS recorder driving continuously to the end of tape position before stopping. However, immediate corrective action was taken to remedy the situation, and operational constraints were undertaken to preclude the possibility of a recurrence of this situation.

(7) Interference patterns in the AVCS video were induced by the APT, MRIR, and PCM subsystems. In addition, the AVCS vidicon cycle affects telemetry from other subsystem; e.g., the controls subsystem yaw solenoid monitor.

(8) Subsystem tape recorder failed prematurely.

Camera Components

Camera 1, Iris Drive Motor No. 2 Failure

The normal practice is to alternate iris drive motors each day; however no. 2 iris motor of Camera 1 failed to position the iris properly. Telemetry indicated that the iris drive motor failed to perform properly when first activated after launch. Figure 9-4 is a comparison of the performance of the various iris motors of all three cameras. During orbits 54 and 65, the no. 1 iris motor of Camera 1 was powered; during orbit 66, the no. 2 iris motor was powered. Figure 9-4 shows that no. 2 iris motor of Camera 1 failed to maintain proper iris positioning. Since orbit 98, the no. 1 iris motor has been used exclusively for Camera 1 and has shown no evidence of performance degradation.

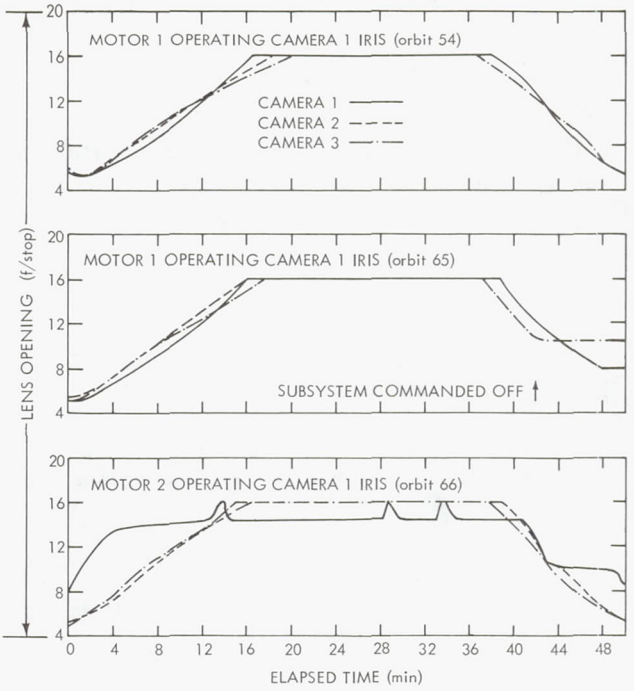

Figure 9-4—AVCS camera no. 1 IRIS drive history.

Camera 2 Shutter Malfunction (Orbit 1309)

During interrogation 1309U, four frames (27 through 24) of video from Camera 2 were almost totally "washed out" (Figure 9-5). The only distinguishable features were faint traces of the fiducial marks. In addition, frame 27 exhibited faint traces of the bottom fiducial line and grey scale. Camera 1 and Camera 3 video remained normal throughout this period.

Each of the three AVCS cameras employs a double-bladed, focal plane shutter assembly (Figure 9-6). The blades are activated by solenoids mounted atop the camera housing energized by pulses generated by multivibrators in the camera electronics module. The blades open the shutter aperture (offset as shown in Figure 9-6) for a predetermined period of time (40 msec). The aperture in blade no. 2 is lined up with the vidicon field-of-view, while the other aperture is below the field-of-view. In this position the shutter is closed. When a pulse energizes solenoid no. 1, shutter blade no. 1 is raised, exposing the vidicon to light. Solenoid no. 2 is energized 40 milliseconds later, and raises shutter no. 2 to close the aperture. Solenoid no. 1 is deenergized 30 milliseconds later (solenoid no. 1 is therefore energized for 70 milliseconds) and solenoid no. 2 is subsequently deenergized 30 milliseconds after solenoid no. 1 is deenergized (solenoid no. 2 is therefore energized for 60 milliseconds). The vidicon is not exposed when blade no. 1 drops to the original position. Since the exposure is both initiated and terminated by raising a shutter blade, the entire vidicon faceplate is exposed uniformly. To reduce the peak current drain on the Power Subsystem, the electronic circuits that activate each camera solenoid are interconnected to provide a 70-millisecond time delay between the triggering of shutter blade no. 1 of each camera.

At the time of exposure of frame 28 in orbit 1309, shutter blade no. 1 of Camera 2 apparently failed to release at the prescribed time. The nature of the malfunction was either mechanical (binding, friction, seizure) or electrical (malfunction in the associated solenoid-enable circuitry resulting in continuous solenoid energization). This condition continued for four frames, whereupon normal operation was resumed. Movement of shutter blade no. 2 was thought to be normal, but shutter blade no. 1 did not shut as rapidly as required. This resulted in nonuniform exposure of the vidicon, the lower part of the vidicon faceplate receiving less incident light. This anomaly, seen as progressive in nature (Figure 9-5), resulted in the appearance of the reticle marks (though very faint) in the area of the first picture (frame 28) closest to the bottom of the vidicon. The bottom edge of the vidicon (Figure 9-6) contains the grey scale which, when processed, appears at the top of the processed print. Thus, the reticles on the lower part of the vidicon appear in the upper part of the processed print, and vice-versa. As time progressed, the reticle marks and grey scale vanished (frames 26 and 27). By frame 25, the reticle marks at the bottom of the vidicon were again visible. After a duration of four frames, the malfunction vanished and has not been observed since.

Camera-3 Flash Tube Malfunction

Each vidicon is equipped with a xenon flash tube, whose output is a short-duration, high-intensity flash of light directed to the faceplate of the vidicon by a prism (Figure 9-7). Attached to the output surface of the prism is a 16-step density transparency that divides the incident light into 16 calibrated steps and thereby permits in-flight calibration/evaluation of each camera. Two pulses of light (T_0-26 sec and T_0-32.5 sec) are required to produce the required illumination of the grey scale transparency. During interrogation 3520R, a frame was received in which the grey scale was absent (Figure 9-8). During subsequent interrogations, A-scope presentations and data indicated intermittent operation of the Camera-3 flash tube. It flashed twice (normal), once, or not at all. This failure did not impair the quality of the video data from this camera, but only negated the built-in calibration analysis feature. The total cumulative number of cycles that the Camera 3 xenon flash tube (S/N 18) had completed before the malfunction was approximately 189,000; this is at the rate of two flashes per picture and includes prelaunch subsystem operating time.

Camera-2 Housing Temperature Telemetry Malfunction

The telemetered value of the Camera-2 housing temperature indicated a decrease from 32.9°C (interrogation 3957, mean temperature) to 25.7°C (interrogation 3958U mean temperature) and subsequently to 18.3°C (interrogation 4164U mean temperature, Figure 9-9). The temperature of the Camera 2 mounting plate, which provides thermal conduction from Camera 2 to the H-frame, did not reflect a corresponding temperature decrease but continued to exhibit a nominal orbit profile of 25.7 ± 1.3°C. The A-scope presentation of the camera grey scale did not show a decrease in camera temperature.

The temperature of the AVCS Camera 2 was approximately 32°C during system operation. The temperature difference between the camera and the mounting plate remained a constant 6°C

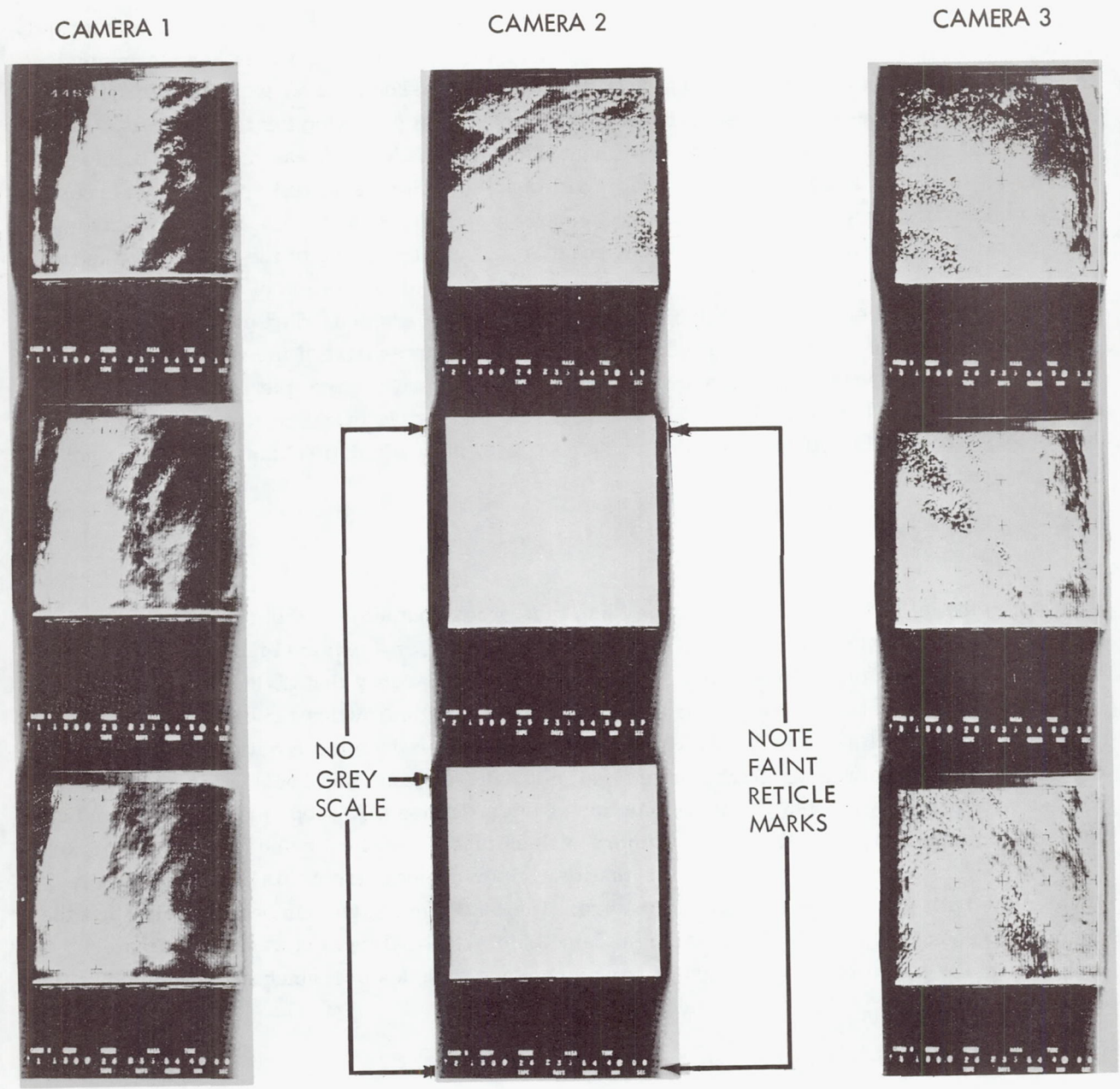

Figure 9-5 — AVCS photographs showing washedout frames of camera no.2.

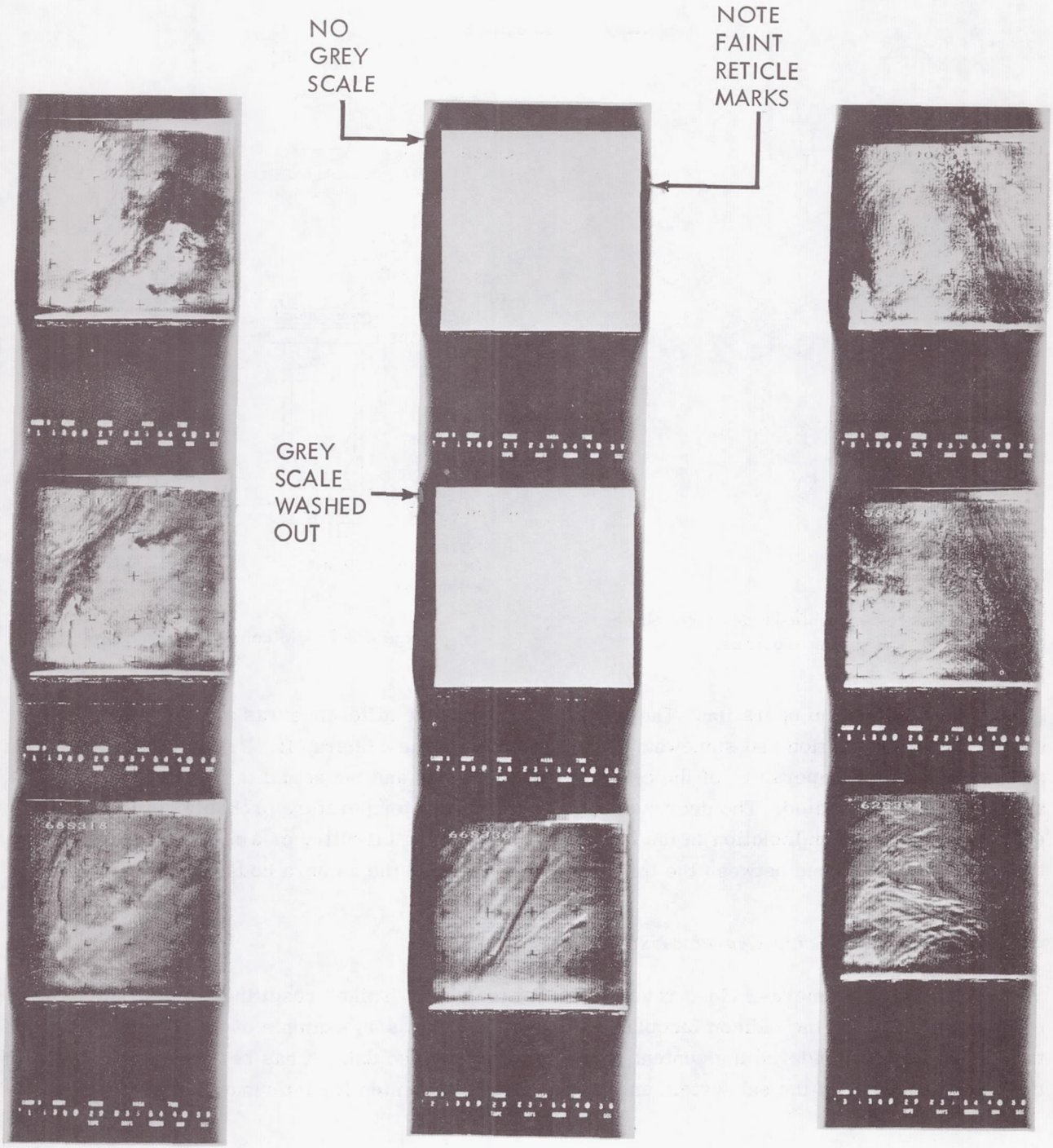

Figure 9-5 (continued) — AVCS photographs showing washedout frames of camera no .2 .

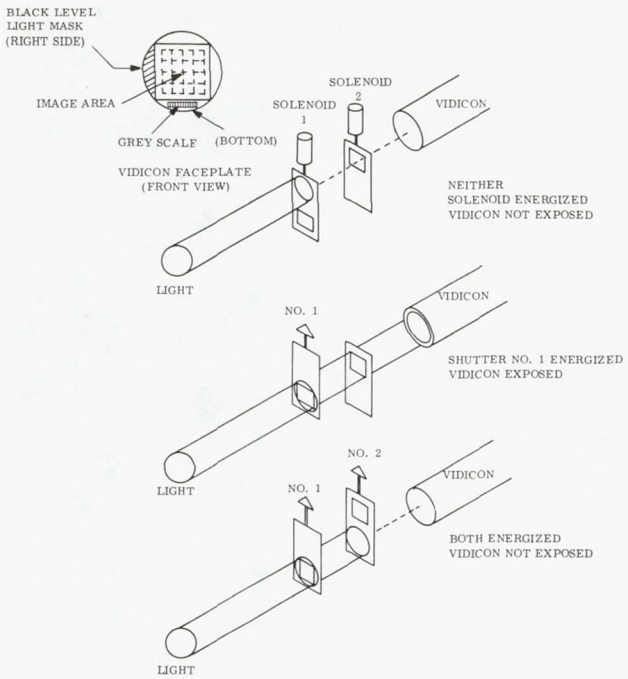

Figure 9-6—Double-bladed focal plane shutter sequence.

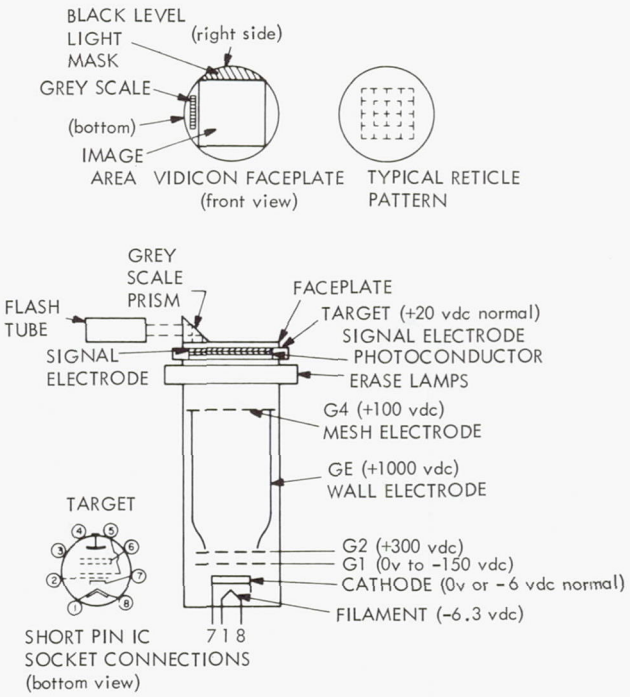

Figure 9-7—Vidicon tube schematic.

irrespective of system operation. The expected temperature difference was approximately 2°C during camera operation and somewhat less than 2°C with the camera off. Hence, it was suspected that the indicated temperature of the camera was erroneous and the actual temperature was probably lower than indicated. The decrease of the telemetered temperature probably resulted from either an electrical malfunction in the telemetry conditioning circuitry or a mechanical degradation of the thermal bond between the temperature sensor and the camera housing.

Camera-2 Grey Scale Characteristics

Evaluation of Camera-2 video revealed a characteristic "spike" resulting from a flaw in the etched grey scale on the vidicon faceplate. Figure 9-10 shows an example of this defect. Although this defect has not hindered the content of the subsystem video data, it has been present throughout the operational life of the subsystem and is, therefore, presented for information purposes.

Camera-1 Focus Degradation

The Camera-1 video focus deteriorated during the 11th month in orbit (Figure 9-11). The fiducial marks, which are etched on the faceplate of the vidicon, have remained in focus, and the related telemetry data given in Table 9-2 do not reveal any anomalistic conditions. The problem,

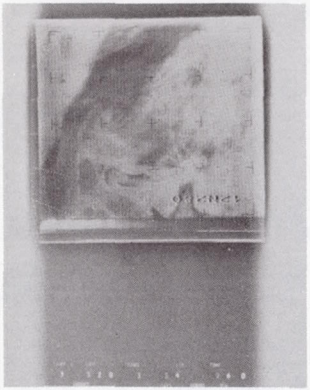

70 mm VIDEO DATA

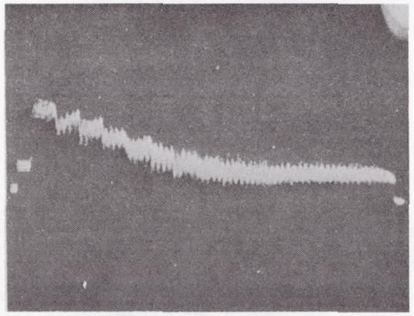

SCOPE PRESENTATION OF GREY SCALE SHOWING NORMAL CAMERA 3 FLASH TUBE OPERATION

(a) ORBIT 3520, NORMAL FLASH TUBE OPERATION (2 flashes)

70 mm VIDEO DATA

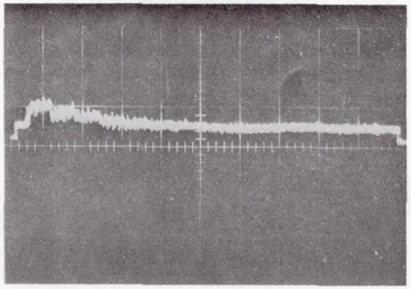

SCOPE PRESENTATION OF UNDEREXPOSED GREY SCALE, RESULTING IN GREY SCALE OF APPROXIMATELY 1/2-NORMAL AMPLITUDE

(b) ORBIT 3959, FLASH TUBE TRIGGERS ONLY ONCE

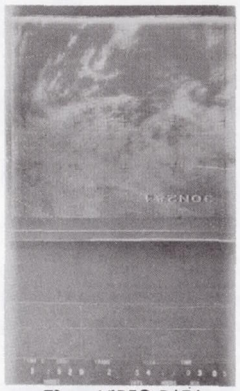

70 mm VIDEO DATA

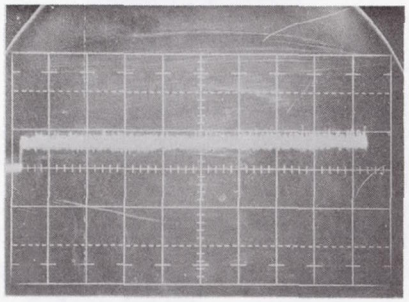

SCOPE PRESENTATION SHOWING ABSENCE OF GREY SCALE DEFLECTION

(c) ORBIT 3520, FLASH TUBE FAILS TO TRIGGER

Figure 9-8—Camera 3 video displays (vertical scale: 0.5 v/cm; horizontal deflection: 5 msec/cm).

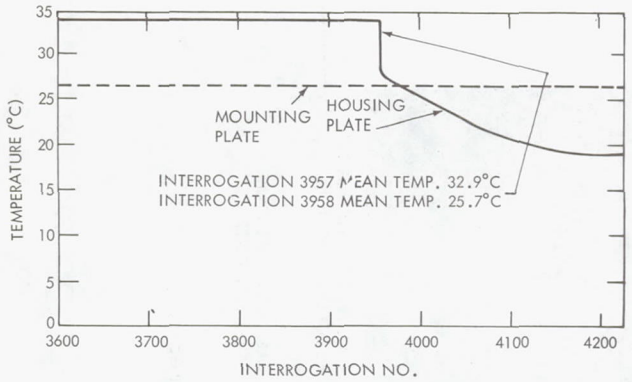

Figure 9-9—Camera 2 housing and mounting plate temperature.

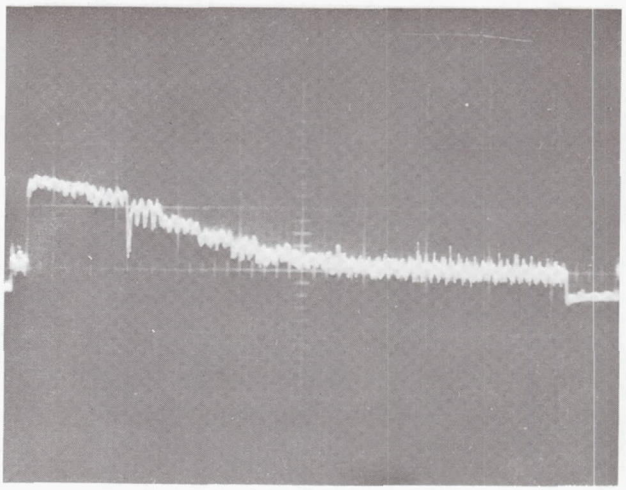

Figure 9-10—Oscilloscope display photographs exhibiting AVCS camera 2 grey scale "spike."

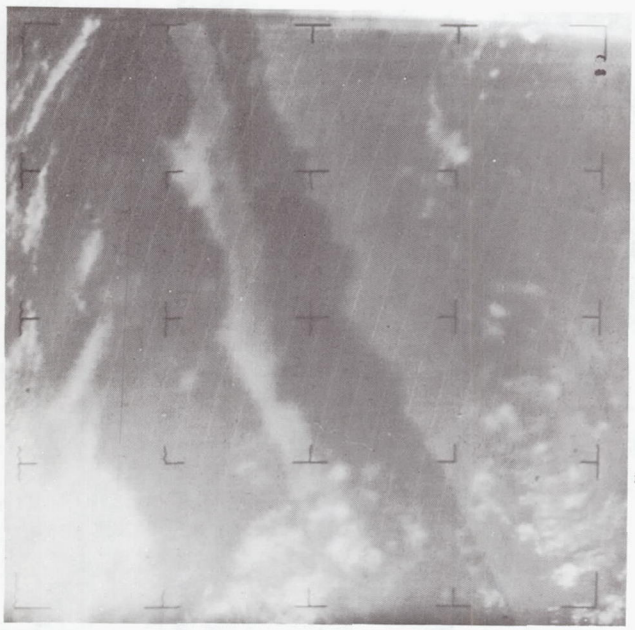

Figure 9-11—AVCS photograph showing loss-of-focus effect on the video of camera 1 (orbit 5154).

Table 9-2

Camera 1 Telemetry Data.

Function No.	Function	Telemetry Voltage (tmv)	
		Orbit 433	Orbit 5158
210	Filament voltage	6.3	6.3
193	Filament current	0.35	0.4
189	Elect. module temp.	4.65 (25°C)	4.7 (24°C)
202	Focus current	2.0	2.0
199	High voltage	4.45	4.45

therefore, is most likely attributable to either a change in the mechanical alignment of the optical system or a change in the optical characteristics of the lenses or the Y-10 yellow filter. Thermal distortion or mechanical shock would cause mechanical alignment changes. It should be noted that the focusing capabilities of Cameras 2 and 3 have not deteriorated.

Electronic Components

Camera-2 Electronics Thermistor Failure

During orbit 692, and intermittently thereafter, the Camera-2 electronics thermistor exhibited radical, intermittent changes indicating instantaneous temperature changes from 24°C

(4.6 tmv) to as low as 4.0°C (5.5 tmv). This has been diagnosed as an electrical failure of either the thermistor temperature sensor or the grounding in the telemetry conditioning circuit.

Extended High-Voltage Cycle (Interrogation 804R)

Between interrogations 788U and 804R, Nimbus II was placed in an APT "coast-through" configuration. During interrogation 788U and before the transmission of the APT coast-through configuration commands, an earth day/earth night transition occurred at approximately 9 seconds into the high voltage portion (T_0 to T + 39.5) of the AVCS cycle. When the AVCS was reactivated during interrogation 804R, the command sequence listed in Table 9-3 was used. During the approximate 64-second period between camera activation and activation of the 6-volt power supply A, high voltage was applied to the cameras.

Table 9-3

AVCS Reactivating Sequence Used During Interrogation 804R.

Command No.	GMT (hr:min:sec)	Command Function
030	16:48:14	AVCS recorder power on
050	16:48:15	Camera 1 on
034	16:48:16	Camera 2 on
210	16:48:17	Camera 3 on
220	16:48:20	6-volt power supply A on

The earth day/earth night transition does not generate a sequence time reset but stops the further sequencing of the timer. Therefore, by the activation of the cameras before the activation of the 6-volt power supply A (which would have generated a sequence timer reset to T_0), the high voltage was immediately applied to the cameras upon camera activation. Not until the 6-volt power supply was activated at 16:49:20 was a sequence timer reset generated, which (immediately being reset to T_0) continued the application of high voltage to the cameras until T_0 + 39.5. This caused the high voltage to be applied to Cameras 1, 2, and 3 for a total time of 104.5, 103.5, and 102.5 seconds, respectively. To prevent a reoccurrence of this problem, operational constraints were undertaken to assure the activation of the 6-volt power supply before camera activation.

Recorder Components

The AVCS tape recorder performance was satisfactory before its premature failure during the fourth month in orbit 1444. Before the failure, the recorder had delivered more than 112,000 pictures of good to excellent quality with no discernible degradation. The recorder exhibited a consistent orbital pressure profile of 17.5 ± 0.5 psi and showed no evidence of long-term pressure degradation.

Residual Video

During recorder playback, prelaunch through failure, video data at times were exhibited between "triplets" because of the incomplete erasure of the recording tape (Figure 9-12). It should be noted that the quality of the received video data was not affected by this phenomenon.

Recorder Drive Voltage Malfunction (Interrogation 1124U)

The AVCS recorder has a dual 400-Hz voltage mode of operation. Its circuitry is such that either a higher voltage or a reduced voltage is applied through a start/run relay to the field winding of the tape recorder drive motor and through a phase shift capacitor to the quadrature winding of the motor. The higher voltage (start) is used to provide high starting torque, which enables the motor to reach synchronous speed within 1 second. After approximately 1 second, a time delay circuit switches the start-run relay to the low-voltage (run) mode and thereby supplies a lower voltage to the motor field windings so that the motor runs at reduced power.

During interrogation 1124U, AVCS playback was commanded during the record portion of the AVCS cycle. Telemetry indicated that the recorder, upon receipt of the playback command, went to the high voltage (start) mode and remained in this mode throughout the entire 8-minute playback sequence; then normal operation was resumed. The most probable cause of this action is improper operation of either the time delay circuit or start/run relay. Operational constraints were undertaken to avoid commanding playback during the record portion of the AVCS cycle. No abnormal recorder temperatures were observed during this extended period of high-voltage application.

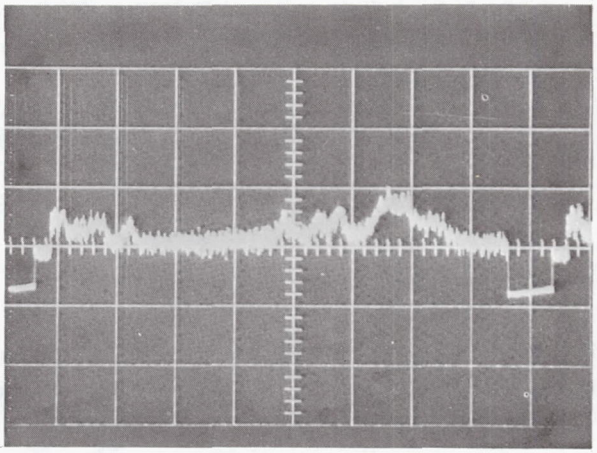

(a) AVCS VIDEO DATA SCAN LINE

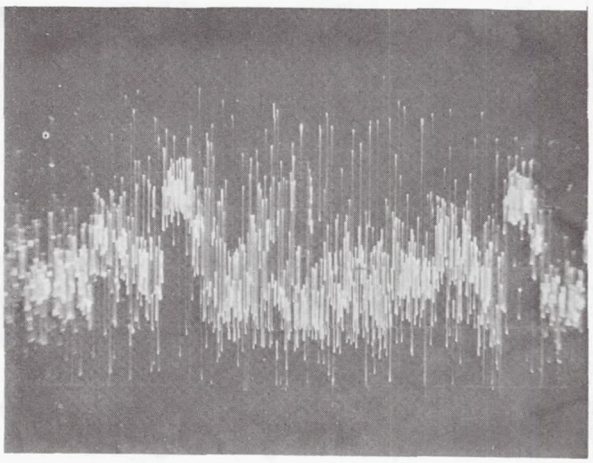

(b) BETWEEN-FRAME RESIDUAL AVCS VIDEO DATA (note residual sync pulses)

Figure 9-12—Oscilloscope display photographs of AVCS video data.

Tape Recorder Failure (Orbit 1444)

During interrogation 1444U, the AVCS was commanded into playback and, after the reception of approximately 1-3/4 pictures, the transmission of both AVCS video data and timing ceased. The playback of the HRIR Subsystem, in progress at the time, was allowed to continue to completion. Upon completion of the HRIR playback, the S-band transmitter remained in transmit. This condition necessitated the transmission of command 032 (AVCS recorder record/S-band off), which terminated the S-band transmission and placed the AVCS recorder in the record mode. Before being placed in the record mode, the AVCS had been in the playback mode for 7 minutes

and 30 seconds versus the normal playback duration of 4 minutes and 30 seconds (29 triplets). Pertinent telemetered AVCS functions are listed in Table 9-4. Telemetry revealed that after the loss of AVCS video and timing the following occurred:

a. The AVCS (including tape recorder) remained in the playback mode,

b. Video and timing were not present at either the output of the playback amplifiers of the AVCS tape recorder, or in the composite signal input to the S-band Transmitter, and

c. Subsystem temperatures and pressures remained normal throughout playback; recorder temperature and pressure were 23.5°C and 14.5 psi, respectively.

Table 9-4

AVCS Telemetry Functions Associated with Tape Recorder Failure (Orbit 1444).

Function	Command No.	Telemetered Value (tmv)		Remarks
		Before Loss of Video and Timing	After Loss of Video and Timing	
Recorder temp.	(213)	1.45 (23.5°C)	1.5 (24°C)	Normal thermal and pressure characteristics were maintained.
Recorder pressure	(214)	4.60 (14.5 psi)	4.60 (14.5 psi)	
Channel 1 P/B Amp.	(219)	0.80	0.00	Video and timing signals were present at the output of recorder playback (P/B) amplifiers before malfunction; not present after malfunction.
Channel 2 P/B Amp.	(220)	1.50	0.30	
Channel 3 P/B Amp.	(221)	1.20	0.30	
Channel 4 P/B Amp.	(222)	0.80	0.00	
Recorder drive volt.	(223)	1.35	1.35	Recorder remained in P/B after loss of signals.
Mux No. 1 osc. level	(225)	3.95	3.95	Invariant levels eliminated systems multiplexers as source of malfunction.
Mux No. 2 osc. level	(226)	3.90	3.90	
Mux No. 3 osc. level	(227)	3.50	3.50	
Mux No. 4 osc. level	(228)	3.80	3.80	
-24.5 vdc mux. supply	(229)	4.95	4.95	Indicated subsystem remained in P/B state.
Mux sum amplifier	(230)	1.5	0.40	Before malfunction, AVCS video and timing were present in the composite signal input to the S-band; after malfunction, only HRIR video and timing present.

Information contained in the AVCS pregridding program revealed that erratic movement of the AVCS recorder tape first began during orbit 1440 and continued until the time of failure. Figure 9-13 is graphic representation of normal characteristics and the erratic characteristics first exhibited during orbit 1440. The erratic time between the reception of the video triplets and the subsequent recorder failure can probably be attributed to increased friction in the tape reel bearings, increased motor bearing friction, or a change in the characteristics of (or failure of) the negator spring.

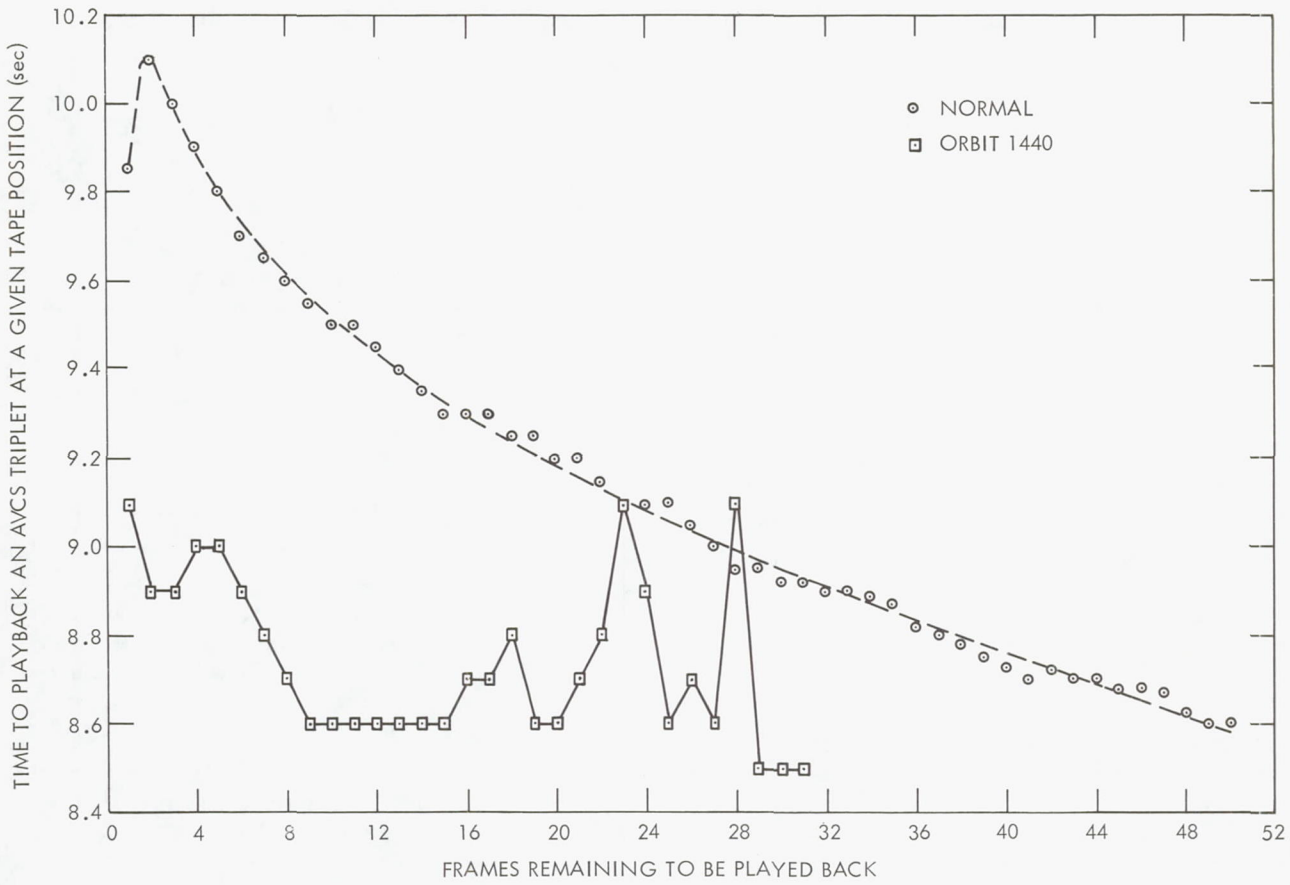

Figure 9-13—Time to play back given AVCS triplets as a function of the number of photograph frames remaining to be played back.

After the recorder failure in an effort to determine the nature of the recorder failure, the prototype recorder (S/N P3) was bench-tested at the GE Valley Forge Space Technology Center. Samples of the startup current drawn by the recorder were photographed during normal and simulated failure modes. The current drawn by the prototype recorder during normal and failure modes was then correlated with that drawn by the flight recorder before and after the failure. (The capability of the HRIR Subsystem to record the spacecraft regulated bus current was used to obtain the necessary data.) However, the current-drawing characteristics of the recorder before and after the failure were not consistent enough to allow precise identification of the source of the

failure. A summary of the experiments performed to reinstate recorder operation is presented in Table 9-5.

Table 9-5

Summary of AVCS Experiments.

Orbit	Experiment/Result
1602 to 1694	Playbacks attempted at random throughout this period; none produced modulation; recorder power on throughout period
1695	Recorder power turned off following unsuccessful playback attempt
1696 to 1788	Playbacks attempted throughout this period with recorder power off; produced no modulation
1789	Recorder power turned on
1790 to 1890	Same as 1602 to 1694
1891	Playback produced 3 seconds of video and timing; data contained two recorder startup cycles which were recorded during separate orbits
1892	Playback attempt produced 3 seconds (in bursts) of video data only (Note 1)
1893	Playback attempt produced no modulation
1895	Same as 1892
1896	Same as 1893
1908	Same as 1892
1909	Playback attempted which produced no modulation; day/night override activated; two-camera operation instituted (Note 1)
1910	Playback attempt produced 3 seconds of video data (3 cameras) only (no timing); (Note 1) day/night override turned off
1912	Recorder power turned off
1915	Recorder power turned on
1920	Same as 1892 (recorder power turned off)
1921	Playback attempted, no modulation present; recorder power turned on
1922 to 1936	Various attempted playbacks produced no modulation
1936 to 2000	System in record, 2-camera day-time operation
2001 to 2107	Playbacks attempted at random throughout this period; none produced modulation; system operated in 2-camera, day operation only
2108	Playback attempt produced 3 seconds (in bursts) of video data only
2108 to 2400	Same as 2001 to 2107
2391	Three-camera operation resumed; pseudo-direct pictures obtained thereafter

Note (1) The frequency bandpass of the timing channel of the AVCS multiplexer is 10 Hz, and of the three video channels, 130 Hz. To obtain timing information, the recorder must be running at 90% of normal speed, under which speed the frequency spectrum of the AVCS timing would be outside the bandpass capabilities of its associated circuitry. After orbit 1891, only short bursts of video (without timing) were received. It was decided that after orbit 1909, only two cameras at a time would be energized. A system of selective rotation of cameras was instituted to assist, in the event of future operation of only video data, in the time correlation of the data received.

S-band Components

The performance of the S-band transmitter was excellent with no indication of long-term degradation in power, pressure, or frequency stability. Transmitter pressure after 1 year in orbit averaged 27.5 psi. This compares favorably to the initial 27.8 psia averaged during the first 30-day orbital period.

Premature S-band Termination (Interrogation 909U)

During interrogation 909U, S-band transmission ended abruptly after 53 seconds of transmission. Simultaneously, telemetry indicated that -24.5-vdc power was removed from the AVCS multiplexer, but the AVCS recorder, HRIR recorder, and multiplexer remained in the playback mode. It was suspected that a spurious U960 command was received, which resulted in the premature termination of the S-band transmission. Further substantiation was not possible since the prime FM demodulator was in use at the time.

S-band Signal Strength

The relationship between the received signal strength of the 5-watt Nimbus II S-band Transmitter and the slant range/antenna elevation angle is shown in Figure 9-14.

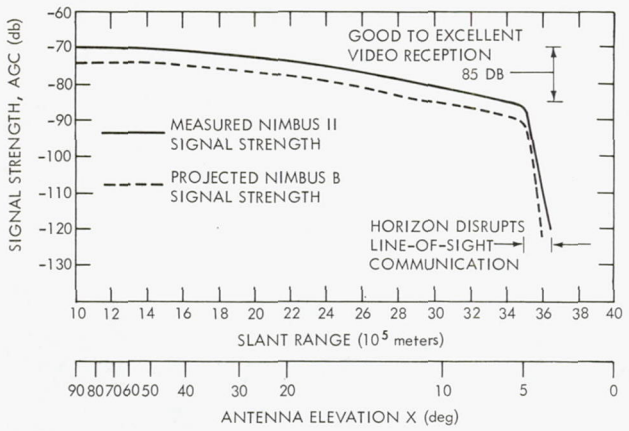

Figure 9-14—S-band signal strength versus range.

The quality of the video data received at elevation angles of 6 degrees (signal strength -85 db) is good to excellent and comparable to that received at higher elevation angles. For antenna angles of less than 6 degrees, as the local horizon disrupts line-of-sight communication, the signal strength decreases rapidly to the noise threshold of the received -120 db with a corresponding degradation in data quality. The incorporation of 2-watt S-band transmitters on Nimbus B will result in a 4-db decrease in signal strength. However, signal strength should be sufficient for the reception of high-quality data at elevation angles of 10 degrees so as not to require special consideration in regard to antenna elevation in the scheduling of S-band interrogation (the only restraint is an antenna elevation of 10 degrees and above the local horizon). Measurements for the foregoing analysis were taken during orbits 319, 498, 4692, 4772, and 5171. The signal strength and slant range values are comparable. This indicates that the power output of the S-band transmitter has not degraded significantly through the first year in orbit.

VIDEO QUALITY

The quality of the AVCS video has been generally satisfactory. Radio frequency interference of various origins, discussed in following subparagraphs, degraded the quality of the subsystem

data and has been the major shortcoming of the overall video quality. Before the failure of the subsystem tape recorder in orbit 1444, the recorded data showed no evidence of recorder degradation. Since the recorder failure, pseudo-direct pictures have been the only medium by which sensory data have been received. During the 13th month in orbit, Camera 1 experienced a loss of focus which degraded the quality of this camera's video. Cameras 2 and 3 continued to perform satisfactorily and show no evidence of long-term degradation.

Vidicon Response

The transfer characteristics of the three vidicons have remained consistent and have indicated little evidence of long-term vidicon degradation (Figure 9-15).

Interference

The following subparagraphs describe the major AVCS shortcoming—its susceptibility to interference generated not only from within the subsystem (high voltage chopper) but also externally generated interferences (APT, MRIR, PCM beacon).

MRIR Transmitter Interference

Before the failure of the MRIR Subsystem tape recorder, the playback of MRIR data during the period that the AVC Subsystem was recording resulted in the obliteration of the video of Camera 2 and a shifting of the video level of Camera 3 towards "white" while the video of Camera 1 was unaffected by the MRIR transmissions (Figures 9-16 and 9-17). This interference was present consistently until the failure of the MRIR Subsystem tape recorder in orbit 985 eliminated the necessity of MRIR transmitter operations.

Beacon Transmitter Interference

Beacon transmitter interference which amplitude-modulates the AVCS video was the most serious impediment to overall video quality. Two sources have contributed to this interference (Figure 9-16)—the 10-kHz time code modulation of the beacon carrier during transmission of real-time A PCM data and the 15-kb PCM data transmission rate during stored A PCM playback.

During APT Subsystem or HAX operation, the level of AVCS video shifts slightly, which makes the 10-kHz beacon interference more pronounced on the photograph (refer to Section 10). Figure 9-18 illustrates the effect of APT operation on the AVCS video.

Since the failure of the PCM Subsystem tape recorder, AVCS pictures ranging from good to excellent have been obtained by commanding the PCM Subsystem tape recorder into playback. With the PCM tape recorder inoperative, there was no modulation on the beacon carrier and, therefore, neither 15-kHz nor 10-kHz interference in the pictures. Figure 9-19 illustrates this principle and is typical of the quality of the data received.

ORBIT 313U

CAMERA 1: ORBIT 3187
CAMERAS 2 AND 3: ORBIT 5450

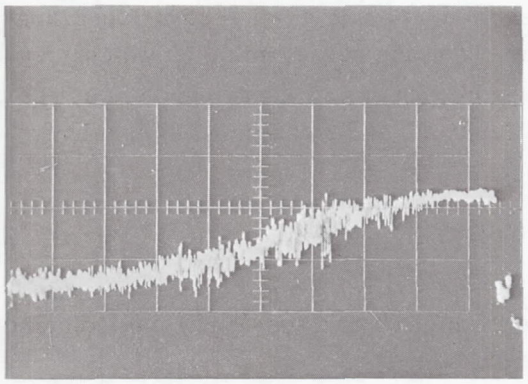

CAMERA 1

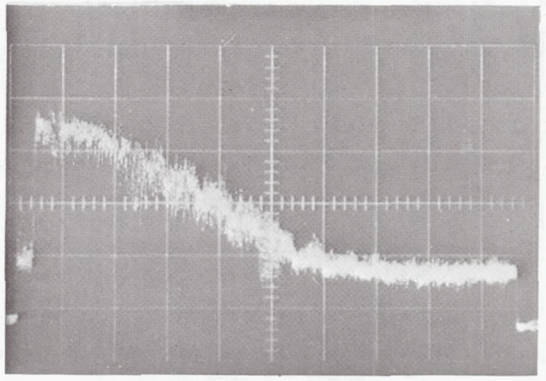

FLASH TUBES OF CAMERA 1 BECOME INTERMITTENT (orbit 3250) AND SUBSEQUENTLY FAILED

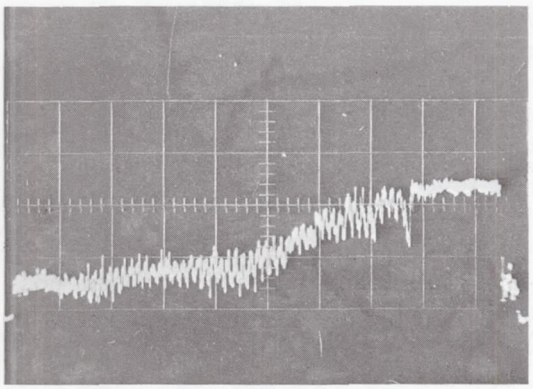

CAMERA 2

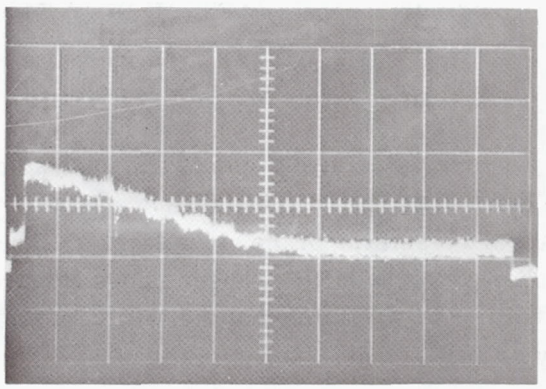

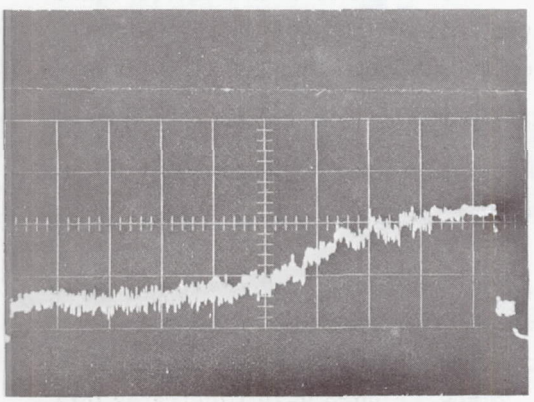

CAMERA 3

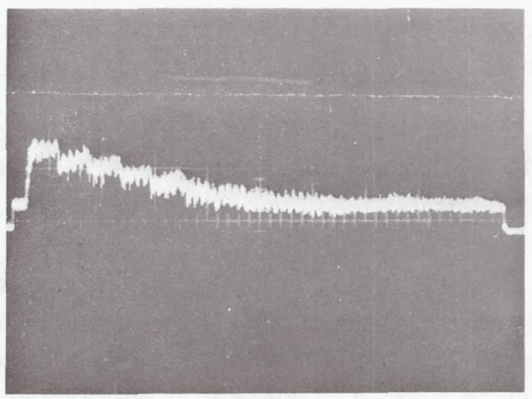

Figure 9-15—AVCS photographs showing grey-scale video transfer characteristics.

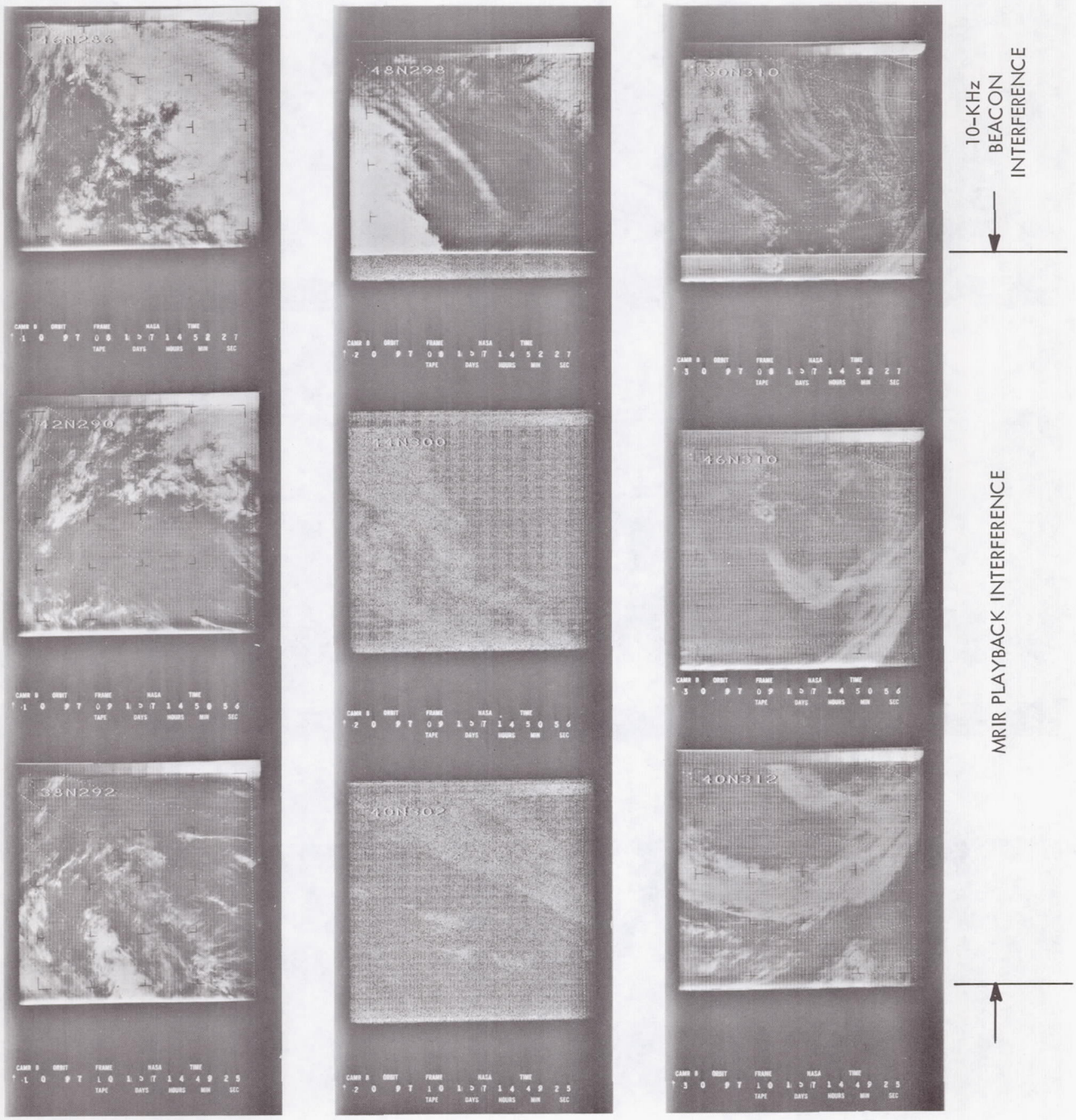

Figure 9-16— AVCS photographs of MRIR transmitter interference patterns.

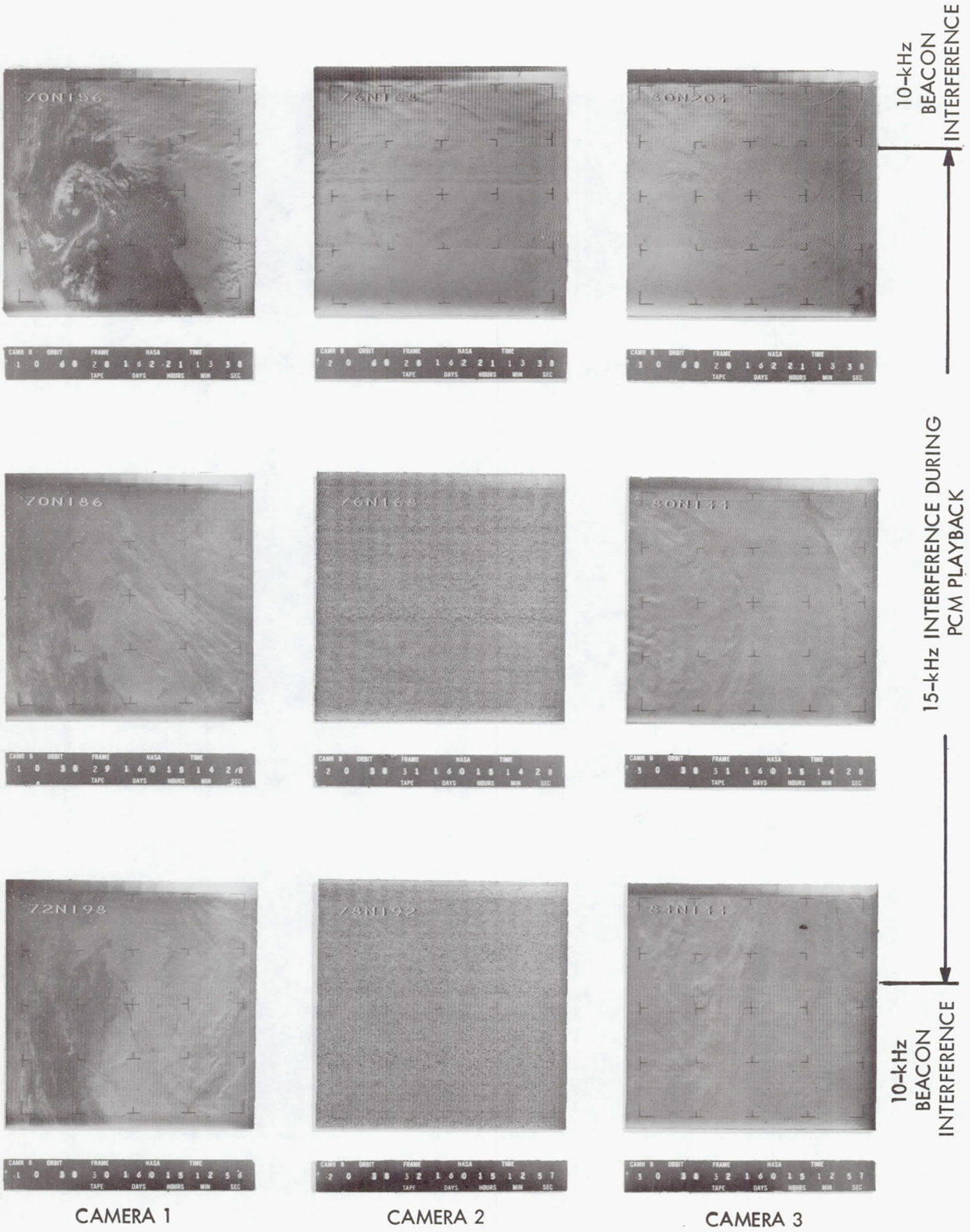

Figure 9-17—AVCS photographs of PCM Beacon transmitter interference patterns.

Figure 9-18—AVCS photographs showing 10-kHz interference increasing with APT subsystem in ON mode (orbit 8U).

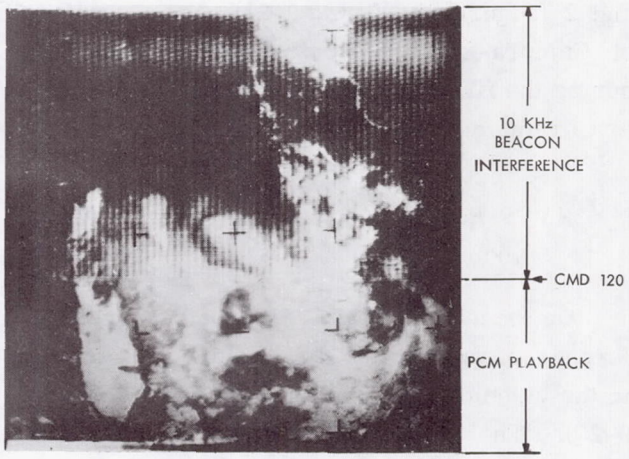

Figure 9-19—AVCS (orbit 4399) photograph showing transition from 10-kHz Beacon interference to period of interference-free data during PCM playback mode.

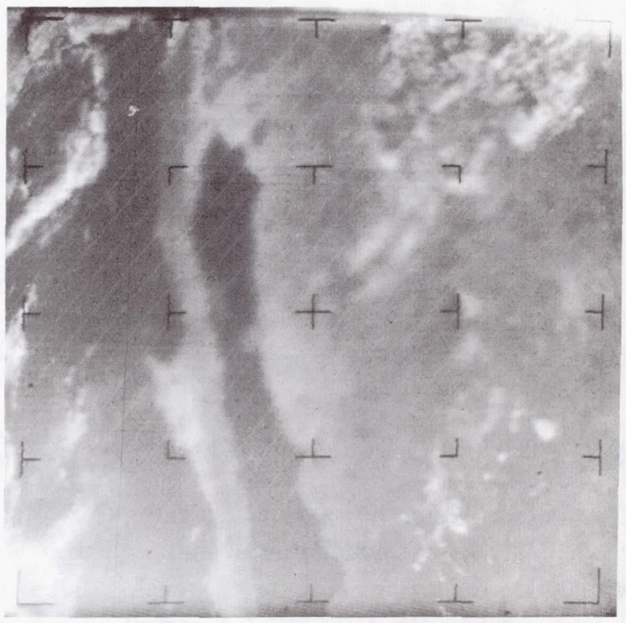

Figure 9-20—AVCS camera no. 1 photograph showing high-voltage chopper interference.

Microphonics

Microphonics of approximately 3.5 kHz sometimes appeared on the video of Cameras 1 and 2 (Figures 9-20 and 9-21). The magnitude of Camera-2 microphonics increased slightly during the first year in orbit while that of Camera 1 remained free of microphonic interference.

AVCS High-Voltage Converter (Chopper) Interference

On occasions, faint AVCS chopper interference of approximately 3.3 kHz was present in the video of Camera 1 only (Figures 9-11 and 9-20). The origin of this interference is the high-voltage converter circuitry in the AVCS camera electronics. This type of interference was rather rare and did not seriously degrade the overall video quality.

APT Transmitter Interference

Interference at 2400 Hz (Figure 9-21), originating from the APT Subsystem, which used a 2400-Hz AM subcarrier, was present in the video of Camera 2 only when the 10-kHz modulation was removed from the beacon (during PCM playback. This interference was minor and was not evident when the heavy 10-kHz beacon interference was present.

AVCS 50-kHz Timing Signal Interference

During the 10th and 11th month in orbit, interference occasionally was exhibited which was believed to result from the crosstalk between the 50-kHz AVCS timing signal and the video channels in the ground station video demultiplexer. This interference severely degraded the quality of the video data (Figure 9-22). It was suspected that an amplifier inserted in the data link between the Data

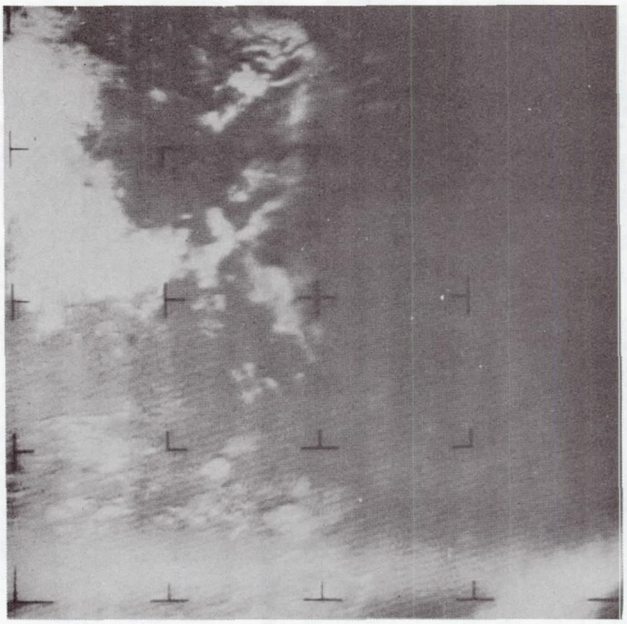

Figure 9-21—AVCS photograph showing APT subsystem transmitter interference. Shaded vertical bars, thought to be interference from 2400-Hz APT subsystem AM subcarrier during orbit 4399. Diagonal interference pattern in lower portion of photo is microphonics resulting from mechanical vibration of the internal elements of the vidicon.

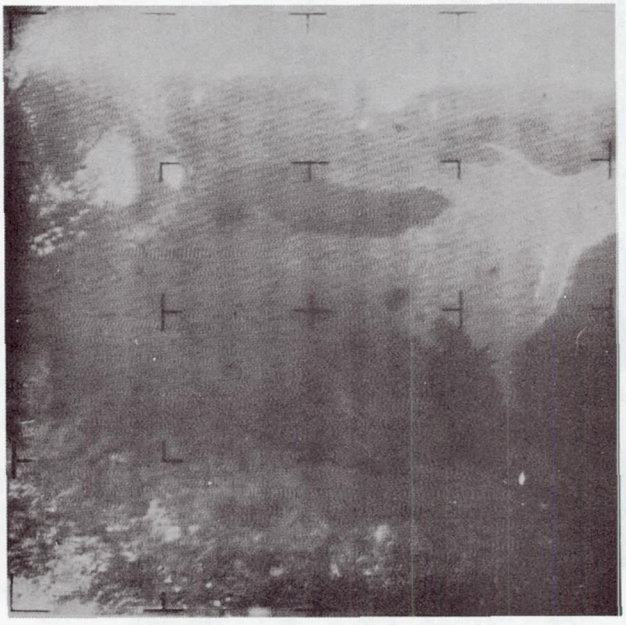

Figure 9-22—AVCS photograph showing 50-kHz timing signal interference.

Acquisition Facility at Rosman, North Carolina and the Nimbus Data Handling Station at Goddard Space Flight Center may have caused this problem; when the amplifier was removed, the interference disappeared and has not recurred.

Night Photography

During interrogation 1849R, a direct picture of Hurricane Inez was attempted using the reflected light from a full moon as a light source. The reflected moonlight intensity was below the threshold light intensity of the vidicons and the resulting pictures were without discernible video information. This experiment represented the first orbital execution and demonstrated the operational ability of the following commands:

Command	Function
056	AVCS Day/Night Override ON
002	AVCS Direct Picture
044	AVCS Day/Night Override OFF

Table 9-6

AVCS Anomalies.

Anomaly	Cause	Remarks
Camera 1 iris failed to maintain proper orbital profile resulting in improperly exposed photographs	Failure of iris drive no. 2 of Camera 1	Since failure, iris drive no. 1 used exclusively and has shown no evidence of degradation in performance
Four frames of Camera 2 video completely washedout (orbit 1309)	Shutter malfunction	Anomaly did not reoccur
Grey scale of Camera 3 improperly illuminated (orbit 3520)	Failure of either flash tube of associated electronics	A-scope presentations indicated intermittent operation of Camera 3 flash tube subsequent to orbit 3520
Telemetered value of the housing temperature indicated a substantial decrease from 32.8°C (orbit 3958)	Malfunction in telemetry conditioning circuitry or mechanical degradation of thermal bond between temperature sensor of camera housing	Temperature of camera mounting plate did not show corresponding decrease
Loss of focus in the video of Camera 1 during 11th month in orbit	Change in the characteristics of Camera 1 lens system	Focus of Cameras 2 and 3 video remaining satisfactory
Telemetered value of temperature of Camera 2 electronics indicated instantaneous temperature changes of 20°C (orbit 692)	Electrical failure of either thermistor temperature sensor or grounding in telemetry conditioning circuitry	----

Table 9-6

AVCS Anomalies (Continued).

Anomaly	Cause	Remarks
Loss of video data and timing during interrogation 1444U	Tape recorder failure	Recorder failure eliminated data storage capability of this subsystem
Video data obliterated during MRIR data transmission	MRIR transmitter interference	Failure of MRIR tape recorder eliminated necessity of MRIR transmitter operation
10 and 15-kHz interference	Beacon transmitter interference	10-kHz real time A code interference 10 kHz - 15 kb stored A PCM data interference
Microphonics, Cameras 1 and 2	Vibration of internal elements of vidicon	Occasionally present
3.3-kHz interference (Camera 1)	AVCS high-voltage converter circuitry	Rarely present
2400-kHz interference (Camera 2)	APT transmitter interference	----

SECTION 10

APT SUBSYSTEM AND HAX

INTRODUCTION

The performance of the Automatic Picture Transmission (APT) Subsystem continues to be entirely satisfactory although a gradual shift in the dc level of the video has occurred. This shift, however, can be compensated by the ground station processing equipment. Before the failure of the HRIR Subsystem tape recorder, the HAX Module (DRIR Subsystem) provided excellent, interference-free, real-time transmission of HRIR video.

A summary of APT Subsystem anomalies is presented in Table 10-6.

DESCRIPTION

The APT Subsystem (Figure 10-1) is a supplementary meteorological system that provides real-time transmission of cloud-cover photography to local ground stations for weather observation and forecasting applications. The HAX Module, which is used in conjunction with the APT Subsystem, provides the capability of transmitting real-time HRIR video. The APT Subsystem, consisting of a camera assembly, electronics module, automatic sync generator (ASG), and a VHF transmitter, is programmed for continuous operational cycles of picture-taking and transmission.

The 1-inch storage vidicon tube is equipped with a wide-angle, 107.8-degree (across the diagonal) Tegea Kinoptic f/1.8 lens with a focal length of approximately 5.7 millimeters. The image is limited to a square (84 by 84 degrees) by the scan pattern used in the vidicon. The ground coverage at an altitude of 600 nm is in the order of 1250 by 1250 nm. Assuming a circular orbit, the 208-second picture cycle results in the foregoing ground coverage with overlaps of approximately 300 nm. The APT Subsystem has a linearity of ±0.5 percent and a resolution of approximately 1-1/2 to 2 miles per scan line with a total scan of 800 lines.

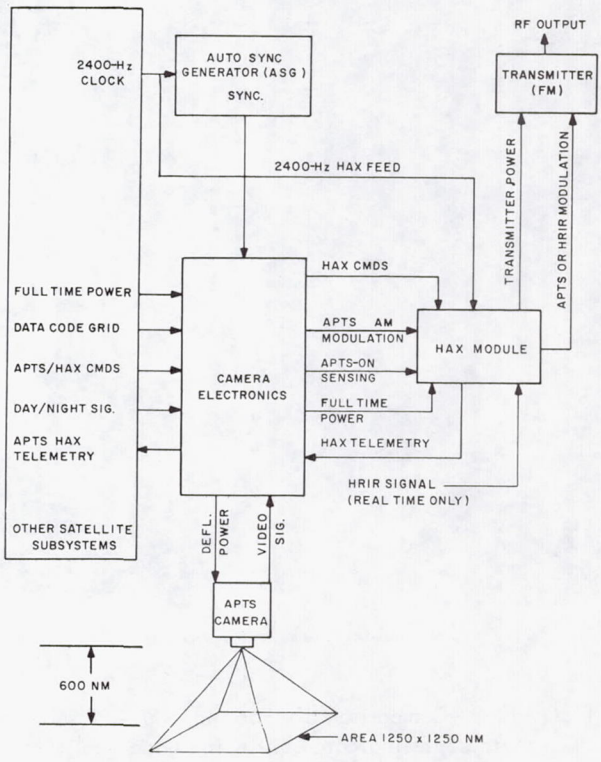

Figure 10-1—APT subsystem block diagram.

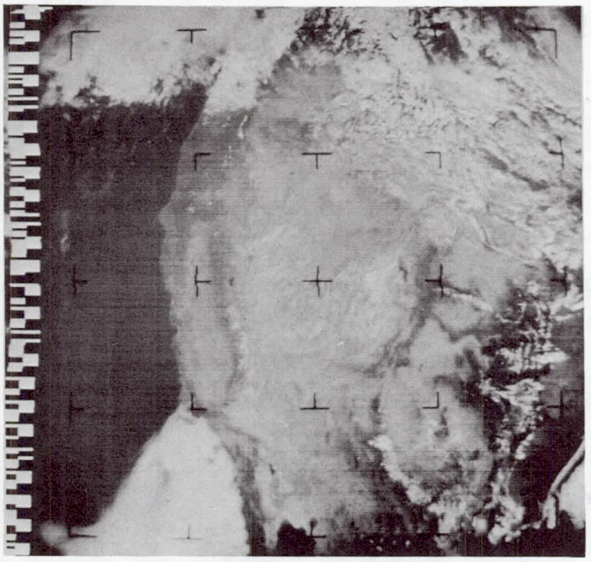

(a) WESTERN UNITED STATES, JULY 12, 1966 (orbit 372)

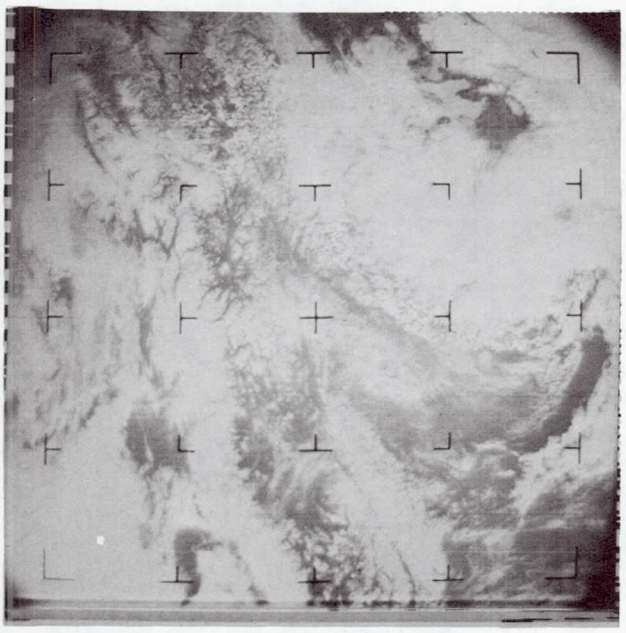

(b) NORTHWESTERN CANADA, JULY 7, 1967 (orbit 5172)

Figure 10-2—Comparison of 1966 and 1967 APT subsystem photographs indicate continuing good quality.

Sensitivity of the subsystem is 10,000 foot-lamberts for highlight brightness (whitest white). The cutoff point, below which noise is an influencing factor, is 500 foot-lamberts. The signal-to-noise ratio is 32 db or greater.

To the formerly unoccupied blanking margin along the side of the APT picture, has been added a data code and grid (DCG), which permits the transmission of orbital information and time code as an integral part of the APT Subsystem video. These data are obtained from four storage memory locations of the spacecraft clock, plus the time of the vidicon exposure from the spacecraft clock.

The vidicon tube in the APT camera is exposed by an electromechanical focal plane shutter for 10 milliseconds. The image impinged on the vidicon faceplate is stored electrically, and, because of the nature of the vidicon tube, it is available for slow readout (200 seconds). During readout, the video information is sampled by a pulse technique rather than by a continuous readout, because this method affords a better signal-to-noise ratio for the slow readout rate of the APT Subsystem. During readout, the vidicon scanning beam is pulse-modulated by applying pulses to the vidicon cathode. The beam sampling rate is 1140 times per horizontal line, and the duty cycle (the ratio of the pulse duration time to the pulse repetition time) is 12 percent. The readout, as seen at the output of the vidicon amplifier in the camera sensor assembly, consists of amplitude-modulated pulses. A video detector in the camera electronics module then detects the information, producing a continuous analog readout. The detected signal then is used to amplitude-modulate the 2400-Hz subcarrier (derived from the Nimbus clock), resulting in a double-sideband modulated subcarrier with sidebands of 1600 Hz above and

below the subcarrier frequency. For transmission, the 2400-Hz AM subcarrier is applied to the solid-state 5-watt transmitter, which has an integral frequency modulator. The result is a 136.95-MHz FM signal which is transmitted to the ground by means of a quadraloop antenna.

For the transmission of real-time HRIR video, the APT VHF transmitter is energized, and the HRIR video signal is applied to the modulator in the HAX Module. The signal which is applied to the APTS FM transmitter is identical with the signal otherwise obtained from the APT electronics module.

On the ground, the signal is received by a circularly polarized antenna, fed into an FM receiver and processed by facsimile recording equipment to produce a real-time cloud cover picture of the locale of the particular ground station. The ground station will automatically receive a picture sequence from the beginning of a 208-second picture frame. At the beginning of this 208-second period, a 300-Hz start tone, transmitted to the ground for 3 seconds, automatically shifts the facsimile equipment from the standby to the operation mode. During the next 5 seconds, phasing pulses transmitted to the ground station automatically synchronize the facsimile equipment with the vidicon scanning beam. The image printout follows for 200 seconds, and is reproduced line-by-line on the facsimile equipment as it is scanned in the vidicon. Processed sensory data are presented in the format shown in Figure 10-2.

FLIGHT OBJECTIVES

Flight objectives for the APT and HRIR Subsystems are given in Tables 10-1 and 10-2, respectively.

Table 10-1

APT Subsystem Flight Objectives.

Flight Objectives	Remarks	
	6 Months	13 Months
Demonstrate the capability of the APT Subsystem to provide high quality photographs of the earth's surface and cover and transmitting same in real time	The performance of the subsystem was entirely satisfactory.	The APT Subsystem continued to perform satisfactorily. A gradual shift in the dc level of the video occurred, but this was compensated for in the ground processors.
Prove feasibility of providing ephemeris data (DCG) to APT users via the satellite	The DCG portion of the APT Pictures proved to be a complete success.	The DCG continued to be satisfactory.

Table 10-2

DRIR Flight Objectives

Flight Objective	Results	
	6 Months	13 Months
Demonstrate the feasibility of direct readout of high resolution infrared data using the APT transmitter	The HAX Module provided good quality, interference-free transmission of infrared video from the HRIR Subsystem until orbit 2455, at which time the HRIR tape recorder failure precluded further reception of data.	The status is the same as mentioned under the 6-month results.

ELECTROMECHANICAL PERFORMANCE

The Electromechanical performance of the APT Subsystem was satisfactory with the exception of the characteristics discussed in the following subparagraphs. Subsystem telemetry has not indicated the presence or development of any anomolistic conditions. A summary of subsystem performance is presented in Table 10-3.

Inadvertent Triggering of Camera Shutter

The APT Subsystem camera shutter was triggered immediately following separation by a voltage transient, recording a picture of the adapter and the forward bulkhead of the Agena (Figure 10-3).

Table 10-3

APT-HAX Performance Summary.

Requirements		Results
General		
300-Hz start tone	Distinct, no losses	Satisfactory
12.5-msec phasing pulse	Distinct, no losses	Satisfactory
Data Code and Grid (DCG)	Always correct	Partially satisfactory (1)
Camera Performance		
Resolution	Over 500 lines	Satisfactory
Distortion	0.5% V&H	Satisfactory
Focusing	Consistent with resolution	Satisfactory
Shading, contrast	Negligible deteriorating compared with pre-launch test data	Satisfactory (2)
Quality	Uniform	Satisfactory
Telemetry	Adherence to calibration and stability	Satisfactory (3)
HAX Performance		
Picture quality	Uniform	Satisfactory
Telemetry	Adherence to calibration and stability	Satisfactory
Transmitter Performance		
Frequency	136.950 MHz ± 0.01%	Satisfactory
Power	3.5 to 4.5 watts	Satisfactory (4)
Telemetry	Adherence to calibration and stability	Satisfactory
Operability	Dependable execution of commands	Excellent
Compatibility	Compatible with other subsystems (RFI)	Partially satisfactory (5)
Reliability	Reliable continuous operation	Excellent

Notes:
(1) The DCG signal was susceptible to upsets caused by noise entry into the command receiver (refer to Section 7 for details). The APT has reliably transmitted DCG information provided by the clock subsystem.
(2) A shift in the dc level of the video occurred which requires compensation at the ground station to utilize the full dynamic range of the video (refer to Section 10).
(3) Refer to Section 10.
(4) Refer to Section 10.
(5) The APT/HAX operation results in a shift in the signal level of the AVCS video into the FM modulator (refer to Section 9). HAX command execution times required spacecraft operational mode planning (refer to Section 10).

The known dimensions of the Agena and the camera optical characteristics indicated that the launch vehicle was then 9.8 feet from the spacecraft. Assuming that the separation springs imparted the expected 4.4-fps velocity, the indicated time of shutter cycling was thus 2.22 seconds after separation. The photograph of the Agena forward bulkhead and spacecraft adapter was read out at initial subsystem turn-on in orbit 5U. Vidicon storage capability was thoroughly demonstrated, as the image was stored almost 7-1/2 hours, instead of the normal average of 204 seconds.

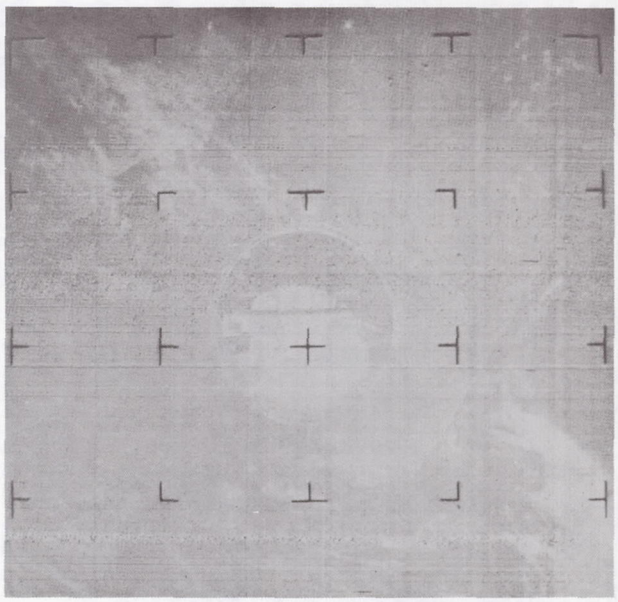

Figure 10-3—APT photograph of Nimbus II adapter 2.2 seconds after separation. (Circular adapter is seen as "shadow" in center of photograph.)

HAX Commanding

A clock upset occurred during the Ulaska station pass on orbit 28. Subsequent investigation showed that the upset coincided with the time of execution of a HAX OFF command. At this time, the AVCS was on and the S-band transmitter was warming up. A visicorder readout of the HRIR video signal showed a 1-volt peak-to-peak transient in the 4-volt signal level with a damped oscillation having a 60 msec period and visible for a 0.4 sec duration. The time code was disrupted, showing several "14" digits in the binary-coded-decimal signal. A clock time upset occurred during the thermal-vacuum test phase on February 19, 1966. When the execution of the HAX OFF command resulted in electrical transients causing a clock upset, operational procedures were instituted that prevented recurrence of this problem by prohibiting a HAX OFF switching event during S-band transmitter operation.

APT-HAX Subsystem Grounding

APT and HAX Module operation induced extraneous ground currents that produced a negative shift of -0.10 vdc in the ground potential of the spacecraft. This is evidenced by the shift of telemetry values for various functions and by a shift in the overall video level of AVCS Camera 2 during APT Subsystem operation. Table 10-4 is a comparison of selected telemetry values during APT and HAX operation.

Data Code and Grid

The APT Subsystem Data Code and Grid was continually susceptible to upset by noise entry into the clock subsystem (refer to Section 7). The APT Subsystem reliably transmitted DCG information supplied by the clock subsystem. On occasions, the DCG has exhibited an offset

Table 10-4

Telemetry Shift Correlation.

Telemetry Function No.	Function Description	Correlation Remarks	
		APT Operating	HAX Operating
199	AVCS Camera 1 high voltage	(+) Positive 2 PCM count shift during APT operation	(+) Positive 2 PCM count jitter induced during HAX operation
200	AVCS Camera 2 high voltage	(+) Positive 2 PCM count shift during APT operation	No change
201	AVCS Camera 3 high voltage	(+) Positve 2 PCM count shift during APT operation	No change
251	APT power amplifier drive	4.4 tmv	4.5 tmv
252	APT DC converter low voltage	4.6 tmv	4.8 tmv
253	APT DC converter high voltage	5.15 tmv	4.2 tmv
254	APT transmitter power output	3.9 tmv	3.9 tmv to 3.95 tmv (ripple) induced during HAX operation

pattern (Figure 7-7). This has been attributed to the phasing relationship between the readout of an APT picture scan line and the 1-Hz clock signal which synchronizes the release of the DCG signal by the clock. Additional discussion is presented in Section 7.

Transmitter Power Output Telemetry

The telemetered value of the power output of the APT transmitter increased from 3.2 tmv (final preshipment antenna tuning) to 3.5 tmv post-launch orbital average and finally to 4.05 tmv (Table 10-5). Prelaunch testing indicated that the telemetry monitor of transmitter power output is sensitive to VSWR changes in the system quadriloop antenna. The change in the telemetered value most probably resulted from a change of the antenna input impedance and tuning because of outgassing of absorbed moisture rather than because of a change in the actual RF power output of the transmitter.

Table 10-5

Telemetered Value of APT Transmitter Output.

Orbit	Telemetry Value (tmv)
(Prelaunch)	3.2
6	3.5
100	3.85
200	3.85
300	3.95
600	3.95
800	4.05
5000	4.05

VIDEO QUALITY

The APT video ranged from good to excellent quality. Occasional interference patterns, discussed below, and a dc change in the video level, which is compensatable in ground station processors, have been the only anomalies associated with the APT video. There was no evidence of long-term degradation in the vidicon (Figure 10-2) or associated subsystem electronics. The HAX video (Figure 10-4) was of satisfactory quality and free of interference patterns, with the exception of those associated with the HRIR subsystem radiometer (sunlight interference, detector cell overheating, etc.; refer to Section 11).

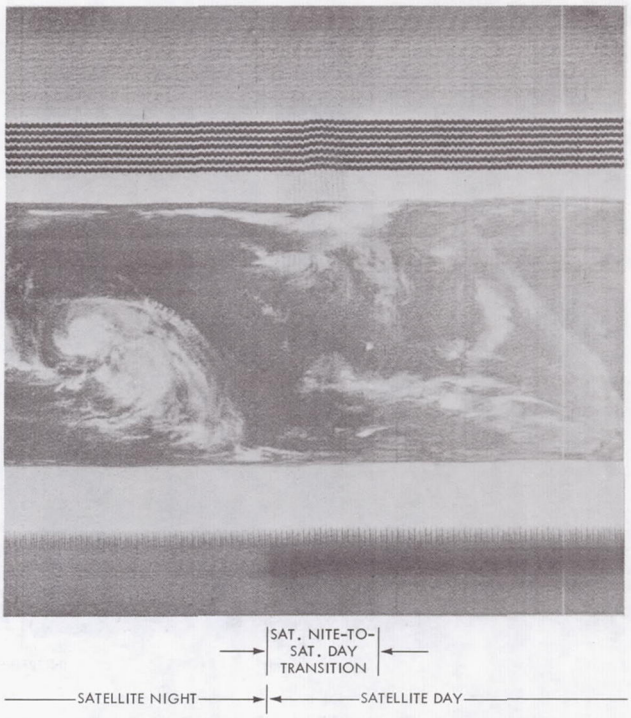

Figure 10-4—HRIR-HAX photograph of hurricane Alma (June 6, 1966) showing sunlight input at transition from satellite day to satellite night.

Vidicon Defects

Belmish spotting and dark scan lines resulting from imperfections within the photoconductor or insulator layer of the subsystem vidicon have been continuously present in the APT video (Figure 10-5). The magnitude of the imperfections has increased slightly after launch but not enough to seriously impair the video content of the APT photographs.

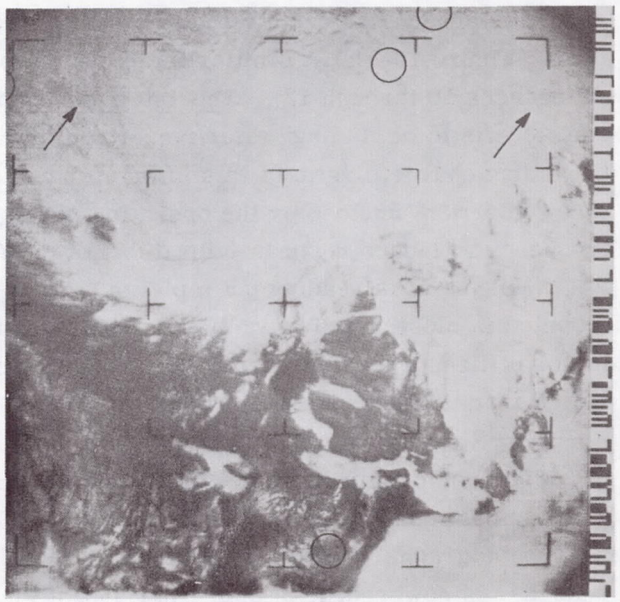

Figure 10-5—APT subsystem photograph showing vidicon blemish spotting (circles) and dark scan-line (arrows) imperfections.

Microphonics

Microphonic interference from 0.7 to 0.9 kHz has occurred occasionally. The interference has increased in magnitude as the vidicon aged, affecting approximately one-eighth of the picture area during the 13 months after launch to approximately one-fifth of the picture area currently (Figure 10-6). This can be attributed to mechanical degradation of the rigidity of the vidicon internal elements. This interference should not be confused with the interference associated with the playback of the HRIR Subsystem tape recorder to be discussed below.

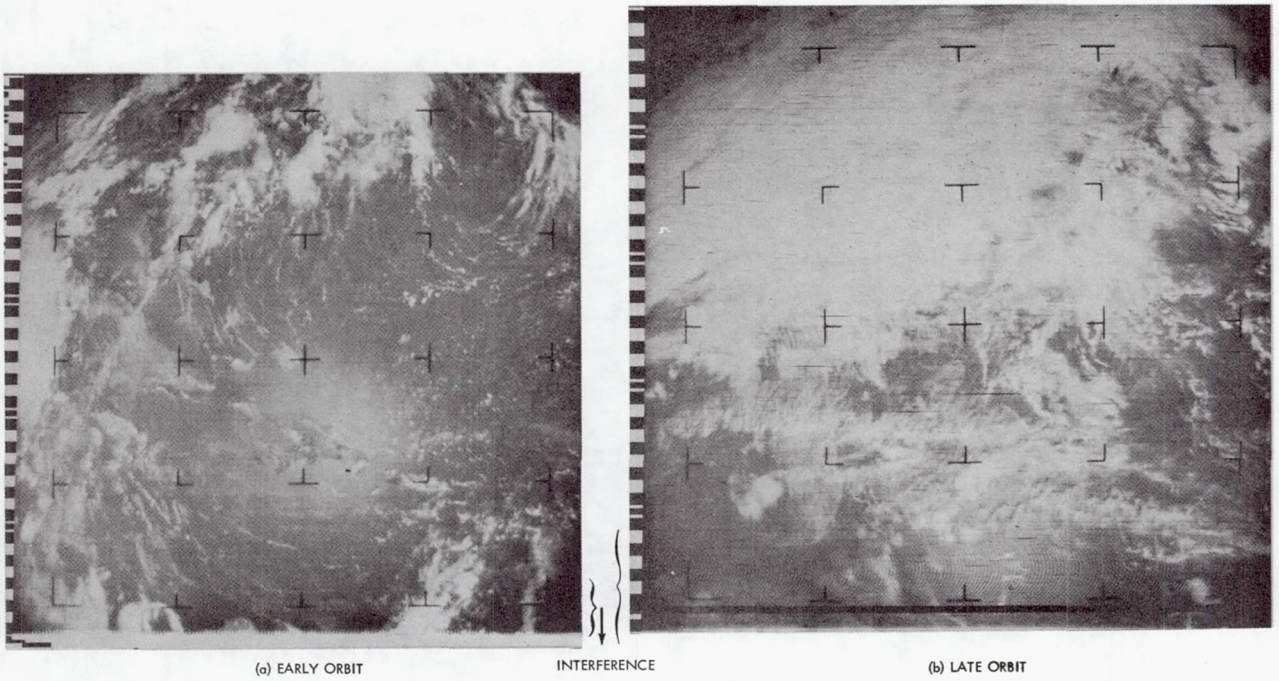

Figure 10-6—Comparison of APT subsystem photographs showing 0.7- to 0.9-kHz microphonic interference during early and later orbits.

HRIR Recorder Interference

Interference has occurred occasionally when the HRIR recorder was powered in the playback mode (Figure 10-7). A similar interference occurred during prelaunch testing (Figure 10-8 and References 10 through 13). The interference varied between 0.8 kHz and 1 kHz and showed the characteristic of "fading" after removal of the HRIR recorder power. The varying frequency and the fading characteristic of this interference suggest that the interference is of a mechanical nature (vibration) induced by the operation of the HRIR recorder, which has sufficient magnitude and frequency to induce resonant vibrations of the APT vidicon internal elements during the time the APT Subsystem is reading out a picture. The APT vidicon and the HRIR recorder are mechanically mounted in close proximity on the H-frame structure of the spacecraft, and the HRIR recorder motor utilizes a 400-Hz signal as a drive source. Therefore, the interference most probably resulted from the second-order harmonic of the HRIR recorder power.

Upon removal of HRIR recorder power, the interference becomes noncoherent and fades out as the vibrations dissipate. This type of interference can seriously impede the usefulness of the APT photographs. However, since this interference is present only during that time the HRIR recorder is powered, less than 4 percent of the pictures are affected. This interference should not be confused with the microphonic interference between 0.7 and 0.9 kHz, which appears randomly at the top end of the photographs (that portion of the photograph immediately following the 300-Hz start tone and phasing portion; see Figures 10-6 and 10-7).

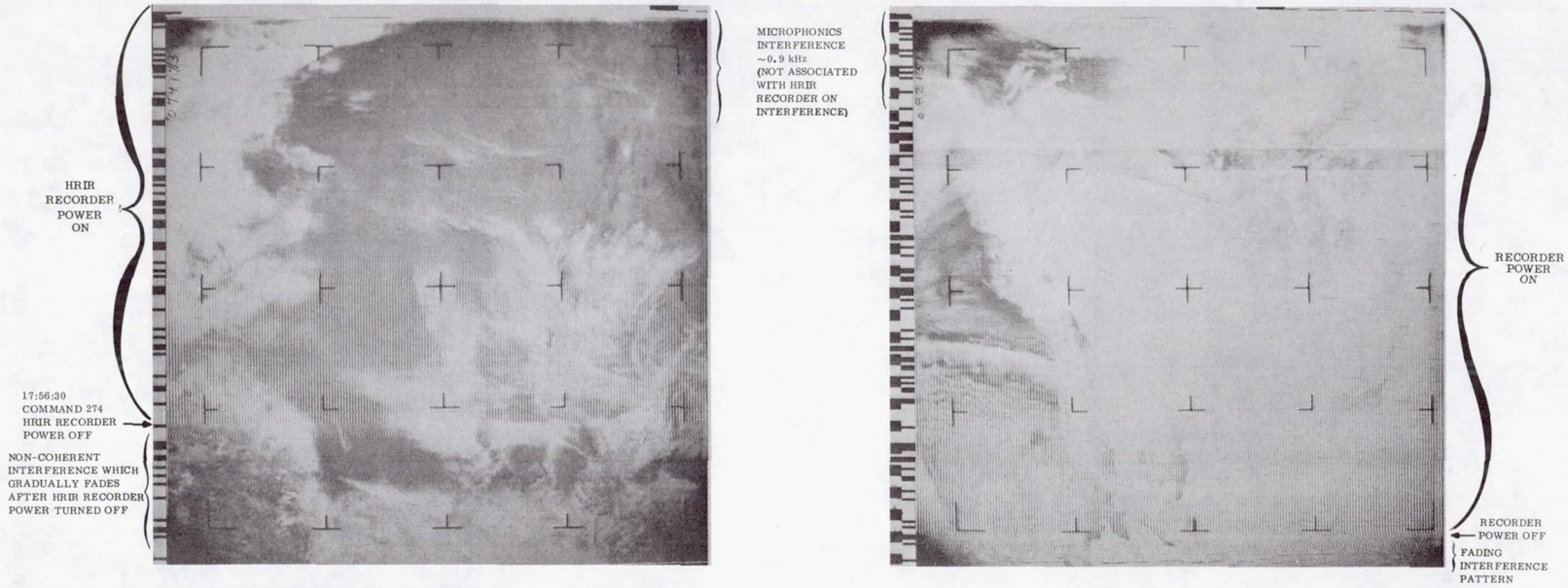

Figure 10-7—APT subsystem photographs showing fading effect of HRIR interference when power is removed from HRIR recorder.

DC Level Shift

The characteristics of the APT amplitude modulation (Figure 10-9) reflect a gradual dc level shift in the video during the second 6-month period of flight. Before the level change, black-signal input drove the modulated video to approximately 8 percent of the white DCG level and, with a white input, approximately 85 percent of the white DCG level. Currently, the black modulates the video to approximately 30 percent of the dc white level, and white to approximately 110 percent of the DCG white level. Graphic presentation of this phenomenon (Figure 10-10) indicates the occurrence of a dc shift of the video toward white. Fortunately, compensation for the level change can be made within the ground station processing equipment either by

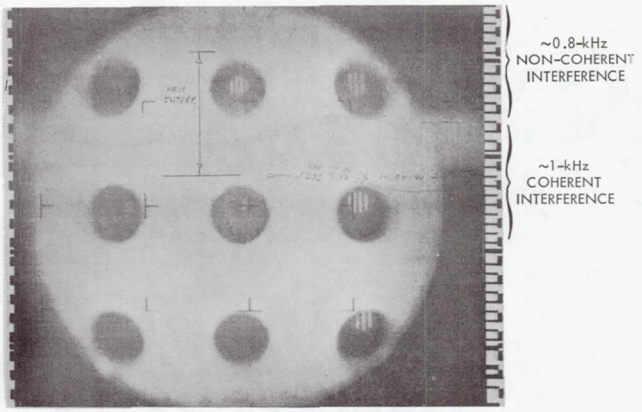

Figure 10-8 — APT subsystem prelaunch photograph of target (during thermal-vacuum testing) showing HRIR interference.

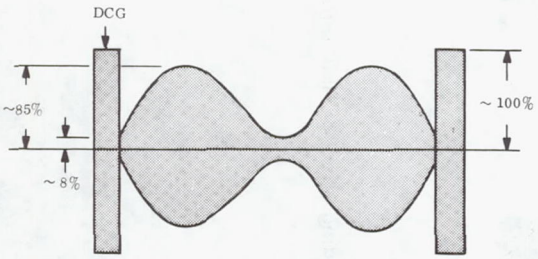

INITIAL POST-LAUNCH MODULATION LEVEL REPRESENTATION IN WHICH PEAK VIDEO WHITE LEVEL WAS ~ 85% OF WHITE DCG LEVEL AND BLACK ~ 8% OF WHITE DCG LEVEL.

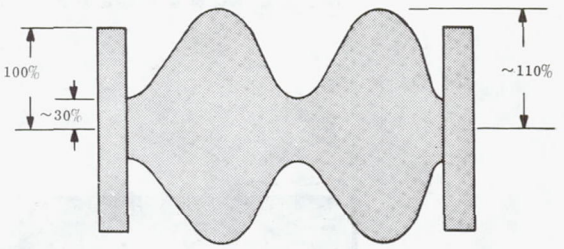

CURRENT MODULATION LEVEL REPRESENTATION IN WHICH PEAK VIDEO WHITE LEVEL IS ~ 110% OF WHITE DCG LEVEL AND BLACK ~ 30% OF WHITE DCG LEVEL

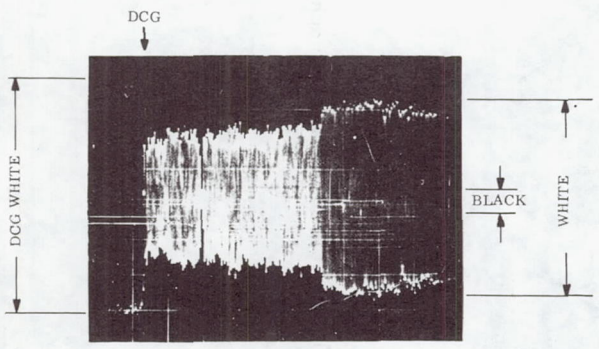

A-SCOPE PRESENTATION OF AMPLITUDE-MODULATED APT VIDEO

(a) Orbit 4338

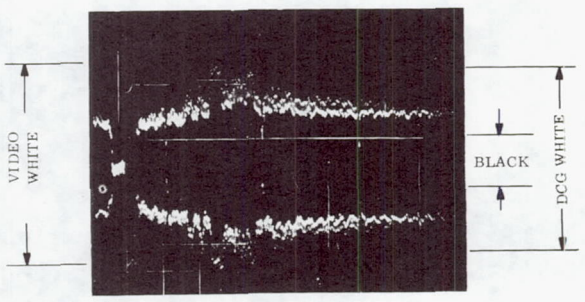

A-SCOPE PRESENTATION OF AMPLITUDE-MODULATED APT VIDEO

(b) Orbit 6

Figure 10-9—Comparison of APT subsystem video characteristics. (Oscilloscope photographs showing test-launch and late orbit characteristics.)

artificially inducing a negative dc bias or by altering the transfer characteristics of the ground station video processor. The following example illustrates this condition: The photographs in Figure 10-11 were received during orbits 404 and 4338. Both were processed with identical ground station transfer characteristics and signal levels. A level shift toward white is evident.

Alteration of the processor transfer characteristics enabled the production of the photograph shown in Figure 10-12 as further verification of the level change. Measurements were made of the "black" video level utilizing night photography during orbit 4898 (Figure 10-13).

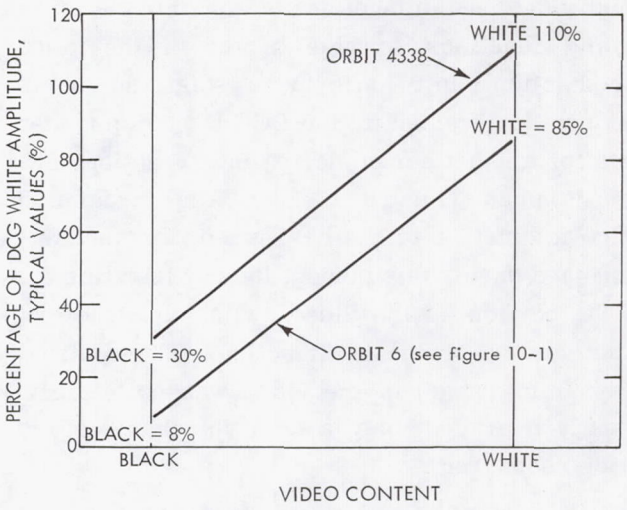

Figure 10-10–APT subsystem signal-level shift.

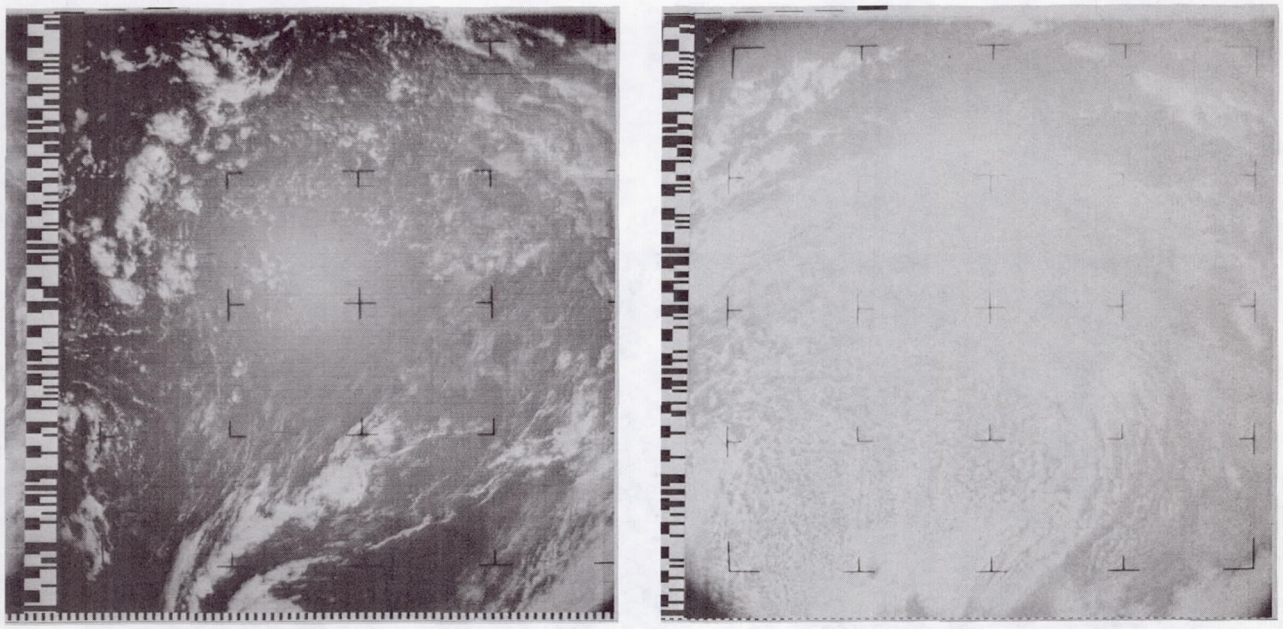

(a) PHOTOGRAPH RECEIVED APRIL 13, 1967 (orbit 4438)

(b) PHOTOGRAPH RECEIVED JUNE 14, 1966 (orbit 404)

Figure 10-11—Comparison of APT subsystem photographs showing shift toward white.

A-scope presentation of the modulated video shows: (1) the black fiducial level has increased to approximately 30 percent of the white level contained in the DCG and (2) the black video level has increased to approximately 70 percent of the white level contained in the DCG.

The dc level change can probably be attributed to a malfunction within the video switching which (in addition to proper time-sequencing the 300-Hz start tone, DCG, phasing information,

and video) establishes the dc bias for the foregoing functions for the driver of the video modulation. In an attempt to isolate the origin at the dc level shift, the DCG was commanded off for a short period during interrogation 4864 at Rosman (Figure 10-14). The modulation characteristics of the APT video remained unchanged during this period, thus eliminating the DCG portion of the video switching circuitry, the source of the malfunction. The contrast (dynamic range) of the video was not significantly degraded; only a dc level change of the video occurred.

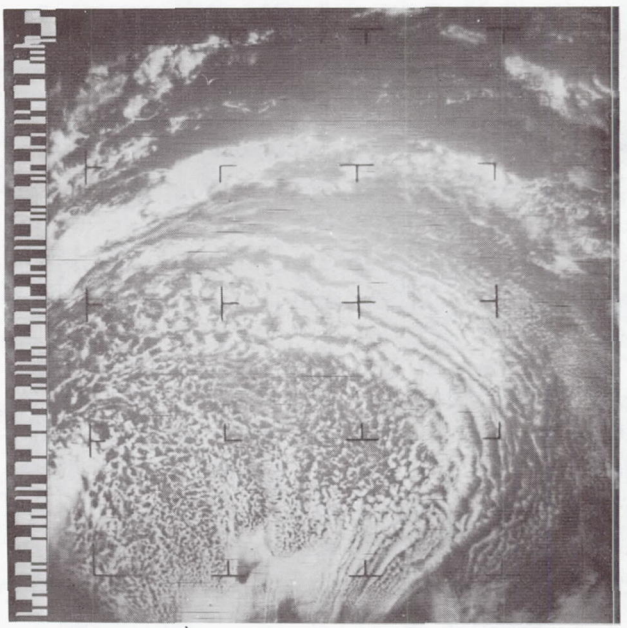

Figure 10-12--APT subsystem photograph (orbit 4438) showing shift in transfer characteristics as a result of alteration of the processor.

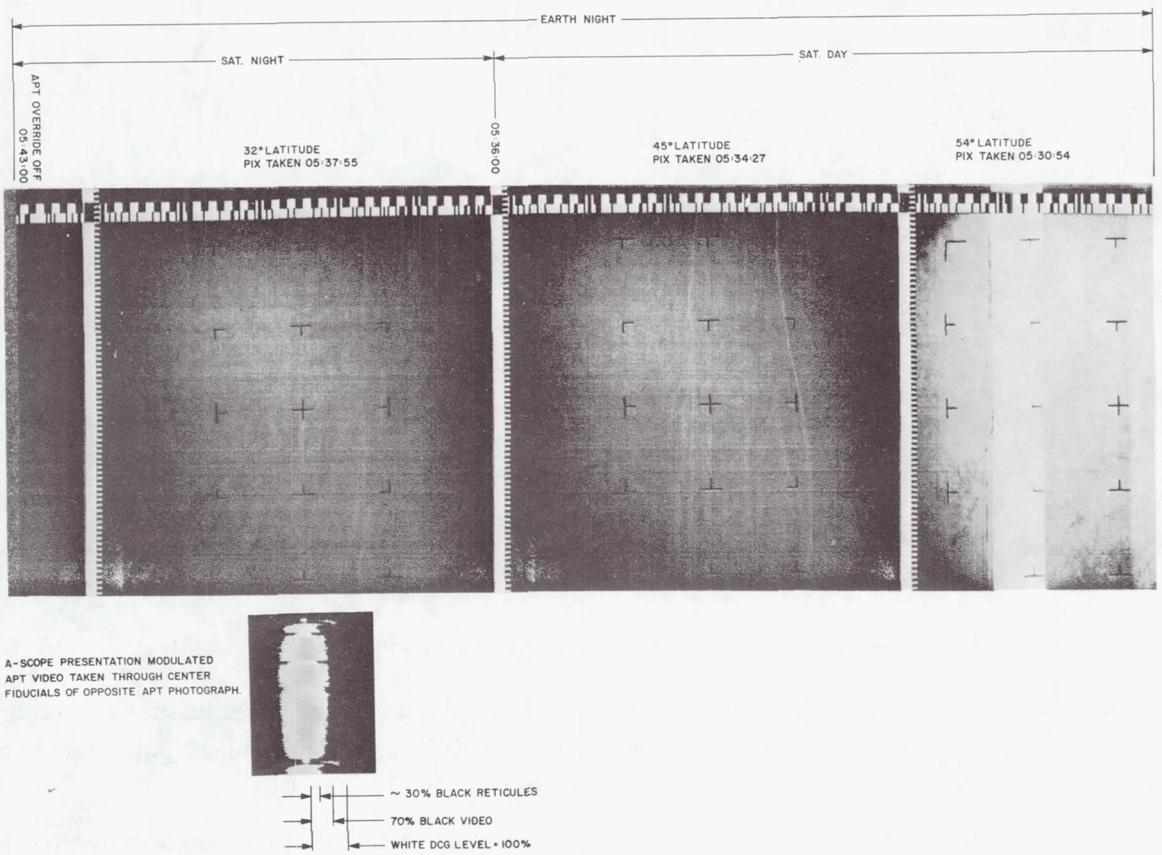

Figure 10-13—APT subsystem night photographic sequence (interrogation 4898R).

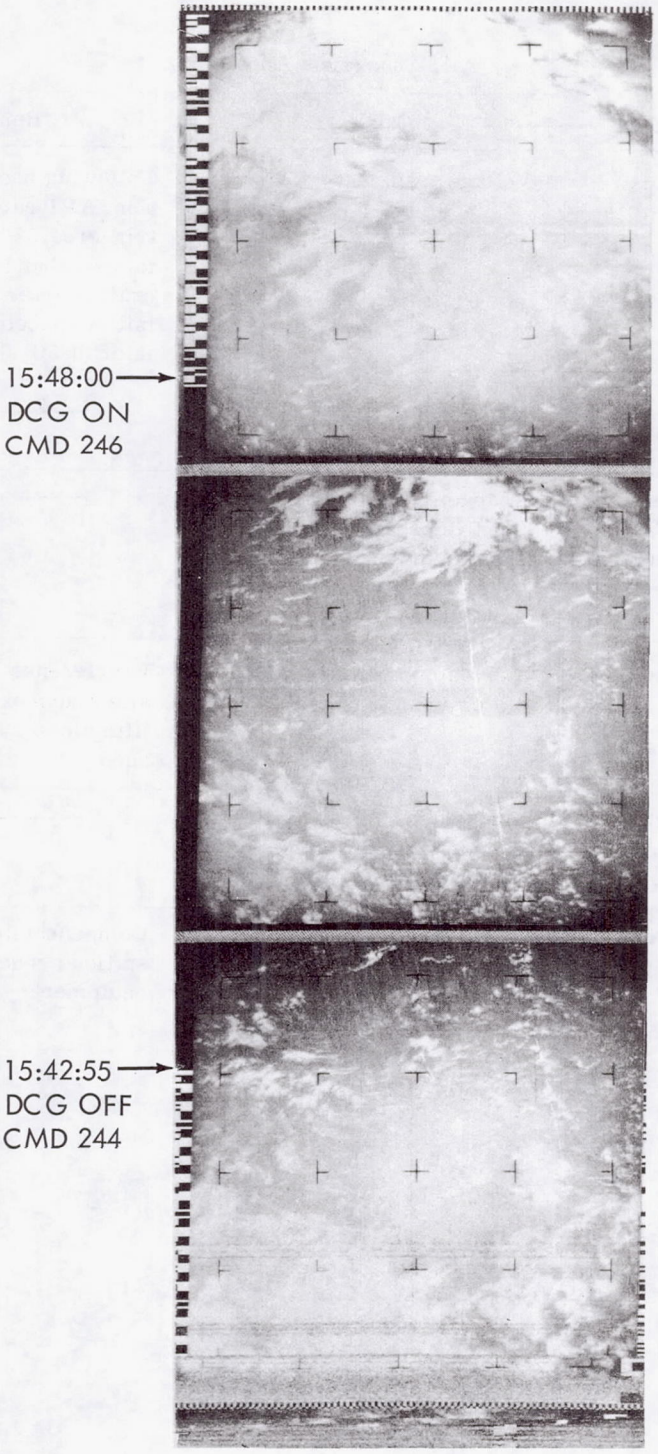

Figure 10-14—APT subsystem photographic sequence during which data code and grid was commanded OFF/ON (interrogation 4864R).

Table 10-6

APT Subsystem Anomalies.

Anomaly	Cause	Remarks	B*
Inadvertent triggering of APT camera shutter	Voltage transient	Following booster separation, APT camera shutter triggered. Photo of Agena forward bulkhead and spacecraft adapter was readout at initial spacecraft turn-on in orbit 5U	No
APT DCG "dogleg"	Clock 1-Hz and APT sequence timer phasing	----------	No
Telemetered value of transmitter output changed from 3.5 TMV (Orbit 6) to 4.05 TMV (Orbit 800)	Change in the tuning and input impedance of subsystem antenna due to outgassing of absorbed moisture	----------	Yes
Microphonic interference	Vibration of vidicon internal elements	Interference increased to affect approximately one-fifth picture area as vidicon aged	No
HRIR recorder-induced interference (0.8 kHz to 1 kHz)	Mechanical vibrations induced by operation of HRIR tape recorder	----------	No
Change in dc level of video	Probable malfunction within video switching section of camera electronics	Compensatable in ground station processing equipment	No

*Anomaly related to Nimbus B.

SECTION 11

HRIR SUBSYSTEM

INTRODUCTION

The performance of the High Resolution Infrared Radiometer (HRIR) Subsystem was excellent until orbit 2455 when the subsystem tape recorder failed. No further sensory data have been received from this subsystem. Overheating of the detector cell decreased the signal-to-noise ratio of the video, causing a corresponding degradation of the video quality. Subsystem calibration remained in good agreement with prelaunch calibration curves and showed no evidence of long-term degradation.

DESCRIPTION

The HRIR Subsystem measures the thermal radiation in the spectral band between 3.48 to 4.17 microns, thereby mapping nighttime cloud cover and cloud-top temperatures by sensing the difference in radiation intensity as emitted by clouds and the earth's surface. The HRIR Subsystem (Figure 11-1) is composed of a scanning radiometer, associated electronics, a four-channel magnetic tape recorder, and a multiplexer which permits data transmission to data acquisition facilities via an S-band data link.

The single-channel scanning radiometer (Figure 11-2) measures radiance temperatures between 210° and 300°K with a noise equivalent temperature difference of 1°C for a 250°K background. The radiometer uses a lead selenide (PbSe) photoconductive cell that is radiation-cooled to -75°C by a black cooling patch at the bottom of a highly reflective gold-coated horn. The horn is oriented to view cold space during the entire orbit, and the patch is suspended by thin wires to reduce heat conduction from the housing.

The radiometer has an instantaneous field-of-view of 8.7 milliradians that, at an altitude of 600 nm (1110 km), corresponds to a subsatellite ground resolution of 5 nm (8 km). The scan mirror is inclined 45 degrees to the axis of rotation which is coincident with the spacecraft velocity vector (assuming no yaw attitude error). The optical scan path thus lies in a plane perpendicular to the orbital motion. The radiation reflected from the scan mirror is chopped at the focus of a 4-inch f/1 modified Cassegrainian telescope. It is then refocused at the detector by a reflective relay containing a 3.5- to 4.1-micron filter. A scan rate of 44.7 revolutions per minute permits continuous scanning in the neighborhood of the subsatellite track, with increasing overlap toward the horizon.

In contrast to television, no image is formed within the radiometer; the radiant energy is modulated by interrupting the reflected energy from the mirror with a mechanical chopper, sensed, amplified, and rectified; then a video bandwidth from dc to 280 Hz is generated. The video

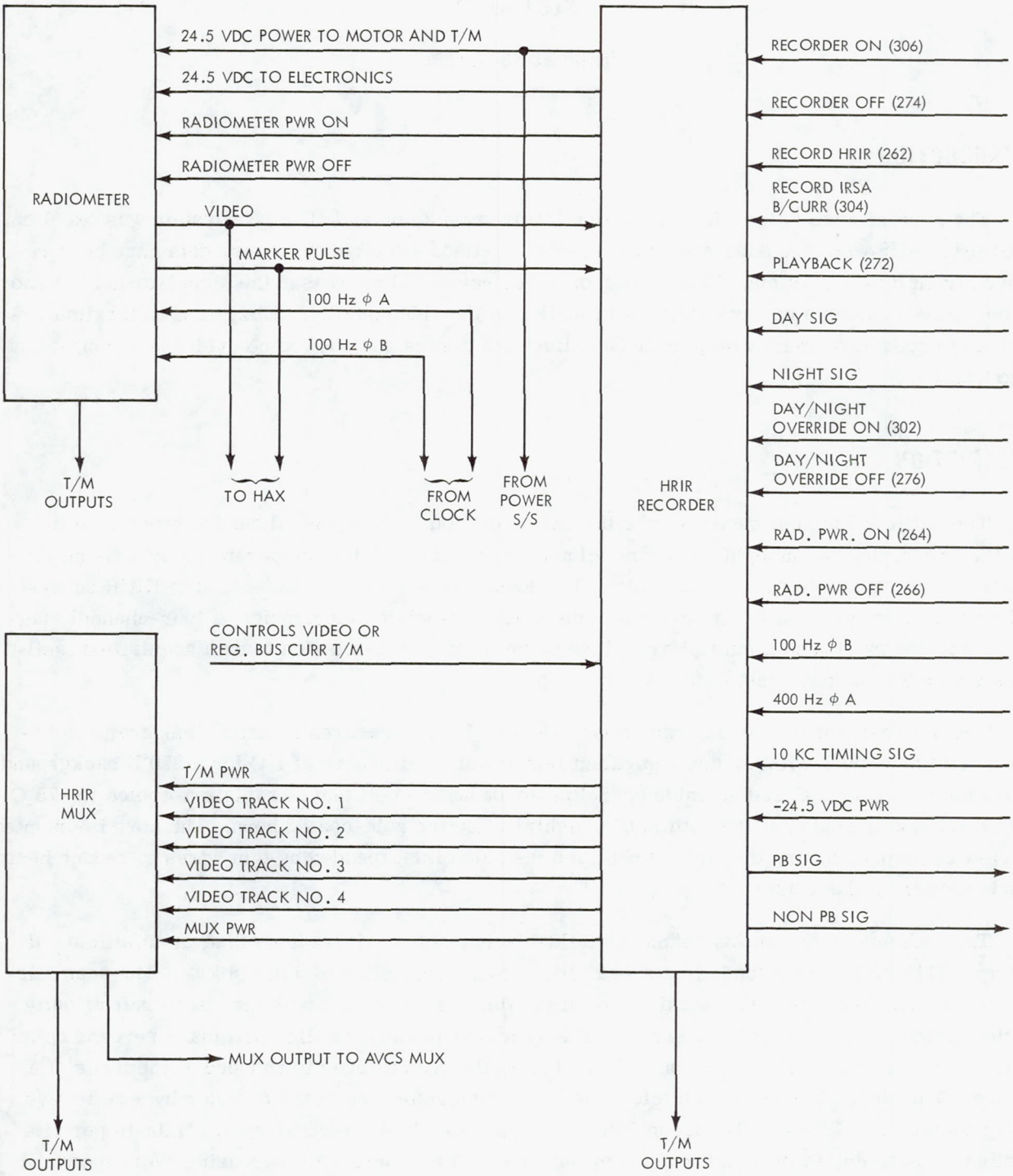

Figure 11-1—HRIR signal flow diagram.

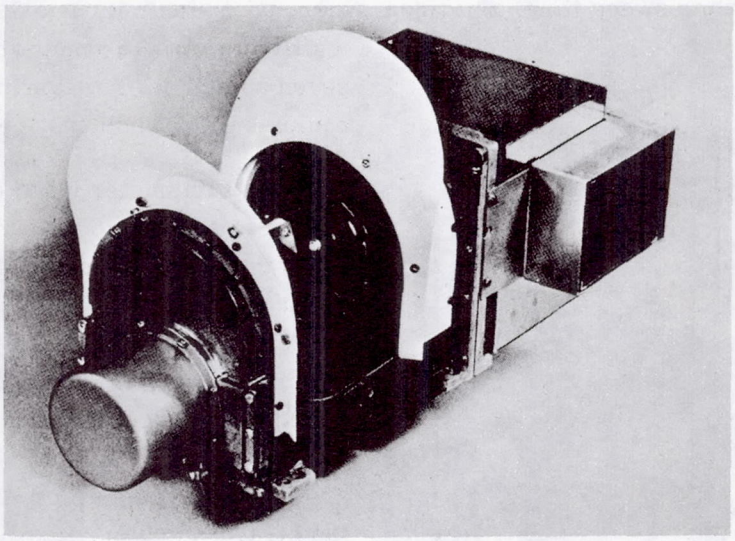

(a)

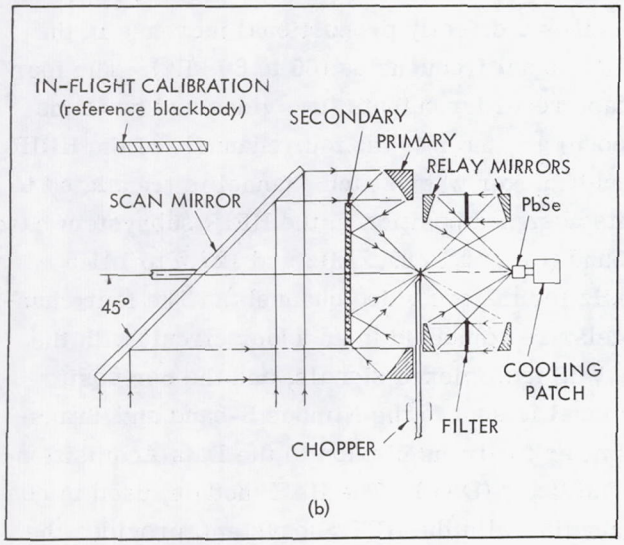

(b)

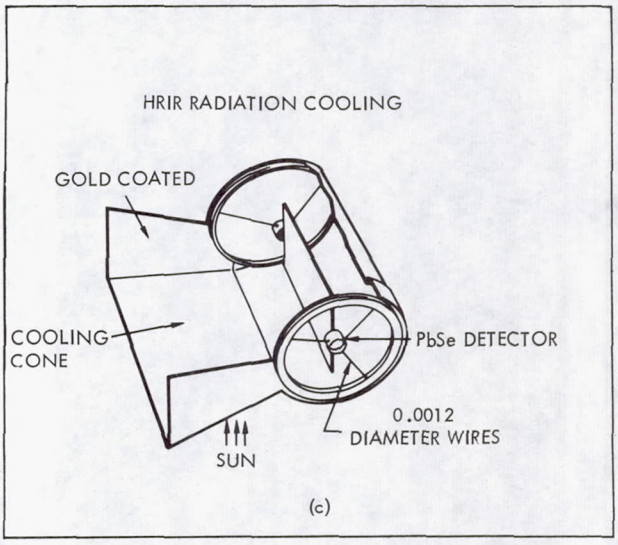

(c)

Figure 11-2—(a) High Resolution Infrared Radiometer, (b) optical system schematic, (c) lead-selenide detector radiative cooling system.

amplitude varies as the radiometer scan mirror continuously rotates the field-of-view of the detector through 360 degrees in a plane normal to the spacecraft velocity vector. The detector views sequentially the in-flight blackbody calibration target (which is a part of the radiometer housing), outer space, earth, and outer space and then returns to intercept the in-flight blackbody target. At the initiation of the space sweep time, a permanent magnet on the mirror axis triggers a gate and multivibrator. The multivibrator then generates seven pulses used to synchronize the ground equipment that displays the data.

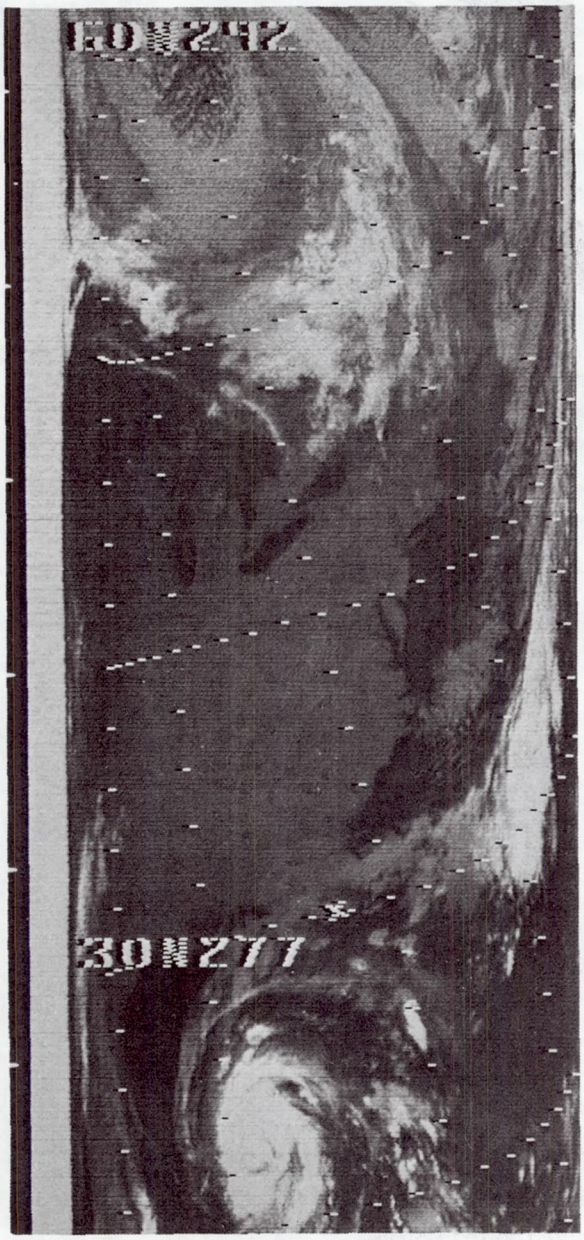

Figure 11-3—Typical high-quality HRIR subsystem video data (orbit 1929).

The radiometer video output (0 to -6.4 vdc) is sent to an FM modulator. The modulator converts the radiometer voltage to frequency-modulated signals (8.25 to 10 kHz) that are recorded on one track of a 4-track tape recorder. Simultaneously, 10-kHz AM timing signals from the Nimbus spacecraft clock are placed on a second track on the tape. When these two tracks are completely recorded, the direction of the tape travel is automatically reversed and the recording continued on the other two tracks. The recorder accepts data at a tape speed of 3.75 inches per second and, upon command, plays back all four channels simultaneously at 30 inches per second. The 8-to-1 playback speedup causes a directly proportional increase in the FM signal frequencies (66 to 80 kHz). The four tape recorder outputs (two video and two time code) are fed into the four channels of the HRIR multiplexer where each channel is translated to its assigned position in the HRIR subsystem base band (i.e., 55 to 69.5 kHz and 127.5 to 141.5 kHz for the two video channels). The four channels are combined in an adder circuit with the AVCS multiplexed signals, and the composite signal is sent to the Nimbus S-band and Transmitter for transmission to the Data Acquisition Facilities (DAF). The HAX module, used in conjunction with the APT Subsystem, provides the capability of transmitting real-time HRIR video.

At the DAF, the HRIR information is demultiplexed and recorded on magnetic tape and then transmitted to the Goddard Space Flight Center,

Greenbelt, Maryland, where the FM signal is demodulated, synchronized, gridded, and displayed by a photofacsimile recorder. The facsimile recorder converts the radiometer output electrical signals into a continuous strip picture, line by line, on 70-mm film. Blanking circuits in the recorder reject unwanted sections of each line scan. Only the earth scan and, for calibration purposes, very small portions of the space scan and the radiometer housing scan are recorded on the film strip. Figure 11-3 illustrates a sample of the format of the Nimbus II HRIR data. In addition to the analog video processing, the analog magnetic tape is fed into an A/D converter, which uses a CDC 924 computer to prepare a digital tape. This tape then is processed by the IBM 7094 computer which prepares a reduced radiation data tape called the Nimbus Meteorological Radiation Tape-HRIR (NMRT-HRIR), which can be used to generate grid point maps or to accomplish special scientific analyses.

FLIGHT OBJECTIVES

The flight objectives of the HRIR Subsystem were to demonstrate the capability of the subsystem to record high quality infrared (IR) measurements of the earth's surface and cover and provide real-time IR to the HAX Module. At 6 months, the HRIR subsystem performed satisfactorily until the tape recorder failed during orbit 2455. This failure precluded further reception of data from the HRIR Subsystem, which had provided good quality data to the HAX Module before the failure. At 13 months, the subsystem status had remained unchanged after orbit 2455.

ELECTROMECHANICAL PERFORMANCE

The electromechanical performance of the HRIR Subsystem has been satisfactory with the exception of the failure of the subsystem tape recorder. A summary of subsystem performance is presented in Table 11-1.

Recorder Pressure

The pressure of the subsystem recorder versus time in orbit is presented graphically in Figure 11-4. The pressure-temperature relationship has followed the universal gas law and has shown no evidence of long-term pressure degradation.

Tape Recorder Failure

During interrogation 2455R, the HRIR Subsystem was commanded into playback. After 1 minute and 2 seconds, modulation of the S-band carrier ceased even though the subsystem remained in the playback mode. Command 032 (AVCS Recorder Record/S-Band OFF) was transmitted to terminate the S-band transmission; this was followed by command 274 (HRIR

Table 11-1

HRIR Subsystem Performance Summary.

Function	Requirement	Outcome
Radiometer		
Mirror rotation	44.7 rpm	Satisfactory
Thermal control		
Detector cell	Maintain temperature between -70 and -80°C	Failure (1)
Radiometer	Maintain reference surface temperatures between 5 and 15°C	Partially satisfactory (2)
Housing	Maintain electronics housing temperature between 10 and 20°C	
Calibration	Maintain constant signal input/output relationship	Partially satisfactory (3)
Shading	Constant relationship between output photographic shading and input earth signal	Failure (4)
Sync pulses	Generation of 7 pulses of 5.5-volt amplitude and 12-millisecond duration	Satisfactory
Video bias	Generation of video bias inversely proportional to video amplitude	Satisfactory
Recorder/Multiplexer		
Data recovery	Record and play back data without distortion	Satisfactory
Telemetry	Adherence to calibration and stability	Satisfactory
Operability	Dependable command execution	Satisfactory (5)
Compatibility	Compatibility with other subsystems (RFI)	Satisfactory
Reliability	Capable of continuous 6-month operation	Partially satisfactory (6)

Notes:
(1) Orbital temperature -64°C obtained at times which signal-to-noise ratio of video reduced.
(2) During continuous (day and night) operation, radiometer and housing temperatures reached 18° and 28°C, respectively.
(3) Data calibration had to be constantly corrected for varying detector cell temperature.
(4) Sunlight interference, both direct and reflected, together with varying detector cell temperature prevented a constant relationship between video output level and input earth signal.
(5) During interrogation 1452U, the HRIR playback command (272) did not result in any apparent HRIR playback. A second playback command was issued whereupon data were received.
(6) Overheating of detector cell prohibited full-time (day and night) subsystem operation. After having achieved 6-month operation, subsystem tape recorder failed during orbit 2455.

OFF). The individual events in this sequence are listed below. The associated functions follow in Table 11-2.

Time	Event
15:27	End of HRIR playback of interrogation 2454R; HRIR Subsystem into standby

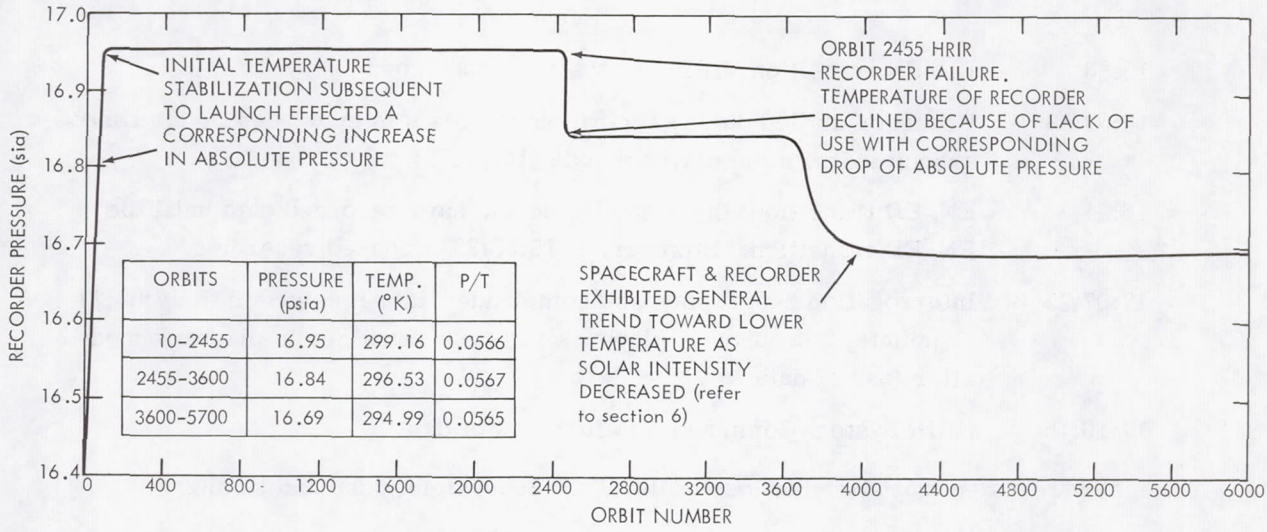

Figure 11-4—HRIR pressure versus time in orbit.

Table 11-2

HRIR Subsystem Telemetry Functions.

Function		Telemetered Level		Remarks
Name	No.	Before Loss of Video and Timing	After Loss of Video and Timing	
Recorder temp. (hot)	102	28.0°C	28.8°C	Temperature of the recorder power inverter which supplies power to the drive mechanism is monitored by Function 102. An increase in this temperature is indicative of a larger power drain on the inverter
Recorder temp. (cold)	092	27.3°C	27.3°C	
Recorder pressure	104	17.0 psia	17.0 psia	Normal pressure characteristics were maintained
Inverter output	105	3.00 tmv	3.00 tmv	Elimates power inverter as source of malfunction
		(millivolt, rms)	(millivolt, rms)	
Channel 1 P/B amp.	109	0.51	0.11	Video and timing signals were present at the output of recorder's P/B amplifiers before malfunction; not present subsequent to malfunction
Channel 2 P/B amp.	110	0.17	0.05	
Channel 3 P/B amp.	111	0.38	0.05	
Channel 4 P/B amp.	112	0.54	0.12	
MUX No. 1 osc. level	114	3.95 tmv	3.95 tmv	Invariant levels eliminate system multiplexers as source of malfunction
MUX No. 2 osc. level	115	3.95 tmv	3.95 tmv	
MUX No. 3 osc. level	116	4.10 tmv	4.10 tmv	
MUX No. 4 osc. level	117	4.35 tmv	4.35 tmv	
MUX output	118	1.55 tmv	0.05 tmv	Before malfunction, HRIR video and timing were present in the composite signal output of the HRIR MUX; absent after malfunction
-24.5 vdc MUX supply	119	4.95 tmv	4.95 tmv	Indicates system remained in P/B mode

Time	Event
15:33	ED/EN transition; HRIR Subsystem into record
15:53:33	Recorder stalled during record mode; this was evidenced by the time associated with the playback data (15:53:33).
16:31	EN/ED transition; the recorder should have recorded data until the EN/ED transition. However, at 15:53:33 it ceased recording.
17:07:25	Interrogation 2455R playback commanded data received until 17:08:27 (1 minute, 2 seconds of playback); system remained in playback mode after loss of data
17:10:15	HRIR System Command off after loss of data

Telemetry revealed that after the loss of the HRIR Subsystem video and timing:

a. The HRIR Subsystem, including the tape recorder, remained in the playback mode.

b. Video and timing were not present at either the output of the playback amplifiers or in the composite signal input to the S-band transmitter.

c. The recorder's power inverter exhibited an abnormally high temperature increase at the time of failure. This could have resulted from a higher current drain by the motor when it stalled (Figure 11-5).

The received HRIR video data indicated that the recorder moved erratically and finally stalled during the record period between interrogations 2454R and 2455R. During the playback of interrogation 2455R, speed variations occurred throughout the approximate 62-second playback before the loss of modulation. At the time modulation was lost, the tape position was approximately 13 minutes and 9 seconds from the end-of-tape positions (99 seconds of playback time). Visicorder presentations (Figure 11-6) indicate that at the instant of failure, the reverse data-playback rate increased, and the forward data-playback rate decreased. This may have resulted from a "skewing" of the tape as it passed over the playback heads.

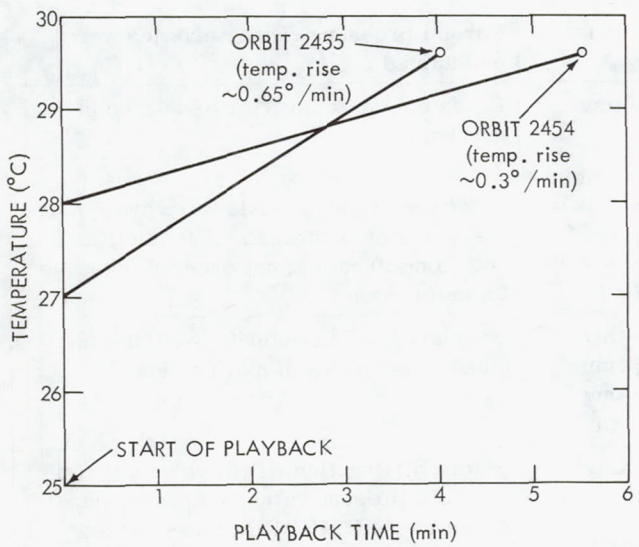

Figure 11-5—Correlation of inverter temperature during normal and failure playback.

The last 220 seconds of counter-clockwise playback (discussed under Timing Amplitude Variations) were accompanied by sharp increases in recorder flutter and wow. The failure in playback occurred in this degraded region at approximately 99 playback seconds from the end of the tape; the record failure also occurred in this region at approximately 162 playback seconds from the end of the tape.

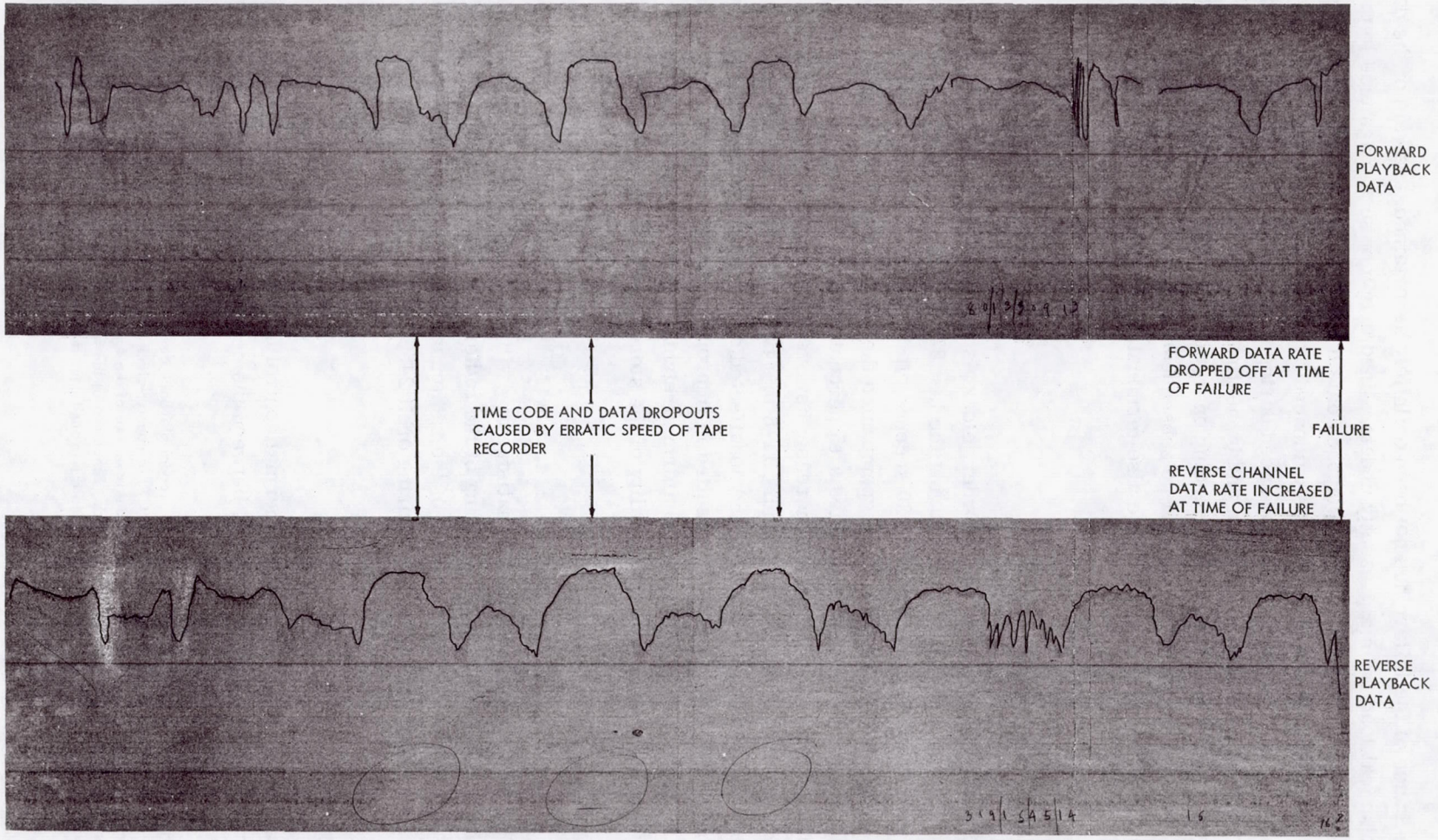

Figure 11-6—Visicorder presentation of HRIR recorder failure data (orbit 2455).

Although the cause of the failure has not been definitely ascertained, analysis of the data indicates that a mechanical load from a presently undetermined origin of such magnitude to prevent tape movement resulted in the loss of HRIR playback data during interrogation 2455R. The additional loading of the recorder drive motor was evidenced by a rise in the temperature of the recorder power inverter and by the erratic tape speed during this playback. Attempts have been made to restart the recorder by cooling the system and by heating it. The system was cooled by removing recorder power; it then was heated by extending operation in the playback mode. Neither method was successful in restarting the recorder and no subsequent data have been received in the playback mode from the HRIR Subsystem. This failure also terminated the receipt of IR data from the HAX Module.

Timing Amplitude Variations

Before the failure of the subsystem recorder, clockwise* HRIR timing had consistently exhibited a 25 percent decrease in amplitude during the last 220 seconds of counter-clockwise playback and, correspondingly, during the first 220 seconds of clockwise playback (Figure 11-7). A sharp increase in recorder flutter and wow accompanied the decrease in time code. The amplitude of the counter-clockwise HRIR timing exhibited a 15 percent decrease in amplitude during this period. The length of tape affected did not increase; however, the magnitude of the degradation over the affected area slowly increased. Figure 11-8 is a typical flutter and wow strip recording showing the transition between the affected and nonaffected areas of the tape. This was probably caused by a degradation of the tape which resulted in improper tape tracking. Such degradation may have been in the form of ribboning, nonuniform stretching, or wrinkling of the tape area in question. This anomaly did not affect the quality of the stored video data.

VIDEO QUALITY

The quality of the HRIR video has been satisfactory with the exception of the degraded signal-to-noise ratio of the data caused by overheating of the radiometer detector cell. There is no evidence of any degradation in the performance of the radiometer or associated electronics before the failure of the subsystem tape recorder during orbit 2455.

Detector Cell Temperature

The combination of active and passive thermal control of the HRIR detector cell failed to maintain the temperature of the detector cell between the desirable limits of -70° to -80°C. The

*The HRIR tape recorder is a 4-channel (track), magnetic tape, record-playback device which records and plays back in one of two directions of rotation. The direction is considered clockwise (CW) or counter-clockwise (CCW) when viewing the top of the tape recorder. Video and timing information are recorded simultaneously on two of the four channels and played back simultaneously; the same recording heads used for recording are used for playback. Since two of the tracks are recorded in the CW direction and two in the CCW direction, two tracks contain timing signals for use in the ground equipment to identify and select for display first the two channels recorded most recently.

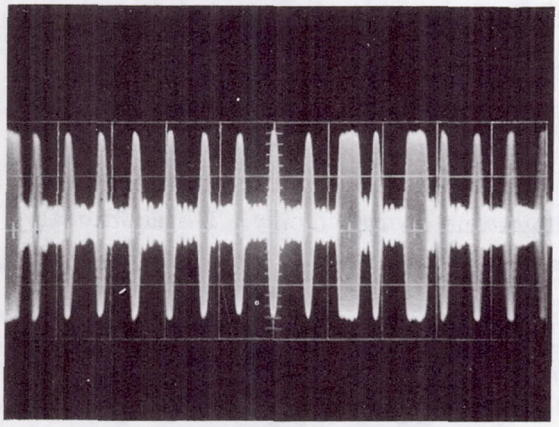

(a) NORMAL AMPLITUDE OF CW TIMING

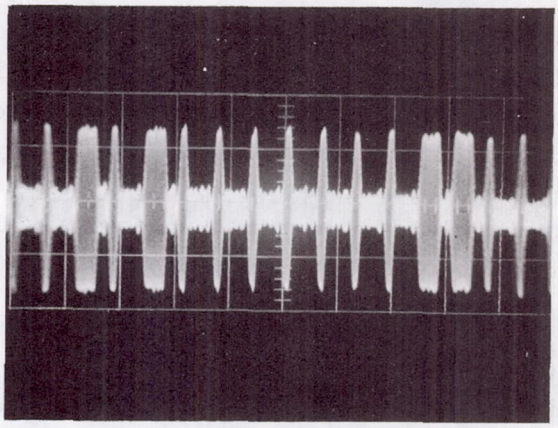

(b) NORMAL CCW TIMING AMPLITUDE

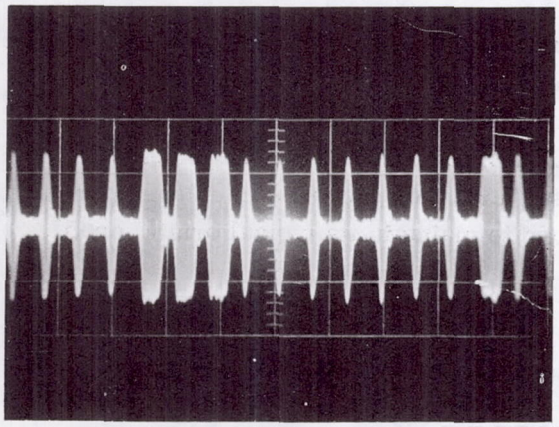

(c) DEGRADED AMPLITUDE OF CW TIMING

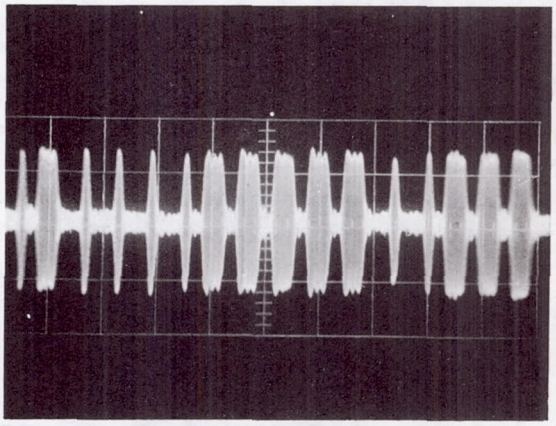

(d) DEGRADED CCW TIMING AMPLITUDE

Figure 11-7—HRIR subsystem timing amplitude degradation.

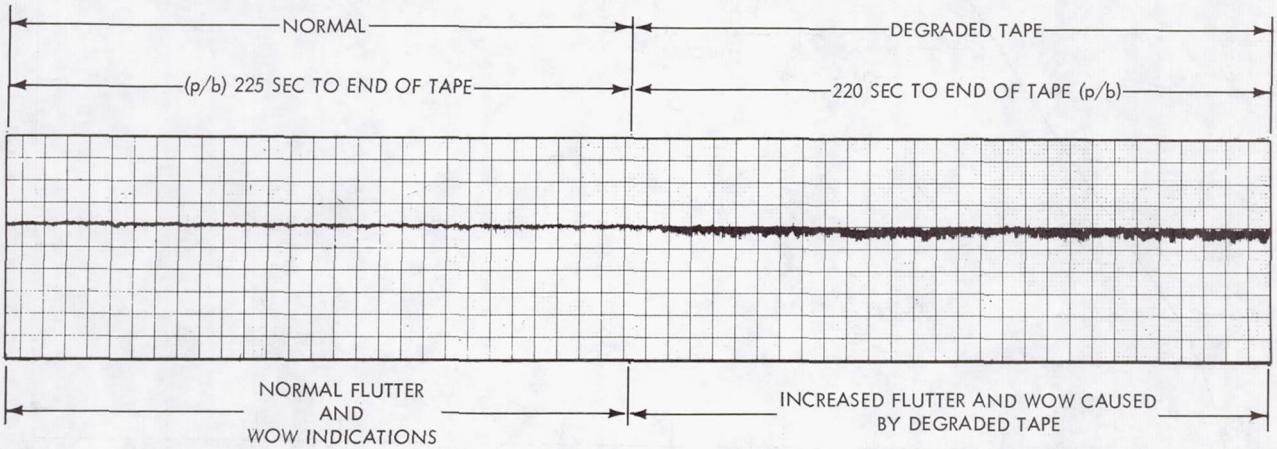

Figure 11-8—Typical flutter and wow strip recording showing transition between degraded and normal conditions.

time in orbit-versus-temperature profile of the detector cell is presented in Figure 11-9. Before the failure of the subsystem recorder, the detector cell temperature orbital profile had been -65.6 ± 1°C, and data of excellent quality were received. After the recorder failure, a decrease of the orbital temperature profile to -67 ± 0.5°C resulted since the radiometer electronics were no longer powered. Continuous day and night subsystem operation was attempted, but a general overheating of the subsystem components necessitated the return to nighttime operation only. The additional thermal loading caused detector cell temperature to increase to -64.0°C.

The elevated detector cell temperature can be attributed to distortion of the inside surface of the cooling cone at the outboard edge, flaking and/or outgassing of the black coating from the cooling patch, or improper operation of the active temperature control loop of the detector cell. Cooling cone distortion results from the high temperature produced by incident solar energy. Such distortion could not only change the cooling characteristics of the cone but could permit solar energy to be reflected to the cooling patch located at the cone apex. The flaked coating particles adhering to the cone gold surface could have changed the cone's thermal characteristics as well as those of the cooling patch itself.

To evaluate the performance of the active temperature control loop of the detector cell, power to the HRIR radiometer (including the active temperature control loop of the detector cell) was removed during interrogation 4520 and reinstalled 110 minutes later during interrogation 4521. It was anticipated that if, in fact, the temperature control loop of the detector cell had malfunctioned, removal of the power to the control loop would have caused a marked decrease in cell temperature. This did not occur; the detector cell temperature continued to maintain its typical orbital profile

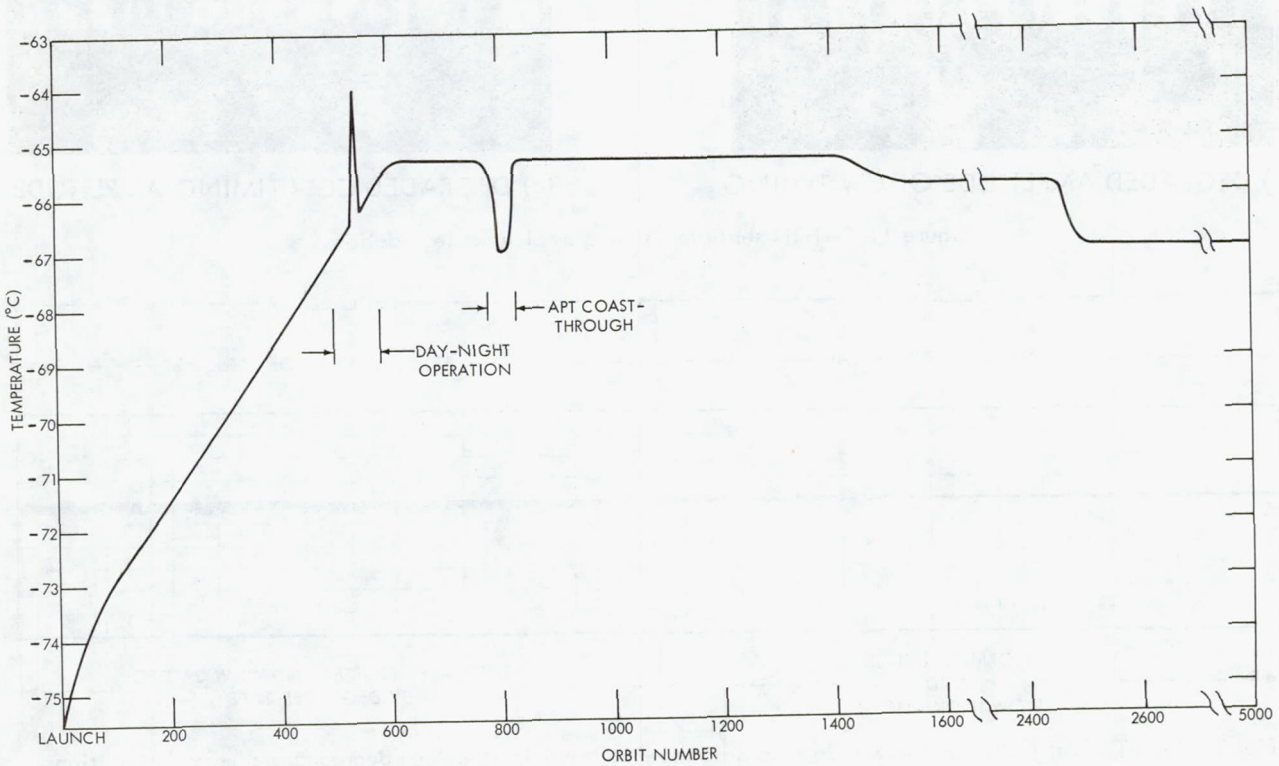

of 67 ± 0.5°C. Although laboratory tests have failed to duplicate this problem, it is presently believed that the most probable cause of the overheating of the detector cell is flaking or outgassing of the cooling patch black coating.

Sunlight Interference

The mirror-shield portion of the Nimbus II HRIR radiometer housing (Figure 11-2) was designed to prevent incident solar radiation from entering the radiometer, assuming normal spacecraft altitudes, at a mean orbital altitude of 500 nautical miles. In the 600-nm orbit which Nimbus II attained, direct sunlight enters the detector cell at the satellite night/day transition and raises the entire video level to almost the same height as the sync pulses. Figure 11-10 shows a normal line of HRIR video (Figure 11-10a) becoming obliterated by direct sunlight entering the radiometer (Figure 11-10b). The mirror, in scanning the radiometer housing receives additional sunlight reflected from the housing. As the spacecraft proceeds, more light enters directly. The reflection ceases, and the mirror, in scanning the radiometer housing, blocks input sunlight (Figure 11-10c). Later the radiometer housing blocks out the remaining sunlight, and the slow time constant of the bias circuit allows the signal to become slightly negative (Figure 11-10d). Sunlight obliterates all video information for approximately 1-1/2 to 2 minutes. During the period of sunlight interference, the HRIR bias circuit functions properly, slowly reducing the bias bulb voltage in proportion to video signal amplitude. Thus overall video amplitude decreases slowly. As the sunlight is blocked by the radiometer housing, the video output decreases below its pre-interference level, because of the lower bias bulb voltage (Figure 11-11). This allows the video signal to reach

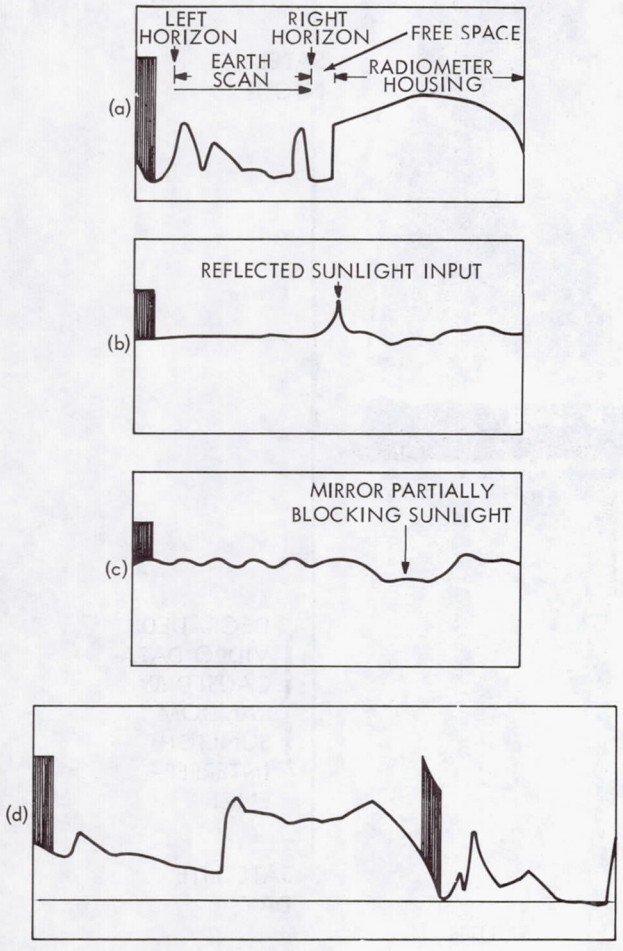

Figure 11-10—HRIR sunlight interference during satellite night/day period.

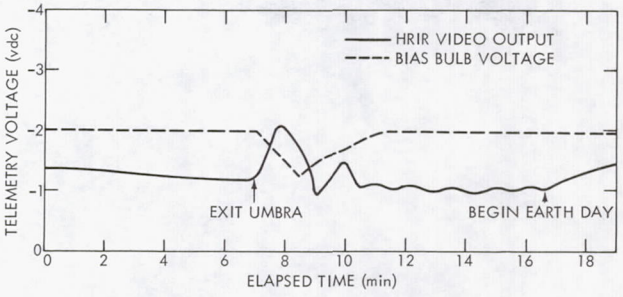

Figure 11-11—Sunlight input effects shown on HRIR telemetry.

negative levels, the condition for which the bias bulb was installed to prevent underexpected conditions. At the satellite day/night transition, sunlight is reflected from the radiometer housing into the detector cell. This is of much lower intensity than the direct sunlight at the satellite night/day transition and merely degrades video slightly for approximately 2 minutes (Figures 11-12 and 11-13).

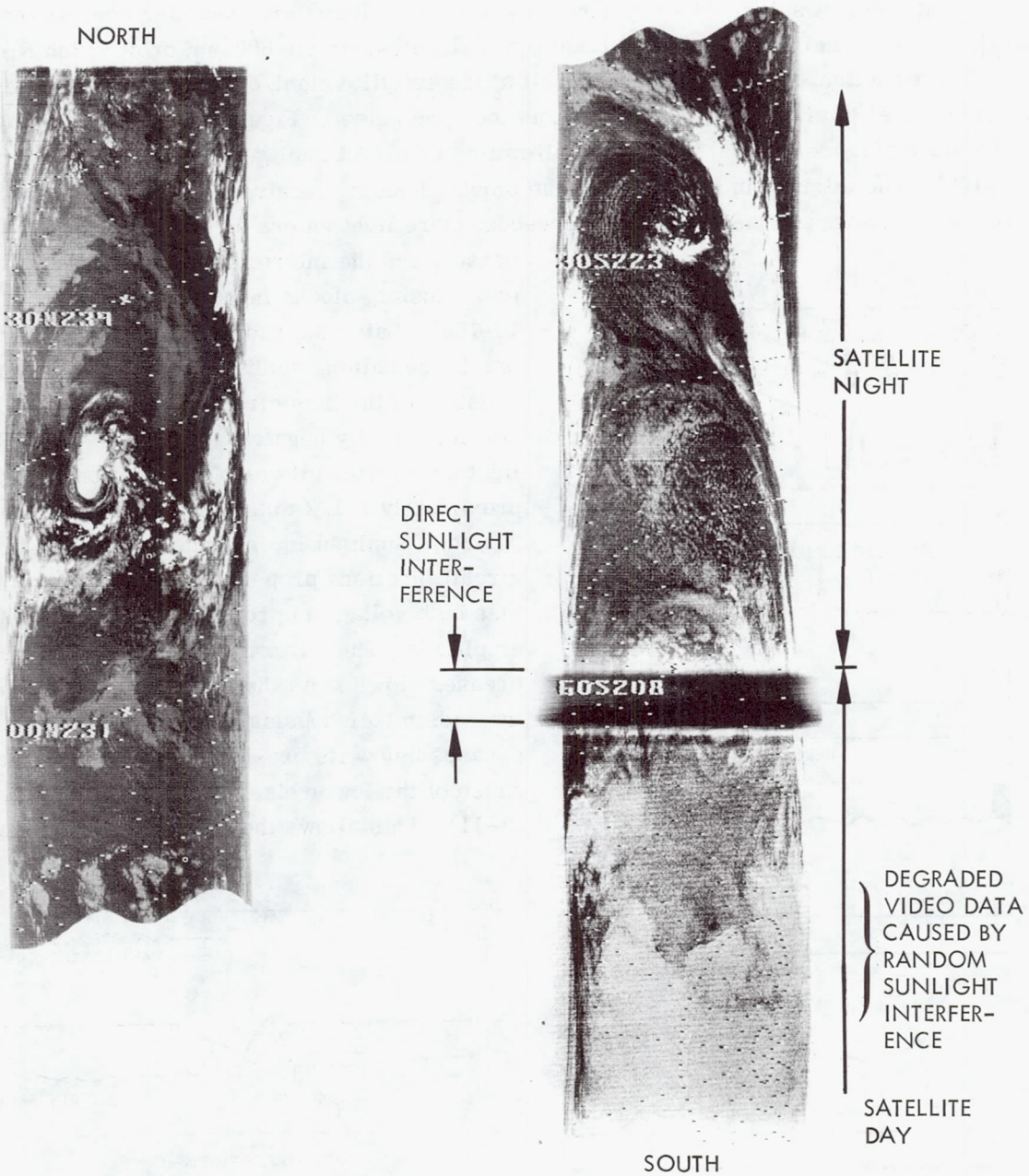

Figure 11-12—HRIR video data showing degradation caused by incident solar radiation.

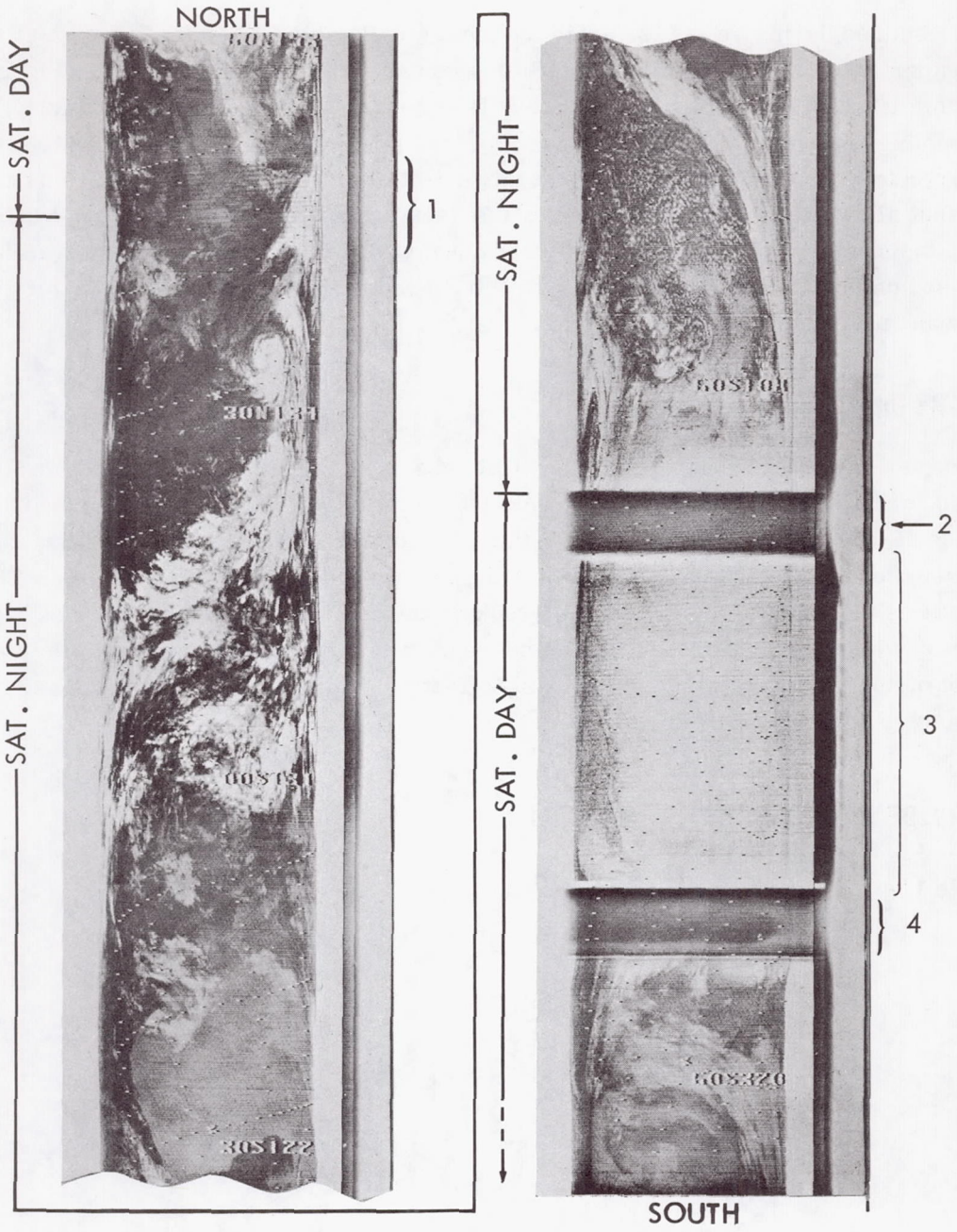

1. REFLECTED SUNLIGHT INPUT AT SATELLITE DAY-TO-NIGHT TRANSITION
2. DIRECT SUNLIGHT INPUT AT SATELLITE NIGHT-TO-DAY TRANSITION
3. DATA DEGRADATION RESULTING FROM IMPROPER DETECTOR CELL TEMPERATURE REGULATION (south pole gridding shown)
4. DIRECT SUNLIGHT INPUT RESULTING FROM ROLL-YAW ATTITUDE ERRORS

Figure 11-13—HRIR video data showing degradation caused by attitude errors (South Pole vicinity, orbit 1122).

Data obtained during orbit 1122 exhibited a degradation similar to the direct sunlight interference experienced at the satellite night-to-day transition at this orbit position (Figure 11-13). Analysis of the video data indicated a negative 5-degree roll error spacecraft attitude. Roll/yaw cross-coupling polarity dictates that a negative yaw error will result from a negative roll error. A yaw correction, combined with a large negative roll error, had turned the HRIR detector into a position that allowed direct sunlight to enter the detector cell, resulting in degraded HRIR video data until the spacecraft had restabilized in roll and yaw. As a corrective measure, the mirror shields used on the Nimbus B radiometer have been redesigned to permit satisfactory radiometer performance at orbital altitudes of 600 nm.

200-Hz Interference

Throughout the operational life of the HRIR Subsystem, the HRIR video contained faint 200-Hz interference (Figures 11-14 and 11-15). This interference was observed during prelaunch testing (Reference 13) and was attributed to a 200-Hz, 50-millivolt ac noise signal accompanying the -24.5-vdc regulated bus power entering the HRIR radiometer on the day/night power line. The radiometer amplifies the noise to a level between 200 and 250 millivolts and superimposes this on the radiometer video output. Although this interference was continuously present in the received video, it was not of sufficient magnitude to seriously affect the overall quality or usefulness of the video data.

SUMMARY OF HRIR SUBSYSTEM ANOMALIES

Table 11-3 summarizes the anomalies of the HRIR Subsystem.

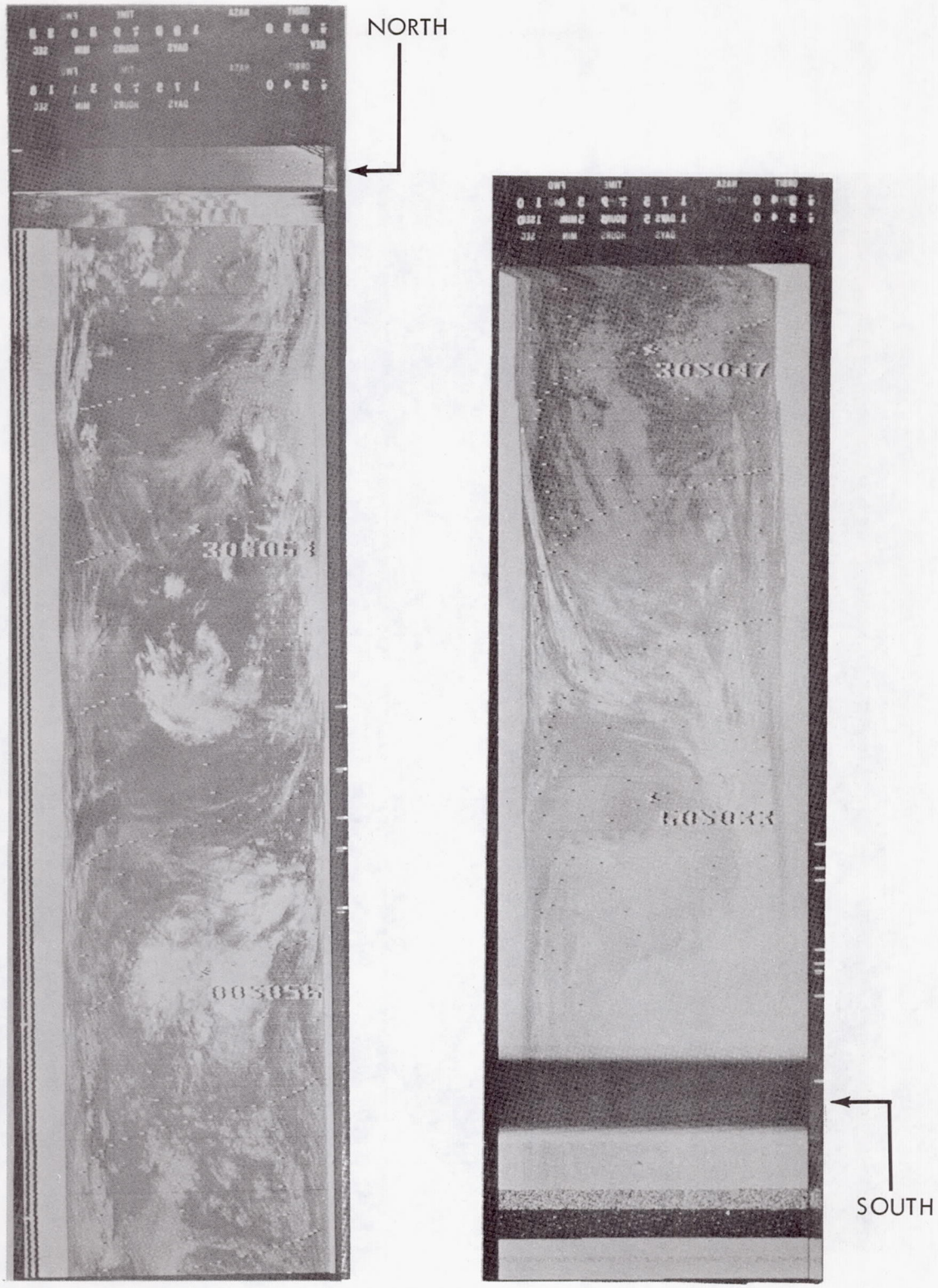

Figure 11-14— HRIR video data showing degradation of signal-to-noise ratio caused by elevated detector cell temperature (South Pole vicinity, orbit 5400).

Figure 11-15—HRIR photograph showing 200-Hz interference (faint diagonal lines).

Table 11-3

HRIR Subsystem Anomalies.

Anomaly	Cause	Remarks	B*	Corrective Action
Loss of video data and timing during interrogation 2455R	Tape recorder failure	Recorder failure in playback mode eliminated data collection and storage capability of this subsystem	No	Nimbus B will utilize dual HDRSS tape recorders for increased reliability
Amplitude variations in timing signals	Recorder tape degradation	Correlatable to increase in flutter and wow	No	----------
Decrease in signal-to-noise ratio from 20 (detector cell temperature -75°C) to 8 (detector cell temperature -64°C)	Change in thermal characteristics of cooling cone or cooling patch	----------	Yes	----------
Degradation in quality of video at satellite night-to-day and day-to-night transitions	Sunlight interference	Mirror shields on Nimbus II radiometer designed for 500-nm orbital altitude	Yes	Nimbus B mirror shield redesigned for 600-nm orbital altitude
200-Hz interference	200-Hz ac signal riding on -24.5-vdc radiometer power bus	----------	Yes	----------

*Anomaly Nimbus B-related.

SECTION 12

MRIR SUBSYSTEM

INTRODUCTION

The performance of the Medium Resolution Infrared Radiometer (MRIR) Subsystem was excellent until orbit 985 when the tape recorder failed. Since then, no sensory data have been received. Telemetry data received during orbit 1170 indicated that the radiometer chopper motor failed to restart after being off for several orbits. Attempts to reinstate the recorder and chopper motor operation proved futile. The calibration of the radiometer and telemetry remained in good agreement with the Santa Barbara Research Center calibration curves and exhibited no evidence of long-term degradation. A block diagram of the MRIR Subsystem is shown in Figure 12-1.

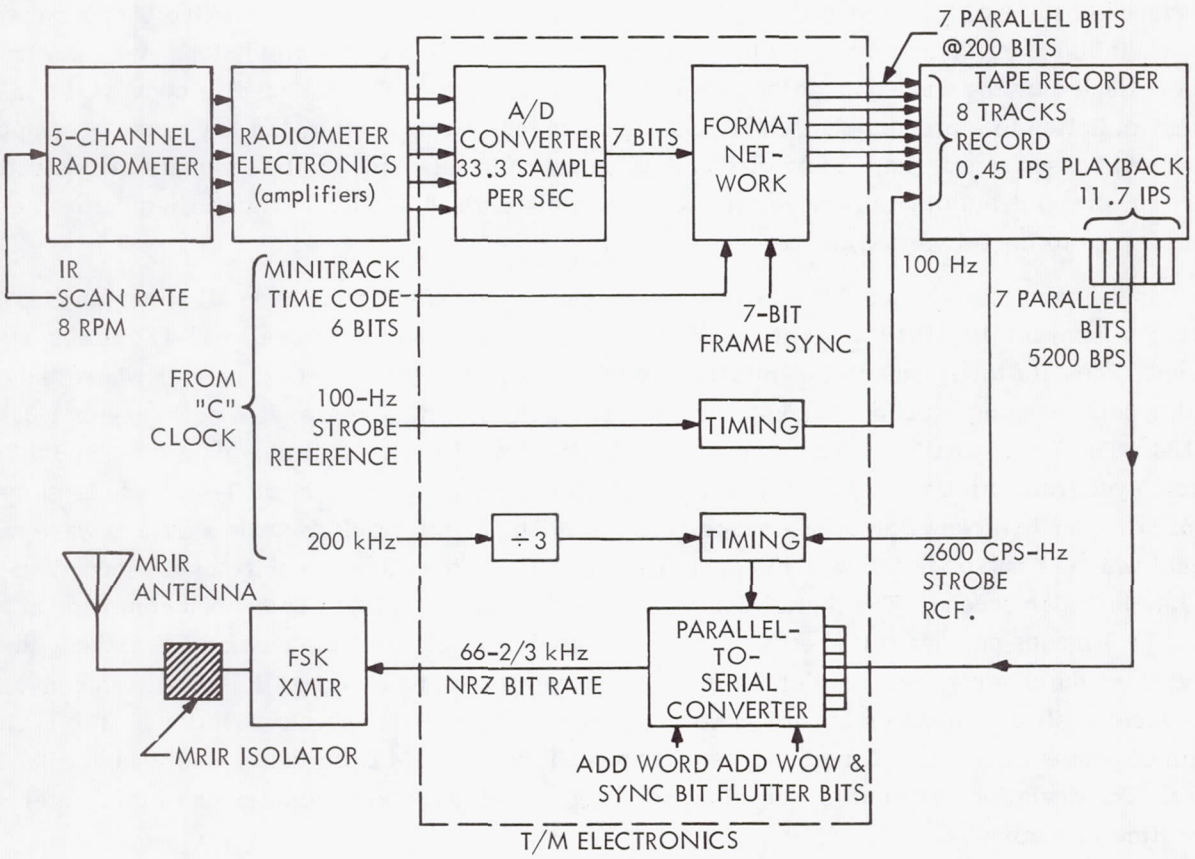

Figure 12-1—MRIR subsystem block diagram.

DESCRIPTION

The MRIR Subsystem measures the earth's terrestrial and atmospheric radiation and reflected solar radiation in five different spectral bands between 0.2 and 30 microns. The subsystem is composed of a 5-channel scanning radiometer, electronics module, telemetry electronics module, tape recorder, isolator, and antenna.

The radiometer optics consist of a single elliptically-shaped plane, aluminum scan mirror set at an angle of 45 degrees with the scan axis, five Cassegrainian telescopes, a chopper disc common to all five channels, a field stop, a filter, a condensing element, and a bolometer for each of the five channels. The radiometer scan mirror scans the earth through 360 degrees in strips perpendicular to the orbital track; it has an instantaneous field-of-view of 2.85 degrees (50 milliradians), and the resolution for a 600-nm altitude is 29.9 miles at the subsatellite point. The aperture diameter of each telescope is 1.72 inches. The effective f number of the objective optics is 2.44.

Two Roters No. 113C-11, hysteresis-synchronous motors drive the radiometer scan mirror and chopper disc. The shaft speed of the motors is 2000 rpm with an output torque of 0.1 oz.-inch. Speed reducing gears provide a scan mirror shaft speed of 8.0 rpm and a chopper disc shaft speed of 240 rpm. Radiation from the target scene is reflected from the rotating scan mirror to the apertures of the five telescopes and is imaged by the telescopes in the plane of the chopper disc. The radiation is modulated at 60 Hz by the chopper disc, limited by the field stops, filtered, and then collected by the condensing elements onto the bolometers. The bolometers convert the incident radiation to a proportional electrical signal which is amplified by the low-noise preamplifiers and passed to the radiometer electronics module. In this unit, the five signals are detected in synchronous detectors to remove the 6.0-Hz modulation and are further amplified before being transferred to the telemetry electronics module.

Inputs from the spacecraft clock (100-Hz, 2-phase and 200-kHz) provide all timing pulses required to operate the MRIR Subsystem. Each channel is sampled periodically 33-1/3 times per second. The data then passed sequentially through analog gates to an A/D converter where the analog data, ranging between 0 and -6.4 volts, are digitized with a conversion accuracy of 1 part in 128. The 7-bit parallel radiometer data are formatted with a 7-bit timing data word and a 7-bit frame synchronization word to produce a 60-millisecond main frame. Each 7-bit word is stored in parallel on 7 tracks of an 8-track tape recorder. The eighth track records a square wave clock signal which is out-of-phase with the data bits recorded on the other seven tracks. Record speed is 0.45 inch per second. The digital data stored on the tape are played back upon command at a 26:1 (11.7 inches per second) speedup ratio. Pulses developed from the clock track trigger the readout of the other seven parallel tracks into storage flip-flops of a parallel-to-series converter. The logic system eliminates errors introduced from tape recorder speed variations. The serial train of pulses thus created frequency-shift-keys a 1.75-watt FM transmitter operating at 137.2 MHz. The deviation selected is ±25 kHz, providing a minimum modulation index of 0.8. Interrogation time is 4 minutes.

Ground station processing is performed by a Telemetrics 670 digital computer with an electronics image system photorecorder as peripheral equipment. Processed sensory data are presented in the format shown in Figure 12-2.

The spectral regions covered by the radiometer are shown in Figure 12-3. The curves shown in solid lines are the normalized spectral responses of the five radiometer channels, and the curves

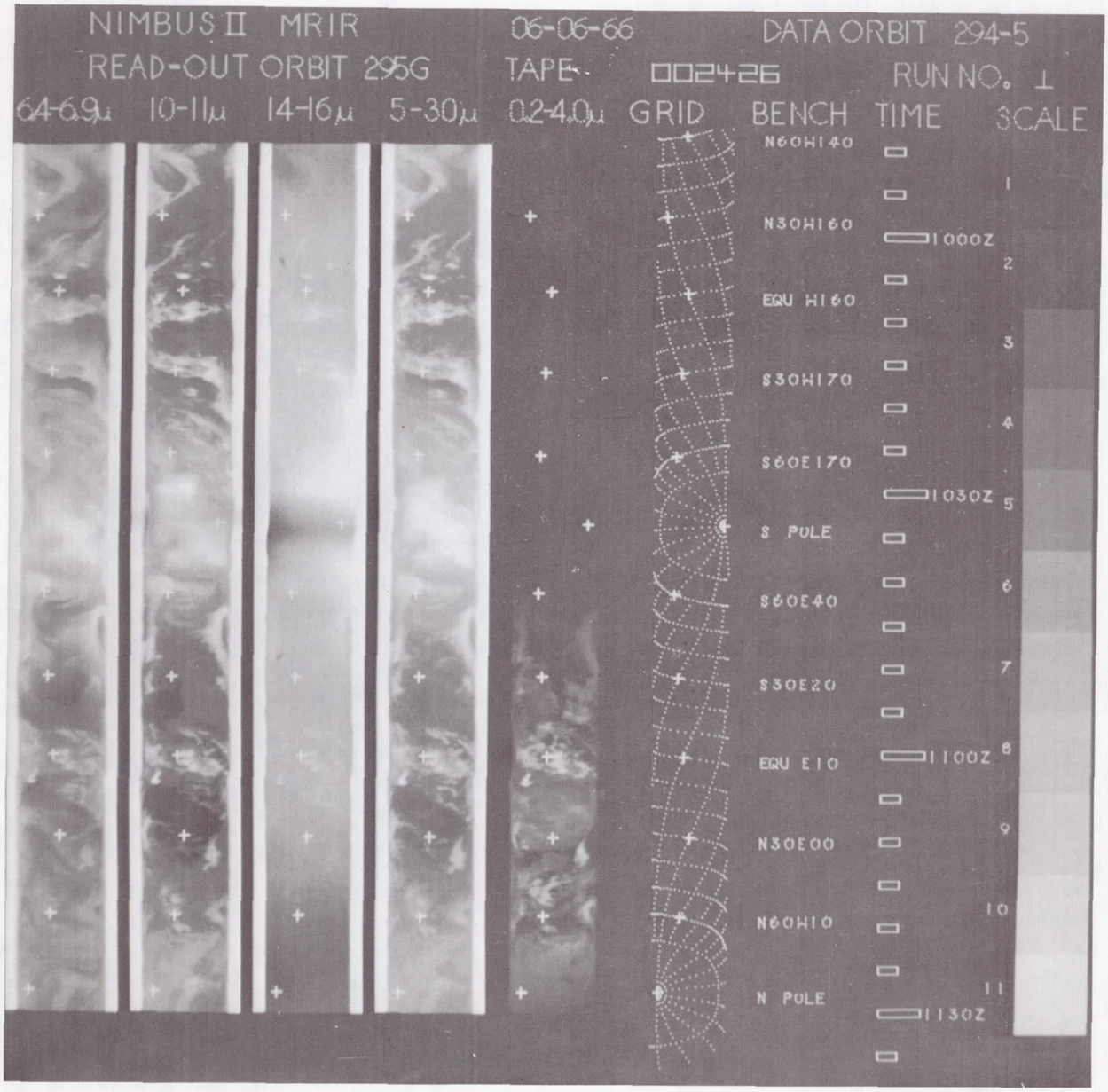

Figure 12-2—MRIR data format (orbit 294).

shown in dotted lines are the normalized transmission curves of the filters used in the five channels. The difference observed between the spectral response and the filter transmission is chiefly caused by the variation of bolometer response with wavelength, and by the dip in spectral reflectivity at 0.8 micron of the aluminized reflecting surfaces used in the radiometer.

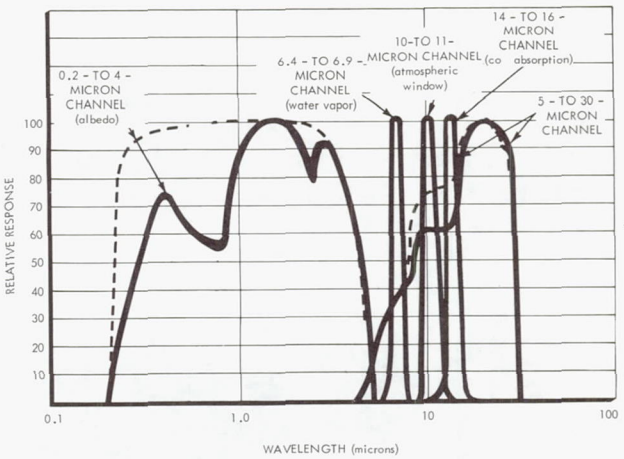

Figure 12-3—Filter and relative spectral response of Nimbus II 5-channel radiometer.

FLIGHT OBJECTIVES

The flight objectives of the MRIR Subsystem were to demonstrate the ability to measure the earth's terrestrial and atmospheric radiation and reflected solar radiation in five different spectral bands between 0.2 and 30 microns. At 6 months, the subsystem had performed excellently until orbit 985, when a tape recorder malfunction eliminated the data recording capability. Also, the radiometer chopper motor failed during orbit 1170. At 13 months, the subsystem status had remained unchanged since orbit 1170.

ELECTROMECHANICAL PERFORMANCE

The electromechanical performance of the MRIR Subsystem was excellent with the exception of the failure of the tape recorder and radiometer chopper motor which is discussed in following subparagraphs. The pressure of the subsystem recorder has remained steady at 14.9 psia. MRIR analog recordings indicated that the subsystem recorder had operated properly before the failure, and that the radiometer mirror rotation speed was within 10^{-4} rpm of the specified 8 rpm. A summary of the subsystem performance is presented in Table 12-1.

Tape Recorder Failure

During orbit 985 the carrier frequency lost modulation after 2 minutes and 48 seconds of playback. At this time, all telemetry indications were normal except playback motor current and record motor power supply (Refer to Table 12-2 for telemetry readings). Telemetry indicated that the momentum compensation motor had stalled. Additional playbacks were attempted in orbits 986, 187, and 988 (refer to Table 12-3 for sequence of events). In orbit 987 the telemetry indicated that the playback motor also had stalled. This condition could have been caused by tape breakage and the subsequent jamming of the motors, or the motors could have stalled of their own accord.

Analysis of the MRIR on/off playback programming from orbit 778 to the time of failure indicated that the tape splice was located at the record/playback head at the time of the playback command just before acquisition for pass 985U. This playback was programmed for, and lasted,

Table 12-1

MRIR Performance Summary.

Function	Requirements	Outcome
Radiometer		
Mirror rotation	8 rpm	Satisfactory
Chopper rotation	4 rps	Failure (1)
Thermal control	Maintain housing at +23°C	Satisfactory (2)
Calibration	Maintain constant signal input/output relationship	Satisfactory
Shading	Output photographic shading/earth signal input relationship constant	Partially satisfactory (3)
Telemetry	Adherence to calibration and stability	Satisfactory
Recorder		
Data recovery	Records and plays back data without distortion	Satisfactory
Drive speed ratio	To play back at 26 times record speed	Satisfactory
Telemetry	Adherence to calibration and stability	Partially satisfactory (4)
Telemetry electronics		
Flutter and wow correction	Add additional digits to recorder output to maintain 66.67-kilobit rate	Satisfactory
Transmitter output		
power	1.5 watts minimum	Partially satisfactory (5)
frequency	137.20 MHz (±13.523 kHz)	Satisfactory
Telemetry	Adherence to calibration and stability	Satisfactory
Operability	Dependable command execution	Satisfactory
Compatibility	Compatibility with other subsystems (RFI)	Partially satisfactory (6)
Reliability	Capable of continuous 6-month operation	Failure (7)

Notes:
(1) Radiometer chopper motor failed during orbit 1170
(2) Radiometer housing temperature telemetry indicated orbital temperature profile of 19 ± 2°C
(3) Sunlight interference at satellite night-to-day transition resulted in erroneous measurements in the vicinity of the South Pole
(4) Recorder motor telemetry indications varied from 3.4 to 3.8 tmv because of hysteresis changes in the core of the transformer in the telemetry sensor; Playback motor drive current telemetry increased from 6.2 to 6.35 volts before recorder failure, because of increased friction within tape recorder or possible shift of telemetry sensor calibration
(5) Telemetry indicates transmitter power output increased during initial 400 orbits from 1.35 watts to 1.5 watts and remained constant thereafter
(6) MRIR playback induced severe interference into AVCS video
(7) Subsystem tape recorder and radiometer chopper motor failed prematurely

Table 12-2

Telemetry Readings Related to MRIR Recorder Failure.

Telemetry Function \ Orbit No.	Telemetry Value (tmv)					
	980	985	986	987	988	5252 (one year in orbit)
Chopper rotation monitor	3.45	3.5	3.4	3.5	3.45	0.00‡
Radiometer -10 vdc	3.0	3.0	3.0	3.0	3.0	3.0
Chopper 1 temp.	2.4	2.4	2.35	2.35	2.4 (17°C)	3.0 (12°C)
Chopper 2 temp.	2.4	2.4	2.35	2.3	2.4 (17°C)	3.0 (11.8°C)
Radiometer housing temp. 1	2.2	2.15	2.15	2.1	2.2 (19°C)	2.7 (14.8°C)
Radiometer housing temp. 2	2.3	2.3	2.25	2.15	2.3 (18°C)	2.75 (14.1°C)
Radiometer electronics temp.	1.9	1.9	1.85	1.9	2.1 (21°C)	2.4 (18.3°C)
Recorder motor	4.6*	4.6*	---	---	---	5.4†
Power supply (P/B)	---	4.9†	4.95†	5.3†	5.35†	5.4†
Recorder motor current	3.6	3.55	3.6	3.5	3.7	3.7
P/B motor current	6.35*	6.35*	5.15†	---	6.35†	6.35†
Recorder deck temp.	2.6	2.6	2.6	2.6	2.55 (22.5°C)	2.25 (18.7°C)
Recorder housing temp.	2.5	2.6	2.6	2.55	2.5 (22°C)	2.3
Recorder pressure	2.85	2.85	2.85	2.8		
T/M electronics temp.	2.6	2.55	2.5	2.5	2.7 (24°C)	3.10 (20.1°C)
Transmitter temperature	1.35	1.3	1.35	1.4	1.4 (21°C)	1.7 (18.7°C)
Transmitter power out record	2.3	2.3	2.3	2.3	2.3	2.0
	4.8	4.8	4.85	4.9	4.9 (1.5 watts)	4.9 (1.5 watts)

*Modulated
†Unmodulated
‡Radiometer chopper failed during orbit 1170

Table 12-3

MRIR Recorder Failure Event Chart.

Orbit No.	GMT (hr:min:sec)	Cmd No.	Remarks
985U	07:31:19	214	Loss of modulation after 2 min., 48 sec of P/B (not noticed on pass)
986U	09:17:35	214	No modulation present
	09:18:19	206	To verify electronics on
	09:70:00	216	To terminate P/B
987U	11:02:19	214	No modulation present
	11:07:16	204	Turn off electronics
	11:14:42	222	Turn off radiometer
	≈11:15:00	360	Turn on radiometer
988U	12:48:36	206	Turn on electronics
	12:48:53	214	No modulation present (timed out OK)
	12:50:58	222	Turn off radiometer
	12:51:18	360	Turn on radiometer
	12:53:31	214	No modulation present (timed out OK)
	12:58:08	204	Turn off electronics

1 minute and 41 seconds. The recorder then went into record for a period of 1 minute and 38 seconds before going into the playback, which failed after 2 minutes and 48 seconds. Expressing the tape length in playback time, a total of 4 minutes and 33 seconds was used from the start of the first playback until the loss of modulation during the second playback. The normal tape length would be 4 minutes and 30 seconds. This would indicate that the tape splice was at, or near, the playback head at the time of failure. Unsuccessful attempts were made to restart the motors by lowering and raising the recorder temperature.

During the cooling-off procedure, the electronics and radiometer were turned off for periods of approximately 20 seconds up to four orbits with little change in the recorder temperature. The warmup procedure, attempted on several different occasions, consisted of placing the system in playback at the end of each playback until the end of the Alaska interrogation. Then 10 playback commands were stored to be executed at 5-minute intervals with the last one to be executed just before the next Rosman, North Carolina interrogation. At Rosman, the continuous playback sequence was performed again through Alaska, this time storing 12 playback commands scheduled to start at the Alaska interrogation and to be executed every 5 minutes. During the double interrogations, the recorder temperatures remained fairly constant at 26 to 27°C, while the transmitter temperature went from 22 to 27°C on one occasion and up to 30°C on another. Table 12-4 is a summary of the experiments performed in attempting to reinstate recorder operation.

Table 12-4

Experiments Performed in Attempting to Reinstate Recorder Operation.

Interrogation No.	Results
1220U	Radiometer, recorder and electronics power activated, followed by attempted P/B; when no carrier modulation was observed, the subsystem was placed in record, and power was removed from the radiometer, recorder, and electronics
1232U	Radiometer/recorder power activated
1233U	Radiometer/recorder power turned off/on, then power applied to the electronics, and P/B commanded; when no modulation was received, subsystem was placed in record, electronics power turned off, and radiometer/recorder power on
1237R	Same as 1233U
1240U	Same as 1233U
1243R	Radiometer/recorder turned off for 2 minutes; power reapplied to the radiometer/recorder and electronics P/B commanded; when no modulation was received, subsystem was placed in record and electronics power turned off
1245U	Same as 1233U
1246U	Electronics power applied and subsystem placed in record for approximately 4 minutes, followed by P/B; no modulation received, and P/B allowed to time out and go into the record mode; subsystem left in record for one orbit
1247U	Playback commanded and allowed to time out and go into record mode; no modulation was received; electronics power turned off; radiometer/recorder remained powered for three orbits

Table 12-4

Experiments Performed in Attempting to Reinstate Recorder Operation.

Interrogation No.	Results
1250R	Electronics power applied, and subsystem placed in record module for approximately 4 minutes, followed by P/B (with no modulation); playback was allowed to time out, and electronics turned off
1253U	Radiometer/recorder turned off/on, electronics power applied, and P/B commanded; after approximately 1 minute of unmodulated carrier, subsystem placed in record, and electronics power removed
1256R	Electronics power applied, P/B commanded and allowed to time out and go into record mode; subsystem left in record mode; no modulation present
1257R	P/B commanded and allowed to time out; no modulation present; electronics power removed after P/B completed
1259U	Electronics power applied, and P/B commanded and allowed to time out; no modulation present; electronics power removed after P/B completed
1264R	Same as 1259U
1267U	Same as 1259U
1270R	Same as 1259U
1273U	Same as 1259U
1276R	Electronics power applied, and P/B commanded and allowed to time out; no modulation received; following completion of P/B, electronics, radiometer and recorder power removed and subsystem remained off for remainder of the period covered by this report
1629R	Radiometer, recorder, and electronics power activated, followed by an attempted playback; when no carrier modulation was observed, power was removed from the radiometer, recorder, and electronics
1922R	Electronics power activated; radiometer and recorder power was applied; then removed at approximately 30-second intervals for duration of pass in an attempt to reinstate chopper rotation; results were negative, and power was therefore removed from the radiometer, recorder, and electronics
2308R	Electronics power activated; radiometer and recorder power was applied, then removed at approximately 30-second intervals for duration of pass in an attempt to reinstate chopper rotation; results were negative
2309U	Playback commanded and allowed to time out and go into the record mode; no carrier modulation was observed; power was removed from the radiometer, recorder, and electronics
3678U	Radiometer, recorder, and electronics power activated; radiometer chopper motors continued to remain inoperative; system left in record mode for one orbit
3679R	Playback commanded; no modulation was received; playback timed out, and system went into record mode; no carrier modulation was observed; power then was removed from the radiometer, recorder, and electronics
3958U	Same as 3678U
3959R	Same as 3679R
4810U	Radiometer, recorder, and electronics power activated followed by an attempted playback; when no carrier modulation was observed, power was removed from the radiometer, recorder, and electronics
5252U	Same as 4810U

Radiometer Chopper Failure

Table 12-5

Telemetry Readings Related to Chopper Failure (System in Record Mode).

Orbit Number	Chopper Motor Telemetry Value (tmv)
1162	3.45
1167	3.45
1170	0.00
1176	0.00
1177	0.00
1178	0.00

Upon application of power to the MRIR radiometer during interrogation 1170R, telemetry showed that the MRIR radiometer chopper (S/N F-6) was not rotating (Table 12-5). Power to the radiometer had been removed during orbit 1167 (before blind orbits). The chopper motor was known to have had marginal starting characteristics at low temperatures. Before launch, a +7°C environment was considered critical. Before the failure, the temperature had reached +14°C. Average normal orbital operating temperature was +19°C. During prototype spacecraft testing both the P-2 and F-2 radiometer choppers stopped rotating after approximately 2000 hours of operating time. During spacecraft thermal-vacuum testing, the F-6 (flight) radiometer chopper had stopped rotating after approximately 1800 hours of operation. This failure occurred while the chopper was rotating. The flight failure occurred after the chopper had been turned off for three orbits and could not be restarted. Continual rotation is recommended for optimum performance.

A decision was made to repair the failed F-6 radiometer rather than replace this unit with the backup F-5 radiometer. The F-6 flight radiometer had approximately 1800 hours of operation (after refurbishment) when it failed to rotate during interrogation 1170R. As a corrective measure, and for increased readability, the bearing retainers utilized in the MRIR radiometer which will be flown on Nimbus B have been redesigned. This modification is expected to give the radiometer the reliability necessary to meet Nimbus B operational requirements.

VIDEO QUALITY

The MRIR video was of excellent quality with the exception of the two problems discussed in the following paragraphs. There was no evidence of any degradation in the performance of the radiometer or associated electronics before the failure of the subsystem tape recorder during orbit 985.

APT Transmitter Interference

During initial interrogations, data were obtained utilizing a receiver bandwidth of 300 kHz. The MRIR data received in this manner were severely degraded by RF interference originating from the APT transmitter because of the close proximity of the APT transmitter frequency (136.95 MHz) to that of the MRIR (137.2 MHz). This necessitated the use of a 100-kHz receiver bandwidth and precise receiver tuning to obtain optimum data quality (Figures 12-4 and 12-5). Interference subsequently was experienced at the Rosman DAF and was determined to originate from a cooling fan

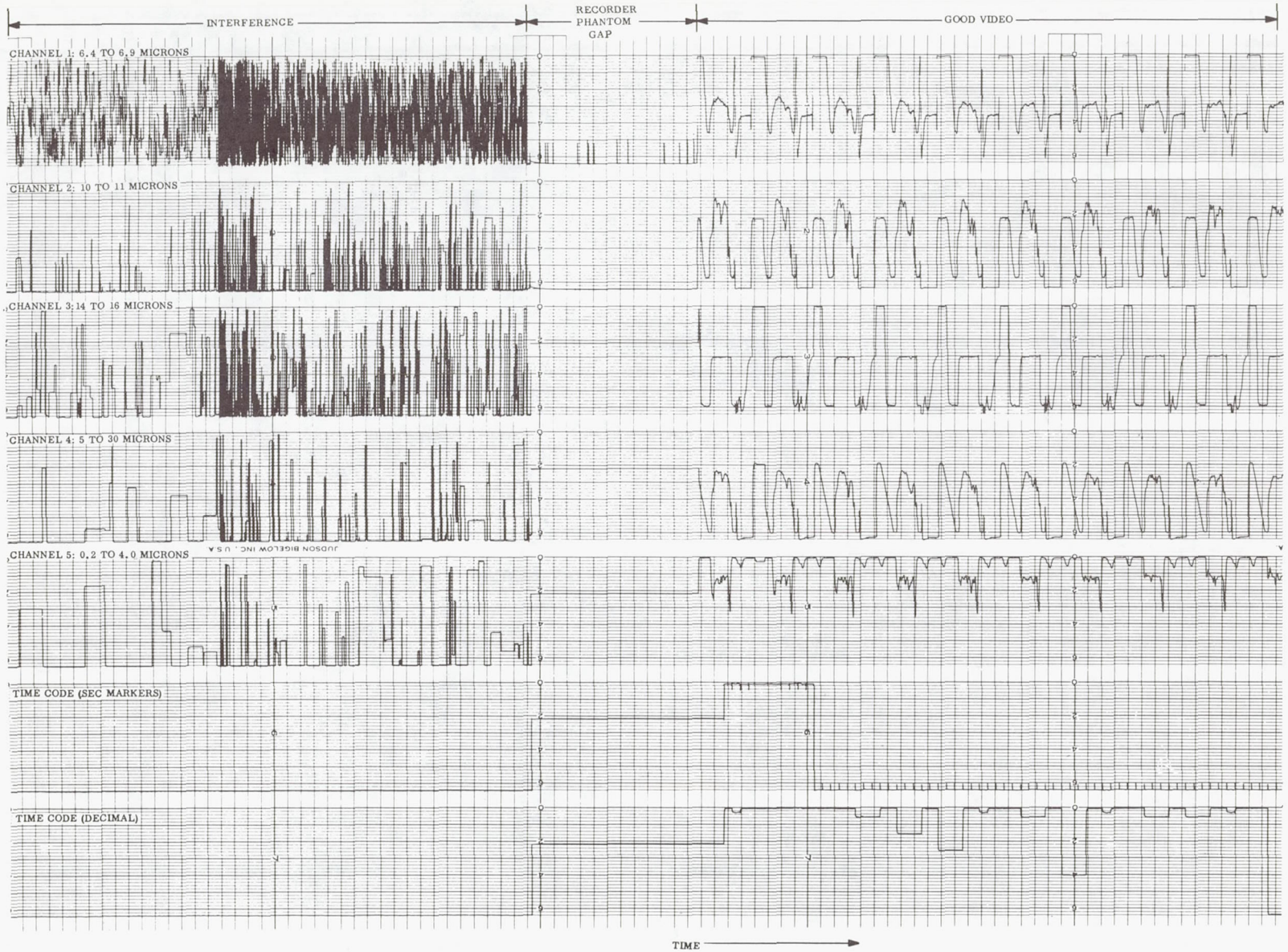

Figure 12-4—MRIR video brush recording showing APT subsystem interference at ground-station receiver.

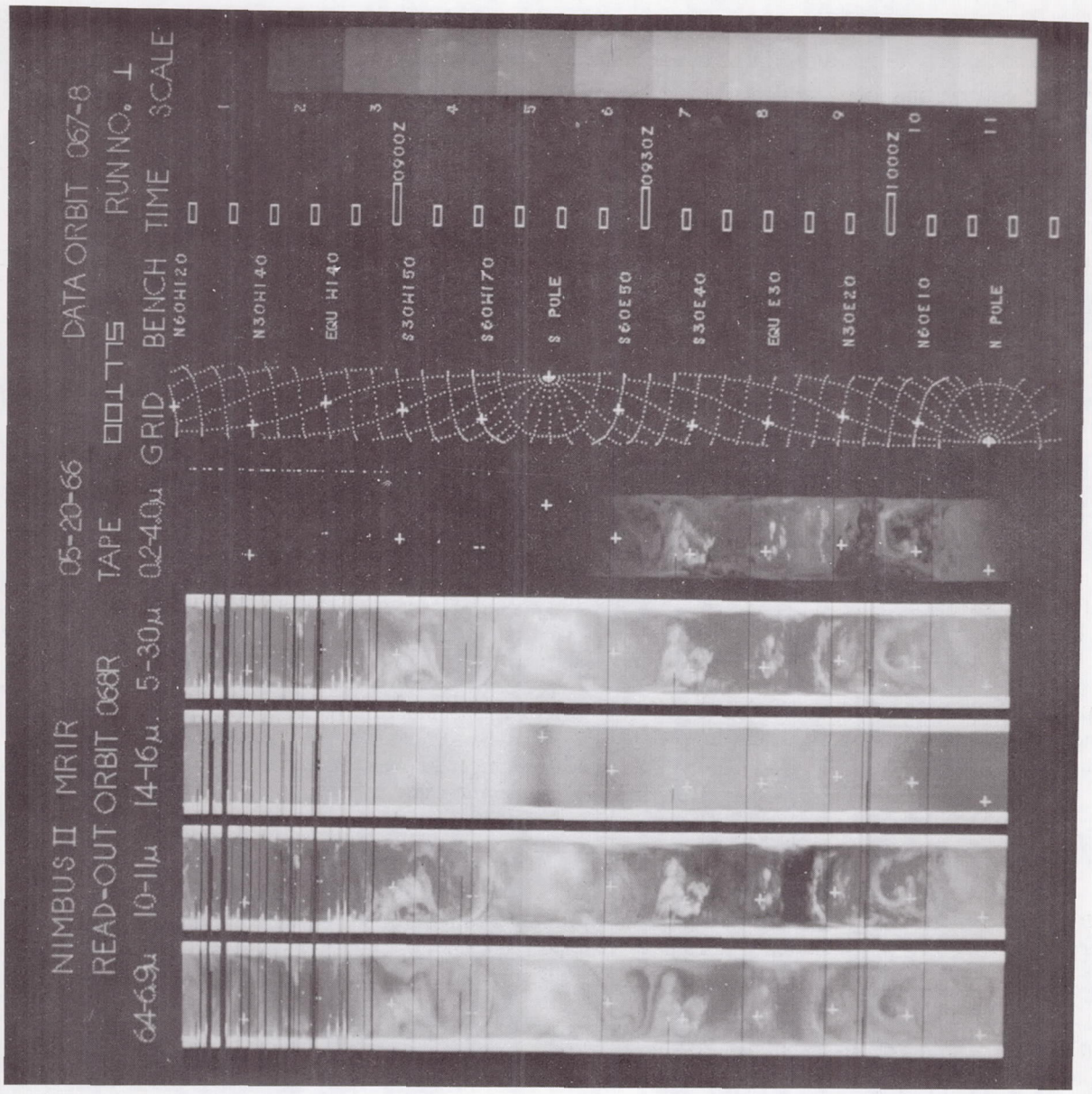

Figure 12-5—MRIR video showing sunlight effects at South Pole region and interference sync losses.

motor in the antenna-mounted electronics. Elimination of the foregoing interference sources enabled the consistent reception of excellent video data of the quality contained in Figure 12-2.

Sunlight Interference

During satellite night-to-day transition periods, direct sunlight entered the optics of the 6.4 to 6.9, 10 to 11, 14 to 16, and 5 to 30-micron channels of the radiometer. In the 0.2 to 0.4-micron

channel, sunlight entered during the space scan portion of the cycle and therefore was not visible in the photographs. In the other channels, the Cassegrainian secondary mirror was heated, resulting in erroneous indications of a "hot" band in the vicinity of the South Pole (Figure 12-5). As a corrective measure, a sun shield which occludes a greater angle than the present radiometer housing structure has been added to the Nimbus B radiometer and is expected to eliminate the sunlight interference.

Table 12-6

MRIR Subsystem Anomalies.

Anomaly	Cause	Remarks	B*	Corrective Action
MRIR P/B motor drive current telemetry increased (initial 400 orbits)	Possible increase loading of P/B motor caused by increased friction within the tape recorder or possible shift of telemetry sensor calibration	T/M showed gradual increase for expected 6.2 tmv to 6.35 tmv (full scale)	No	N/A
MRIR record motor drive current indicated change (separation, orbit 28U)	Hysteresis changes in sensor transformer core	Coincident with power transients at HAX OFF command (orbit 28U) and at squib firing at separation	No	N/A
MRIR (sunlight interference on three channels)	Direct and reflected sunlight interference	Shielding should have been designed for a 600-nm orbit in place of 500-nm design	Yes	A sun shield has been added to the Nimbus B radiometer which includes a greater angle than the present radiometer housing structure
MRIR tape recorder failure in orbit 985	Stalled P/B and compensation motors possibly because of tape breaking	Attempts to restart tape recorder in P/B mode failed	No	Nimbus B will utilize dual HDRSS tape recorder for increased reliability
MRIR chopper motor stopped rotating in orbit 1070	Probable increase in friction in chopper motor bearing system	Chopper motor known to have marginal starting characteristics at low temperatures	Yes	Bearing retainers for the Nimbus B radiometer have been redesigned for increased lubricant protection and efficiency

*Anomaly related to Nimbus B.

SECTION 13

CONCLUSIONS

Nimbus II was launched successfully into a near-circular orbit on May 15, 1966; it performed well during the 13-month period ending 15 June 1967 (orbit 5275). All major mission objectives were met. The favorable orbit and satisfactory performance of all systems resulted in nearly full-global meteorological coverage by the spacecraft on a daily basis. With the near-circular 600-nm orbit achieved, the nominal number of daily interrogations obtained at the two Data Acquisition Facility (DAF) stations amounted to ten passes at Fairbanks, Alaska (Ulaska) and four passes at Rosman, North Carolina. Pass-time ranged from 10 to 15 minutes.

Many improvements over previous Nimbus models performed successfully. The improvements in the Solar Array Drive (SAD), for example were completely successful. The reduction in the size of the pitch nozzle, along with the reduced gating duration, successfully eliminated the pitch oscillation that was experienced with Nimbus I. The ability to measure the earth's terrestrial and atmospheric radiation and reflected solar radiation using five spectral bands was demonstrated successfully by the MRIR Subsystem. Also, the Data Code Grid (DCG) experiment incorporated into the APT Subsystem pictures performed satisfactorily.

Direct readout HRIR (DRIR) was transmitted by the APT transmitter for 1370 hours before the failure of the HRIR Subsystem tape recorder eliminated this capability. The success of this experiment is highlighted by the growth of stations with the capability of receiving the DRIR signal (7 at launch to approximately 51 at the time of failure).

The major problem encountered by Nimbus II was the failure of tape recorders:

a. PCM (orbit 949)

b. MRIR (orbit 985)

c. AVCS (orbit 1443)

d. HRIR (orbit 2455)

The sensory data output exceeded that of Nimbus I on the 15th day of flight; at the end of 13 months in flight, the total number of photographs accumulated and total operating time for the sensory subsystems were as given in Table 13-1. A summary of the individual subsystem performance follows.

SEPARATION SUBSYSTEM

Following launch the Separation Subsystem behaved normally. The 2.5-second timer caused paddle-unfold; initial stabilization was smooth, rapid, and complete in all three axes within 7 minutes after spacecraft/booster separation. The clock was upset (similar to test experience), and one word was lost in the PCM multicoder causing short-term loss of synchronization.

Table 13-1

Nimbus II Sensory Data Outputs Through Month 13.

Subsystem	Operation	Total This 31-day Period (May 16 to June 15, 1967)	Accumulated to Date (May 15, 1966 to June 15, 1967)
AVCS	Total camera cycles	38,400	429,149
APT	Hours Total pictures	365 6317	4860 84,115
HRIR	Night orbit swaths	------	2005
	Day orbit swaths	------	185
	Orbits of operation for recording regulated bus current	------	215
DRIR	Hours	------	1370
AVCS	Photographs retrieved	130*	114,003†
MRIR	Day/night orbit swaths	------	789

*Total (approximate) frames of AVCS direct pictures since 16 May 1967.
†Includes approximately 1670 frames of AVCS direct pictures.

POWER SUBSYSTEM

The Power Subsystem performed well throughout the flight. The solar array output in orbit 1 was 13.6 amperes, and the average array output at the end of 13 months in orbit (orbit 5275) was 9.85 amperes, which is sufficient power for present spacecraft operation. The solar array experienced normal degradation caused by particle damage and ultraviolet irradiation, and two solar panel failures (orbit 1066 and orbit 4384). Battery performance was excellent with no battery degradation observed. Voltage regulation of the spacecraft primary and auxiliary buses was maintained well within the prescribed tolerances.

CONTROL SUBSYSTEM

The Control Subsystem effectively maintained Nimbus II in an earth-oriented attitude within 1 degree in all axes in the absence of cold cloud disturbances. Solar array pointing accuracy was maintained, and the Solar Array Drive (SAD) control loop ran as anticipated at the low-torque setting. The SAD motor temperature was maintained well within its prescribed limits and currently is averaging +25.4°C, the average temperature for 13 months in orbit being +24 ± 3°C. The control gas consumption was low, with the system averaging one roll gate every other orbit and one pitch gate every 3-to-4 orbits. The yaw pneumatics were turned off as planned in orbit 5 to conserve control gas. At launch, there were 16.43 pounds of control gas available; on June 15, 1967,

there were 13.40 pounds remaining. At this rate, there are approximately 26,000 orbits worth of gas remaining—equivalent to approximately 5.4 years.

THERMAL SUBSYSTEM

The Thermal Subsystem control of Nimbus II was good. For the 13-month period, the average sensory ring temperature was +21 ± 2°C; the average center section temperature +23 ± 3°C; and the average control housing temperature +24 ± 5°C. Day-to-night variations in average temperatures were approximately 2°C. All batteries are running cooler now with a minimum temperature of approximately +18°C, and a maximum of approximately +25.5°C, compared to +21.2°C minimum and 26.5°C maximum during the period of full spacecraft operation. The average ring temperature is now +19.2°C.

There were three failures in the Thermal Subsystem: (1) The AVCS Camera-2 temperature telemetry point failed; (2) thermal control shutter 15 position monitor failed open, followed by occasional intermittent shorting; and (3) thermal control shutter 13 position monitor read random positions.

Most thermistors exhibited a cyclic temperature characteristic related to the orbit of the spacecraft. The excursions of these temperature variations remained essentially the same throughout flight while their level shifted because of the varying intensity of the sun and internal power dissipation.

PCM SUBSYSTEM

The PCM Subsystem performed well for the first 949 orbits, at which time a failure of the PCM tape recorder precluded further receipt of stored data. Real-time data are still being received and have proved to be of sufficient quantity and quality to properly evaluate the spacecraft and to make any necessary adjustments.

COMMAND SUBSYSTEM

Clock stability, with the exception of two upsets early in flight, was well within specification, gaining only approximately 1 millisecond per orbit. There have been no significant problems with the ground-to-spacecraft command link during interrogations. Two types of problems have been encountered, neither of which affect spacecraft operation. One problem was noise entry into the clock memory, resulting mainly in erroneous data in the APT Subsystem DCG. The second problem was the large number of unencoded command executions which resulted in switching the primary and redundant receiver FM demodulation selection relay and switching the power supply feedback amplifier relay.

Approximately 85,000 commands have been issued to the spacecraft since launch. Commands are issued at ranges of 3900 km (slant range) with a SATAN transmitter having a nominal output of 2.5 kilowatts.

RF SYSTEMS

All RF links were satisfactory. Usable PCM data were received at signal levels ranging from -85 to -120 dbm; good S-band data were received in the range of -70 to -90 dbm with elevation angles as low as 4 degrees. Satisfactory MRIR transmissions have provided usable data between -80 and -105 dbm. The APT signal interfered with the MRIR signal during early operations when the ground receivers had a 300-kHz bandwidth; however, this problem was eliminated by changing to 100-kHz bandwidth operation of the MRIR receiver. Usable APT signals were received with amplitudes ranging from 5 to 110 microvolts, allowing up to five pictures to be received on each pass.

AVCS SUBSYSTEM

The performance of the AVCS was satisfactory until orbit 1444 when the subsystem tape recorder failed, thus eliminating data storage capability. Since that time pseudo-direct pictures represented the only medium by which subsystem data could be received. Throughout the 13-month period, the most serious impediment to overall quality was RF interference. The cameras are still being cycled during the earth-day portion of the orbit; however, one camera has experienced loss of focus, although it is still usable. Picture quality from a cloud coverage standpoint was satisfactory and superior to Nimbus I although landmark identification was not as good because of the higher altitude orbit and the use of the Y-10 filter.

APT SUBSYSTEM

The performance of the APT Subsystem was satisfactory. Picture quality from a cloud coverage standpoint was superior to Nimbus I, but terrain detail was not as good. A gradual shift in the dc level of the video occurred which, however, can be compensated for by the ground station processing equipment. The DCG continues to successfully disseminate ephemeris data to APT users.

HRIR SUBSYSTEM

The HRIR Subsystem picture quality was extremely good with no interference pattern and high-frequency noise that existed in Nimbus I. This improvement effectively doubled the HRIR resolution. There was, however, a saturation of the video signal caused by direct sunlight on the detector cell when the satellite was at the satellite night-to-day transition. In addition, the detector cell temperature gradually increased after launch, stabilizing at -66°C. This overheating

decreased the signal-to-noise ratio of the video, causing minor video degradation. The performance was good until orbit 2455, at which time the subsystem tape recorder failed, thus precluding the continued reception of data.

DRIR SUBSYSTEM

Before the failure of the HRIR Subsystem tape recorder, the HAX Module provided excellent, interference-free, real-time transmission of HRIR data. The failure of the HRIR tape recorder precluded the further receipt of DRIR video.

MRIR SUBSYSTEM

The performance of the MRIR Subsystem was excellent until orbit 985 at which time the subsystem tape recorder failed, precluding further receipt of data. After this, during orbit 1170, telemetry data indicated that the radiometer chopper motor had also failed. The technique developed for presenting photographically the output of the five radiometer channels was very effective.

Goddard Space Flight Center
National Aeronautics and Space Administration
Greenbelt, Maryland, February 12, 1968
604-21-75-01-51

REFERENCES

1. "Instruction Manual, Solar Conversion Power Supply Subsystem," RCA Document No. AED-M-1798, Rev. 2, Feb. 18, 1966.

2. Rasmussen, R., "Nimbus II Power Subsystem Post-Launch Analysis, Solar Array Performance," RCA/AED Report No. SP-W-784, July 1966.

3. Rasmussen, R., "Nimbus II Power Subsystem Post-Launch Analysis, Orbits 3100 to 5700," RCA/AED Report No. SPW 717, Sept. 25, 1967.

4. Brindley, W., and Rasmussen, R., "Nimbus II Power Subsystem Post-Launch Analysis, Orbits 1 to 3100," RCA Report No. SPW 912, April 28, 1967.

5. Pizzini, G., and Barcus, R., "Nimbus II Separation Sequence Telemetry Evaluation," General Electric Company, Valley Forge Space Technology Center, Program Information Release 41J1-27.

6. Klammer, R., "Dynamic Control System Error Evaluation for Nimbus II, Utilizing Telemetered Flight Data," General Electric Company, Valley Forge Space Technology Center, Program Information Release 41M1-000-458, July 26, 1967.

7. Greaves, J., "Operation of NIMBUS Data Utilization Center," Allied Research Association Document 9G26F, Appendix C, Feb. 1967.

8. McNaney, J., "NIMBUS II Monthly Flight Evaluation Report No. 10," General Electric Document No. 67SD4280, Mar. 31, 1967.

9. "Final Report, Nimbus C (Flight 302), Integration Testing Review and Evaluation," Section 8-1, General Electric Document No. 66SD4280, Mar. 15, 1966.

10. "Nimbus C Thermal-Vacuum Tests," General Electric Company Document No. 66SD4267, pp. 5-7, Mar. 15, 1966.

11. "Nimbus C Electrical Vibration Test Report," General Electric Company Document No. 66SD4259, pp. 3-6, Mar. 15, 1966.

12. "Nimbus C Integration and Testing Final Report," General Electric Company Document No. 66SD4300, pp. 4-4, Mar. 15, 1966.

13. "Engineering Evaluation Report on the Flight No. 302, Sensory Ring Thermal Vacuum Testing," General Electric Company Document No. 65SD4450, pp. 4-40, Oct. 12, 1965.

Appendix A

Summary of Nimbus II Anomalies

Table A1 lists the Nimbus II anomalies covered by the report period.

Table A1

Summary of Nimbus II Anomalies.

Anomaly	Cause	Remarks	Corrective Action	B*
Clock upset (1st)	Occurred during separation	Orbit 1U; reset clock to accurate time	Fire pyros from unreg. bus	Yes
Clock upset (2nd)	HAX OFF command executed during S-band transmission	Operational procedures modified to preclude recurrence of problem		Yes
AVCS Camera 1 iris failed to maintain proper orbital profile resulting in improperly exposed photographs	Failure of iris drive no. 2 of Camera 1	Since the failure, iris drive motor 1 has been used exclusively; it has shown no evidence of degradation in performance		No
Regulated bus exceeded regulator tolerance	Paddle unfold squib fire	Occurred at separation; feedback amplifier did not switch	Fire pyros from unreg. bus	Yes
Regulated bus exceeded regulator tolerance	HAX commanded on during S-band transmission	Occurred during orbit 28U; feedback amplifier did not switch	Change operational procedure	Yes
Roll solenoid gating	Earth/spacecraft magnetic field interaction	Max. roll flywheel momentum, periodically stored each orbit, has been greater than predicted; this increased more frequent solenoid gating to occur than expected (because of IR disturbances)	N/A	Yes

*Anomaly related to Nimbus B.

Table A1

Summary of Nimbus II Anomalies (Continued).

Anomaly	Cause	Remarks	Corrective Action	B*
Solar array motion during satellite night	Caused by noise on the 400-Hz ac power supply outputs which are used for the SAD and flywheel motors, motor drive amplifier reference phasing, and for the SAD sun sensor preamplifiers	SAD frequency advances 0.5 to 1.0 degree in position after it has settled at the night rest position during satellite night	N/A	Yes
SAD shaft tracking deviations	A negative yaw error adding to the existing 10-degree orbit plane misalignment, resulting in a total misalignment between the sun line and vehicle in excess of 10 degrees which, in turn, produces uneven shading of the shaft sun sensor	This anomaly has not been noted between orbit position 90 and 180 degrees; it is thought that the relatively quiet roll performance in this region has kept yaw excursions to a minimum and hence shaft sun sensor shading has not occurred	N/A	Yes
Deviation of thermal control shutters on controls package		Shutters 1 and 2 finally assumed an open position of 28 degrees which is approximately 20 degrees more than would be expected when compared to the associated panel temp.	N/A	Yes
Microphonics, AVCS Cameras 1 and 2	Vibration of internal elements of vidicon	Occasionally present		No
Decrease in HRIR signal-to-noise ratio from 20 (detector cell temperature -75°C) to 8 (detector cell temperature -64°C)	Change in thermal characteristics of cooling cone or cooling patch			Yes
AVCS video data obliterated during MRIR data transmission	MRIR transmitter interference	Failure of MRIR subsystem tape recorder eliminated necessity of MRIR transmitter operation		No
3.3-kHz interference ON AVCS Camera 1	AVCS high-voltage converter circuitry	Rarely present		No

*Anomaly related to Nimbus B.

Table A1

Summary of Nimbus II Anomalies (Continued).

Anomaly	Cause	Remarks	Corrective Action	B*
Telemetered value of temperature of AVCS Camera 2 electronics indicated instantaneous temperature changes of 20°C (orbit 692)	Electrical failure of either thermistor temperature sensor or grounding in telemetry conditioning circuitry			No
Thermal control shutter 15 position monitor malfunction	Monitor failed open, followed by occasional intermittent shorting	Shutter 15 indicated possible erratic movement with positions ranging from 10.08 to 25.6 degrees and back to zero allowing no apparent correlation with the sensing plate temperature	No fix planned (B circuitry different)	
Spurious execution of unencoded commands	Modulated RF signals in vicinity of spacecraft	Spurious unencoded commands caused switching of the primary and redundant receiver FM demodulated selector relay and the switching of the power supply feedback amplifier selector relay but did not affect spacecraft performance; corrected by having STADAN stations at Quito (Ecuador) and Santiago (Chile) transmit an unmodulated carrier whenever spacecraft in range	Require 2 unencoded commands simultaneously; clock design change	Yes
Telemetered value of APT transmitter output changed from 3.5 tmv (orbit 6) to 4.05 tmv (orbit 800)	Change in the tuning and input impedance of subsystem antenna caused by outgassing of absorbed moisture			Yes
Loss of data words during stored A-data playback	Tape wearout (reason unknown)	By orbit 940, the PCM tape recorder exhibited three blank spots of 6, 9, and 2 words in length, that increased with time		Yes
AVCS continuous playback mode	Power supply commanded off during record cycle	Corrective operational procedures put into effect		No

*Anomaly related to Nimbus B.

Table A1

Summary of Nimbus II Anomalies (Continued).

Anomaly	Cause	Remarks	Corrective Action	B*
10-kHz and 15-kHz interference on AVCS pictures	Beacon transmitter interference	10-kHz A-real time code interference; 15 kHz - 15 kbts A-stored PCM data interference		No
Inadvertent triggering of APT camera shutter	Voltage transient	Following booster separation, APT camera shutter triggered; photo of Agena forward bulkhead and spacecraft adapter was readout as initial spacecraft turn on in orbit 5U		No
HRIR recorder induced interference (0.8 kHz to 1 kHz) in APT pictures	Mechanical vibrations induced by operation of HRIR tape recorder			No
Microphonic interference in APT pictures	Vibration of vidicon internal elements	Interference increased to affect approximately one-fifth picture area as vidicon aged		No
Degradation in quality of MRIR video at satellite night-to-day and day-to-night transitions	Sunlight interference	Mirror shields on Nimbus II radiometer designed for 500-nm orbital altitude	Nimbus B mirror shield redesigned for 600-nm orbital altitude	Yes
HRIR video degradation	Direct and reflected sunlight interference	HRIR designed for 500-nm orbit; detector cell sun shield should be redesigned for 600-nm orbit		Yes
MRIR P/B current telemetry increase	Possible increased loading of P/B motor caused by increased friction within tape recorder or possible shift of telemetry sensor calibration	T/M showed gradual increase for expected 6.2 tmv to 6.35 tmv (full-scale)	N/A	No
MRIR record motor drive current indicated change	Hysteresis changes in sensor transformer core	Coincident with power transients at HAX OFF command (orbit 28U) and at squib firing at separation	N/A	No

*Anomaly related to Nimbus B.

Table A1

Summary of Nimbus II Anomalies (Continued).

Anomaly	Cause	Remarks	Corrective Action	B*
MRIR (sunlight interference on three channels)	Direct and reflected sunlight interference	Shielding should have been designed for a 600-nm orbit in place of 500-nm design	A sun shield has been added to the Nimbus B radiometer which occludes a greater angle than the present radiometer housing structure	Yes
Thermal control shutter 13 position reading random positions	Failure of shutter position monitor			Yes
Unencoded command execution while command receiver being jammed	Two stations radiating at same time caused a beat frequency unencoded command	A 30-sec interval between end of transmission by a station and start of transmission of next station has been started		Yes
Nonexecution of stored commands and DCG upsets	Noise entry into clock memory			Yes
Long beep tone indicating only one copy of command entering memory	Noise entry into clock memory			No
APT DCG "dogleg"	Clock 1-Hz and APT sequence timer phasing			No
Shift in beat pattern between PCM sampling rate and Clock 1-Hz and 10-Hz T/M monitors	PCM/clock phasing	Possibly an extraneous shift in PCM logic of 2 msec or an odd multiple of 2 msec during A-stored P/B	N/A	Yes
Stored A-data dropout (orbit 718R)		Suspected problem with propagation medium or DAF (no repetition)	N/A	Yes

*Anomaly related to Nimbus B.

Table A1

Summary of Nimbus II Anomalies (Continued).

Anomaly	Cause	Remarks	Corrective Action	B*
Clock master oven temperature reading 1 PCM count low during S-band transmission	Grounding problem within spacecraft	EMI effect on T/M levels	Nimbus B has better grounding system and tighter control on output impedances	Yes
2 PCM count shift of Cameras 1, 2, and 3 high-voltage levels during APT operation	Extraneous ground current induced by APT-HAX module causing -0.1 tmv shift of ground potential of spacecraft			No
Four frames of AVCS Camera 2 video completely washed-out (orbit 1309)	Shutter malfunction	Anomaly did not reoccur		No
Amplitude variations in HRIR timing signal	Recorder tape degradation	Correlatable to increase in flutter and wow		No
200-Hz interference on HRIR video data	200-Hz ac signal riding on -24.5 vdc radiometer power			Yes
PCM tape recorder failure in orbit 949	A stalled P/B motor is the most probable cause of failure	Still receiving good quality real-time A data.		Yes
MRIR tape recorder failure in orbit 985	Stalled P/B and compensation motors (possibly caused by tape breaking)	Attempts to restart tape recorder in P/B mode failed.	Nimbus B will utilize dual HDRSS tape recorder for increased reliability	Yes

*Anomaly related to Nimbus B.

Table A1

Summary of Nimbus II Anomalies (Continued).

Anomaly	Cause	Remarks	Corrective Action	B*
MRIR chopper motor stopped rotating in orbit 1070	Probable increase in friction in chopper motor bearing system	Chopper motor known to have marginal starting characteristics at low temperatures	Bearing retainers for the Nimbus B radiometer have been redesigned for increased lubricant protection and efficiency	Yes
Solar array outout decreased about 0.6 ampere during orbits 1065 to 1070		Solar array still produces sufficient power for normal spacecraft operation		Yes
Loss of AVCS video data and timing during interrogation 1444U	AVCS tape recorder failure	Recorder failure eliminated data storage capability of this subsystem		No
Loss of HRIR video data and timing during interrogation 2455R	Tape recorder failure	Recorder failure in playback mode eliminated data collection and storage capability of this subsystem	Nimbus B will utilize dual HDRSS tape recorders for increased reliability	No
Execution of encoded command (not commanded)	Probable noise entry into clock memory	PCM Power Supply 1 turned on in blind orbit period (orbits 2805 to 2807)		
Command tape out of sync	Sync problem in command ground station between time computer and transmitter modulator	On two occasions this resulted in clock memory being advanced through more locations than intended; this wiped out a stored command		
Grey scale of AVCS Camera 3 improperly illuminated (orbit 3520)	Failure either of flash tube or associated electronics	A-scope presentations indicated intermittent operation of Camera 3 tube after orbit 3520		No

*Anomaly related to Nimbus B.

Table A1

Summary of Nimbus II Anomalies (Continued).

Anomaly	Cause	Remarks	Corrective Action	B*
Telemetered value of the AVCS Camera 2 housing temperature indicated a substantial decrease from 32.8°C (orbit 3958)	Malfunction in telemetry conditioning circuitry or mechanical degradation of thermal bond between temperature sensor of camera housing	Temperature of camera mounting plate did not show corresponding decrease		No
Solar array decreased about 600 milliamps between orbit 4000 and orbit 4720		Solar array continues to produce sufficient power for normal spacecraft operation		Yes
Change in dc level of APT video	Probable malfunction within video switching selection of camera electronics	Compensatable in ground station processing equipment		No
Loss of focus in the video of AVCS Camera 1 during 11th month in orbit	Change in the characteristics of Camera 1 lens system	Focus of Cameras 2 and 3 video remaining satisfactory		No
2400-kHz interference on AVCS (Camera 2)	APT transmitter interference			No

*Anomaly related to Nimbus B.